910

DISC-GEOMETRY RELUCTANCE MOTORS

Thesis presented to the University

of London for the award of

the degree of Ph.D.

by

Peter David EVANS, B.Sc.(Eng), A.C.G.I.

March, 1977

Department of Electrical Engineering,
Imperial College,
London, S.W.7.

Abstract

This thesis is concerned with a.c. disc-shaped electrical machines, and in particular with disc geometry reluctance motors.

Chapter One contains a topological investigation of disc induction machines in which alternative stator and rotor configurations are identified. Some novel stator designs are presented which belong broadly to the class of "transverse flux" machines, and which have simple laminated structures. Quantitative assessment of the various machines is provided.

Chapter Two introduces the principles of reluctance motor operation, reviews their development and summarises the design considerations for salient pole and segmented rotor machines. It is seen that the relatively high end winding leakage reactance of low pole number disc machines will have an adverse effect on reluctance motor performance. These remarks precede an investigation of preferred types of disc reluctance motors, two of which are studied in the remainder of the thesis.

Chapter Three describes a computer-oriented method for simulating the performance of a double-sided salient pole disc reluctance motor under all operating conditions. The salient pole disc shaped rotor is represented by an equivalent electrical network and subdivision of the rotor circuits into sets of parallel-connected filament coils produces good quality predictions from a small number of rotor circuits.

Chapter Four presents theoretical and experimental results for the double sided reluctance motor considered in Chapter Three. These include its steady-state behaviour at synchronous and asynchronous speeds, and its transient start-up characteristics.

Chapter Five describes the test results obtained with a prototype single sided segmented rotor disc reluctance motor when operated with a large airgap between stator and rotor. They are shown to correlate well with existing methods of analysis, but the large airgap causes considerable degradation of synchronising performance. The characteristics of the normal force that exists between the stator and rotor at synchronous speed are investigated.

ACKNOWLEDGEMENTS

The author wishes to express his gratitude to Professor Eastham for his encouragement, inspiration and guidance with the work described in this thesis. Much is owed to him.

Professor Laithwaite kindly gave his timely tactical assistance and the many discussions with Dr. Hugh Bolton were invaluable. Thanks are due to them both.

Appreciation of the excellent service provided by the Engineering Workshop at Imperial College is extended to Colin Jones and his staff. Both experimental motors were constructed there, and John Kenny deserves particular thanks for his work on them.

Thanks are also proffered to Agnes Balchin who typed the text with an expert touch.

List of Principal Symbols

A_1	stator area enclosed by a short pitched coil
A_2	stator area outside a short pitched coil
A_s	area of one degree segment of stator
b_1, b_2	flux densities produced by short pitched coil in uniform airgap
b_m	flux density at m^{th} stator segment.
B_R, B_Y, B_B	flux density distributions produced by red, yellow and blue phase windings, respectively, in a uniform airgap
B'_R, B'_Y, B'_B	flux density distributions produced by red, yellow and blue phase windings, respectively, in a non-uniform airgap
B_g	rms value of sinusoidal airgap flux density distribution
B_n, b_n	rms and instantaneous values of normal component of airgap flux density
B_t, b_t	rms and instantaneous values of tangential component of airgap flux density
B_d, B_q	rms values of direct and quadrature axis components of airgap flux density
d_r	general diameter on disc motor
d_B	backing iron depth
d_s	slot depth
D_o	outer diameter of disc motor core
D_i	inner diameter of disc motor core
D_m	mean diameter of disc motor core
D_r	diameter of cylindrical stator bore
f	supply frequency
F_n	normal force
F_{nd}	normal force due to direct axis component of flux density
F_{nq}	normal force due to quadrature axis component of flux density
g	magnetic airgap between stator and rotor
g_1	magnetic airgap on direct axis of salient pole machine (Chap.3); channel depth in segmented rotor machine (Chap.5)
g_2	magnetic airgap on quadrature axis of salient pole machine
g_i	equivalent airgap due to iron circuit

g_d, g_q	equivalent uniform airgaps of the direct and quadrature axis machines
G	goodness factor
h'	effective segment depth
i	instantaneous phase current
I_d, I_q	direct and quadrature components of rms phase current
J_s	stator surface current density
J_R	rotor surface current density
J_L	current loading of stator winding
J_k	moment of inertia
k_{er}	end ring factor
k_s	slot packing factor
k_p	coil pitch factor
k_1	winding factor of fundamental harmonic
ℓ	inter-segment semi-distance
L_e, L_g	end winding lengths of surface and gramme-ring windings respectively
L	stack length (Chap.1); leakage inductance (Chap.3); main inductance (App.2)
M_{ab}	mutual inductance between coil system a and coil system b
N_c	number of turns per coil
N	number of turns per phase
p	number of pole pairs
$P_{s,r}$	stator and rotor magnetic potentials
R	mean radius of machine
R_1	primary phase winding resistance
R_2	secondary resistance
s	per unit slip
s_o	per unit slip at the start of the synchronising cycle
t	time
t_r	rotor thickness
T_a	asynchronous torque
T_b	braking torque
T_c	torque produced by a cylindrical machine
T_D	torque produced by a disc machine
T_e	electrical torque
T_r	reluctance torque
u	rotational speed of rotor

v	instantaneous phase voltage
V	rms phase voltage
V_L	rms line voltage
V_{dm}, V_{qm}	direct and quadrature axis components of rms phase airgap voltages
w_s	slot width
W	stator width
$\delta W, \delta W_e, \delta W_m$	small changes in work done, electrical input energy, and stored field energy respectively
W_{md}, W_{mq}	direct and quadrature axis components of airgap-stored energy
x_c	magnetising reactance of uniform airgap machine
x_d, x_q	direct and quadrature components of magnetising reactance (excluding leakage inductance)
x_l	leakage inductance
X_d, X_q	direct and quadrature axis components of motor reactance (including leakage reactance)

α	slot pitch
β	pole arc to pole pitch ratio
β_p	pitch of stator coil
β_T	tooth width to tooth pitch ratio
γ	channel arc to pole pitch ratio
γ_i	density of iron
γ_c	density of copper
δ	voltage-related load angle
δ_i	current-related load angle
$\delta_{max}, \delta_1, \delta_f, \delta'_f$ δ_o	angles related to synchronising cycle of a reluctance motor: defined in Fig. 5.12
λ	flux linkage
Λ	permeance
ρ_r	surface resistivity of rotor
ρ_c	resistivity of copper
τ_p	pole pitch
ϕ	power factor angle
μ_o	permeability of free space
ω	rotational frequency, in radians per second

CONTENTS

CHAPTER ONE

The Topology of Disc-Shaped Electric Machines

1.1 Introduction

There is a general class of rotating electric machines which may be called disc machines. Their essential topology is illustrated in Fig. 1.1 in which a single sided disc motor is compared in a stylised form with a conventional cylindrical motor. The shape of a disc machine can be arrived at by putting a conventional machine through two notional transformations. This is shown for a stator only in Fig. 1.2. Firstly, the cylindrical machine is cut radially and unrolled to give a linear machine (Fig. 1.2(a) and (b)). Secondly, the two ends of the linear stator are re-joined while keeping the active surface of the motor flat (Fig. 1.2(b) and (c)). The resulting stator is 'doughnut' shaped and the accompanying rotor would be disc shaped. The characteristic dimensions of the disc motor are its inner and outer core diameters, D_i and D_o respectively. These are related to the corresponding dimensions of the cylindrical machine, stack length L and stator bore D_r by:

$$\begin{aligned} D_o &= D_r + L \\ D_i &= D_r - L \end{aligned} \qquad \text{or} \qquad \begin{aligned} D_r &= \frac{1}{2}(D_o + D_i) \\ L &= \frac{1}{2}(D_o - D_i) \end{aligned} \qquad (1.1)$$

Preliminary inspection of the disc machine configuration shown in Fig. 1.2(c) indicates that several problems may be associated with its manufacture and operation. For example, the stator core illustrated in Fig. 1.2(c) cannot be built up from standard laminations and is consequently expensive to fabricate. Also, under operating conditions a large axial force will exist between the stator and rotor. To its credit, however, the disc machine configuration offers real advantages in some applications. For example:

- the stator and rotor of a single sided disc motor can be separated by a leakproof seal. This is advantageous when pumping hazardous or toxic fluids. Also, the heat-producing stator can be situated outside a vacuum enclosure.

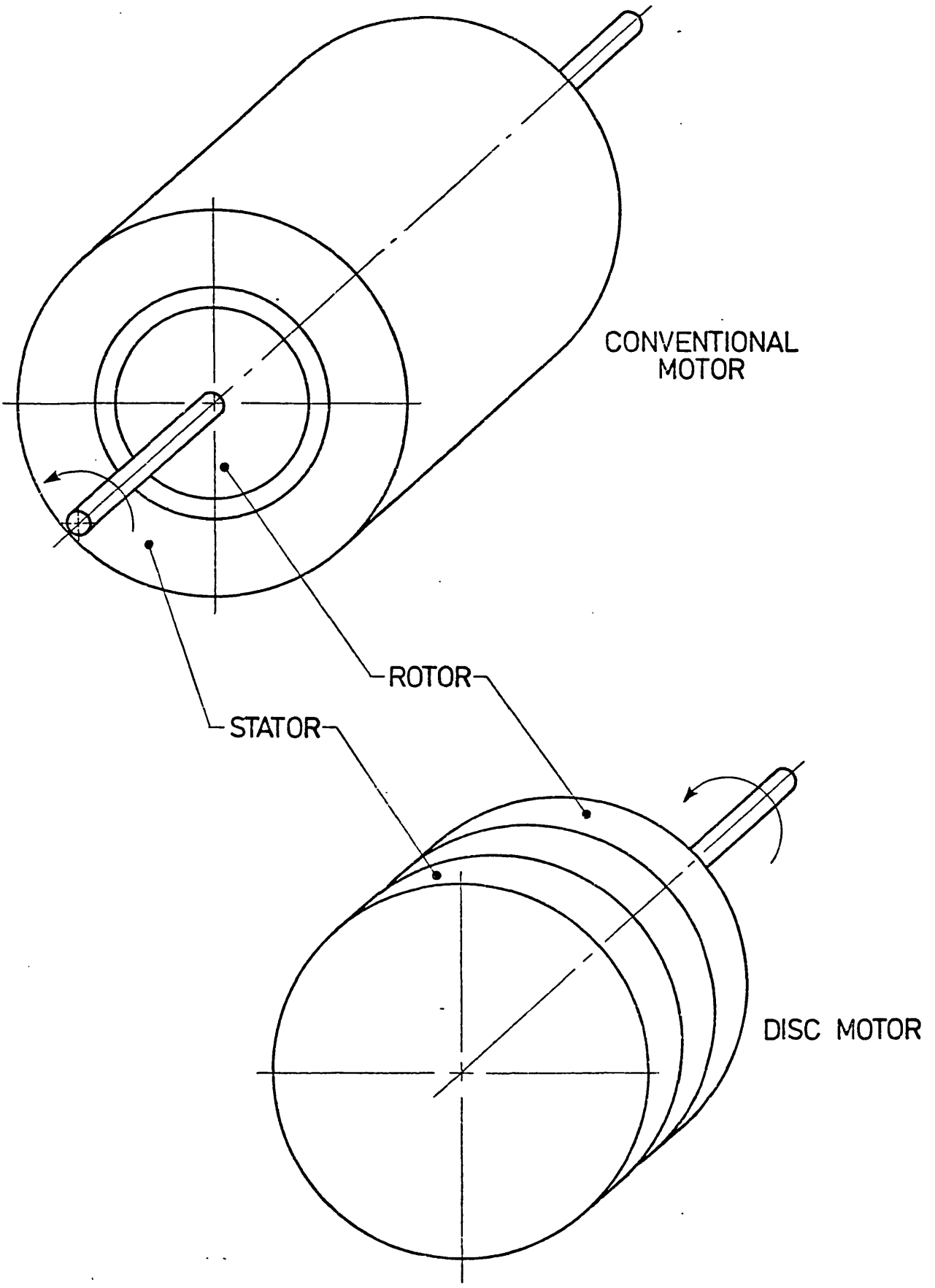

ESSENTIAL DIFFERENCES IN THE SHAPES OF CYLINDRICAL AND DISC MOTORS

FIG.1.1

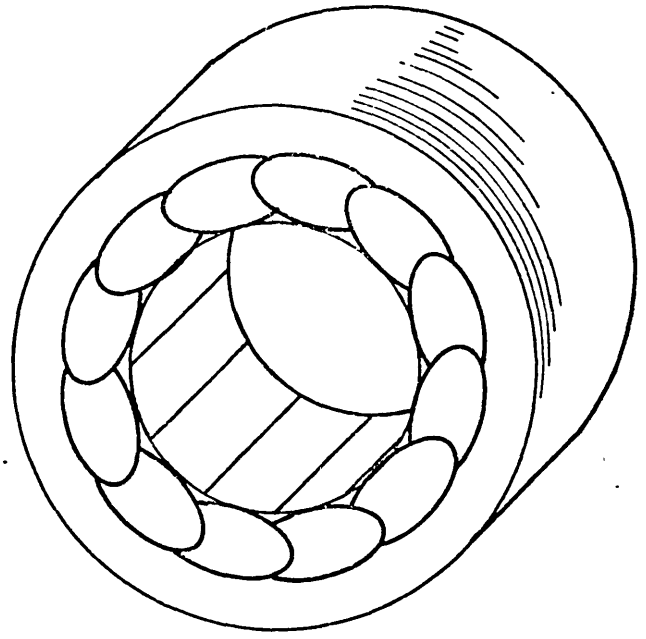

a. stator for cylindrical (conventional) machine

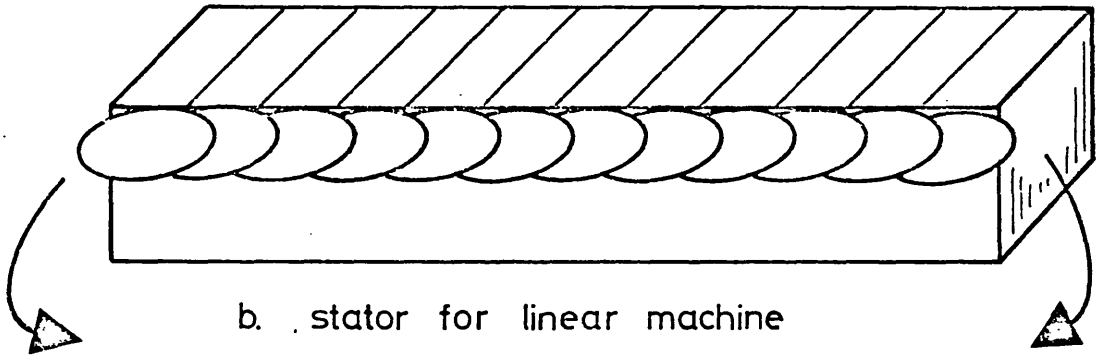

b. stator for linear machine

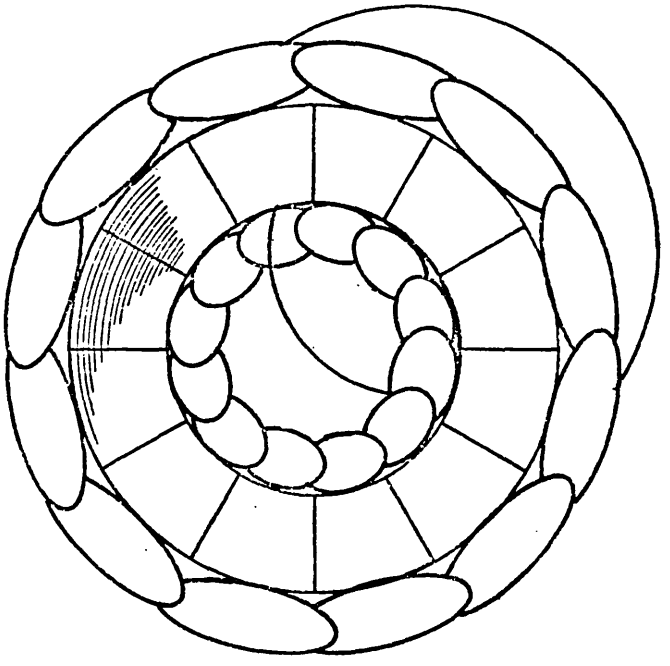

c. stator for disc machine

FIG. 1.2 DERIVATION OF THE SHAPE OF A DISC MACHINE

- the flat profile of the motor has advantages in some situations where a short axial length is required.
- the stator and rotor can be treated as separate units, the rotor being attached to the item to be driven, and the stator secured close to it. This removes the need for belts and pulleys and for separate motor bearings, thus increasing the reliability of the system. In the event of failure the stator can be replaced simply and rapidly.

Disc shaped machines have been designed and constructed for just a few specialised purposes[1],[2],[3]. For example, they are currently produced commercially for domestic central heating pumps in which their leakproof feature is exploited; printed circuit d.c. motors, which use disc shaped rotors have become quite widely used in recent times, especially for computer peripherals and similar control applications; and some disc shaped alternators have been constructed for aerospace applications. There are reasons to believe that the main drawback to disc machines is the expensive techniques that must be used in their manufacture; and that if they were available at prices which compared favourably with conventional machines their use would be more widespread in many areas of application. In view of this, the present chapter on the topology of disc machines has three prime objectives:

i) to identify as many alternative designs for disc-type machines as possible,
ii) to compare quantitatively the principle forms of disc machines with cylindrical machines, and with each other,
iii) to identify the configurations which appear to offer both acceptable operating characteristics and economic methods of manufacture.

Some new machines are presented which appear to lend themselves to simple and inexpensive methods of manufacture.

This thesis is primarily devoted to a study of disc 'reluctance' motors, i.e. motors which use induction torques for starting, but subsequently synchronise under the influence of reluctance torques created by rotor saliency. Discussion, therefore, centres largely around induction and reluctance machines. Other forms of disc motor,

such as d.c. motors, primary or secondary side excited synchronous machines, or permanent magnet machines are not taken into consideration.

1.2 Topological Terminology

Electrical machines can be constructed in so many different forms using several different mechanisms for torque production that it is difficult to conceive of a precise system of classification for them which is both comprehensive and convenient. For the purposes of the present discussion on the topology of induction machines, however, it is necessary to define and adopt a system which enables the essential features of the different machines to be described succinctly.

The basic requirement of an electrical machine is that mechanical forces should be produced on its secondary member (rotor) which is separated from the primary member (stator) by the airgap. This force is created in an induction motor by the interaction of the magnetic flux density in the airgap and the electric currents flowing in the rotor. The only fundamental condition necessary for a useful interaction is that the force, flux and currents have components which are mutually perpendicular. The design of an electric machine is, therefore, concerned with arranging its electric and magnetic circuits with respect to the direction of relative motion between its primary and secondary members in order that the most cost-effective machine can be constructed for a given set of operating conditions. In this respect freedom exists in the design of the shape of the airgap, and in the paths which the electric and magnetic circuits follow outside the airgap region. The general configuration of a motor can, therefore, be defined in the first instance by three terms:

i) Geometry. The shape of the airgap can be defined by a geometrical term. Thus, the conventional shape of motor is 'cylindrical'; the machines under discussion are 'disc' shaped (with a hole in the middle of the disc); so-called linear machines are by this classification 'rectangular'; and other shapes of motor such as 'spherical' and 'conical' have also been made. Motors with conic section geometries provide rotary motion and the 'rectangular' motor produces 'linear'

motion. The 'tubular' linear motor does not appear to fit conveniently into this classification. In all these shapes the flux is usually driven in a direction which is substantially normal to the plane of the airgap.

ii) Direction of flux paths outside the airgap region

The geometry of a motor, as described above, implicitly defines the direction of relative motion between its primary and secondary members. The direction of the flux and current paths outside the airgap are, therefore, most conveniently defined with respect to this direction. Two important alternative paths exist for the flux: it can either be parallel to the direction of motion - usually called 'axial' flux; or it can be 'transverse' to the direction of motion[4].

iii) Direction of current paths outside the airgap region

Two alternative paths also exist for the end windings of the current-carrying coils of the primary member. They can either be in the direction of motion, so that the coils are in the plane of the airgap; these are commonly known as 'surface' windings. Or, if they are transverse to this direction, they are referred to as 'Gramme ring' windings.

It appears that 'transverse' is to 'axial' for the flux as 'Gramme ring' is to 'surface' for the currents. The terminology 'transverse', 'axial', 'surface' and 'Gramme ring' is, therefore, not consistent, but what it lacks in consistency it makes up in familiarity and for this reason has been adopted in the present thesis.

According to the above classification, the conventional electric motor has a 'cylindrical' geometry and utilises 'axial' flux paths and 'surface' windings. This has proved to be a very good arrangement for normal applications, but as demonstrated recently for linear machines[5], an investigation of novel machine configurations must examine critically the alternative arrangements of flux and current paths.

The basic requirement of the rotor of an induction motor is that it should carry the rotor currents which mirror the stator current pattern. In its simplest form it consists of a thin electrically conducting plate or shell which is the same shape as the airgap. This type of rotor is called a 'sheet' rotor. An alternative type of rotor which gives improved performance under some conditions by increasing the airgap permeance consists of discrete conductors aligned in the direction of the main current paths, which are interspersed with magnetically soft iron. This type of rotor is designated a 'cage' rotor after the well-known 'squirrel cage'. These two types of rotor are described in more detail in Section 1.3.2 below.

As described above, a rotor does not contain return paths for the airgap flux; its function is solely to react electrically to the flux which passes through it normally. The arrangement of the electric and magnetic circuits of the primary member, the stator unit, around the rotor is therefore another important topological feature of electrical machines which can be described by two of four terms as follows:

i) 'electrically single-sided' (ess) indicates that the primary excitation of the machine is provided on one side of the rotor only

ii) 'electrically double-sided' (eds) indicates that the rotor is sandwiched between two excited stator units

iii) 'magnetically single-sided' (mss) indicates that a low reluctance flux path is provided on one side of the rotor only

iv) 'magnetically double sided' (mds) indicates that both sides of the rotor are provided with low reluctance paths to carry the main airgap flux

According to these definitions, conventional cylindrical machines are usually 'ess and mds'. Most useful machines have good low reluctance flux paths and are therefore invariably magnetically double-sided. This being the case, the two alternatives which exist are for 'ess' and 'eds' machines. These have been referred to in the context of linear motors simply as 'single-sided' and 'double-sided' machines respectively.

From the above discussion, it appears that the principal features of any configuration of induction machine can be described by six terms:

- geometry
- direction of flux return paths
- direction of current return paths
- type of rotor
- number of primary magnetic circuits
- number of primary electric circuits

and they are used for the following discussion of the topology of disc induction machines. Several other detailed features are usually required to distinguish uniquely one machine from another, and these are introduced as required in the discussion of disc machine configurations which follows.

1.3 Disc machines with axial flux

1.3.1 Introduction

According to the definitions given in Section 1.2 above, a disc motor with axial stator flux paths has the form indicated in Fig. 1.2(c), i.e. the direction of motion and the direction of flux in the backing iron are the same. The stator consequently consists of a strip wound core with radial (or skewed-radial) slots into which a conventional type of winding is inserted. It is directly equivalent in these respects to a conventional cylindrical stator. The backing iron for both 'sheet' and 'cage' rotors which are compatible with this type of stator is also a strip wound core, the preferred path being presented to flux passing circumferentially around the motor.

There appear to be three main configurations for axial flux disc machines, but some variations of these also exist. They are illustrated in cross section in Fig. 1.3 and are described in Sections 1.3.3, 1.3.4 and 1.3.5 below. Their discussion is, however, prefaced by a description of 'sheet' and 'cage' rotors which can in general be used with all the disc motor configurations.

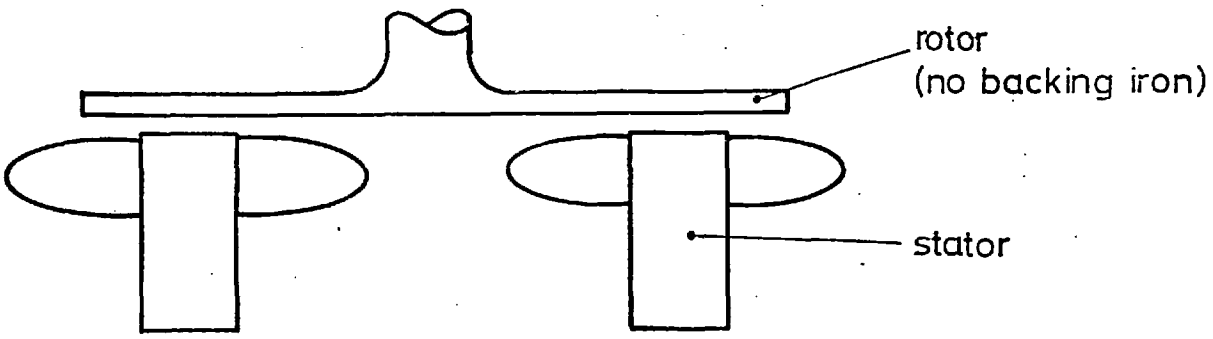

a. electrically & magnetically single sided

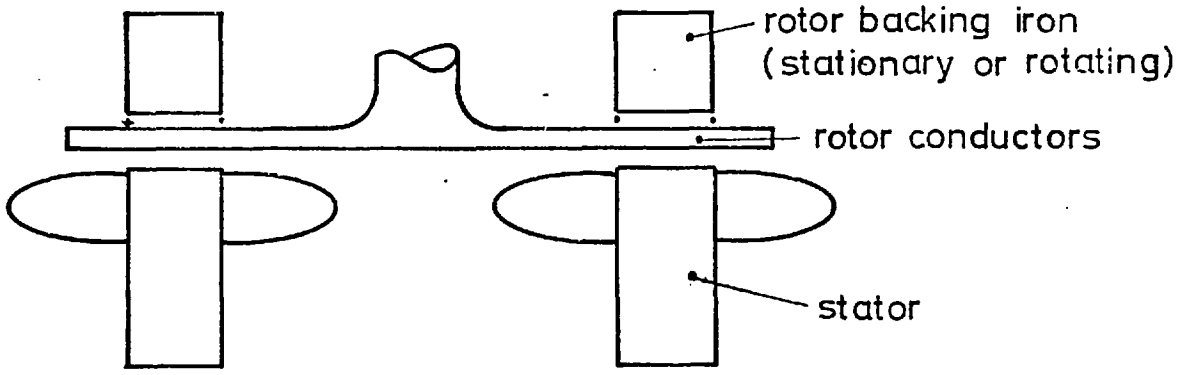

b. electrically single sided, magnetically double sided

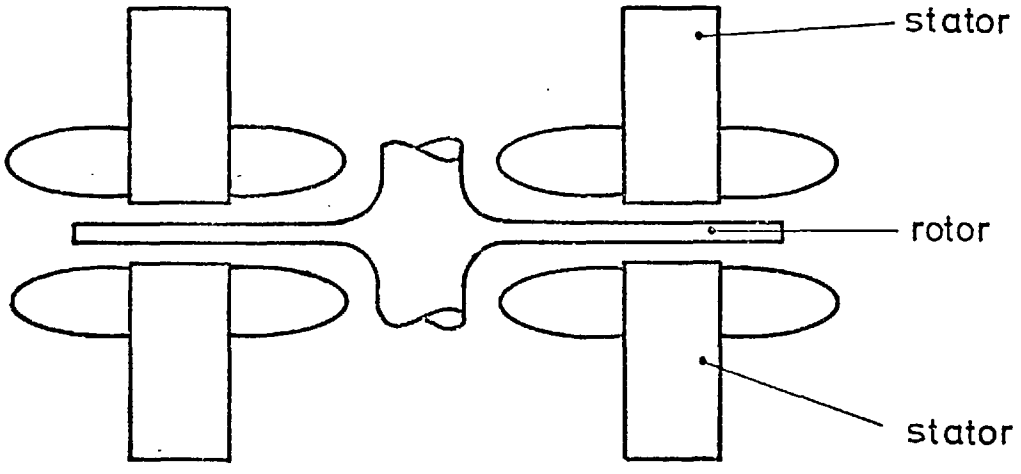

c. electrically & magnetically double sided

FIG.1.3 ALTERNATIVE CONFIGURATIONS OF DISC MOTORS WITH AXIAL FLUX.

1.3.2 Rotor configurations

The disc-shaped rotor demanded by axial flux disc machines can take two basic forms which are analogous to the 'drag-cup' and 'squirrel-cage' rotors of conventional induction motors: they were referred to in Section 1.2 above as 'sheet' and 'cage' rotors respectively.

i) The sheet rotor

A sheet rotor is illustrated in Fig. 1.4(a). It consists essentially of a disc of conducting material (usually aluminium or copper) which can have thickened rims as shown to reduce its end ring resistances. It is usually used in conjunction with a low reluctance flux return path which can be either stationary or an integral part of the rotor. This simple form of rotor is free from slot harmonics and has a low leakage reactance, but inevitably gives the motor a large magnetic airgap, or 'entrefer'.

ii) The cage rotor

Fig. 1.4(b) depicts a rotor which consists of a flat electrically conducting grid embedded in a laminated iron toroid. The rotor conductors are effectively sunk into slots, according to normal practice, in order to decrease the total 'entrefer' of the motor. Like the sheet rotor it must, in the form illustrated, be used in conjunction with low reluctance flux return paths. (Closed rotor slots would usually be required for constructional rigidity of the iron core. Arcuate portions of iron would need to be located between the radial rotor bars if semi-closed slots were to be provided). This form of rotor, which has been investigated by Capaldi[6], would be difficult and expensive to manufacture. A practical version of it with the same basic performance characteristics might consist of a sheet rotor into which steel rivets had been inserted in the active annular region[7].

The nature of the forces exerted on the sheet and cage rotors in a direction normal to the airgap plane is in general different. The sheet rotor experiences forces of repulsion from the stator due to the interaction of the stator and rotor current sheets. These are usually maximum at standstill and reduce as the slip speed falls. The cage rotor, on the other hand, can be either repelled from or attracted to the stator according to the relative sizes of the normal and tangential

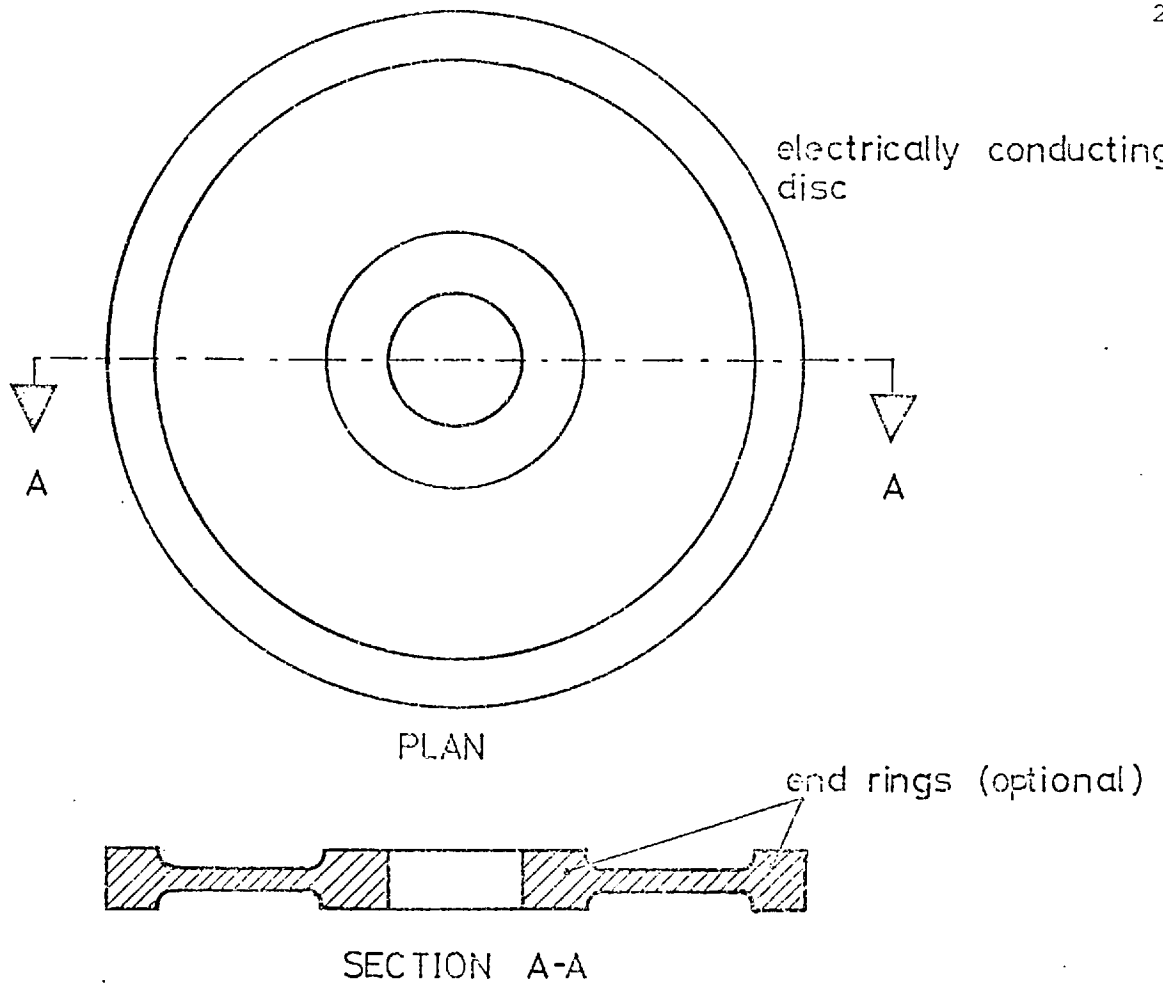

a. SHEET ROTOR

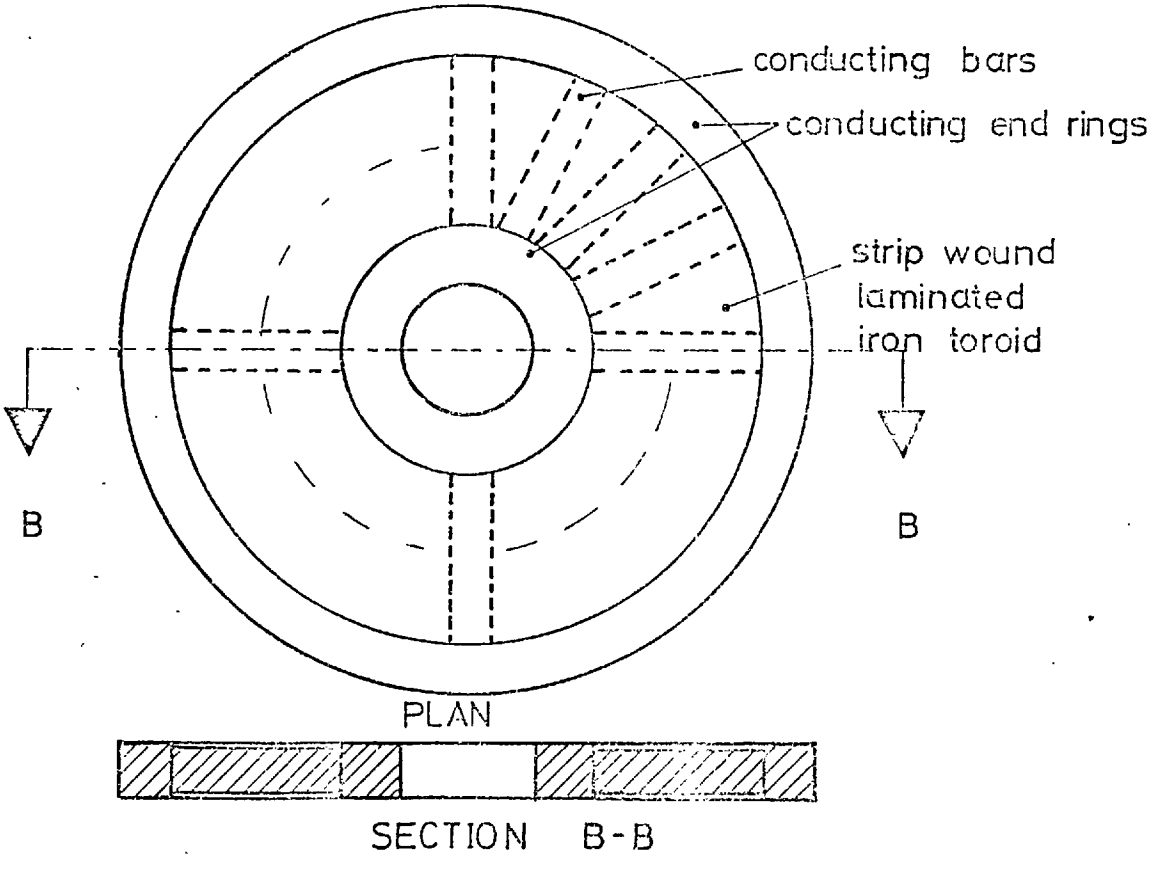

b. CAGE ROTOR

FIG. 1.4 ROTORS FOR A.C. DISC INDUCTION MACHINES

field in the air gap[8]. It can be shown[9] that the time average pressure, F_n, is given by

$$F_n = \frac{1}{2\mu_o}(B_n^2 - B_t^2)$$

where B_n and B_t are the r.m.s. values of normal and tangential airgap flux density respectively. Now B_t is given by $J_s\mu_o$ where J_s is the stator current loading which is proportional to line current, whilst B_n is given approximately by $B_n = \frac{\rho_r J_s}{sv_s}$ where ρ_r is the rotor surface resistivity, v_s is the synchronous speed and s is the per unit slip. Thus, it can be appreciated that both the sign and the magnitude of the normal force are dependent upon the machine design parameters. Normally, the values of these quantities ensure, for a conventional cylindrical squirrel-cage design, that the force is always attractive; but special design conditions can be met where the force is replusive at standstill, zero at some intermediate speed and attractive at synchronous speed[10].

1.3.3 The ess and mss axial flux disc machine

Fig. 1.3(a) illustrates perhaps the simplest axial flux disc machine (AFDM); it is both electrically and magnetically single-sided. The notable feature of this machine is its open magnetic circuit: there is no low reluctance flux return path for the stator flux, and it would sensibly only be used with a sheet rotor.

The effective airgap of such a machine is approximately equal to τ_p/π[11], where τ_p is the pole pitch. Consequently, it has a large equivalent airgap and the resultant low value of magnetising reactance will preclude it from normal applications. It is interesting, however, to consider briefly what form a useful version of this machine might take and its 'goodness', G,[12] gives an indication of this

$$G = \frac{2\tau_p^2 \mu_o f}{\pi \rho_r g K_{er}} \qquad (1.2)$$

By inserting known values for the permeability of free space, μ_o, and the supply frequency, f; assuming that the end-ring factor, K_{er}[13] can be kept below 3.0; substituting τ_p/π for the airgap, g,[11]; substituting ρ_c/t_r for ρ_r, where ρ_c is the resistivity of the rotor material

and t_r is the thickness of the sheet rotor); it can be shown that for a copper rotor which is 0.5 cm thick, say:

$$G = 12.2\ \tau_p \qquad (1.3)$$

For a Goodness factor of 10 therefore (i.e. the maximum torque is produced at 10% slip, assuming that the motor is driven from a constant current supply and that the rotor leakage inductance is zero), the pole pitch would have to be greater than 0.8 m. The mean diameters of 2- and 4-pole machines which satisfy this requirement are 0.52 m (20.5 inches) and 1.04 m (41 inches) respectively.

Although increased rotor conductor thickness and reduced end ring resistance would permit smaller machines to be constructed with the prescribed torque characteristic, in all cases the machine would draw a high magnetising current. It is conceivable, therefore, that this configuration might find a few specialised applications but would certainly not be considered for normal usage. In this event it is given no further consideration.

1.3.4 The ess, mds axial flux disc machine

An immediate improvement to the ess and mds motor above can be made by providing a low reluctance return path, for the flux on the side of the rotor which is remote from the stator, as shown in Fig.1.3(b). This form of disc motor which makes use of a sheet rotor and stationary backing iron is analogous to the cylindrical 'drag-cup' motor. A cage rotor, on the other hand, joined to a backing iron member which rotates with it gives the disc motor which is equivalent to a cylindrical squirrel cage induction motor. These appear to be the two sensible forms of ess and mds axial flux disc machine. The drag-cup analogue provides the low inertia version of the disc machine, in which the rotor does not contain iron, and is consequently not susceptible to the high magnetic forces which are produced between magnetised iron surfaces. The magnetic airgap of this type of rotor is characteristically large, however, being equal to $2g + t_r$, where g is the mechanical clearance between stationary and rotating surfaces and t_r is the thickness of the rotor, and this feature inevitably incurs penalties on the performance of the machine. The squirrel cage analogue can provide the most

efficient form of single-sided disc motor, but usually at the expense of high magnetic forces between the stator and rotor under normal operating conditions. The contributory forces were discussed in Section 1.3.2 above. The physical characteristics of this type of disc motor are compared quantitatively with an equivalent cylindrical motor in Section 1.4 below.

It should also be noted that the iron losses in the stationary backing iron member will be greater than those in the rotating member, with additional penalties on the efficiency of the sheet rotor disc motor.

Two further configurations of ess and mds disc machine theoretically exist. These would combine a sheet rotor with a rotating backing iron member, and a cage rotor with stationary backing iron. But it is difficult to conceive of situations in which either of these would be used in preference to the two described above.

1.3.5 The eds and mds axial flux disc machine

The ess and mds AFDM of the previous section was a direct evolution from the conventional cylindrical motor. It could be considered merely as an alternative geometric arrangement of a motor, and it possessed no intrinsically novel design features. An eds and mds AFDM, which is illustrated in Fig. 1.3(c), is a new type of machine, however, and does not have a commonly occurring cylindrical counterpart. As shown in Fig. 1.3(c) the eds and mds axial flux disc machine consists essentially of two stators arranged face-to-face with a disc shaped rotor situated in the airgap between them. By analogy, its cylindrical counterpart would consist of a cylindrical rotor shell situated between inner and outer cylindrical stator units, both of which carry windings. There are two major drawbacks to this arrangement:

- the constricted radius at the roots of the teeth of the inner stator unit would be liable to magnetic saturation
- a complex bearing assembly would be required to support the cylindrical rotor shell between the inner and outer stators.

Some rotors of this type appear to have been constructed in the past for very specialised applications, but their widespread use has been inhibited by the drawbacks described above. In contrast to this 'double-sided' linear motors are widely used within the restricted area of applications for linear drives[14].

The implications of using a double-sided stator configuration are significant: it can lead to improvements in the electromagnetic properties of the windings and to a better power to weight ratio. These effects have been discussed briefly by Laithwaite and Barwell[14] with respect to linear machines, but are investigated in more detail for disc machines in this section. Throughout the following discussion it is assumed that the windings of the two stators are interconnected so that the main flux is directed normally across the airgap i.e. a north pole on one stator is opposite a south pole on the other. The alternative interconnection, producing like poles opposite each other is effectively the same as mounting two single sided machines face-to-face on the same shaft. (Nasar[1] proposed varying the orientation of one stator with respect to the other in order to modulate the profile of the airgap flux wave).

The benefits arising from the use of a double stator configuration are as follows:

i) Improvements in electromagnetic properties of windings

The implications of using two stators rather than one can best be seen by considering the hypothetical conversion of a single-sided motor (Fig. 1.3(b)) into a double-sided motor (Fig. 1.3(c)). It can be deduced that if the windings previously confined to one stator are equally divided between two stators, the slot depth being reduced accordingly, then for either a sheet or a cage rotor:

- the power output of the motor is substantially unchanged,
- the average electric and magnetic loading of the motor remain constant,
- the magnetising reactance (Xm) of the motor is ideally unchanged, because the same total number of turns is linked by the same main flux,
- the total stator resistance is the same,

BUT - the leakage reactances of the windings are reduced

significantly. In general terms, this is because the number of turns per coil is halved, so that its inductance is reduced by a factor of four; but as there are now two sets of coils connected in series, the net effect is a reduction by a factor of approximately two. This assumes that there is no mutual coupling between the leakage fields of the two sets of windings. Considering the end winding leakage and the slot leakage components separately, the situation can be summarised as follows:

Component of leakage reactance	Formula for leakage reactance (15)	Change in parameter per stator	Overall effect on motor
End windings	$X_{le} = K(qz_c)^2 L_e$	$z_c \times \frac{1}{2}$	$X_{le} \times \frac{1}{2}$
Slot:			
Open slots	$X'_{ls} = Kqz_c^2 W\{\frac{d_s}{3\omega_s}\}$	$z_c \times \frac{1}{2}$ $d_s \times \frac{1}{2}$	$X'_{ls} \times \frac{1}{4}$
Semi-closed slots	$X''_{ls} = Kqz_c^2 W\{\frac{d_s}{3\omega_s} + \frac{h_o}{\omega_o}\}$	$z_c \times \frac{1}{2}$ $d_s \times \frac{1}{2}$	$X''_{ls} \times \alpha$ where $\frac{1}{4} < \alpha < \frac{1}{2}$

where $K = 2\pi\mu_o fp$

$L_e = k_p \tau_p + 0.019$

X_{le} = end winding leakage reactance per phase

X'_{ls} = leakage reactance per phase due to open slot

X''_{ls} = leakage reactance per phase due to semi-closed slot

q = number of slots per pole and phase

z_c = number of conductors per slot

W = stator width

d_s = slot depth

ω_s = slot width

h_o = tooth tip depth

ω_o = slot opening

f = supply frequency

p = number of pole pairs

k_p = fractional pitch of stator coil

τ_p = pole pitch

The above expressions indicate that the use of two wound stator units instead of one reduces the overall motor leakage reactance by at least one half. In the case of open slots, for which it has been assumed that the total depth is filled with conductors, it can be seen that the total slot leakage is divided by a factor of four, because both the slot depth and the number of turns per slot are halved. This gain can only be made, however, when the high level of pole face losses associated with flux ripple from the slot openings can be tolerated. When semi-closed slots are used, the main body of the slot which is filled with conductor for normal designs contributes a relatively small proportion of the total slot leakage (around 25% for some geometries), the remainder being caused by the small opening at the top of the slot. The reduction in slot leakage due to a smaller slot depth is therefore correspondingly less.

From the foregoing discussion it can be seen that the overall effect of using two winding sets instead of one is to reduce leakage reactance and consequently improve the power factor and efficiency of the motor; but these gains are necessarily made at the expense of increased manufacturing costs.

It should be noted that under some circumstances when two windings are being used it might be preferable to forego the maximum reduction in slot leakage in exchange for reduced winding resistance. This can be achieved by retaining the slots at the original single-sided stator size and using wire with twice the cross-sectional area in both stators of the double-sided version.

The relative sizes of the parameters of the stators used for experimental work which is described later in the thesis give an appreciation of the improvements that can be made by using a double stator configuration. Typically, the total leakage reactance of a single 4-pole stator is some 15% of the magnetising reactance when the motor has an entrefer of 1 mm (0.040 in). The open circuit airgap voltage is consequently increased by about 10% by converting from the single to the double sided motor arrangement. Furthermore, approximately 80% of the total leakage reactance is contributed by the end windings, the remainder being caused by the slots. The slots are semi-closed,

and the specific permeance of the main body of the slot is only 25% of the total slot permeance. Hence, halving the slot depth reduces the total leakage reactance by less than 5%, and it is clear that the most substantial improvement in leakage reactance is derived from a reduction in the end winding component.

The corollary of this is that the slots can be deepened to accommodate more conductors without incurring severe penalties: the implications of this are investigated more thoroughly later in this thesis (Section 1.5) where some design criteria for disc motors are examined.

ii) Improvements in power to weight ratio

The transfer of half the windings from a single stator on to the stationary rotor backing iron, thereby creating the double stator arrangement described above, provides the clue for increasing the power to weight ratio of the motor. For if, instead of dividing the windings between the two stators, a second complete stator is added, the double sided motor so formed has the potential for twice the power output, provided the rotor conductors are also increased in size; and this is achieved without adding any more backing iron. The actual effect on the performance of the motor depends upon the type of rotor - sheet or cage - that is being used. When a cage rotor is in position the cross-sectional area of its conductors can be doubled to meet the increase in stator copper, without a significant increase in the air-gap reluctance. In other words, the surface resistivity of the rotor is halved; peak torque is produced at about half the original value of slip; and approximately twice the power output can be obtained from the machine for the same thermal dissipation in the rotor.

The situation is different for a sheet rotor as an increase in rotor conductor thickness necessarily introduces an increase in the size of the 'entrefer'. Part of the benefit from the second stator is therefore absorbed in providing the magnetising current for this additional airgap, and the increase in power output is correspondingly reduced.

Detailed examination of these effects is beyond the scope of the present text, as they are to a large extent determined by second-order effects which are not conveniently treated in a simple analysis. But ultimately the rating of a machine is limited by heat dissipation in the stator and rotor. In this respect, the second stator with a second set of windings has a second major path for heat dissipation through the surface of its backing iron and can therefore dissipate its own I^2R losses. To this extent, therefore, the increased power to weight ratio of double stator machines is potentially realisable.

Unlike the single-sided disc machine in Section 1.3.4 above, which was merely an alternative geometry for a conventional cylindrical machine, the present double-sided rotary motor is peculiar to the disc motor topology. The simple face-to-face arrangement of stator and rotor of the single-sided machine has been forfeited, but normal forces between stator and rotor are largely cancelled out. In addition, the use of two stators enables p.u. leakage reactances to be reduced and the power to weight ratio to be enhanced. The principle characteristics of this motor are compared quantitatively with those of conventional machines in Section 1.4.4 below.

1.4 Quantitative comparison of equivalent cylindrical and disc machines

1.4.1 Introduction

There is every reason to suppose that disc machines will behave in a similar manner to conventional cylindrical machines. They are both rotating electromagnetic devices. Their differing geometries affect the arrangement of their electric and magnetic circuits, but not their essential interactions.

The previous section investigated the possible configurations of disc machines in a qualitative manner, and established that two principal disc machines were viable: the single-sided disc machine which, in one of its forms, was equivalent to the cylindrical squirrel cage induction motor; and the double-sided disc motor which does not have a commonly-occurring cylindrical counterpart. The purpose of this section is to examine quantitatively the physical characteristics of these machines

in relation to an equivalent cylindrical version, in order to determine the relative efficiencies with which their magnetic and electric circuits are utilised. The results of these studies give an appreciation of the penalties that may have to be accepted if disc geometries are adopted, and should also indicate any advantageous features that they may possess.

The following treatment is necessarily simplified and only takes into account the more important features of the motor under consideration: its purpose is to identify underlying trends. Competing designs for a particular application must ultimately be examined in detail, and all the characteristics of the motor which influence its suitability for the proposed duty taken into account.

1.4.2 Equivalent machines

The torque, T_c, produced by a cylindrical machine with stack length, W, and bore D_r, can be expressed by:

$$T_c = (B_g J_R \cos\theta)(\pi D_r W)(\frac{D_r}{2}) \qquad (1.4)$$

where $B_g J_R \cos\theta$ is the force produced per unit of active stator surface area. (θ represents the space phase angle between the airgap flux density, B_g, and the rotor surface current density J_R: it is assumed to be constant). $\pi D_r W$ is the total active stator surface area and $D_r/2$ is the effective torque arm length for the motor.

The torque, T_D, produced by a single sided disc motor that incorporates a cage rotor with integral backing iron cannot be written down in a similar manner for two reasons:

- the torque arm length is not constant over the active surface area but varies from the inner to the outer radii.
- the rotor surface current density is not uniform across the active motor surface.

However, the torque δT_D produced by an infinitely thin circumferential element of the motor surface of width $\frac{1}{2}\delta d_r$ and at diameter d_r is given by:

$$\delta T_D = B_g \pi d_r \frac{\delta d_r}{2} J_R \left(\frac{D_o + D_i}{2d_r}\right) \cos\theta \frac{d_r}{2} \qquad (1.5)$$

where - $B_g \pi d_r \frac{\delta d_r}{2}$ is the flux entering the circumferential element.

- $J_R \left(\frac{D_o + D_i}{2d_r}\right)$ is the rotor surface current density at diameter d_r (J_R being the current density at the mean diameter, $\frac{1}{2}(D_o + D_i)$ of the disc motor).

- θ is the phase angle between B_g and J_R.

B_g, J_R and θ are assumed to be the same for both the cylindrical and disc machines.

Integrating equation 1.5 between the limits of the inner and outer core diameters of the disc motor, D_i and D_o respectively, gives:

$$T_D = (B_g J_R \cos\theta)\left(\frac{\pi}{4}(D_o^2 - D_i^2)\right) \frac{1}{2}\left(\frac{D_o + D_i}{2}\right) \qquad (1.6)$$

This expression, like equation 1.4 above, contains terms for force per unit area, motor surface area and mean torque arm length. It indicates that a disc motor produces the same nominal output as a cylindrical motor with a bore that is equal to the mean diameter of the disc motor.

Equations 1.4 and 1.6 enables equivalent cylindrical and disc machines to be defined. For if $T_c = T_D$:

$$D_r^2 W = \frac{1}{8}(D_o^2 - D_i^2)(D_o + D_i) \qquad (1.7)$$

But, in order to define equivalent machines in terms of one variable each two simplifications are necessary.

Firstly, it is assumed that the cylindrical motor has 'square poles', i.e. that the motor width is equal to the pole pitch. This is expressed mathematically by:

$$W = \frac{\pi D_r}{2p} \qquad (1.8)$$

Secondly, a relationship between the inner and outer diameters of the disc motor can be derived to maximise its output. Re-writing equation 1.6 with the rotor surface current density expressed in terms of the value obtaining at the inner diameter gives:

$$T_D = B_g J R_{D_i} \cos\theta \frac{\pi}{4} (D_o^2 - D_i^2) \frac{D_i}{2} \qquad (1.9)$$

Differentiating equation 1.9 with respect to D_i, assuming that D_o is constant,

$$\left.\frac{\partial T}{\partial D_i}\right|_{D_o=\text{const}} = B_g J r_{D_i} \cos\theta \frac{\pi}{8} [D_o^2 - \frac{D_i^2}{3}] \qquad (1.10)$$

which is equal to zero, and is maximum when

$$\frac{D_o}{D_i} = \sqrt{3} \qquad (1.11)$$

This implies that the maximum output can be obtained from a disc motor when its inner and outer diameters are related by equation 1.11. Campbell[16] derived the same relationship for the maximum power output from a permanent-magnet axial field d.c. machine.

There is a physical reason for an optimum value of the ratio D_o/D_i to exist. As the inner diameter of the motor is made smaller, the active surface area of the motor is increased, tending to improve the output of the motor, but at the same time the slot area of the motor is decreased, which tends to reduce its output.

Substituting the relationships in equations 1.8 and 1.11 into equation 1.7 enables it to be simplified to:

$$\frac{D_r}{D_i} = \sqrt[3]{\frac{(\sqrt{3}+1)p}{2\pi}} \qquad (1.12)$$

Thus, within the constraints defined above, the ratio of the bore of a cylindrical motor, D_r, to the inner diameter, D_i, of an equivalent single sided disc motor depends upon the pole number of the motor. Tabulated results for expression 1.12 are as follows:

p	D_r/D_i
1	0.76
2	0.95
3	1.09
4	1.20
5	1.30
6	1.38

This relationship between the sizes of the two types of motor opens the way for simple calculations of motor weights and dimensions to be made. But some additional assumptions are also necessary. These are:

i) that the depth of backing iron, d_B, in a motor is given by:

$$d_B = \frac{\beta_T \tau_p}{\pi} \qquad (1.13)$$

where β_T is the tooth width to tooth pitch ratio and is assumed to equal 0.5. τ_p is the pole pitch (at the mean diameter of the disc motor).

ii) that the machines have infinite magnetising reactances, so that the stator surface current density, J_s, is equal to the rotor surface current density, J_R. The dangers of making this assumption are reduced by the fact that it is applied to all types of machines, and that parameter ratios only are considered.

iii) that the slot depth, d_s, of a cylindrical motor is given by:

$$d_s = k\, D_r \qquad (1.14)$$

where k is an empirical factor, equal to 0.17. It is approximately correct for machines up to 0.5 m bore. The depth of slot in the disc machine was made equal to the value calculated from equation 1.14 for its cylindrical equivalent.

iv) that the extent by which end windings overhang the motor core is equal to $0.25\ \tau_p$.

v) that all motor coils are pitched over five-sixths of the pole pitch.

1.4.3 Calculation and comparison of parameters of cylindrical and single-sided disc machines

Five parameters were compared for equivalent cylindrical and disc machines. They are:

i) Pole pitch: Stator Width Ratio
ii) Weight of Iron
iii) Weight of Copper
iv) Total Motor Weight
v) Axial Length

The principal dimensions of the cylindrical and electrically single-sided disc machines under consideration are shown in Fig. 1.5.

i) Pole-pitch: stator width ratio

This ratio is defined as unity for the cylindrical machine, because it has been assumed to have 'square' poles. For the disc motor, however, it is given by:

$$\frac{\text{Pole pitch}}{\text{Stator width}} = \frac{\pi}{2p} \frac{(D_o/D_i + 1)}{(D_o/D_i - 1)} \qquad (1.15)$$

The tabulated results for this expression are:

p	$\frac{\text{Pole pitch}}{\text{Stator width}}$
1	5.86
2	2.93
3	1.95
4	1.47
5	1.17
6	0.98

They demonstrate that for common types of motor, i.e. $p \leq 3$, say, the pole pitch of a disc motor is considerably greater than the stator width: for a two pole machine it is almost six times greater. The implications of this is that disc motors generally have long end windings, with adverse effects on resistance and leakage inductance.

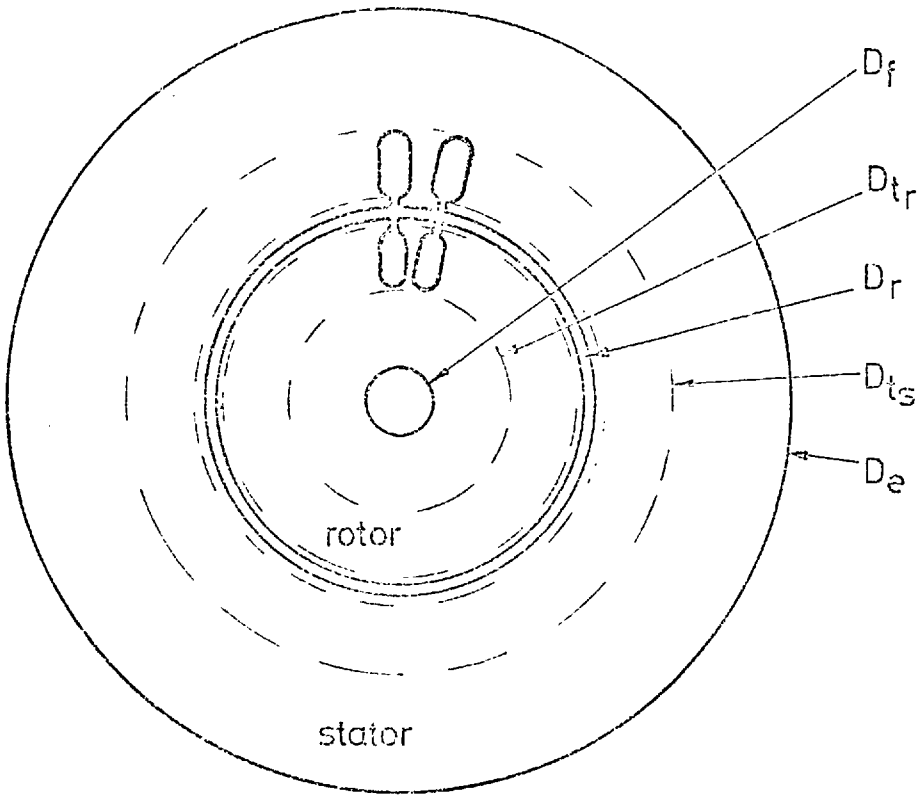

a. cylindrical machine - end view
(iron circuit only)

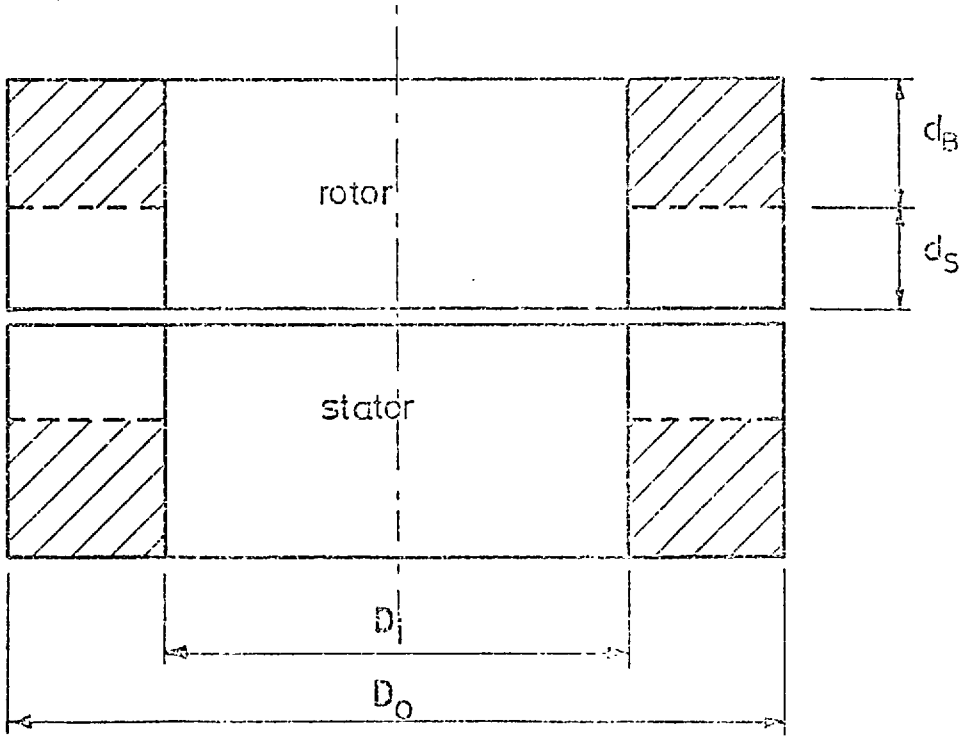

b. disc machine - section
(iron circuit only)

PRINCIPAL DIMENSIONS FOR COMPARISON OF PHYSICAL PARAMETERS OF CYLINDRICAL- AND DISC- MOTORS

FIG. 1.5

ii) Weight of iron

The weight of iron required for a cylindrical machine, $W_{i_{CM}}$, and for its equivalent single sided disc machine, $W_{i_{DM1}}$, can be written down with reference to Fig. 1.5 as:

$$W_{i_{CM}} = \frac{\pi\gamma_i D_r}{8p}\{(\beta_T D_{t_s}^2 - D_{t_r}^2) + (D_e^2 - D_{t_s}^2 + D_{t_r}^2 - D_f^2)\} \quad (1.16a)$$

$$W_{i_{DM1}} = \frac{\pi\gamma_i D_i^2}{2}\{(\frac{D_o}{D_i})^2 - 1\}\{\beta_T d_s + d_B\} \quad (1.16b)$$

where γ_i is the density of laminated iron.

iii) Weight of copper

Similarly, the copper weights, $W_{c_{CM}}$ and $W_{c_{DM1}}$, can be shown to be:

$$W_{c_{CM}} = \pi^2(1-\beta_T)\gamma_c \frac{D_r^2 d_s k_s}{p}(1 + k_p) \quad (1.17a)$$

$$W_{c_{DM1}} = \pi(1-\beta_T)\gamma_c D_i^2 d_s k_s (\frac{D_o}{D_i} + 1)\{(\frac{D_o}{D_i} - 1) + \frac{\pi k_p}{2p}(\frac{D_o}{D_i} + 1)\} \quad (1.17b)$$

where γ_c is the density of copper
k_s is the slot packing factor
k_p is the fraction of a pole over which a coil is pitched.

iv) Total weight

The total weights of the respective machines are clearly given by:

$$W_{CM} = W_{c_{CM}} + W_{i_{CM}} \quad (1.18a)$$

$$W_{DM1} = W_{c_{DM1}} + W_{i_{DM1}} \quad (1.18b)$$

The results of calculations from equations 1.16, 1.17 and 1.18, using the simplifications given above are illustrated on Fig. 1.6 for a range of pole numbers.

It is apparent that the disc motor generally requires less iron, but more copper than its cylindrical counterpart. It is particularly noticeable that the disc motor uses some 80% more copper than the cylindrical motor in a 2-pole version. This is in accordance with the

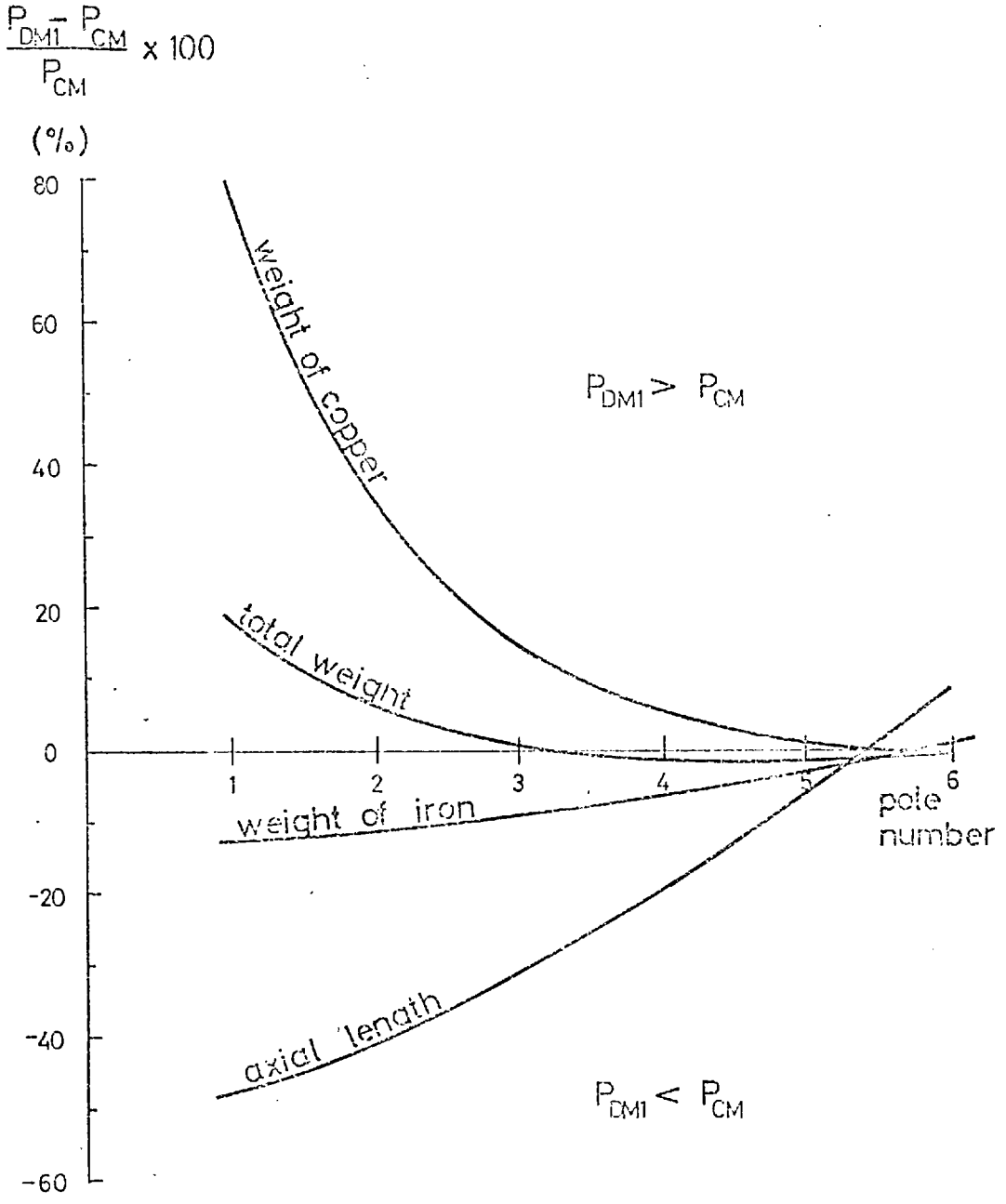

COMPARISON OF THE PHYSICAL CHARACTERISTICS OF CYLINDRICAL- AND SINGLE SIDED DISC- MACHINES

FIG. 1.6

high pole pitch: stator width ratio demonstrated above. There is little difference between the total weights of the two types of machine, however, the discrepancy being most noticeable at low pole numbers when, for example, a 2-pole disc motor is almost 20% heavier than an equivalent cylindrical motor.

iv) Axial length

The axial length of a cylindrical motor includes the overhang of the stator windings: for the disc motor, however, it comprises slot and backing iron depths only. The simplified algebraic expressions for the axial lengths are:

$$AL_{CM} = \frac{3}{4} \frac{\pi D_r}{p} \qquad (1.19a)$$

$$AL_{DM1} = 2(d_B + d_s) \qquad (1.19b)$$

and results of calculations with these expressions are plotted on Fig. 1.6. The disc motor is considerably shorter along its main rotor shaft than the cylindrical motor, this advantage being greatest in low pole number machines. A 2-pole disc motor appears to be about half the axial length of an equivalent 2-pole cylindrical motor.

The profiles of equivalent disc and cylindrical machines are shown in Fig. 1.7 for two- and six-pole versions. The short flat profile of the disc motor is distinctive, but is caused mainly by the different positions of the end windings of the machines with respect to the axis of rotation of the motor shaft.

1.4.4 Calculation and comparison of parameters of cylindrical and double-sided disc machines

One advantage of the double sided disc machine suggested in Section 1.3.5 above was that it could offer an improved power to weight ratio. The reason for this suggestion can be seen in Fig. 1.8. It contains a notional 'kit of parts' for a single sided disc motor which, as shown, can also be used to construct a double sided motor. The main feature is that an effective doubling of output power is produced without an increase in the amount of backing iron required.

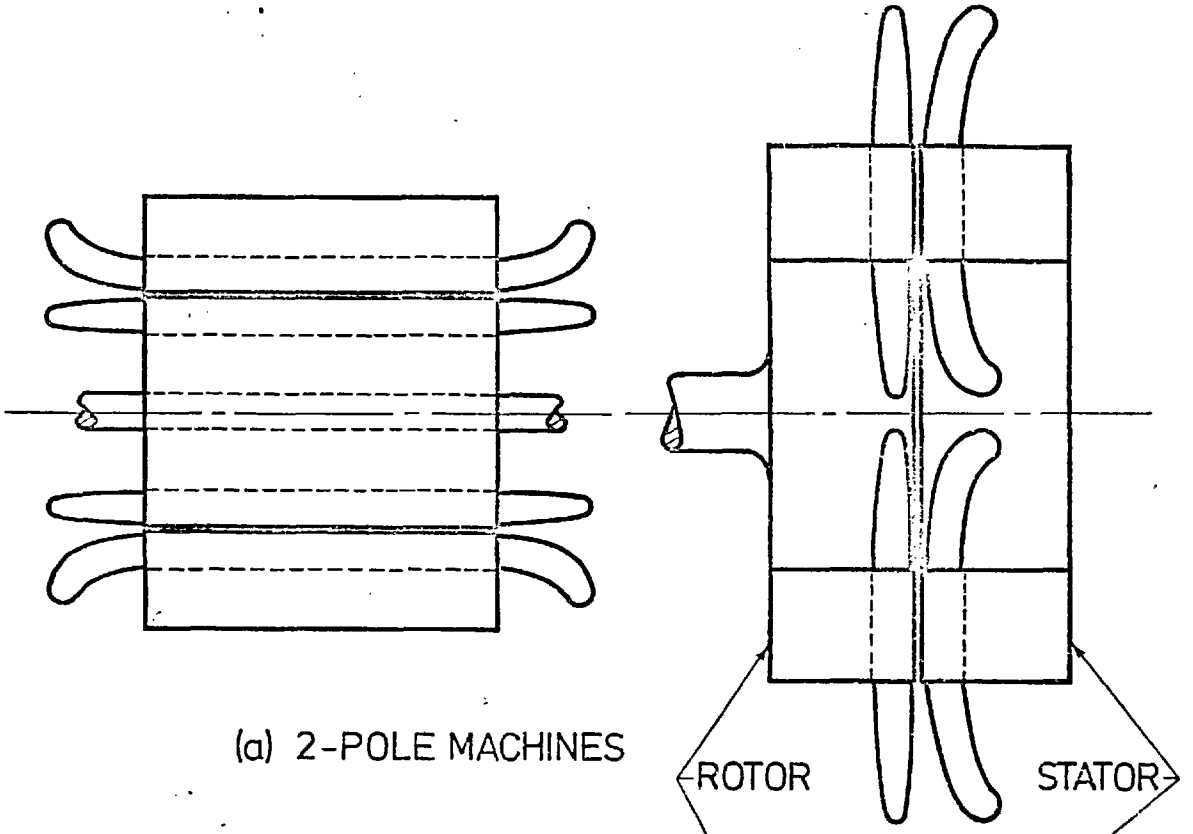

(a) 2-POLE MACHINES

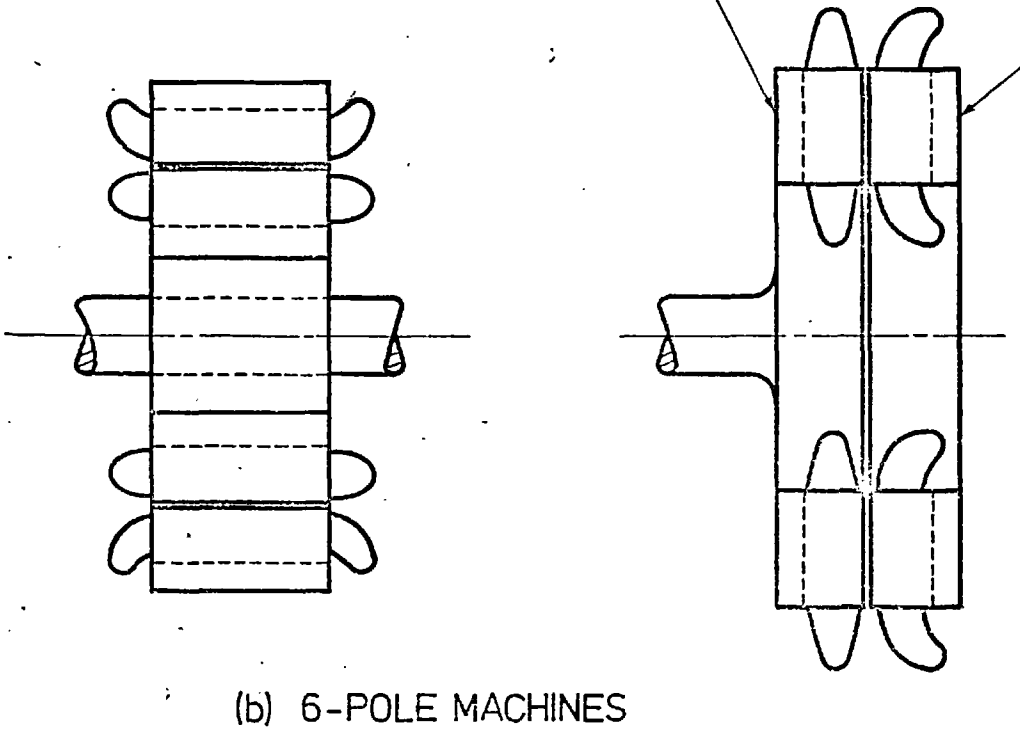

(b) 6-POLE MACHINES

FIG.1.7 COMPARISON OF PROFILES OF EQUIVALENT CYLINDRICAL AND DISC MACHINES (to scale)

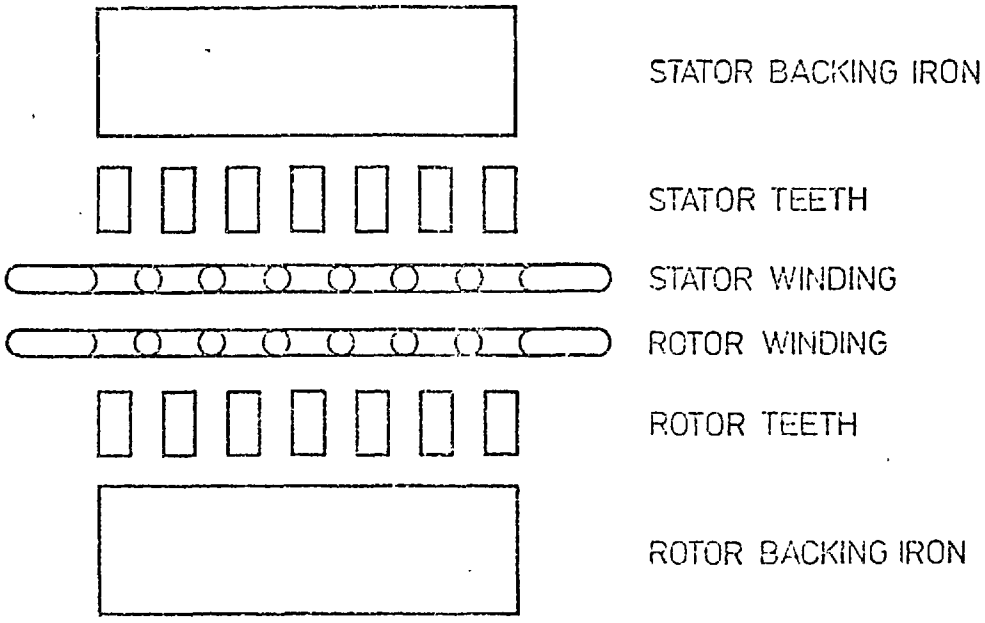

(a) SINGLE SIDED DISC MACHINE

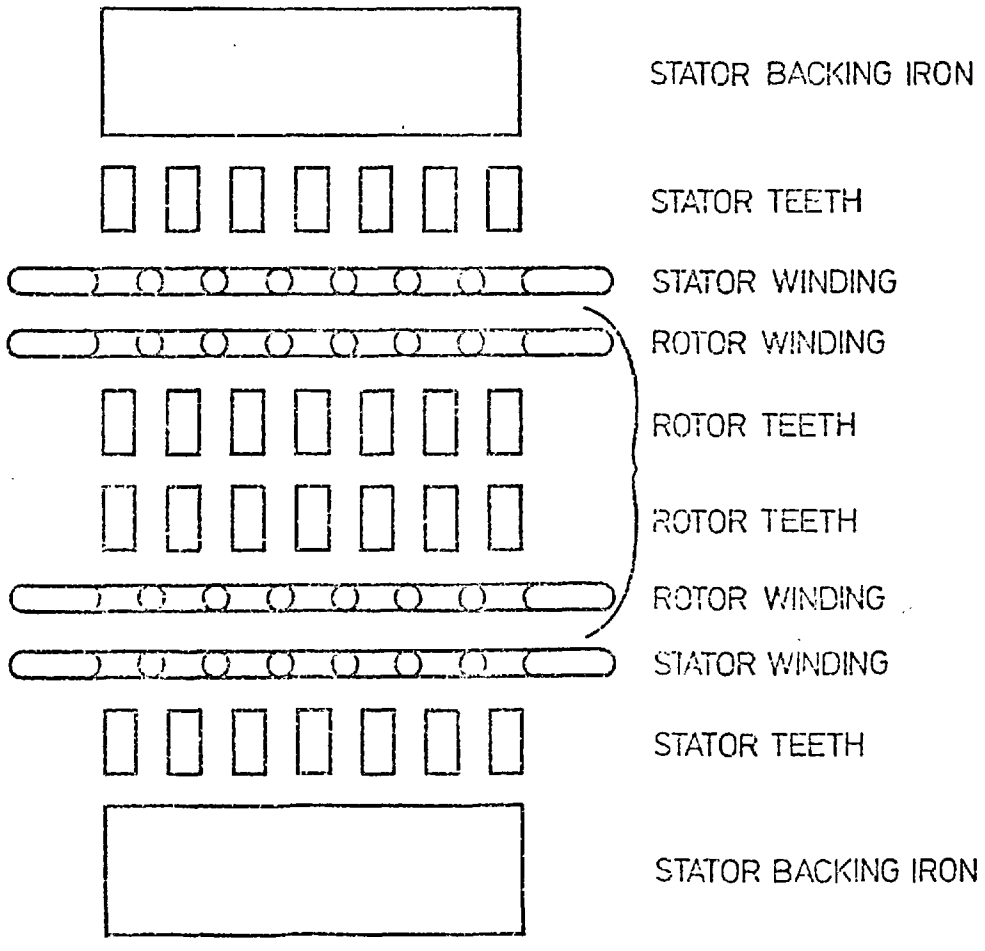

(b) DOUBLE SIDED DISC MACHINE

Fig.1.8 NOTIONAL 'KIT OF PARTS' FOR DISC MOTORS

The weight of iron and copper required for a double sided disc motor, compared with an equivalent cylindrical motor was calculated by a similar method to that used in the previous section. This was achieved by taking into account the fact that the power output of the machine, and the volume of iron and copper were both proportional to D_i^3 for a fixed ratio of D_o/D_i. The results are presented graphically in Fig. 1.9. It can be seen that the relative weights of copper are the same as in the single sided case above, but there is a notable reduction in the iron content of the double sided disc motor compared to a conventional motor. This leads to an overall reduction in the total weight of the disc motor, and it can be seen that double sided disc motors are around 10% lighter than cylindrical motors with comparable output. It should be noted, however, that there is an increase in axial length when the double sided disc motor configuration is used, and disc machines of this type with pole numbers greater or equal to three actually appear to be longer than their cylindrical counterparts.

1.4.5 Conclusions

While fully noting the reservations stated in the introduction to this section about the general method of quantitative comparison that has been used, three main conclusions can be drawn:

- in terms of total weight for a given output disc motors are quite comparable with conventional machines. In fact, there are indications that the double-sided disc motor can produce a better power-to-weight ratio than conventional machines.
- disc motors generally require more copper but less iron than cylindrical motors.
- single sided disc motors have a considerably shorter axial length than cylindrical machines, but this advantage disappears for some types of double-sided disc machine.

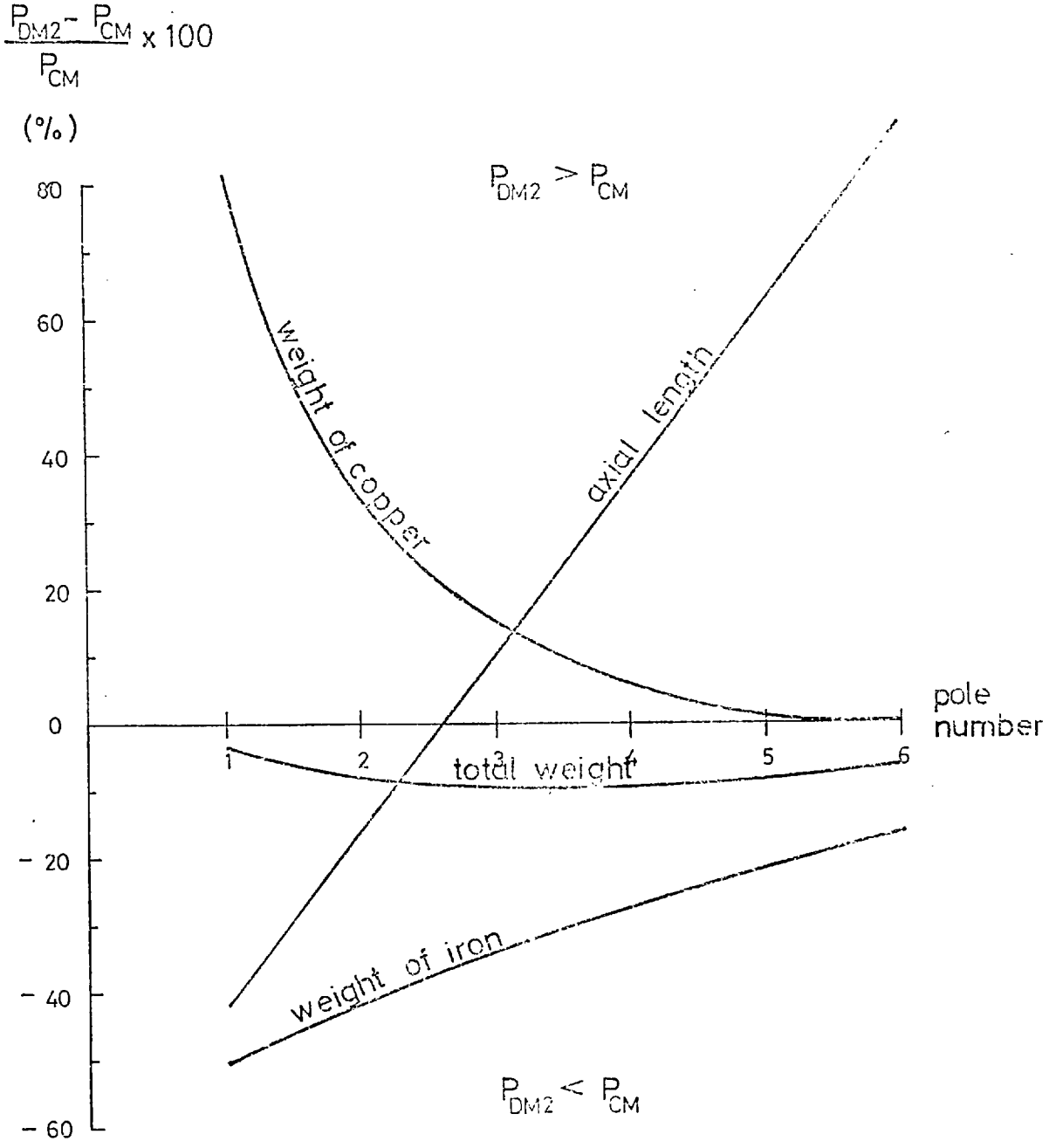

COMPARISON OF THE PHYSICAL CHARACTERISTICS
OF CYLINDRICAL - AND DOUBLE SIDED DISC - MACHINES

FIG. 1.9

1.5 Examination of design criteria for disc machines with axial flux

1.5.1 Introduction

The design of electrical machines is as much an art as a science. For precise application of the physical laws which explain the electromagnetic interactions in them is invariably impossible, and the empirical results from accumulated experience form an important part of the design procedure. These remarks apply particularly to second order electromagnetic effects such as leakage fields, and to thermal conditions. New designs for conventional types of motors are therefore usually based on existing designs and incorporate standard lamination punchings for the stator and rotor assemblies.

A similar fund of experience is not available for disc machines although some of the guiding principles for conventional machine design would be applicable. It is worthwhile, however, to examine some design criteria to ensure that design concepts which are inapplicable or irrelevant to disc machines are not carried over from the established methods of machine design.

To this end the present section examines briefly the implications of the disc geometry on the design of the electric and magnetic circuits of an electric machine. Two specific areas are considered: slot design (and by implication tooth design), and winding design.

1.5.2 Slot design

The main purpose of the slot-tooth arrangement in an induction machine is to minimise its effective 'entrefer'. But to some extent the requirements of teeth and slots are conflicting, for an increase in the slot width - to increase the surface current density - necessarily reduces the tooth width - and hence the average airgap flux density. There is limited scope for augmenting slot area in conventional machines by increasing slot depth because apart from increasing slot leakage, there is a physical constriction for flux at the rotor tooth root as the radius diminishes. This constriction does not exist with disc machines, and it is for this reason that slot dimensions are re-examined here.

Adopting a simplified approach, the airgap flux density (B_g) and rotor current density (J_R) can be expressed in terms of the slot and tooth dimensions (see Fig. 1.10(a)) as follows:

$$B_g = B_{sat} \frac{\omega_t}{y_s} \qquad (1.20)$$

and $$J_R = \frac{I_s}{y_s} \qquad (1.21)$$

where B_{sat} is the saturation flux density of iron

and I_s is the effective slot current: $I_s = k_w N I_L$

where k_w is the winding factor

N is the number of turns per slot

and I_L is the phase current

The force produced by unit area of the machine is given by:

$$B_g J_R \cos\theta = B_{sat} \frac{\omega_t}{y_s} \frac{I_s}{y_s} \cos\theta$$

$$= B_{sat} J_L \cos\theta \, k_s \, d_s \frac{\omega_t (y_s - \omega_t)}{y_s^2} \qquad (1.22)$$

where J_L is the current loading, in Amps/m^2 of the coils and k_s is the slot packing factor.

B_{sat} and J_L can be considered as constants for the present purposes. The optimum tooth width, which allows maximum force production can be obtained by differentiating equation 1.22 with respect to tooth width. Hence

$$\left.\frac{\partial(B_g J_R \cos\theta)}{\partial \omega_t}\right|_{d_s=\text{const}} = \frac{B_{sat} J_L \cos\theta \, k_s}{y_s^2} (y_s - 2\omega_t) d_s \qquad (1.23)$$

which has a maximum when:

$$\omega_t = \frac{1}{2} y_s \qquad (1.24)$$

i.e. when tooth width = slot width.

This result confirms normal practice, and the maximum force is given by:

$$B_g J_r \cos\theta = B_{sat} J_L \cos\theta \, k_s \frac{d_s}{4} \qquad (1.25)$$

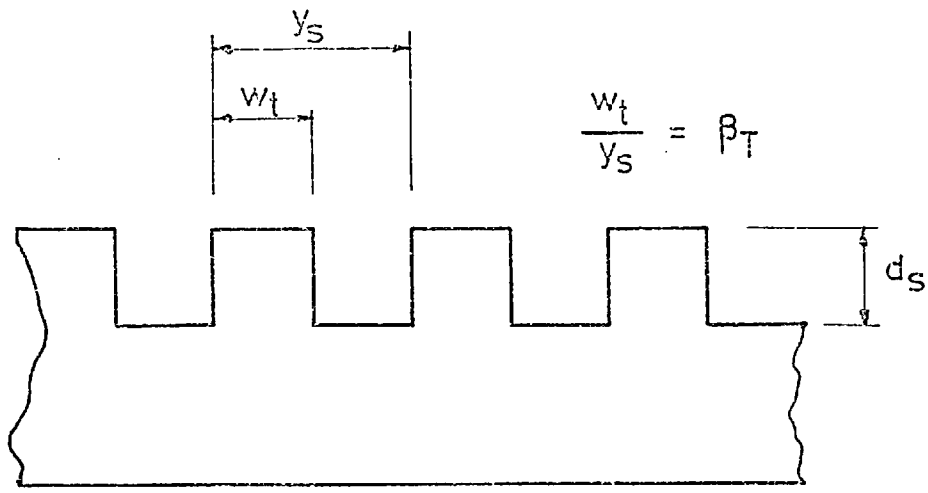

a. slot dimensions

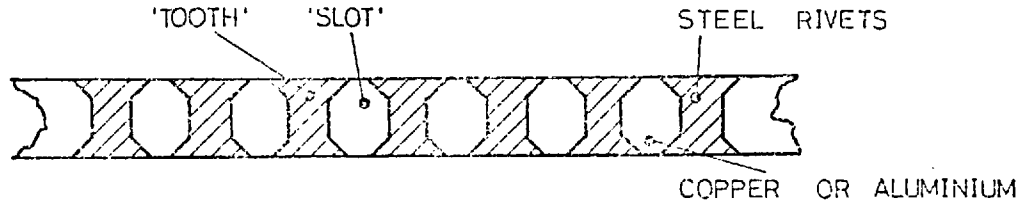

b. section through disc rotor fabricated from a conducting disc and steel rivets

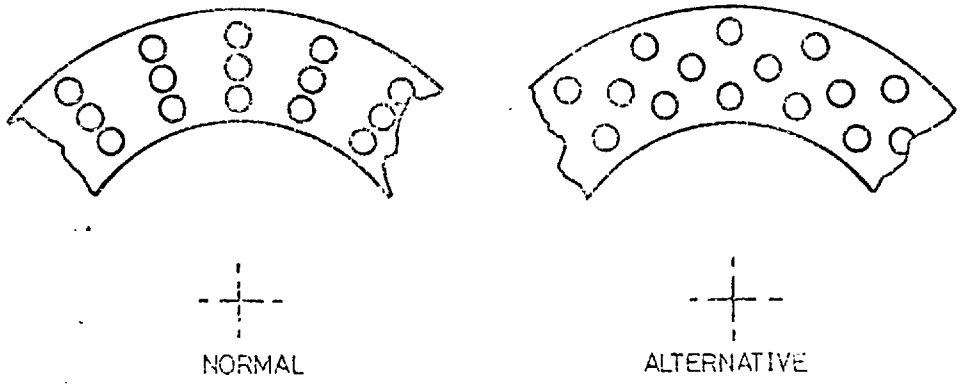

c. rivet pattern in disc rotor

FIG.1.10 ASPECTS OF SLOT DESIGN FOR DISC MOTORS

This expression indicates that the force produced by the motor can be increased by increasing slot depth, but in practice a limit on d_s is set by thermal dissipation and by slot leakage.

Directing remarks at eds machines with cage rotors (of the conducting disc/steel rivet construction - see Section 1.3.2) the following observations can be made on both these constraints:

i) Thermal dissipation:

This is normally the prime constraint which limits the maximum power output obtainable from a given size of motor. The proposed motor has a thin flat profile with a large surface area: volume ratio that assists in direct cooling. The conduction path for heat to the rotor shaft has a relatively thin cross sectional area, but will have a high thermal conductivity (copper or aluminium). An increase in 'd_s' in this rotor is identical to an increase in rotor thickness, and an increase in this dimension automatically enhances the heat conduction path to the rotor shaft. Also important is the fact that the conductors in which most heat is generated are not insulated thermally from the heat induction paths. The indications are, therefore, that this rotor may be able to dissipate more heat and run at a higher temperature than conventional rotors, thereby enabling a greater power to weight ratio to be obtained from this type of motor.

ii) Slot leakage:

It has been shown in Section 1.3.5 that slot leakage tends to be a relatively minor component of total leakage in disc machines, especially when the pole number is low; the contribution by the body of the slot is particularly low when semi-closed slots are used. From this it follows that the slots of disc machines could be made deeper than in conventional machines without seriously affecting the total leakage. This is not necessarily an advantage of disc machines; it only occurs when the end winding leakage reactance is high. However, given that a disc geometry is to be used, and the end winding leakage can be tolerated, it is reasonable to propose that deeper slots should be used, providing thermal conditions are satisfactory.

An increase in stator conductor area which is necessary to balance greater rotor conductor areas can therefore be achieved without severe

penalties (see Section 1.3.5, Improvements in the electro-magnetic properties of windings) by deepening the slots.

In addition to this effect, which would apply if a conventional conductor/slot construction were used for the cage rotor, the proposed rotor made from rivets appears to offer other advantages. (The shape of the 'slot' so formed is illustrated in Fig. 1.10(b): it is double ended but otherwise has a conventional profile). The 'normal' rivet pattern (Fig. 1.10(c)) which might be adopted by extrapolating from conventional rotor construction patterns calls for the rivets to be aligned radially. But the type of pattern, the alternative pattern in Fig. 1.10(c), in which the circumferential arrays of rivets are offset from one another will tend to reduce the slot leakage, perhaps compensating for any increase due to greater slot depths. This alternative pattern also gives a skewed effect to the rotor conductors, but will tend to increase the rotor resistance. The situation appears to be as follows:

- there is no physical limit on the rotor conductor size in a disc machine
- increased rotor conductor sizes might be used to obtain higher mechanical output per unit volume, particularly from an eds machine
- the two main problems associated with this development, namely excessive thermal dissipation and high slot leakage reactance, are not necessarily prohibitive.

A detailed study of these problems would be extremely complex. It cannot be handled by general methods of appraisal and is beyond the scope of the present text. The purpose of the preceeding remarks has been to identify a line of development for disc machines which may prove fruitful.

1.5.3 Winding design

Conventional surface windings are quite suitable for disc machines, and their insertion into the exposed slots on the flat stator surface is probably easier than into the stator bore of a conventional cylindrical machine. However, the relatively large pole pitch to stator width ratio of disc motors with low pole numbers, and the copper losses and leakage reactance associated with the long end windings, suggests that Gramme ring windings might be more suitable. Surface and Gramme ring windings are therefore compared below in terms of their resistance and leakage reactance in order to determine the circumstances under which one or the other holds the advantage.

i) Stator winding resistance

The main end winding lengths of surface wound and Gramme ring coils, L_e and L_g respectively, are given approximately by:

$$L_e = k_p \tau_p \qquad (1.26a)$$

$$L_g = W + 2d_B \qquad (1.26b)$$

where k_p, τ_p, W and d_B were defined in sections 1.4.2 (iii) above, and their ratio is:

$$\frac{L_e}{L_g} = \frac{k_p \tau_p}{W + 2d_B} \qquad (1.26c)$$

For a disc machine, inserting:

$$\tau_p = \frac{\pi}{4p} (D_o + D_i)$$

$$W = \frac{1}{2} (D_o - D_i)$$

and $$d_B = \frac{\beta_T \tau_p}{\pi} = \frac{\beta_T}{\pi} \frac{\pi}{4p} (D_o + D_i)$$

the ratio becomes:

$$\frac{L_e}{L_g} = \frac{\frac{k_p \pi}{4p} (D_o + D_i)}{\frac{1}{2} (D_o - D_i) + \frac{\beta_T}{2p} (D_o + D_i)} \qquad (1.27)$$

which, when $D_o/D_i = \sqrt{3}$, $\beta_T = 0.5$ and $k_p = 5/6$, reduces to:

$$\frac{L_e}{L_g} = \frac{5\pi}{6 + 3.24p} \qquad (1.28)$$

This can be tabulated as follows:

p	L_e/L_g
1	1.72
2	1.26
3	1.0
4	0.83
5	0.71
6	0.62

from which it can be seen that for disc machines with $p \leq 2$, a Gramme ring winding has a lower primary resistance than an equivalent surface winding.

ii) Stator end winding leakage reactance

Draper's formula[15] for the end turn leakage reactance of a double layer surface winding, assuming complete coupling between the end winding is:

$$X_{le} = \frac{\pi}{2} \mu_o f p (q z_c)^2 L_e \qquad (1.29)$$

as defined in Section 1.3.5 above.

The magnetising reactance of a set of coils is also given by:

$$X_m = \frac{6W \tau_p \mu_o f}{\pi g} 2p (q z_c)^2 \qquad (1.30)$$

Assuming that the end turns of a Gramme ring winding approximate to a current sheet, of width $W + 2d_B$. If it has a travelling current wave that is sinusoidally distributed in space and is at the boundary between air and an infinitely permeable region, its effective airgap is τ_p/π[11]. Substituting this into equation 1.30, the end winding leakage reactance of a Gramme ring winding is given by:

$$X_{lg} = 12\mu_o f p (qz_c)^2 (2d_B + W) \qquad (1.31)$$

Hence X_{le}/X_{lg} can be shown to be:

$$\frac{X_{le}}{X_{lg}} = \frac{\pi k_p \tau_p}{12(2d_B + W)} \qquad (1.32)$$

Making the same assumptions as for equation 1.27 above, the ratio can be tabulated as follows:

p	X_{le}/X_{lg}
1	0.45
2	0.33
3	0.26
4	0.22
5	0.18
6	0.16

These results indicate that the leakage reactance of a Gramme ring winding on a disc motor is always more than double that of an equivalent surface winding. Even for a two pole motor which gives the Gramme ring winding its greatest advantage X_{le} is less than half X_{lg}.

Gramme ring windings appear to offer savings in the amount of copper required for a motor with corresponding savings in copper losses, but their associated leakage reactances are very high by normal standards. It should also be noted that the leakage flux produced by Gramme ring end windings circulates in the stator backing iron, which accordingly has to be increased in thickness to accommodate it.

From the above brief consideration of the problems of slot and winding design applied to disc motors, it appears that deeper slots may sometimes be advantageous, and that gramme ring windings should be considered for 2- and 4-pole machines if a high leakage inductance can be tolerated.

1.6 Disc machines with transverse flux

1.6.1 Introduction

Linear motors which utilise flux return paths that are transverse to the direction of motion were conceived quite recently[4]. The lay-

outs of typical transverse flux linear machines are compared with that of an axial flux machine in Fig. 1.11. It can be seen that while conventional winding configurations may be used, the flux is confined to transverse paths outside the airgap region. This arrangement reduces the depth of backing iron required for long pole pitch machines, and was in fact first proposed for high speed traction motors in which the pole pitch is large compared with the motor width.

Two reasons might suggest that the transverse flux topology is worthy of consideration for disc machines. These are: the basic similarity between some aspects of linear and disc machine geometries; and the fact that the pole pitch of low pole number disc machines tends to be large compared to its width. But the transverse flux disc machine also appears to have one important advantage over the axial flux version which does not feature in equivalent linear machines. It is that the stator core of a transverse flux disc machine can be made up from standard blocks of laminations. This is in contrast to the axial flux disc machine, the stator core of which is usually manufactured by an expensive process which involves machining the slots into a circular strip wound core. The transverse flux disc motor may therefore be a cheaper form of motor to manufacture than its axial flux counterpart.

A quantitative investigation of disc motors with transverse flux paths is undertaken in the following section with a view to establishing viable forms of transverse flux disc motors. They are compared with their axial flux counterparts in terms of their physical characteristics.

1.6.2 A quantitative assessment of disc machines with transverse flux

It is difficult to determine the best form of stator for a transverse flux disc motor (TFDM) without making some calculations to ensure that its magnetic and electric circuits can be arranged in a physically acceptable way. This section describes simple topological analyses which were undertaken for two types of motor - a 'C' core and an 'L' core version - in order to arrive at viable forms. They are compared quantitatively with equivalent axial flux disc machines.

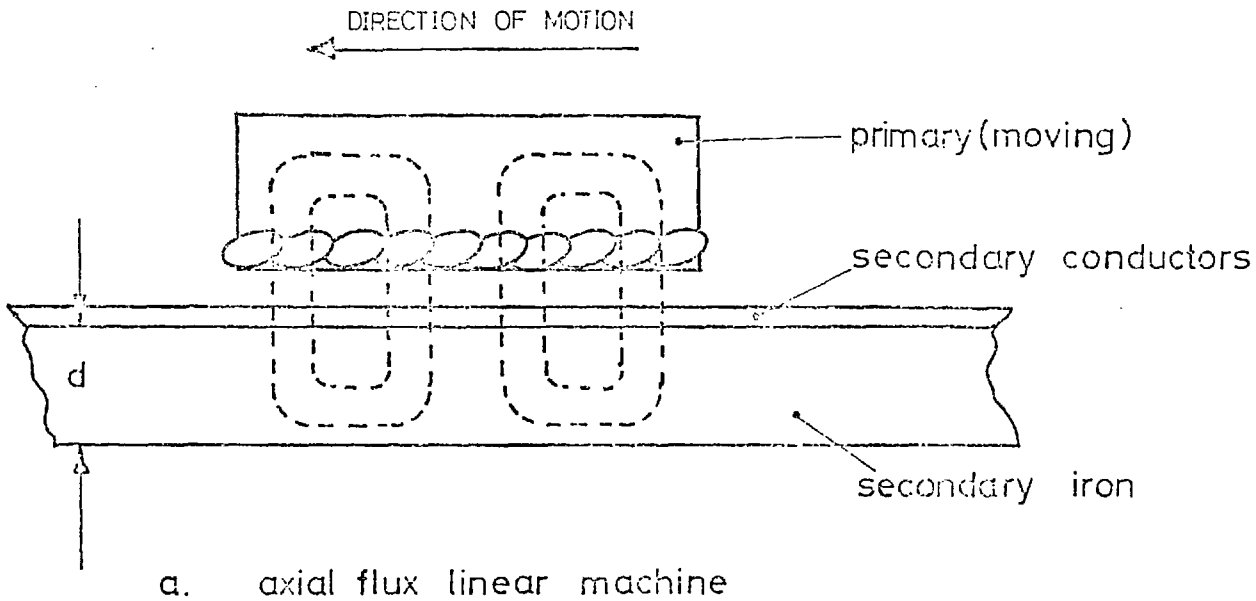

a. axial flux linear machine

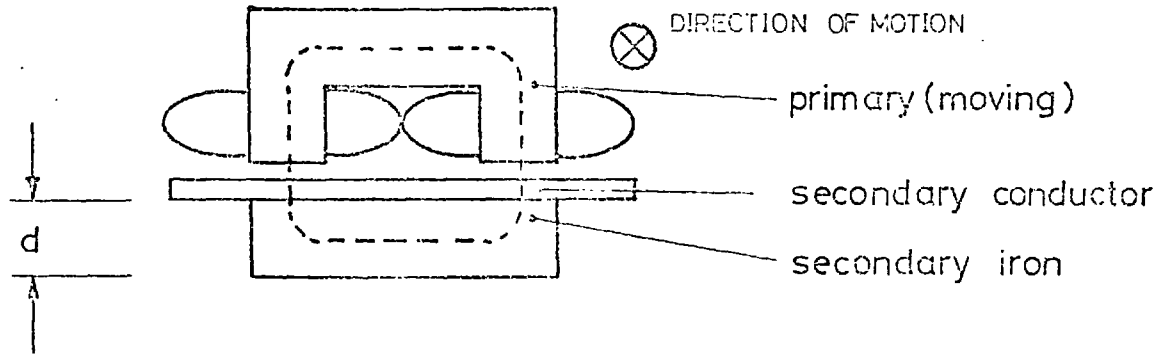

b. 'C' core transverse flux linear machine

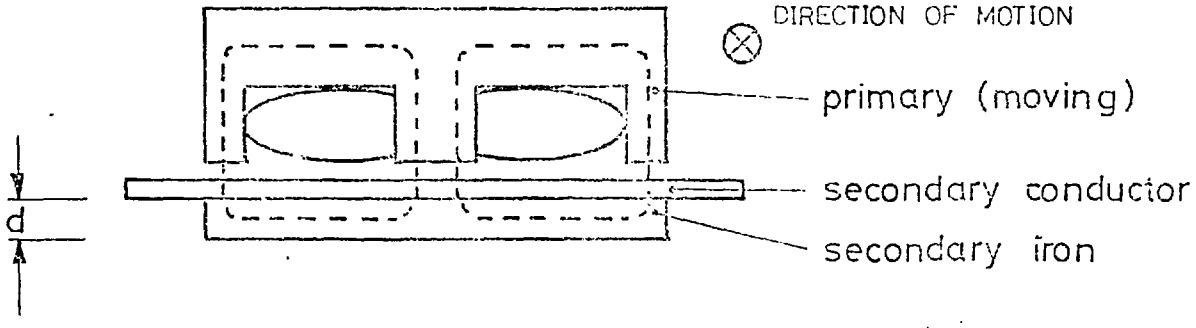

c. 'E' core transverse flux linear machine

FIG.1.11 COMPARISON OF FLUX PATHS IN AXIAL AND TRANSVERSE FLUX LINEAR MACHINES

i) The 'C' core transverse flux disc motor

By analogy with linear transverse flux machines, the stator of a TFDM would consist essentially of radially disposed 'C' or 'E' cores. These cores can in general be strip wound or made up from laminations. A more detailed study of the magnetic and electric circuit requirements, however, shows that this simple design does not necessarily lead to a sensible transverse flux disc motor, unless of course the mean diameter of the motor is large compared with its width, but this is not generally the case. Problems arise from two basic requirements which are not easily compatible: the cross sectional area of the inner and outer limbs of the 'C' cores must be equal in order that their magnetic loading is uniform; and the space between the limbs must be wide enough to accommodate the end turns of the stator windings. For these reasons it was found that perhaps the obvious arrangement, in which the inner limbs of the 'C' cores were close packed and the outer limbs carried the stator windings is not a viable motor. Typically, for a 2-pole motor, the tooth width to tooth pitch ratio of the outer limbs, which comprise the active motor surface, would be less than one quarter. This is not a satisfactory condition for most induction motors. This motor would incidentally require half the amount of core iron but more than four times the amount of copper of its axial flux counterpart.

In contrast to this, the motor illustrated in Fig. 1.12(a) & (b) appears to be a suitable arrangement for a disc motor with transverse flux paths. The windings are placed around the inner limbs which can be set to give the desired tooth width to tooth pitch ratio (usually around 0.5), and the outer limbs provide the flux return paths. It is likely that under some conditions the stator windings could be placed around both outer and inner limbs, as this would reduce their leakage reactance for the reason given in Section 1.3.5 above. Clearly, there are also advantages to be gained in extending the rotor conductors over the outer limbs, as the force produced at this radius will contribute considerable torque. With this in mind an improved primary magnetic circuit might take the form illustrated in Fig.1.12(c). The outer flux return path is provided by a strip wound circular core to reduce tooth ripple effects at the outer diameter of the motor. This latter form of motor was compared quantitatively with an equivalent axial flux disc machine: the symbols used for the dimensions of the two machines are indicated in Fig. 1.13.

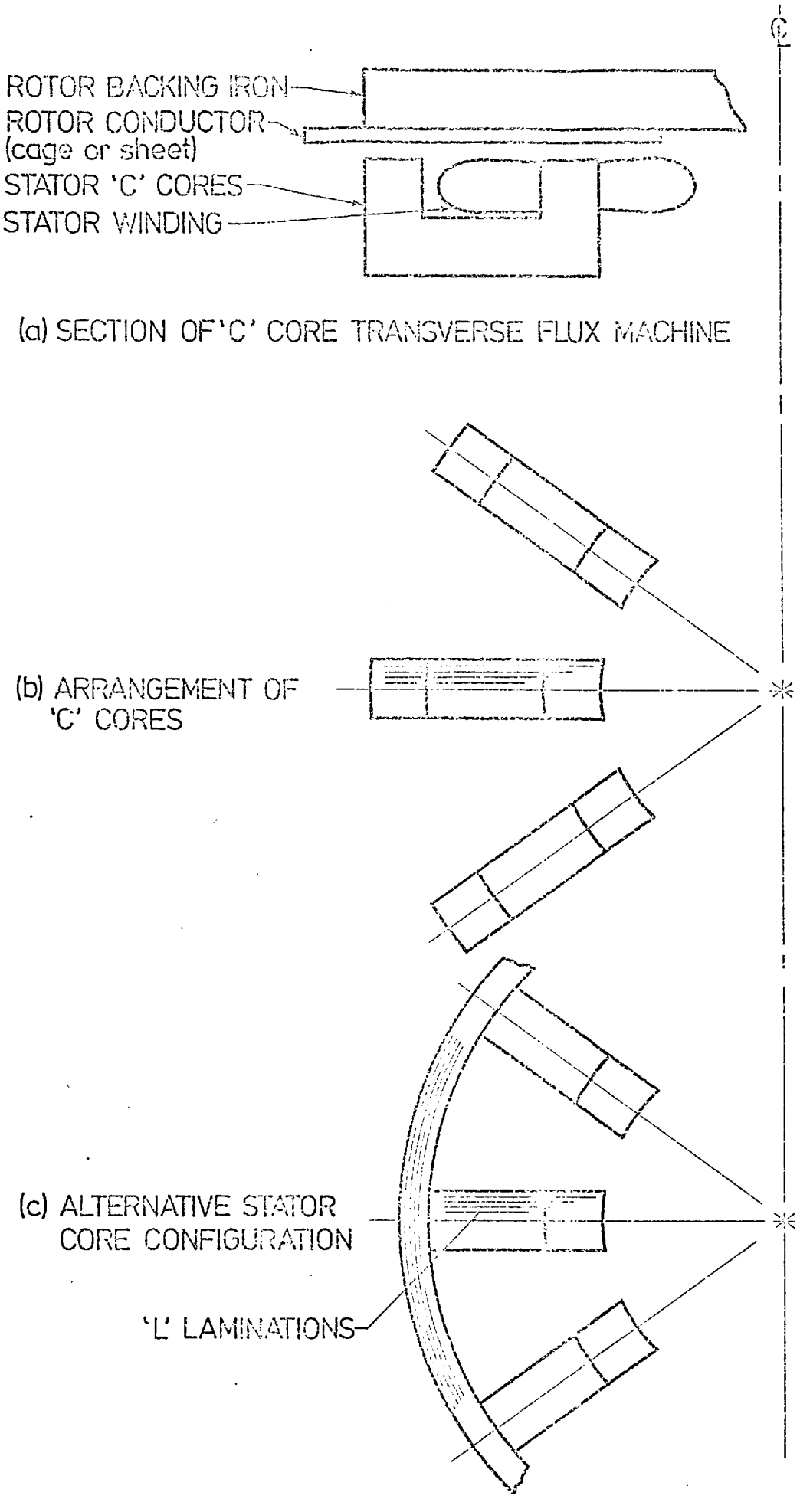

FIG.1.12 TYPICAL CONFIGURATIONS OF 'C' CORE TRANSVERSE FLUX DISC MACHINES

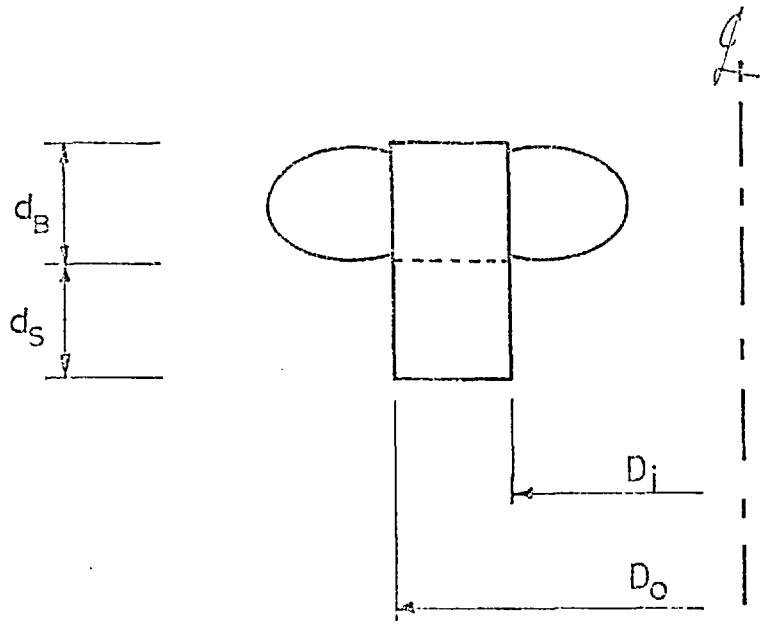

a. axial flux disc motor

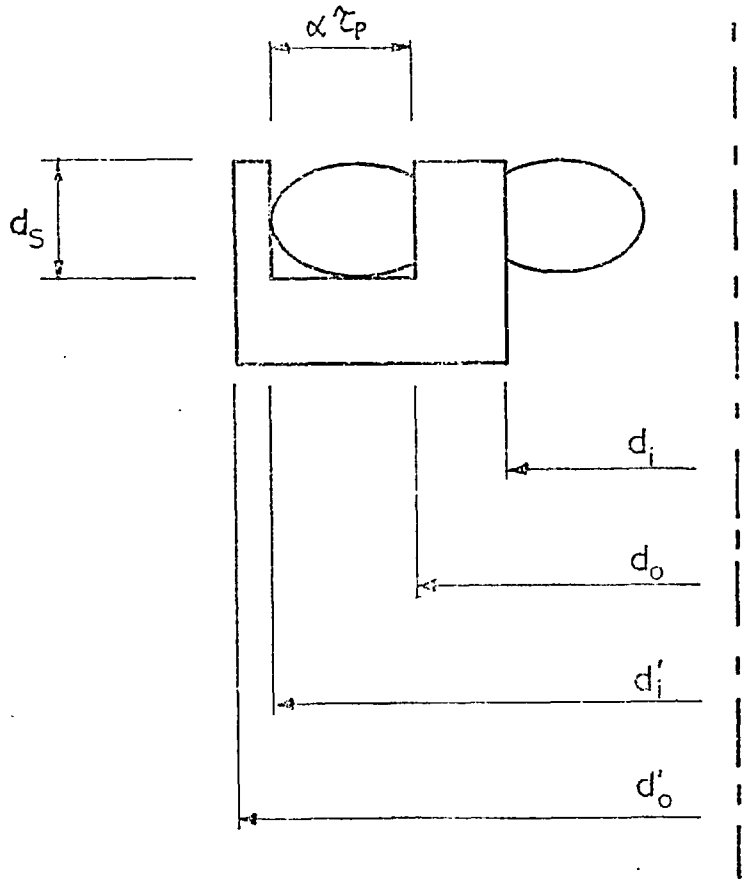

b. 'C' core transverse flux disc motor

FIG. 1.13 DIMENSIONS FOR EQUIVALENT AXIAL FLUX- AND 'C' CORE TRANSVERSE FLUX- DISC MACHINES

The comparison was based on the following assumptions:

i) The total magnetic airgap is the same for both machines, and the same winding is used on both machines (on the inner limbs of the transverse flux motor). Although the TFDM has two airgaps per pole, compared with the single airgap per pole of the AFDM, it is assumed for the present purposes that the extra airgap length in the TFDM is offset by the short flux path in the core iron. This implies that the core iron operates at a relatively high magnetic loading.

The total rotor surface current density is therefore the same for both machineswhen operating at the same stator current loading. It is given by

$$J_{RA} = B_g \frac{\pi f}{2p\rho_r} (D_o + D_i) \qquad (1.33(a))$$

for the axial flux motor

$$J_{RT_i} = B_g \frac{\pi f}{2px\rho_r} (d_o + d_i) \qquad (1.33(b))$$

for the inner limbs of the transverse flux motor

$$J_{RT_o} = B_g \frac{\pi f}{2px\rho_r} (d'_o + d'_i) \qquad (1.33(c))$$

for the outer limbs of the transverse flux motor
where ρ_r is the surface resistivity of the axial flux motor rotor, and the surface resistivity of the transverse flux rotor - in the area of inner and outer limbs - is $x\rho_r$ where x is an unknown factor.

$$\text{As } J_{RA} = J_{RT_i} + J_{RT_o} \qquad (1.34)$$

it can be shown from equations 1.33 that:

$$x(D_o + D_i) = d_o + d_i + d'_o + d'_i \qquad (1.35)$$

ii) The inter-limb distance on the transverse flux motor which accommodates the end windings is equal to $\alpha\tau_p$ where α is an empirical constant - equal approximately to 0.25 - and τ_p is the pole pitch at the inner diameter of the motor cores.

Hence $d_i' = d_o + 2\alpha\,\tau_p$ (1.36(a))

and $d_i' = d_o + \frac{\alpha\pi}{p}\,d_i$ (1.36(b))

iii) The return path for the flux at the outer limbs of the transverse flux motor has the same area as the flux path at the inner limbs.

Hence, $\beta_T(d_o^2 - d_i^2) = (d_o'^2 - d_i'^2)$ (1.37)

iv) The value of $D_o/D_i = \sqrt{3}$, as derived in Section 1.4.2 above, and β_T is set at 0.5 for both motors.

The torque produced by the axial and transverse flux motors can be equated in the form:

$$B_g J_{RA} \frac{\pi}{4}(D_o^2 - D_i^2)\frac{D_i}{2} = B_g J_{RT_i}\frac{\pi}{4}(d_o^2 - d_i^2)\frac{d_i}{2} + B_g J_{RT_o}\frac{\pi}{4}(d_o'^2 - d_i'^2)\frac{d_i'}{2} \quad (1.38)$$

from equation 1.6 above, into which

$$J_{RT_i} = \frac{d_o + d_i}{x(D_o + D_i)}\,J_{RA} \quad (1.39(a))$$

and $$J_{RT_o} = \frac{d_o' + d_i'}{x(D_o + D_i)}\,J_{RA} \quad (1.39(b))$$

derived from equations 1.33 above can be substituted, and the equation simplified to:

$$x(D_i)(D_o + D_i)(D_o^2 - D_i^2) = d_i(d_o + d_i)(d_o^2 - d_i^2) + d_i'(d_o' + d_i')(d_o'^2 - d_i'^2) \quad (1.40)$$

Using equations 1.36 and 1.37 to obtain expressions for d_o' and d_i'; equation 1.35 to give x (all in terms of D_o, D_i, d_o and d_i); and choosing an arbitrary value for D_i (and hence D_o), d_o can be calculated from equation 1.40 for particular values of d_i.

These calculations were performed for a 2-pole machine, for which the transverse flux motor is likely to be most advantageous. Two values of inner diameter were chosen for the transverse flux motor, 4 inches and 6 inches, and the results were as follows:

For D_i = 4.0 inches, D_o = 6.93 inches;

d_i (in)	d_o (in)	d'_i (in)	d'_o (in)	x
4.0	6.63	9.77	10.46	2.82
6.0	7.54	12.25	12.67	3.52

These motors are illustrated to scale in Fig. 1.14. It can be seen that the overall diameter of the motors including end windings are not dissimilar, but that the rotors for transverse flux motors would be considerably larger than for the axial flux motor. The rotor surface resistivity for the transverse flux motor is approximately three times that of the axial flux motor.

The ratios of the iron and copper requirements for the stator of these motors and the ratio of their axial lengths are as follows (parameter for transverse flux motor divided by parameter for axial flux motor):

d_i	Iron	Copper	Axial Length
4	1.10	0.98	.98
6	0.87	1.76	.74

It can be seen that when the internal core diameters of both types of machine are the same, the amounts of iron and copper required for the stator construction are very similar. Increasing the diameter of the transverse flux motor reduces the iron weight, increases the amount of copper and decreases the axial length.

It is interesting to note that approximately 30% of the transverse flux motor torque is provided by the inner limbs, and 70% by the outer. The tractive force produced by both sets of limbs is therefore approximately equal.

The conclusions arising from these results, which are necessarily very approximate, are that there is no reason for the motor to be rejected on the grounds of excessive iron or copper requirements, and that the rotor diameter for a transverse flux motor is considerably

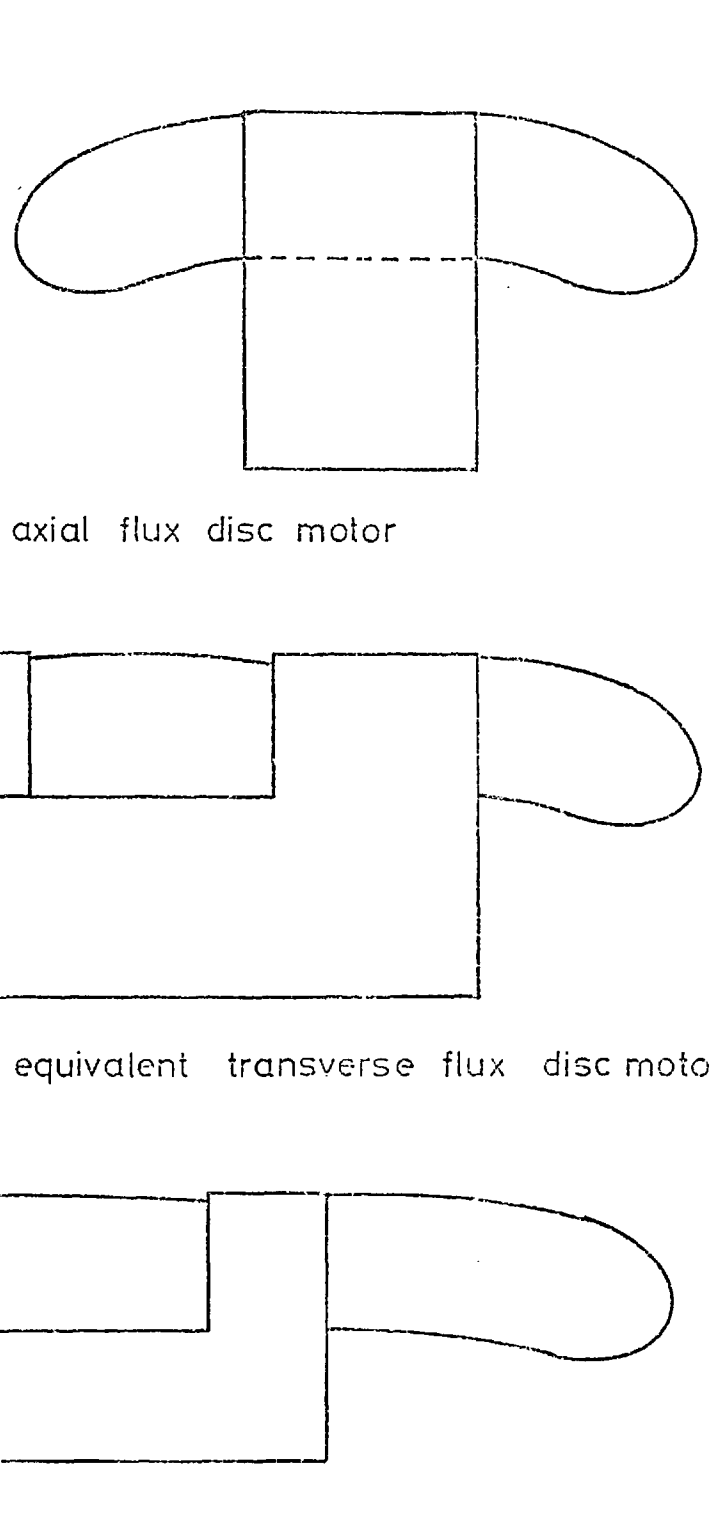

a. axial flux disc motor

b. equivalent transverse flux disc motor, d_i = 4.0 in.

c. equivalent transverse flux disc motor, d_i = 6.0 in.

FIG. 1.14 COMPARISON OF PROFILES OF EQUIVALENT AXIAL - AND TRANSVERSE - FLUX DISC MOTORS. (to scale)

greater than for an equivalent axial flux disc motor. This general form of transverse flux disc, therefore, appears to have considerable potential and may be regarded as a real alternative design when disc motors are under consideration for a specified application. In particular, the form of this motor which utilises windings on both inner and outer limbs gives considerable flexibility in overall motor design.

ii) The 'L' core transverse flux disc motor

The 'C' core motor in its various forms described above is essentially a linear motor that has had its ends joined together to form a rotary disc motor. A second distinct form of transverse flux disc motor also exists which has no linear counterpart. It exploits the circular geometry of the disc motor to eliminate one of the limbs of the 'C' core and is therefore designated the 'L' core motor. It is illustrated in Fig. 1.15. The flux paths are transverse with respect to the direction in which the force is produced, but diametral in relation to the geometry of the motor. The cross sectional area of the iron across a diameter of the machine must therefore be capable of carrying the pole flux of the machine. In the form shown in Fig. 1.15(a), only strip wound cores provide a path for the flux across the middle of the machine which does not require it to pass normally through laminations: stacks of graded 'L' shaped laminations arranged in the manner shown in Fig. 1.15(a) would not provide good flux paths for the diametral flux. An alternative arrangement is illustrated in Fig. 1.15(b). It consists of a pile of disc laminations for the central position with the 'teeth' arranged around the edge.

An important feature of this type of motor is that it has one airgap per pole: other transverse flux machines have two. Compared to an axial flux stator, therefore, the airgap reluctance is the same, and the reluctance of the stator iron path is shorter by a factor of $\pi/2$. (Flux crosses a diameter instead of passing around a semi-circumference).

The active motor surface of this form of motor is very similar to that of an equivalent axial flux motor. The implication of this is that the same diameter rotor can be used for both types of machine.

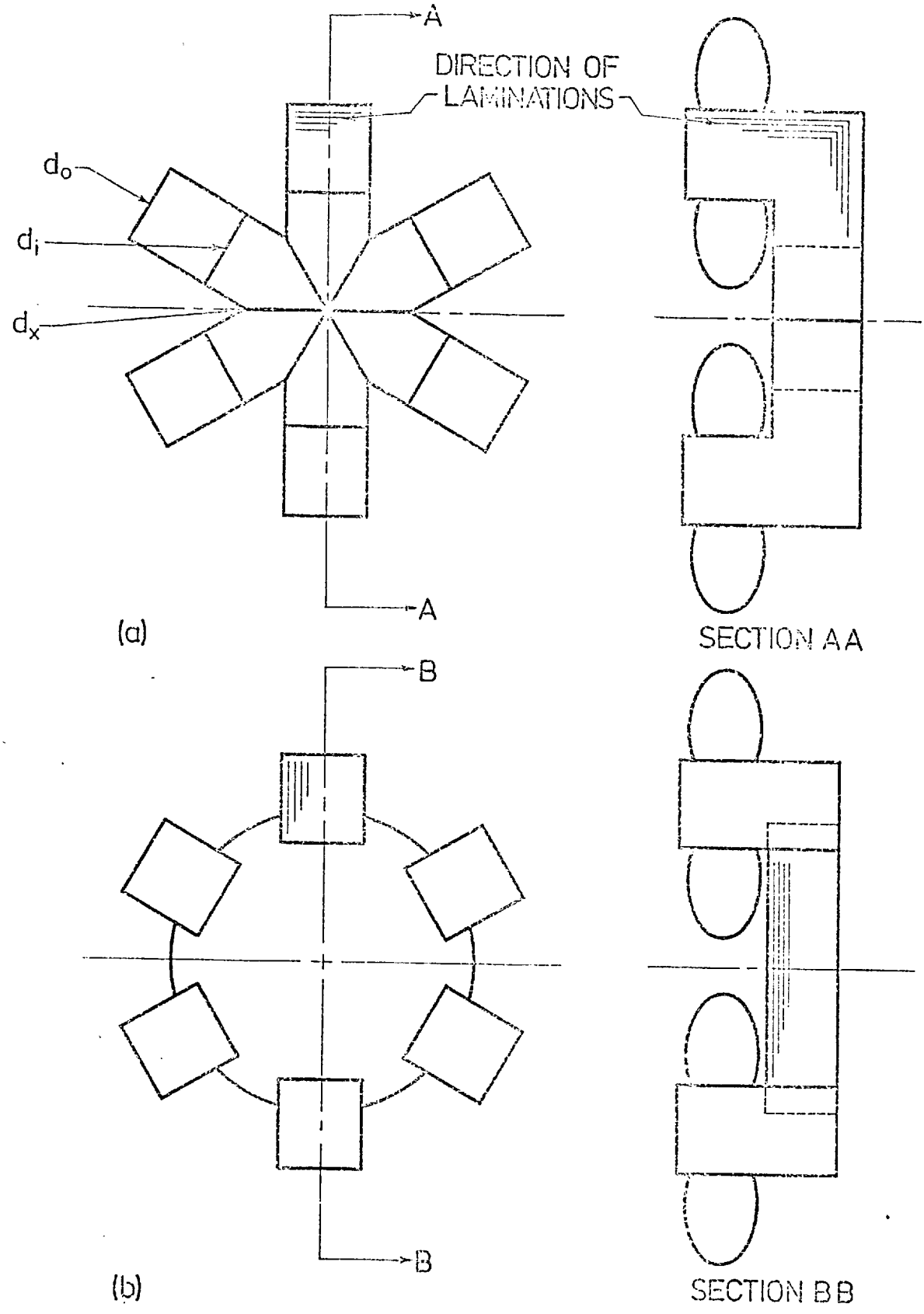

FIG.1.15 'L' CORE TRANSVERSE FLUX DISC MOTORS

This contrasts with the 'C' core transverse flux motor which required a considerably larger diameter rotor than its axial flux counterpart.

Comparing transverse flux motors of this type with equivalent axial flux machines, it can be seen that identical rotors can be used for both, and that theoretically identical stator windings are also suitable. The amount of iron required for the stator core must be calculated however. The weight of iron in the core of an axial flux stator is given by:

$$W_{i_A} = \frac{\pi \gamma_i D_i^2}{4} \left\{ \left(\frac{D_o}{D_i}\right)^2 - 1 \right\} \{ \beta_T d_s + d_B \} \qquad (1.41)$$

from equation 1.16(b) above. In terms of the symbols shown on Fig. 1.15(a), the weight of iron in the 'L' core transverse flux motor can be written down as:

$$W_{i_T} = \frac{\pi}{4} (d_o - d_i) \{ d_s \beta_T (d_o + d_i) + d_x (d_o - d_x) + \frac{d_x}{2} \} \qquad (1.42)$$

where $d_x = \frac{\beta_T}{2} (d_o + d_i)$ (1.43)

Calculations using these expressions indicated that the volume of iron for equivalent 2-pole axial flux and 'L' core transverse flux disc machines are the same, to within 1%.

It appears, therefore, that this type of motor suffers no greater penalties compared with axial flux disc motors, but has the advantage of simpler construction.

Two alternative designs of the 'L' core motor which seem to be particularly suitable for low cost manufacture are illustrated in Fig. 1.16. Fig. 1.16(a) contains a variation of the motor shown in Fig. 1.15(b) in which the teeth surrounding the central stack of discs are 'L' shaped. This enables the stator core assembly to be held together by a simple cup and plate arrangement as shown. A suitable rotor for this type of motor, however, is still a relatively difficult and expensive item to manufacture. Typically, it would consist of

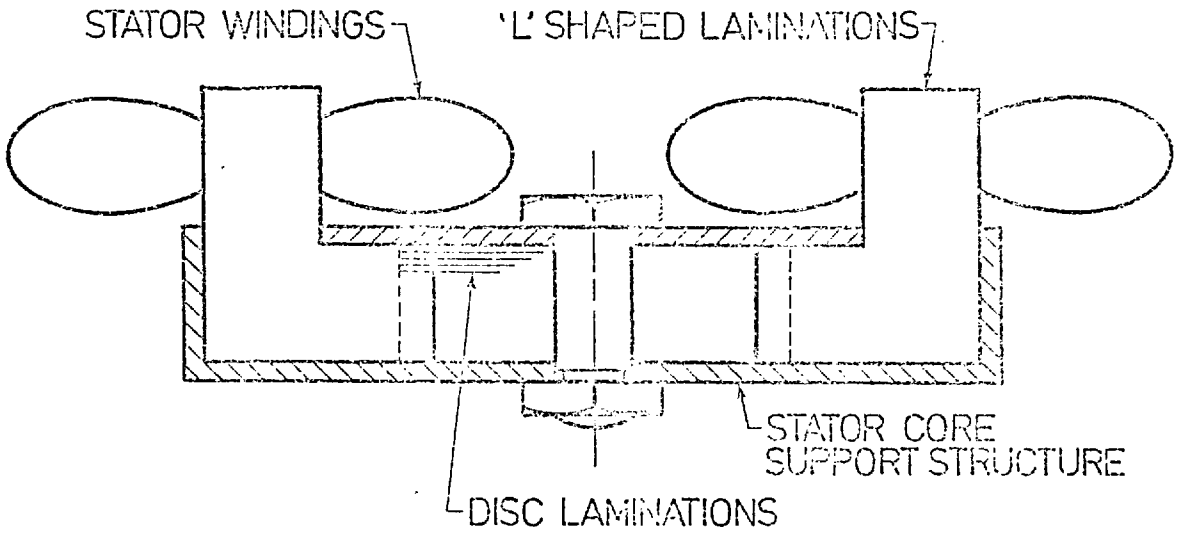

(a) SIMPLE METHOD OF CONSTRUCTION (Diametral Section)

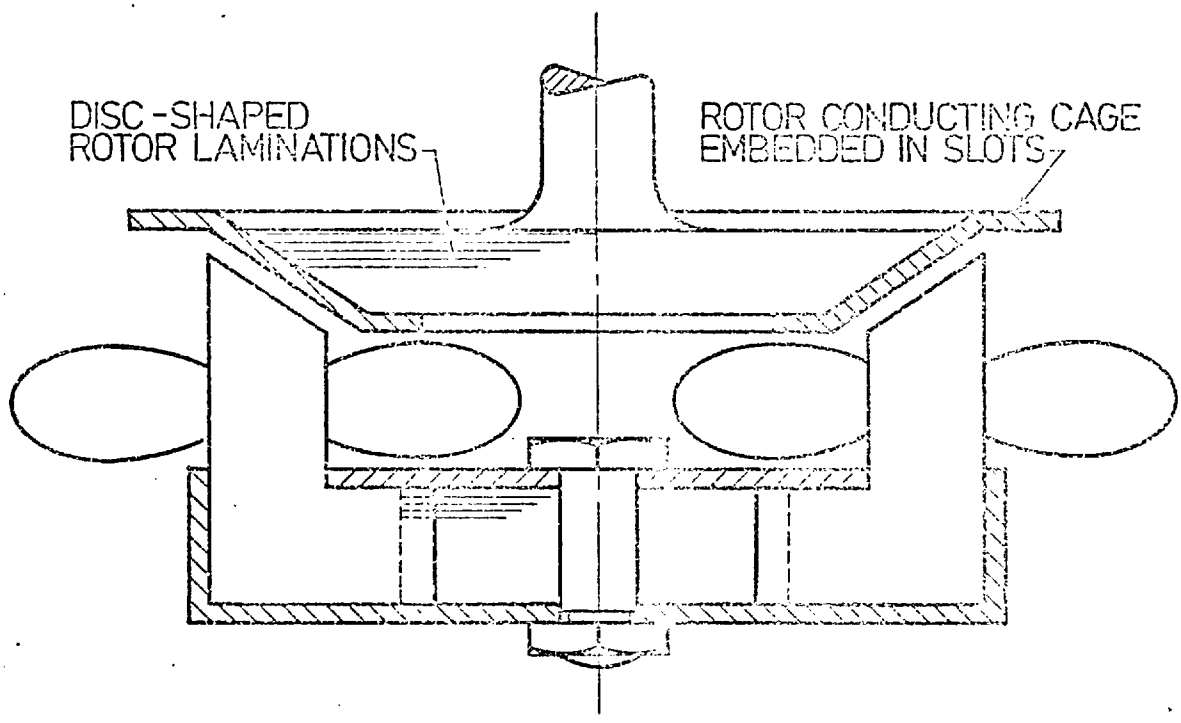

(b) DISC LAMINATED ROTOR, AND REDUCED THRUST FORCE ON ROTOR SHAFT (Diametral Section)

FIG.1.16 IMPROVED DESIGNS FOR PRACTICAL 'L' CORE TRANSVERSE FLUX DISC MOTORS

a solid iron disc which was slotted to accommodate the conducting cage, or grid. Fig. 1.16(b) illustrates a motor design which seems to eliminate the need for slotting the rotor core. The motor can be seen now to have a conical shape, but this allows graded sizes of disc laminations to be used for the rotor core construction. The rotor thickness needs to be around one-third of the width of the stator in order that the pole flux can pass through a diametral section of the rotor without saturation. If the rotor disc punchings contain slots, they can accept a conducting rotor cage which has been punched from a flat sheet of material. Thus all components of this form of motor, except the stator winding, can be produced by punching or pressing processes.

1.6.3 Alternative configurations for transverse flux disc machines

The preceding section has identified the two most promising forms of stator for transverse flux disc machines. They were referred to as 'C' core and 'L' core machines because of the basic shape of lamination that was required to make up their stator cores. Just like the axial flux disc motor configurations described in Section 1.3 above, the 'C' and 'L' core stators can be arranged in different electrically and magnetically single and double sided motor configurations. To some extent the relative advantages of the alternative arrangements are similar for transverse flux machines as for axial flux machines (Section 1.3), especially as far as the 'L' core motor is concerned; but some notable differences do arise and they are as follows:

i) The ess and mss machine

The open magnetic circuit of this type of motor gives it a large magnetic airgap, and as discussed in Section 1.3.3 above, for the axial flux disc motor the large magnetising current drawn by the motor gives it a poor overall performance. In the case of the 'C' core motor, however, the airgap is related to the inter-limb distance, rather than to the pole-pitch, and for this reason its performance might be better than that of an 'L' core TFDM or an AFDM. Nevertheless, it is unlikely to be a useful machine for normal applications.

ii) The ess and mds machine

The behaviour of an ess, mds machine depends largely upon the rotor: it can have 'sheet' or 'cage' conductors and stationary or rotating backing iron. The similarity of the 'L' core TFDM to an AFDM enables it to use conveniently a rotor with axial flux paths; but the most efficient rotor for a 'C' core motor would appear to take the shape illustrated in Fig. 1.17.

Solid (unlaminated) rotor backing iron sections also seem to offer a simple way of accommodating the predominantly transverse flux path. Investigations by Chalmers and Mulki[17] with cylindrical machines indicate that solid iron can be used with some success, especially in f.h.p. machines.

Although the 'L' core TFDM, like the axial flux motor, has one airgap per pole, the 'C' core TFDM has two airgaps per pole and might therefore be less tolerant of sheet rotors in which the rotor conductor creates an inherently large magnetic airgap.

iii) The eds, mds TFDM

Both the 'C' and the 'L' core TFDM's are likely to operate most successfully in the eds and mds configuration with the conducting sheet/steel rivet type of rotor described in Section 1.3.2 above. The behaviour of the double sided 'L' core TFDM is likely to be very similar to the double sided axial flux disc motor, but the 'C' core motor can take on a modified form. Its straightforward shape is illustrated in Fig. 1.18(a), in which the flux is assumed to be driven normally across the airgap. An alternative form, however, is illustrated in Fig. 1.18(b): the magnetic paths of the two stators can be seen to be physically coupled, unlike any other form of double sided motor discussed so far, and the number of airgaps per pole has been reduced to one.

There appear to be two sensible types of double-sided transverse flux disc motor: one uses two 'L' core stators; and the other, the modified 'C' core stators illustrated in Fig. 1.18(b). They can both be constructed from laminated components and use a simple rotor construction. While being more complex in structure, and hence more

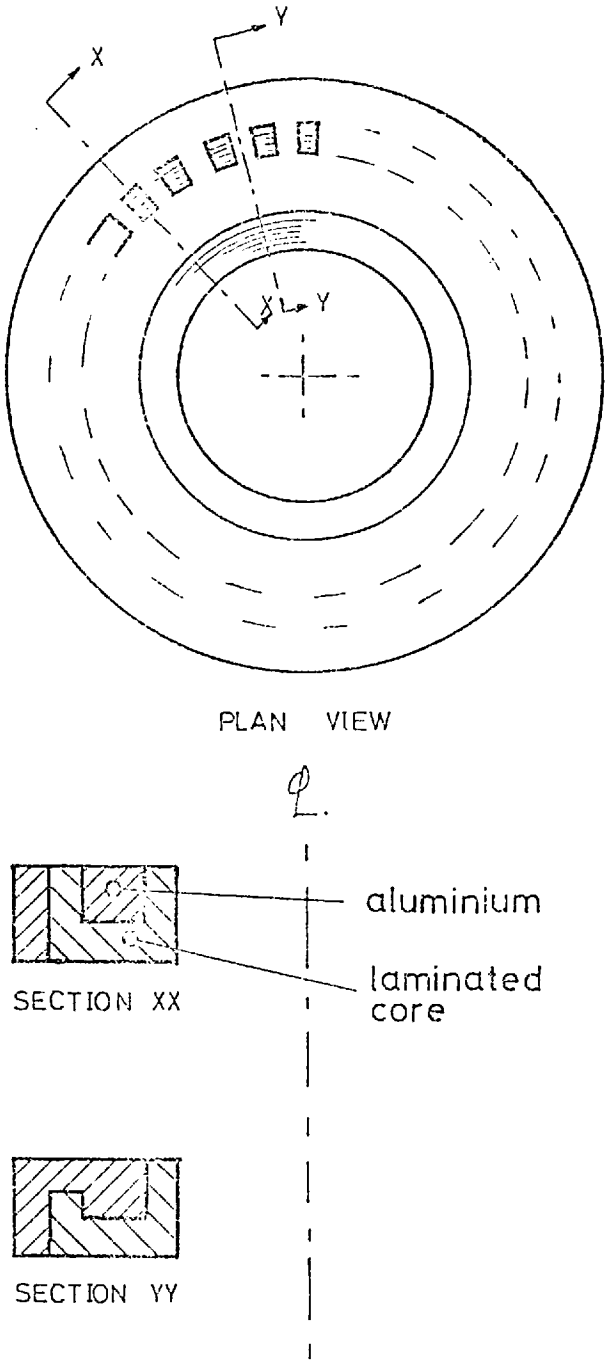

FIG. 1.17 LAMINATED ROTOR FOR SINGLE SIDED 'C' CORE TRANSVERSE FLUX DISC MOTOR

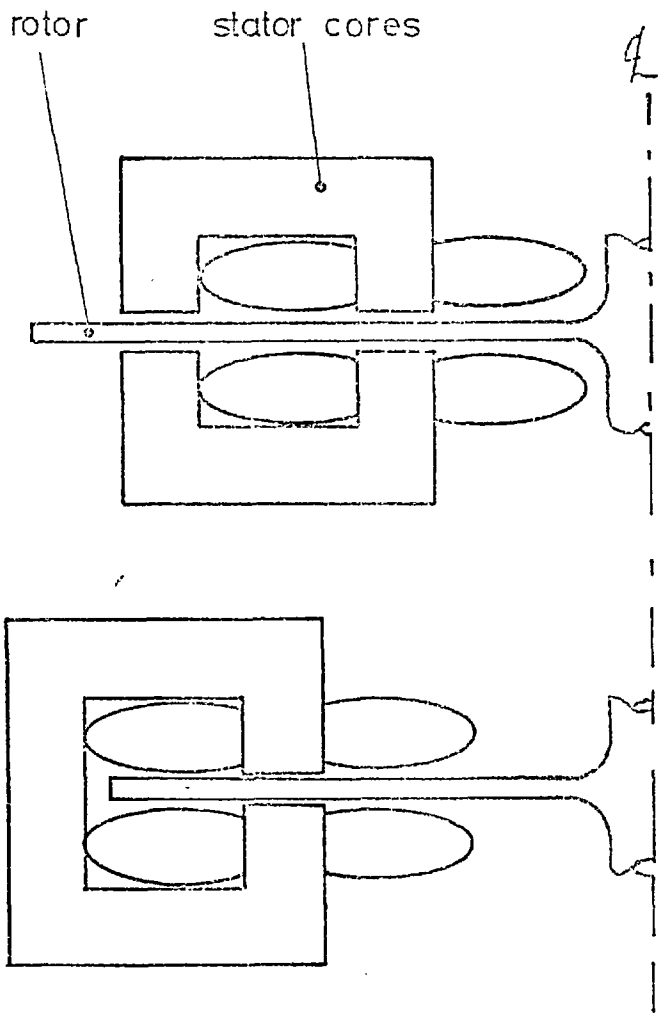

a. Double-sided 'C'-core transverse flux disc motor.
(2 airgaps per pole)

b. Double-sided 'C'-core transverse flux disc motor with improved magnetic circuit.
(1 airgap per pole)

FIG. 1.18 DOUBLE-SIDED TRANSVERSE FLUX DISC MOTOR

expensive, than single sided machines they do not suffer from the need for robust thrust bearings to accommodate the axial force between stator and rotor(like single sided machines) and offer the advantages of double sided operation discussed in Section 1.3.5 above.

iv) Reduced normal force between stator and rotor

A net normal force often exists between the stator and rotor of a single sided disc machine. Two geometrical methods can be used to reduce the effect of this force. In the first, shown in Fig. 1.19(a), the outer edge of the rotor is used as the return path for the flux. This construction halves the net magnetic force between stator and rotor, and the motor may be considered as a hybrid disc/cylindrical type. In the second, illustrated in Fig. 1.19(b), the shape of the airgap becomes conical. The net axial force acting on the rotor shaft is therefore the resolved component of the normal force between the stator and rotor surfaces. Both of these methods of construction, of which numerous variations exist, retain the essential geometrical advantages of the single sided disc motor.

It is also conceivable that the axial force between the stator and rotor can be controlled by the electromagnetic design of the machine, as suggested in Section 1.3.2 above. But the extent to which this can be achieved must await the results of further work.

1.7 Conclusions

The purpose of this chapter has been to give an introduction to the topology of disc machines. It has attempted to identify alternative types of disc machines, examine their relative advantages and disadvantages, compare them with conventional cylindrical machines, and establish the general design criteria and constraints that might apply to them.Quantitative methods of comparison have been pursued wherever possible, although necessarily at a very general level. In so far as the quality of performance of a machine is frequently governed by 'second order' effects, such slot leakage, the conclusions provided by the various comparisons can do no more than indicate general trends. They are presented as such.

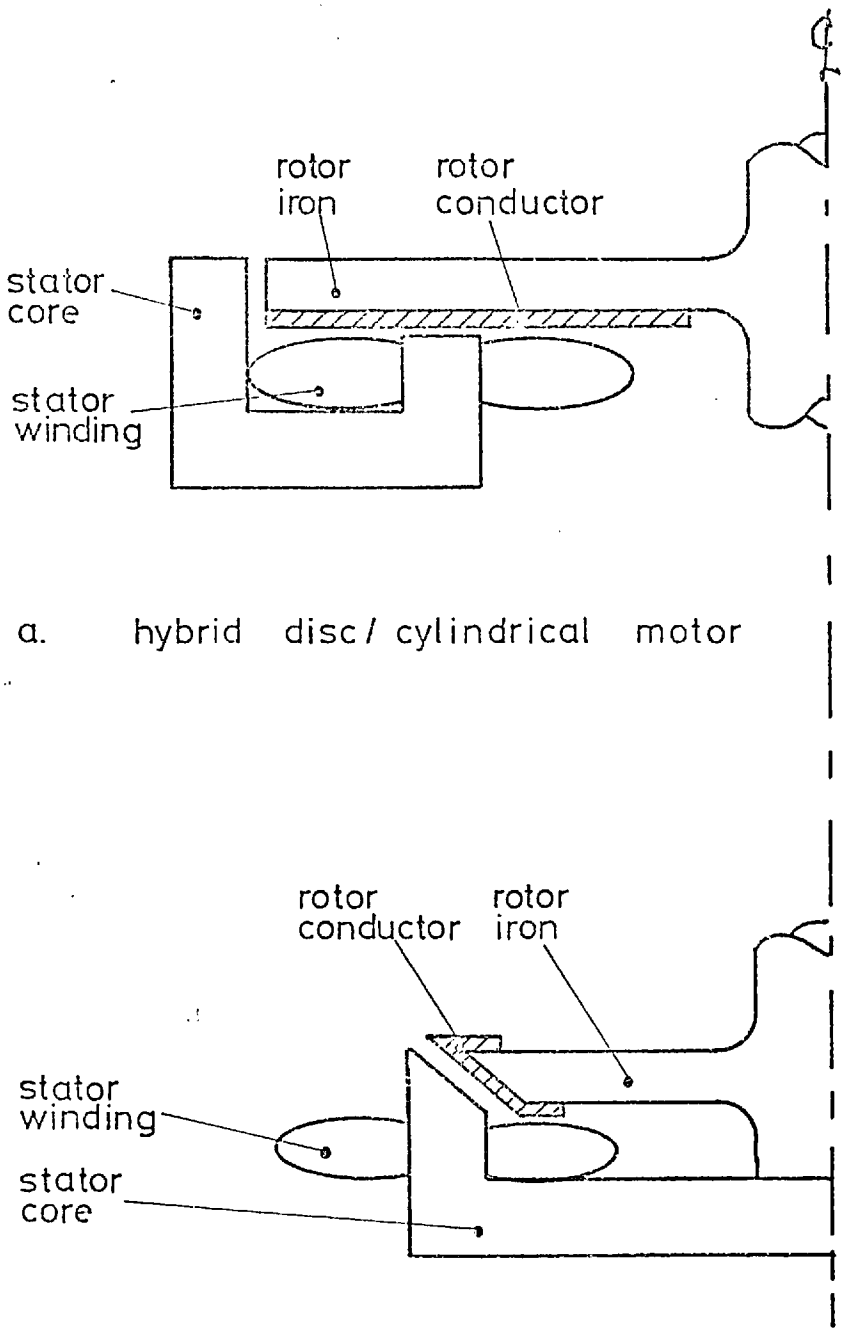

a. hybrid disc / cylindrical motor

b. 'conical' motor

FIG. 1.19 ALTERNATIVE MOTOR SHAPES FOR REDUCED NORMAL FORCE BETWEEN STATOR AND ROTOR

The natural disc shaped derivative of the conventional cylindrical machine was shown to be the disc motor with axial flux paths. In general, it requires more copper and less iron than the cylindrical machine but has approximately the same total weight. The transverse flux disc motor is very similar to the axial flux version in these respects, and therefore stands in the same relation as it does to the conventional motor. Both types of disc motor suffer a relatively high leakage reactance, especially with low pole numbers, but under these conditions their axial length is about half that of a cylindrical motor: they have short and flat profiles. The p.u. leakage reactance of double sided disc motors is less than that of single sided motors, but in this configuration they lose the simple face-to-face construction and the short axial length which has been the attractive feature of disc machines in most of the restricted applications for which they have been used. An interesting property of the double sided motor is its power to weight ratio. It appears to have a weight which is some 10% lower than an equivalent cylindrical machine. This feature seems worthy of further investigation.

The theoretical optimum relationship between the inner and outer core diameters of a disc machine was found to be $D_o/D_i = \sqrt{3}$. Departure from this ratio in either direction can probably be justified for particular cases, but it gives an indication of the general shape that a disc motor should take.

Perhaps the most important difference between cylindrical and disc machines is the effect of the normal forces between stator and rotor. These forces largely cancel themselves out in a cylindrical machine, but are present as a thrust load on the shaft bearings in a single sided disc motor. Some physical designs were suggested which reduce this effect and in some applications the fluid dynamic thrust forces of pumps and fan can be used to counteract these forces. But in any event they can often be accommodated by normal thrust bearing assemblies and need not cause insurmountable problems.

At a technical level, therefore, disc motors do not present serious disadvantages with respect to cylindrical machines that are not compensated for in some applications by their own special features.

To some extent, the move from cylindrical to disc motor simply exchanges one set of constraints for another, the former however being more familiar to the motor designer. The big difference between them lies in their respective suitabilities for economic manufacture.

As little or no attention appears to have been given to the transverse flux disc motor, the relative merits of cylindrical and disc machines would have been judged with respect to the axial flux form of disc motor, which requires inherently expensive manufacturing methods. It is probably for this reason that disc motors have not achieved widespread use. This drawback seems to disappear with transverse flux disc machines, and there are reasons to suggest that they need be no more expensive to manufacture than cylindrical machines if a development and investment programme can be justified to establish large-scale manufacturing techniques.

Chapter 1: References

1. Nasar, S.A., "An Axial-Airgap, Variable-Speed, Eddy-Current Motor", Trans. IEEE, 1968, PAS-87, pp. 1599-1603.

2. Campbell, P., "A New Wheel Motor for Electric Commuter Cars", Electrical Review, 10th March 1972, pp. 332-333.

3. Campbell, P., "'Pancake' Shaped d.c. Motor for Efficient Fan Drives", Electrical Review, 8th March 1974, pp. 211-212.

4. Laithwaite, E.R., Eastham, J.F., Bolton, H.R., Fellows, T.G., "Linear Motors with Transverse Flux", Proc.IEE, 1971, 118 (12), pp. 1761-1767.

5. Laithwaite, E.R., "Linear Electric Motors", Mills and Boon Ltd., 1971, pp. 30-31.

6. Capaldi, B., "The Theory and Performance of a.c. Axial Flux Machines", Ph.D. Thesis, 1973, University of Warwick.

7. Williams, F.C. and Laithwaite, E.R., "A Brushless Variable Speed Induction Motor", Proc.IEE, 1954, 102A, pp. 203-210.

8. Eastham, J.F. and Laithwaite, E.R., "Linear Induction Motors as Magnetic Rivers", Proc.IEE, 1974, 121, (10), p. 1099.

9. Carpenter, J.C., "Surface Integral Methods of Calculating Forces on Magnetised Iron Parts", IEE Monograph No. 342, August 1959.

10. Freeman, E.M. and Lowther, D.A., "Normal Force in Single-Sided Linear Induction Motors", Proc.IEE, 1973, 120 (12), pp. 1499-1506.

11. Tipping, D., "The Analysis of Some Special Purpose Electrical Machines", Ph.D. Thesis, 1964, Victoria University of Manchester.

12. Laithwaite, E.R., "The Goodness of a Machine", Proc.IEE, 1965, 112, (3), pp. 538-541.

13. Russell, R.L. and Norsworthy, K.H., "Eddy Currents and Wall Losses in Screened-Rotor Induction Motors", Proc.IEE, 1958, 105A, pp. 163-175.

14. Laithwaite, E.R. and Barwell, F.T., "Application of Linear Induction Motors to High-Speed Transport Systems", Proc.IEE, 1969, 116, (5), pp. 713-724.

15. Draper, A., "Electrical Machines", 1956, Longmans, Green & Co.

16. Campbell, P., "Principles of a Permanent-Magnet Axial-Field d.c. Machine, Proc.IEE, 1974, 121, (12), pp. 1489-1494.

17. Chalmers, B.J. and Mulki, A.S., "New Reluctance Motors with Unlaminated Rotors", Proc.IEE, 1970, 117, (12), pp. 2271-2272.

CHAPTER TWO

Reluctance Motors

2.1 Introduction

When a discrete piece of magnetically soft iron is placed in a magnetic field, a force or torque is exerted on it which tries to move it to the position in which the energy stored in the magnetic field is maximised: this is consistent with the potential energy of the system as a whole being minimised. This is a general description of the way in which reluctance forces manifest themselves. For example, if a shaped iron rotor is situated in a magnetic field, as shown in Fig. 2.1(a), it will experience a torque tending to align its axis of minimum reluctance - its 'direct' axis - in the direction of the magnetic field. If pivoted and free to rotate, the rotor will come to rest in this aligned position; the airgap flux density, and hence the airgap-field-stored energy are thus maximised. The same type of force is exerted in the linear arrangement illustrated in Fig. 2.1(b). In this case the iron slug, which is displaced from its symmetrical position by a distance x, experiences a force which acts to return it to the position which is symmetrical with respect to the magnetic field, i.e. when $x = 0$.

Reluctance forces of this type can be explained qualitatively in terms of the magnetic poles, the so-called 'salient poles'. These are attracted to the magnetic poles that are setting up the field in the same way that a piece of iron is attracted to a magnet. Quantitative assessment of reluctance forces, however, is usually most conveniently achieved through consideration of the change in stored energy (or coenergy) associated with small displacements of the iron member with respect to the magnetic field.

Pure reluctance forces are exploited in devices such as stepper motors which rely upon switched d.c. supplies to create a rotating field that drives a salient pole rotor in synchronism with it. They also occur as incidental components of synchronous torque in conventional synchronous machines which have salient poles. This thesis

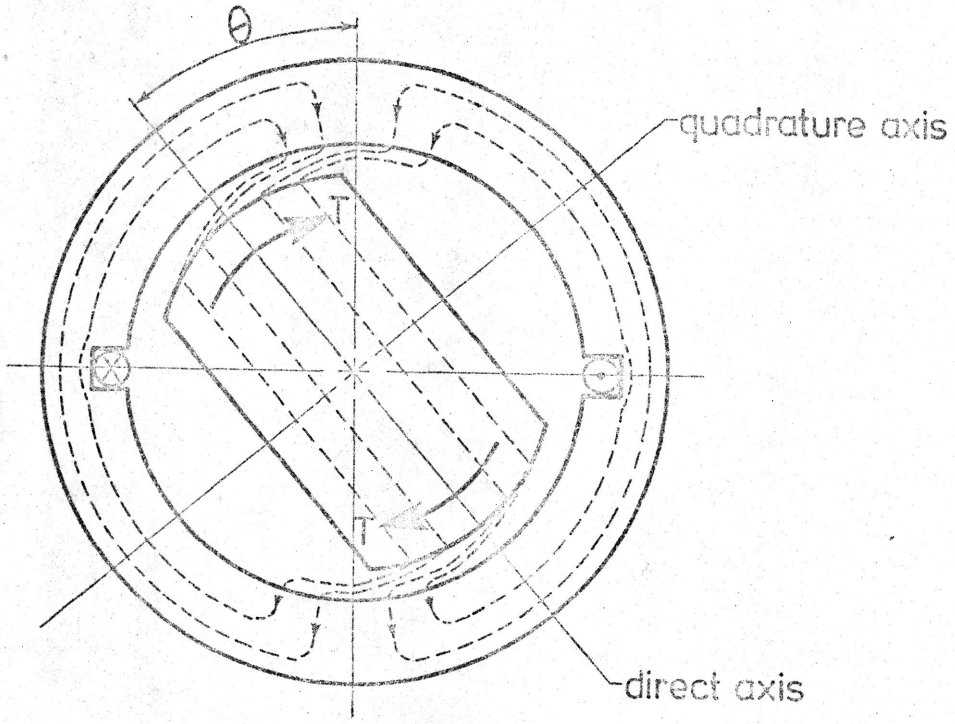

(a) RELUCTANCE TORQUE

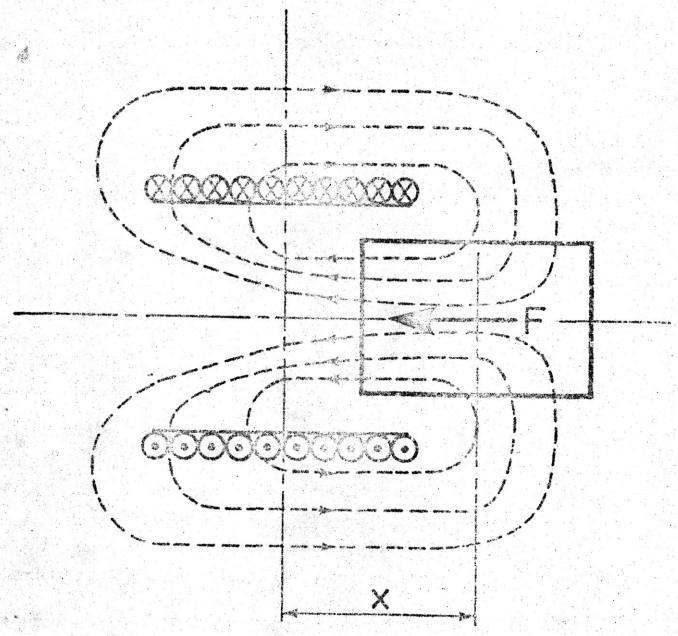

(b) RELUCTANCE FORCE

FIG.2.1 EXAMPLES OF RELUCTANCE FORCES

is largely concerned with a third class of machines, however, which use reluctance forces to provide an essential feature of their operating characteristics. A full description for them is "induction-start reluctance motors". This recognises the fact that they utilise induction torques for starting, but operate at synchronous speed under the influence of reluctance torque. They are commonly known as 'reluctance' motors, and are hereinafter referred to as such. The concept of the reluctance motor can be understood with reference to Fig. 2.1(a). If the magnetic field is rotated slowly, the iron rotor will also rotate in step with the magnetic field. As the frequency of rotation is increased, the rotor will speed up and maintain synchronism with the field for as long as the retarding torques on the rotor (friction, windage and load) do not exceed the reluctance torque. As the load on the rotor increases its direct axis will fall back with respect to the axis of the magnetic field; i.e. angle θ in Fig. 2.1(a) increases. The reluctance torque increases as θ increases and under ideal conditions the reluctance torque is maximum when θ, in Fig. 2.1(a), is greater than 45°. Fluctuations in mechanical load are accomodated automatically by adjustments to this angle.

A different situation would exist if the iron rotor of Fig. 2.1(a) were inserted into an already-rotating magnetic field. As the poles of the magnetic field slipped past each end of the rotor, it would be subjected to forces which varied cyclically about zero at twice the slip frequency: there would be zero time-average rotational force. Reluctance torque is therefore an essentially synchronous property and a net unidirectional torque is only produced when there is zero slip between the rotor and the stator field. As an accelerating torque is not produced by reluctance action under asynchronous conditions, it is clear that a self-starting reluctance motor that is to operate from a fixed frequency supply must rely upon an alternative torque-producing mechanism for reaching synchronous or near synchronous speed.

The simplest form of reluctance motor which demonstrates the asynchronous-induction and synchronous-reluctance torque mechanisms is produced by modifying the magnetic circuit of the rotor of a standard squirrel cage induction motor. For if, for a 2-pole motor, two diametrically opposite portions of the rotor iron are machined

away, the rotor becomes magnetically salient and hence capable of producing synchronous reluctance torque; but also possesses a conducting cage to provide asynchronous induction torques for starting purposes. Thus, after switch-on, the rotor accelerates under the influence of induction torques. As synchronism is approached, the induction torque falls off in a characteristic manner, but the rotor is subjected to pulsations of reluctance torque at twice the slip frequency as the stator field slowly sweeps past the salient rotor poles. Under favourable load conditions the unidirectional reluctance torque exerted during one quarter cycle is sufficient to accelerate both rotor and its coupled load into synchronism. At synchronous speed the fundamental component of rotor current is zero, induction torque is substantially zero and the motor maintains synchronism under the action of reluctance torque alone. The maximum torque which the motor can exert before synchronism is lost, the 'pull-out' torque, is invariably greater than the effective torque that is produced by the motor in achieving synchronism, the 'pull-in' torque.

Thus, it can be seen that reluctance effects can be used as the main torque producing mechanism in simple, robust, brushless synchronous electric machines.

It has been shown that reluctance forces are essentially magnetic forces exerted by magnetic fields on ferromagnetic materials placed in them. Historically, they were the first type of electromagnetic forces to be discovered and consequently formed the basis of the earliest types of motors, dating back to around 1830. Before investigating the design criteria for modern reluctance motors, therefore, it is interesting and instructive to review briefly the historical development of reluctance motors in the context of the general development of electric machines.

2.2 The historical evolution of the reluctance machine

A particularly interesting description of the development of reluctance motors has been given by Anderson[1]. And Cruickshank[2] gave a brief but thorough review of the publications which trace its progress. Some of the early motors constructed by Wheatstone and others have also been catalogued and described by Bowers[3]. This

section is therefore intended to give but a brief description of reluctance motor development from the early days of electric motors through to the modern commercially produced versions. It outlines the varying fortunes of the machine against other advances in electrical engineering, and identifies the major steps in its development.

The first electric motor ever made is often attributed to Professor del Negro of Padua University in 1830, just one year before Faraday discovered the principles of electromagnetic induction. By 1840 Robert Davidson of Aberdeen, who pioneered reluctance motors in Britain, had demonstrated an electrically driven railway vehicle; and at the same time W.H. Taylor of the U.S.A. was producing similar machines for driving small lathes. These early machines invariably relied upon the attraction of soft iron armatures by d.c. excited solenoids; the latter were switched sequentially to provide continuous motion. The inherent drawback of these machines arises from the fact that the attractive forces between armature and solenoid fall off rapidly as the distance between the interacting iron surfaces increases; this means that effective forces can only be produced during a small displacement of the armature. Many ingenious configurations were conceived to try and minimise this difficulty, including the "eccentric electromagnetic engines" of Wheatstone[3] and the 4-cylinder electric engine of Thomas Allan[3].

During the second half of the nineteenth century, there appears to have been little electric motor development, but reluctance motors generally lost ground to d.c. machines. The lack of interest was probably due to the fact that there was no need for electric tractive power: the steam engine, with all its vested interests was a satisfactory and fashionable source of primary power. The development of electric machines that was undertaken was devoted mainly to the improvement of electric generators for use with lighting systems.

The reciprocal nature of motors and generators appeared to have dawned quite slowly. Although Lenz realised this fact in 1838 and Gramme and Siemens some time later, it wasn't until 1873 that it was demonstrated publicly. This took place at the Vienna Exhibition, using two of Gramme's machines.

Towards the end of the nineteenth century there was renewed interest in electrical machines. Bailey demonstrated the production of a rotating field by the interconnection of a two-phase supply and a two-phase distributed winding in 1879, and Tesla produced a viable form of induction motor in 1887. By the end of the nineteenth century most of the common types of electrical machines that we know to-day had been devised. Their respective developments were largely dependent upon the conflict between a.c. and d.c. systems which continued from the late nineteenth century (Silvanus P. Thompson published his vindication of a.c. generation and distribution in 1894) until well into the twentieth century.

It has been said that important developments in electrical machines stopped at the turn of the century. What appeared to have taken place was a period of consolidation at the beginning of the twentieth century following the period of prolific invention in the 1880's and 1890's. By 1900, both the squirrel cage and wound rotor induction motors had emerged and the salient pole reluctance motor developed as a close cousin of the former. It provided cheap and reliable synchronous drive which found applications in industrial processes where close speed control was essential. An amusing example of its application cited by Anderson[1] was found in the manufacture of swiss rolls. It appears that "close speed control is essential in view of the negligible tensile strength of the material". As has been stated before, however, the performance of this form of motor was poor and it could not compete with the induction motor; it was only used where its choice was made inevitable by its brushless synchronous mode of operation. A typical rotor of the 'milled cage' salient pole reluctance motor (i.e. the rotor was produced by milling away arcuate portions of a squirrel cage rotor) is illustrated in Fig. 2.2(a). This type of motor was refined by the use of special rotor punchings, Fig. 2.2(b) illustrates a design that was in use before 1950, but the milling process is still occasionally used as an expedient method for small quantity production of special purpose motors.

In 1923, Kostko, in America, was probably the first to realise that it was not the external shape of the motor that was important for reluctance motor operation, but its internal magnetic saliency[4].

He proposed a design of rotor which was substantially cylindrical in shape but which incorporated internal flux guides or flux barriers in the form of appropriately positioned slits. The barriers are aligned in the direction of the flow of flux in the direct axis position, but present additional reluctance to the flux when the rotor is in the quadrature axis position. A rotor lamination stamping proposed by Kostko is illustrated in Fig. 2.2(c). Kostko demonstrated that this type of reluctance motor could produce an output which approached that of a similar size of induction motor. For reasons unknown, Kostko's work appears not to have been followed up at that time. Instead, Trickey[5], Talaat[6], Lin[7] and others continued to refine the salient pole reluctance motor, producing more sophisticated analyses and better design criteria. The main innovation during this period (the 1930's through to the 1950's) was the purpose-made rotor stamping mentioned above. In 1956, however, rotor stampings which incorporated flux guides were brought into commercial production; an example designed by Risch[8] is shown in Fig. 2.2(d).

In the U.K., the work of Lawrenson[9] since 1962 has been directed towards the 'segmented' form of reluctance rotor; a typical rotor stamping is shown in Fig. 2.2(e). It is essentially the limiting version of the flux barrier configuration. The separate iron segments of the rotor are mounted on a non-magnetic arbor and the motor shaft is thereby excluded from the magnetic circuit of the rotor. This form of motor has characteristics which are comparable to equivalent induction motors, and is now in commercial production in sizes which range from fractional horse powers to more than 50 H.P. It is interesting to note that one of Wheatstones reluctance machines of 1840 consists of segments of iron fastened to a non-magnetic (wooden) arbor[3].

In addition to these main developments, other configurations of reluctance motors have been produced in recent years; they all claim performance characteristics that are comparable to the flux barrier and segmented machines. Fong[10] in 1970 devised the so-called "essential barrier" reluctance rotor which uses a very simple form of rotor punching, and is distinguished from the designs of Kostko and Lawrenson by the fact that it requires half the number of barriers

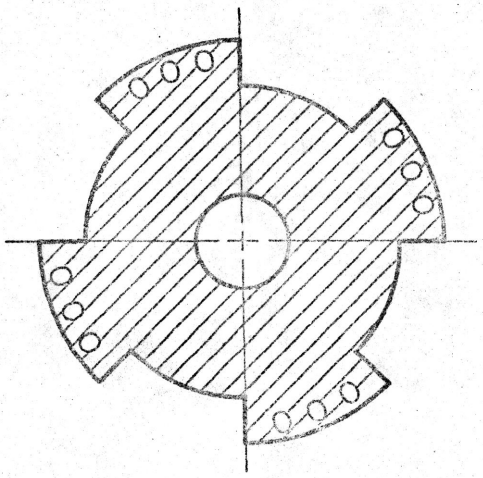

(a) SALIENT POLE
(MILLED ROTOR)

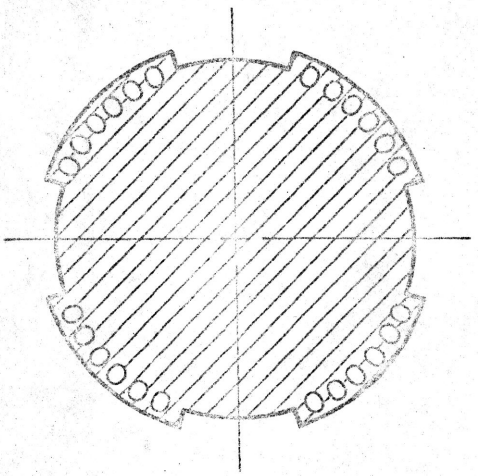

(b) SALIENT POLE
(PURPOSE MADE
LAMINATION)

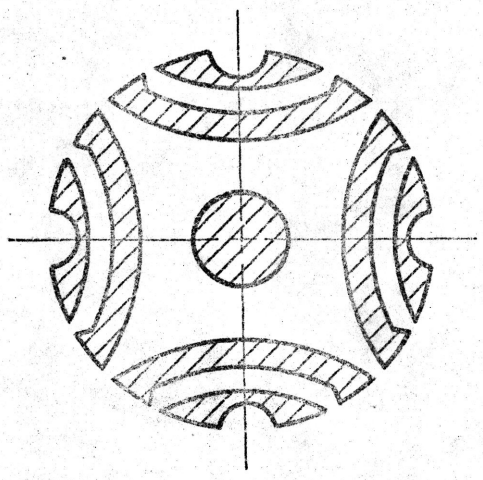

(c) INTERNAL FLUX GUIDES
(KOSTKO 1923)

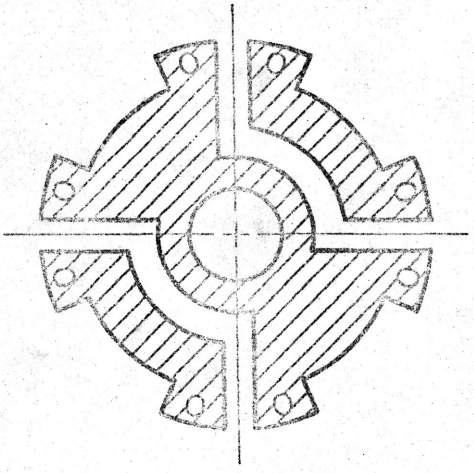

(d) SALIENT POLE
(WITH FLUX GUIDES)
(RISCH 1956)

FIG.2.2 ROTOR MAGNETIC CIRCUITS FOR CYLINDRICAL RELUCTANCE MOTORS/cont.

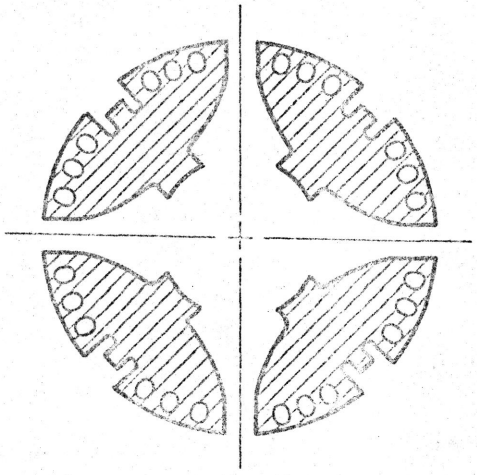

(e) SEGMENTED ROTOR
(LAWRENSON 1964)

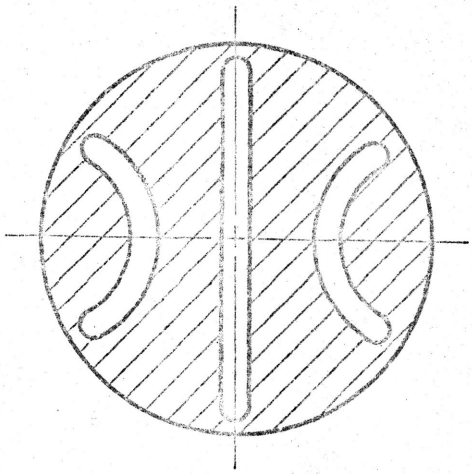

(f) ESSENTIAL BARRIER ROTOR
(FONG 1970)

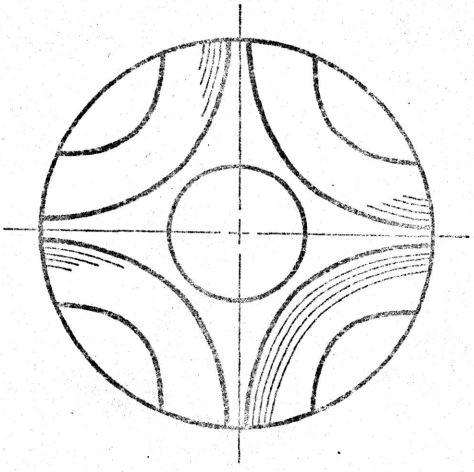

(g) AXIALLY LAMINATED ROTOR
(CRUICKSHANK 1971)

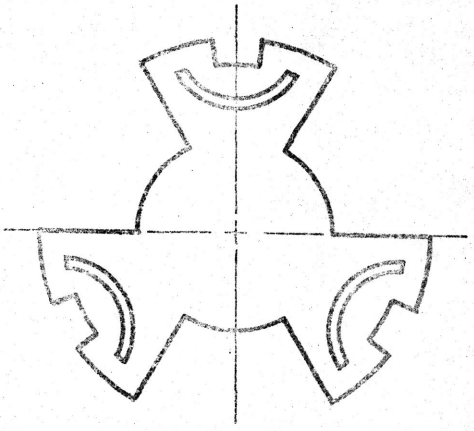

(h) 'SEMIPOLE' ROTOR
(LAWRENSON 1968)

FIG.2.2 ROTOR MAGNETIC CIRCUITS FOR CYLINDRICAL RELUCTANCE MOTORS (cont.)

per pole. A rotor stamping for a six pole "essential barrier" machine is illustrated in Fig. 2.2(f). Cruickshank et al[2] reported an axially laminated anisotropic rotor in 1971. A typical four pole design is shown in Fig. 2.2(g). The principle of operation of this motor is very similar to that of the segmental rotor, but it also exploits the interlaminar reluctance of axially laminated rotor iron. While presented as a novel machine in this country, it also appears as a recommended reluctance motor design in a Russian teaching text book published in 1963[11]. Lawrenson reported a 'semipole' reluctance motor[12] in 1968 which does not appear to have been followed up. It is interesting in that it combines 'salient pole' and 'flux guide' features in the rotor, as can be seen in Fig. 2.2(h).

Although many types of reluctance motor have been conceived and tested, as illustrated above, two main types appear to be in commercial production at the present time: the simple salient pole motor, using special rotor lamination stampings, and the segmented rotor motor of Lawrenson. Some intermediate designs which use flux barriers to enhance the performance of the salient pole motor are also available. Between them they make a substantial contribution to the electric motor drives in use to-day.

Reluctance effects were used to produce the very first motive power from electricity and magnetism, even before electromagnetic induction had been discovered and certainly before its exploitation (more than fifty years elapsed between Faraday's discovery and Tesla's first induction motor). During this century the role of reluctance torques has been in modified a.c. induction machines and in some synchronous machines. It is interesting to note, however, that recent developments in stepper motors, made possible by solid-state technology for suitable drive systems, indicate that pure reluctance torques are being exploited once more to produce viable machines for some present day applications.

2.3 Design considerations for reluctance motors

The two principle types of reluctance motor which are in commercial use at the present time are 'salient-pole' and 'segmented-rotor' machines. They are accordingly given the closest attention in the examination of disc reluctance motors below. Other types of reluctance motor such as the 'semi-pole', the 'essential-barrier' and the 'axially-laminated' which were mentioned in Section 2.2 above are given little further consideration.

Now, before investigating the topology of disc-shaped reluctance motors, the design criteria for good cylindrical motors are examined in order that the implications of adopting a disc motor geometry can be studied critically.

Three distinct modes can be considered to occur in the operating duty of a reluctance motor. These are the asynchronous run-up phase, the synchronisation cycle, and steady state synchronous operation. During the synchronisation cycle the reluctance torques, pulsating at a low slip speed, must take over from the induction torque and drive the rotor plus its coupled load into synchronism. This capability is a very important feature of a reluctance motor and usually determines its rated capacity.

The synchronous torque characteristic of a reluctance motor is well known. The torque appears to vary in a substantially sinusoidal manner with respect to load angle; it is discussed in some detail by Stephenson[13]. At synchronous speed reluctance motors are usually rated for steady state operation at two-thirds of the pull-out torque as this gives an efficient and stable operating point while allowing an adequate margin to handle load fluctuations without loss of synchronism. The synchronous behaviour of a reluctance motor is controlled very largely by its direct and quadrature axis reactances, but the relatively large p.u. stator resistance of smaller machines also has an effect, and tends to reduce pull-out torque produced by a motor. Synchronous torque, T_r, expressed in watts, for a star connected reluctance motor is given by[13]:

$$T_r = \frac{V_L^2}{2} \frac{(X_d - X_q)}{(X_d X_q + R_1)^2} \{ (X_d X_q - R_1) \sin 2\delta + R_1 (X_d + X_q) \cos 2\delta - R_1 (X_d - X_q) \} \quad (2.1)$$

where V_L is the line voltage

X_d and X_q are the direct and quadrature reactances respectively and include the leakage reactance components

R_1 is the stator phase resistance

and δ is the load angle between phase voltage and the quadrature axis

And when $R_1 = 0$, the expression for pull-out torque reduces to:

$$T_{po}\Big|_{R_1=0} = \frac{V_L^2}{2}\left(\frac{1}{X_q} - \frac{1}{X_d}\right) \qquad (2.2)$$

which illustrates the importance of a low value of X_q to obtain a high pull-out torque. In order that the machine operates efficiently, however, a high value of X_d is also desirable.

The synchronising process of a reluctance machine is a very complex phenomenon, and a quantitative description of it is correspondingly difficult. The most precise criterion for synchronisation capability has been produced by Lawrenson and Mathur[14]. The essential problem is that the unidirectional reluctance torque produced during one quarter cycle must be sufficient to accelerate the rotor, plus its coupled inertia, against the load torque, from a sub-synchronous slip speed into synchronism. It is therefore desirable that the rotor achieves the lowest possible slip speed under the influence of its induction torques in order to minimise the speed difference through which the rotor must be accelerated by the reluctance torque. The synchronising capability of a reluctance motor is accordingly enhanced by constructing its rotor with a low electrical resistance.

The properties of a good reluctance motor may therefore be summarised as:

i) high X_d, as close as possible to the value of X_m of the parent induction motor

ii) low X_q

iii) low R_2

For reasons of stability at synchronous speed and acceptable asynchronous performance, however, there are indications that few benefits are obtained by increasing the value of the X_d/X_q ratio beyond 5 or 6. Also,

there is a theoretical optimum value of R_2, below which the synchronising performance of the motor deteriorates[15], but this is rarely encountered in practical machines.

The preceding remarks relate to the terminal characteristics of reluctance machines and to their effect on motor performance. It is now possible to investigate salient pole and segmented rotor reluctance motors and to examine the extent to which their respective geometries restrict the achievement of optimum parameter values.

i) The salient pole reluctance motor

The essential features of a salient pole reluctance motor are illustrated in Fig. 2.3(a): the direct and quadrature axes are indicated, and flux paths associated with each axis position are also shown. The variables which govern the axis reactances are identified in Fig. 2.3(a) as g_1, g_2 and β. Lawrenson[16] expressed x_d and x_q, the armature reactance components of X_d and X_q, in the convenient form:

$$\begin{aligned} x_d &= k_d\, x_c \\ x_q &= k_q\, x_c \end{aligned} \qquad (2.4)$$

where x_c is the magnetising reactance with a cylindrical rotor and uniform airgap of g_1, the factors k_d and k_q being given by:

$$\begin{aligned} k_d &= \frac{g_1}{g_2} + \left(\beta + \frac{\sin \beta\pi}{\pi}\right)\left(1 - \frac{g_1}{g_2}\right) \\ k_q &= \frac{g_1}{g_2} + \left(\beta - \frac{\sin \beta\pi}{\pi}\right)\left(1 - \frac{g_1}{g_2}\right) \end{aligned} \qquad (2.5)$$

The two axis reactances which control reluctance motor performance also include the stator leakage reactance, however, and can be written as:

$$\begin{aligned} X_d &= x_d + x_\ell \\ X_q &= x_q + x_\ell \end{aligned} \qquad (2.6)$$

where x_ℓ is the stator leakage reactance.
Equations 2.6 can be re-written as:

$$\begin{aligned} X_d &= x_c\,(k_d + k_\ell) \\ X_q &= x_c\,(k_q + k_\ell) \end{aligned} \qquad (2.7)$$

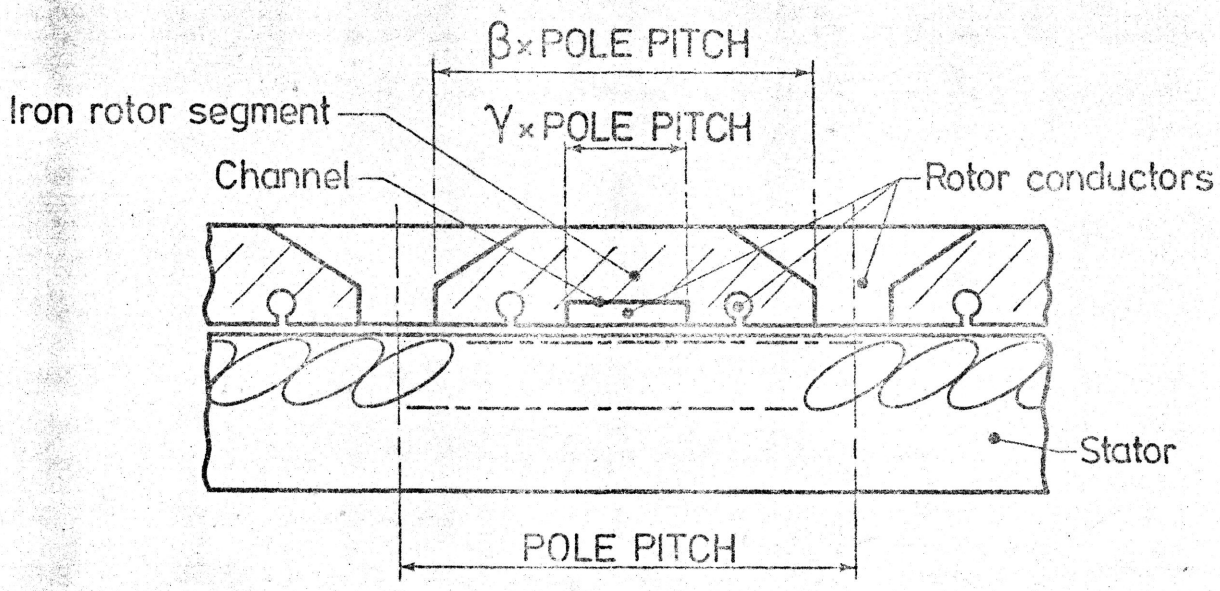

(a) SINGLE-SIDED, SEGMENTED-ROTOR, AXIAL FLUX, DISC RELUCTANCE MOTOR

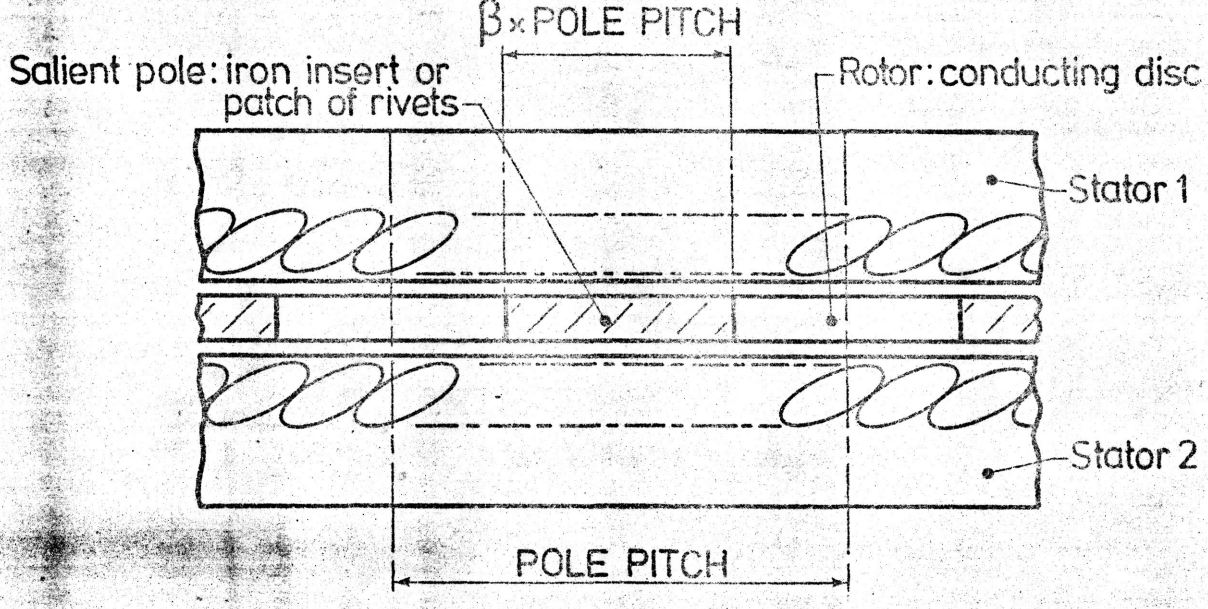

(b) DOUBLE-SIDED, SALIENT-POLE, AXIAL FLUX, DISC RELUCTANCE MOTOR

Fig. 2.6 ESSENTIAL FEATURES OF ALTERNATIVE DESIGNS FOR DISC GEOMETRY RELUCTANCE MOTORS

where $k_\ell = x_\ell / x_c$

and the expression for pull out torque, equation 2.2, takes the form:

$$T_{po}\Big|_{R_1=0} = \frac{V_L^2}{2x_c}\left\{\frac{1}{k_q + k_\ell} - \frac{1}{k_d + k_\ell}\right\} \qquad (2.8)$$

Expressions were also derived[16] for the power factor at pull-out ($\cos \phi_{po}$) and the magnetising current at pull-out ($I_{m_{po}}$) for the case when the primary resistance was zero. They are:

$$\cos \phi_{po}\Big|_{R_1=0} = \frac{X_d - X_q}{X_d + X_q} \qquad (2.9)$$

and

$$I_{m_{po}}\Big|_{R_1=0} = \frac{V}{\sqrt{6}} \frac{[X_d^2 + X_q^2]^{\frac{1}{2}}}{X_d X_q} \qquad (2.10)$$

The influence of β and g_1/g_2 on the main characteristics of a salient pole reluctance motor, as predicted by the simplified analysis given above is summarised in Fig. 2.4 (k_ℓ is taken to be 0.1 for Figs. 2.4(b), (c), (d) and (e)). Two main conclusions can be derived from this Figure:

- the maximum X_d/X_q ratio, maximum pull-out torque and maximum power factor at pull-out are obtained when β is between 0.2 and 0.4. In these respects therefore, β should be around 0.3.

- in contrast to this, the magnetising current of the motor, which may be taken as an indication of the quality of the machine, is very high at low values of β, and judged on this criteria alone, β should be set as close to unity as possible. The deeper significance of the magnitude of the magnetising current concerns its operation as an induction motor. If the magnetising current at synchronous speed is high, the slope, d(Torque)/d(slip), of the induction torque characteristic near synchronous speed will be low: the motor will therefore not achieve a very low slip speed under the influence of this torque component and its synchronising capacity will be correspondingly poor. This is the basic conflict which occurs in the design of salient pole reluctance motors: β should be large for good induction motor performance, and good pull-in characteristics, but should be small for good

g_1/g_2	0.05	0.10	0.25	0.50
KEY	——	·····	- - - -	-·-·-

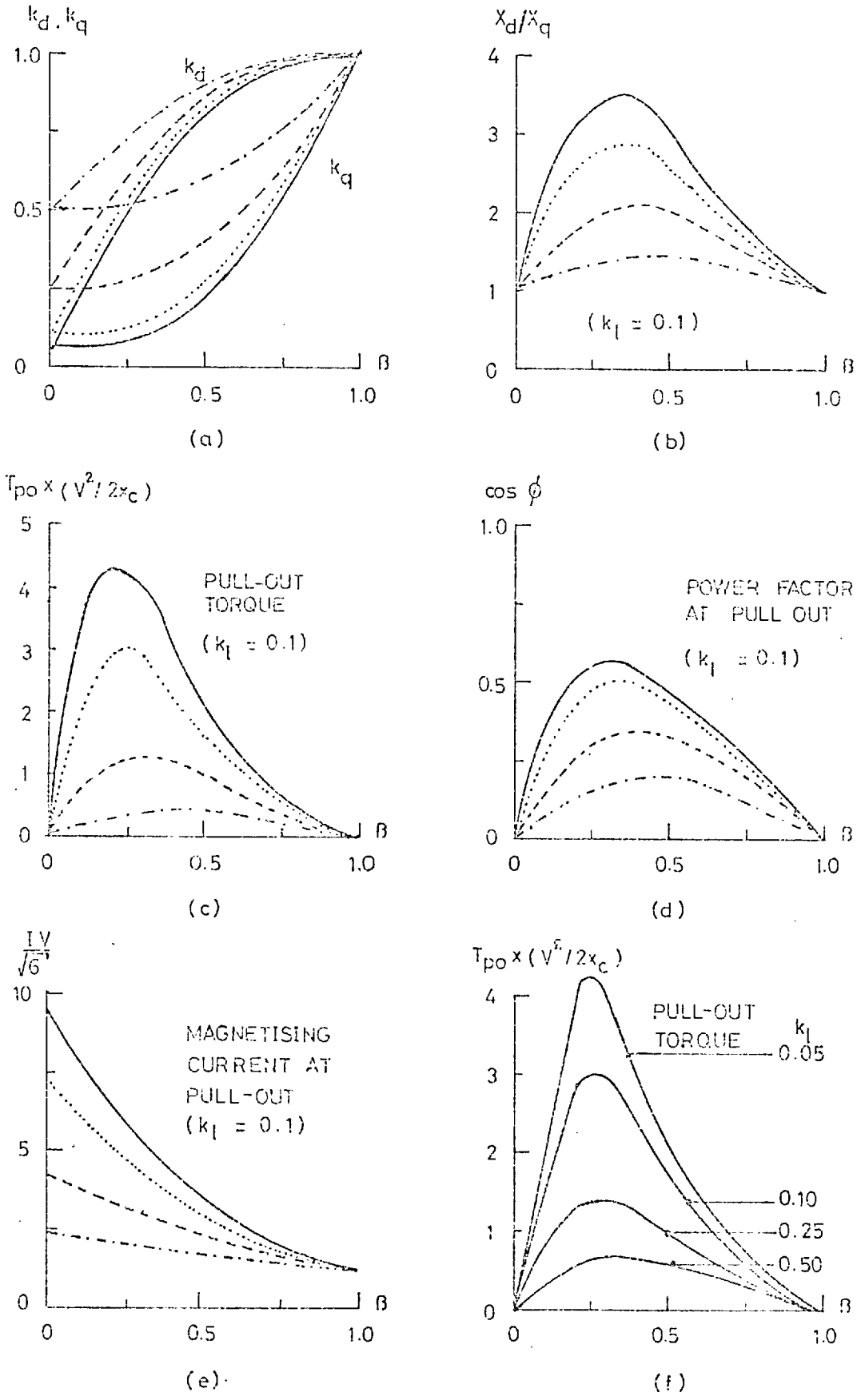

FIG. 2.4 SOME CHARACTERISTICS OF SALIENT POLE RELUCTANCE MOTORS

synchronous performance. In practice, it has been found that a value of β of about 0.5[16] gives the best compromise performance.

Concentrating on a value of β of 0.5, the effect of the ratio g_1/g_2 and of the stator leakage reactance can be examined. From Fig. 2.4(b) it is apparent that the value of the X_d/X_q ratio is sensitive to g_1/g_2. A value of $X_d/X_q = 3$ can only be achieved if g_2 is 20 times greater than g_1; and $g_1/g_2 = 0.25$ limits X_d/X_q to around 2. As g_2 is increased, however, there is a significant increase in magnetising current, as indicated in Fig. 2.4(f).

It was assumed that the stator leakage reactance was 10% of the magnetising reactance ($k_1 = 0.1$) for the calculation of the X_d/X_q, pull out torque, power factor and magnetising current characteristics in Fig. 2.4. Fig. 2.4(f), however, shows the variation of pull out torque for a range of values of k_1 and there appears to be every incentive to minimise the leakage reactance of a reluctance motor.

All the characteristics illustrated in Fig. 2.4 are for the case when the stator resistance is zero. Departure from this ideal case will tend to reduce the pull-out torque that can be expected from the motor.

The above discussion has brought out the factors which contribute to good and bad salient pole reluctance motor design. The quantitative aspects of the discussion were necessarily based on a relatively simple analytical method, but it is nevertheless sufficiently representative to enable the conclusions arising from it to be given full consideration in the topological investigation of disc reluctance motors which follows in Section 2.4.

ii) The segmented rotor reluctance motor

A simple version of a segmented-rotor reluctance motor is illustrated in Fig. 2.3(b). It can be seen that the rotor consists essentially of circumferential iron segments which extend over a substantial portion of the pole arc. When the interpolar space is coincident with the pole centre the iron segments provide a low reluctance path for flux through the rotor: this is the direct axis position.

When the pole arc is opposite the stator pole centre the interpolar space creates a very high reluctance path: this is the quadrature axis position. Flux paths corresponding to these two positions are indicated on Fig. 2.3(b). The special feature of segmented rotor machines is that the flux invariably re-enters the stator iron to bypass the high reluctance presented by the interpolar space when the rotor is in the quadrature axis position. This is because it is generally easier for the flux to cross the motor airgap an extra two times than to negotiate the interpolar gap.

It appears from the mode of operation of the segmented rotor machines that the pole arc to pole pitch ratio will be close to unity, and that its performance will consequently approach more closely that of its parent induction motor.

The effect of β on the performance of the primitive segmented rotor reluctance motor of Fig. 2.3(b) is illustrated in Fig. 2.5: k_d and k_q, X_d/X_q, pull out torque, maximum power factor, and magnetising current at the point of pull out are shown. k_1 is assumed to equal 0.1 for all these calculations. Contrasting these results with similar results for the salient pole motor in Fig. 2.4, it can be seen that low magnetising current, high power factor and high pull out torque can all be achieved if a value of β of between 0.8 and 0.9 is adopted. The slight reduction in the maximum possible pull-out power that must be accepted with this value of β is more than compensated for by the improved synchronising capacity resulting from good induction motor performance.

The results in Fig. 2.5 are derived from an approximate analysis of a very simple motor design. They are representative of the general form of the parameter changes that take place if β is altered, but underestimate the quality of performance that can be achieved with segmented rotor machines.

A practical design for a rotor segment is illustrated in Fig. 2.3(c). The features to be noted are:

- tapered ends which tend to saturate in the quadrature axis position and hence increase interpolar reluctance without substantially affecting the direct axis reactance.

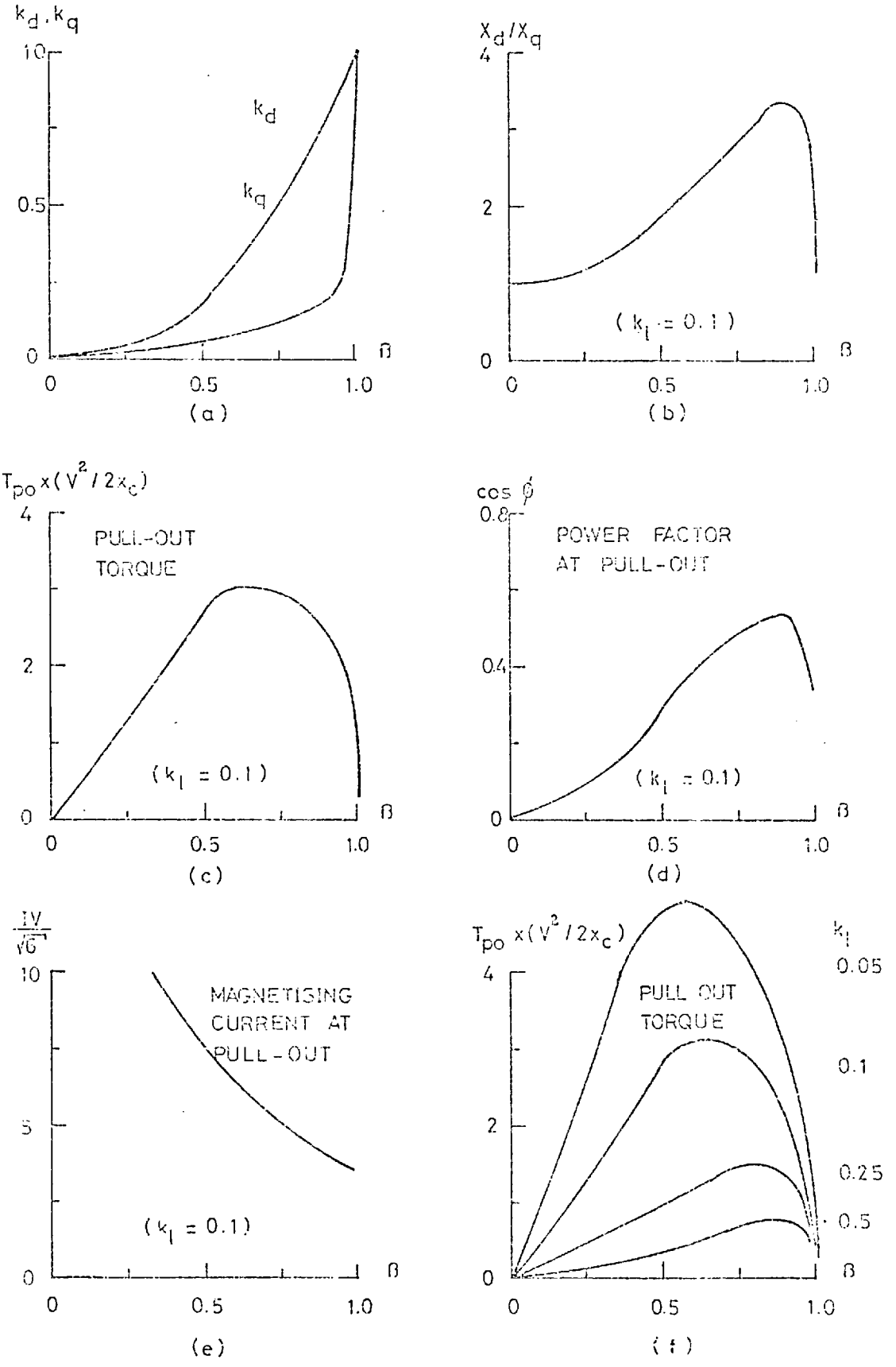

FIG. 2.5 SOME CHARACTERISTICS OF SEGMENTED ROTOR RELUCTANCE MOTORS

- a channel in the centre of the segment which serves two purposes: it further reduces quadrature axis reactance, and provides space for rotor conductors which are particularly effective in enhancing the pull-in capability of the machine in this position. The introduction of the channel can increase the pull-out torque by a factor of almost 2 without adversely affecting the pull-in power.

The notable feature about the mode of operation, and geometry of the segmented rotor machine is that the direct and quadrature axis reactances can be changed almost independently. Greater freedom therefore exists in the choice of these parameters for good motor operation. This should be contrasted with the salient pole motor above in which X_d and X_q were closely interdependent: i.e. a reduction in X_q also brought about a reduction in X_d.

Two main variables could be controlled in the design of a salient pole reluctance motor : β and g_1/g_2 (assuming g_1 was the minimum gap consistent with satisfactory mechanical clearance between stator and rotor). The more complex nature of segmental rotor inevitably introduces a greater number of design variables. The most important ones are:

β - pole arc to pole pitch ratio

γ - channel width to pole pitch ratio

g/g_1 - airgap to channel depth ratio

For good pull-in performance Lawrenson[17] has reported that the preferred values for β and γ are around 0.85 and 0.27 respectively, and that g/g_1 need not exceed about 10, and shows no added benefit above 25.

Whatever the form of reluctance motor, there is always a conflict between the demands of the magnetic circuit of the rotor for good synchronising and good synchronous performance. In the segmented rotor machine this conflict is perhaps less apparent than in the traditional salient pole reluctance motor, but it nevertheless exists. The precise design of a machine will therefore depend upon the operating cycle it is expected to follow. For example, pull-in capacity can be enhanced if high inertia loads are to be synchronised, but only at the expense of a slight deterioration in synchronous performance - and vice versa.

The influence of the disc motor geometry on the important features of segmented rotor reluctance motor design which have been identified above can now be examined.

2.4 General considerations for disc geometry reluctance motors

Disc machines are very similar to cylindrical machines in that they are both rotating electrical machines, and the general principles of induction and reluctance motor operation consequently apply to both. However, the alternative geometry of the disc motor imposes some new constraints on its design while removing others which apply for cylindrical machines. Altogether it adjusts the relative importance of the many features which contribute to the quality of performance of an electrical machine. Chapter One attempted to identify the implications of disc geometries on the design of induction machines; this section outlines the principle effects which the adoption of a disc motor geometry has on reluctance motor performance. Sections 2.5 and 2.6 which follow identify in more detail preferred designs for single and double sided disc reluctance motors.

Two general properties of disc motors which critically affect their performance as reluctance machines can be picked out from discussions given in Chapter One, and from the foregoing sections of the present chapter. They relate to the primary (stator) leakage reactance, and the secondary (rotor) resistance. In addition, the practical running clearances that are required between the stators and rotors of disc motors must also be considered. The effect of these three parameters on disc reluctance machines are now considered in turn.

i) Primary leakage reactance

The primary leakage reactance of a disc reluctance motor can readily be seen to be important. For it has been shown in Section 1.4.3 above that the end winding length, and hence leakage reactance of a low pole number disc motor is considerably greater than that of an equivalent cylindrical machine; and it has been shown in Section 2.3 above that the performance of a reluctance motor depends critically upon the ratio X_d/X_q. X_d and X_q include the primary leakage reactance in the manner of equation 2.6 above, i.e.

$$X_d = x_d + x_1$$

and $$X_q = x_q + x_1$$

so that the larger x_1, the smaller the ratio of X_d and X_q. For a four pole machine, say, the results of Section 1.4.3 above suggest that the end winding leakage reactance of a single-sided disc motor will be some three times greater than that of an equivalent cylindrical machine (this becomes a factor of six for 2-pole machines). If the leakage reactance of a conventional machine is taken to be 10% of the magnetising reactance (although higher values than this are often encountered in well-saturated machines), this implies that the leakage reactance of an equivalent disc motor (neglecting the slot leakage component) will be around 30% of the magnetising reactance. Typically, for an x_d/x_q ratio of 3.0, the increase in leakage reactance from 10% of x_c (see equation 2.4) to 30% of x_c would reduce the value of X_d/X_q from around 2.5 to 2. Alternatively, for an x_d/x_q ratio of 6.0, the reduction in X_d/X_q for the same change in x_1 would be from approximately 4 to 2.7. The implication of these figures is that a segmented rotor machine, with the generally higher x_d/x_q ratio than the salient pole motor will suffer the greater degradation of reluctance properties when constructed in a disc geometry. One possible conclusion arising from these results is that to obtain the same X_d/X_q ratio in cylindrical and disc machines the armature reaction component, x_d/x_q, in the latter form would have to be greater in order to compensate for the higher level of leakage reactance.

The electrically double sided disc motor was shown in Section to have a p.u. leakage reactance which was less than half that of a single sided motor. It would, therefore, appear in this respect to constitute the better form of disc reluctance motor, with a p.u. leakage reactance which is of the same order as conventional machines.

The problem of high leakage reactance in disc machines can perhaps be alleviated slightly by special windings which have low leakage reactances. But there also appears to be a case for increasing the stator width so that the pole pitch to stator width ratio is reduced, and the end winding leakage reactance becomes a smaller proportion of the magnetising reactance. All the figures used immediately above relate to a disc motor in which the outer core diameter, D_c, is $\sqrt{3}$

times the inner core diameter, D_i. If, for example, the ratio of D_o/D_i is increased from $\sqrt{3}$ to 2, in a single sided machine, x_1 could be decreased from 30% of x_c to about 25% of x_c and the deterioration in the X_d/X_q ratio by the leakage reactance component would be reduced accordingly. The reduction in available slot area at the inner periphery of the core that is caused by increased stator width can be offset by deeper slots, for it was indicated in Section 1.5.2 above that this expedient would increase the total leakage reactance by a very small amount.

It would appear therefore that a disc reluctance motor might have greater core widths and slot depths than would normally be used for an induction machine. Conceptually, this suggests that the motor becomes an 'iron' machine, and this is consistent with its operation as a reluctance motor.

ii) Rotor resistance R_2

It is known that the electrical resistance of the rotor cage of a reluctance motor should be low if it is to have a good synchronising capability[15]. Although this can normally be achieved, a physical limit is imposed on the size of a rotor slot in a cylindrical machine by the constriction of flux which occurs at the roots of the rotor teeth if the slots are made too deep. This constraint becomes most significant in smaller machines which tend to exhibit higher per unit values of resistance. In a disc motor there is no such limit on rotor slot depth*. It would therefore appear possible to achieve lower values of rotor resistance in disc machines, and this might have special advantages for small motors. Of particular interest in this respect is a 'Gramme Ring' type of winding[18] for the rotor of a single sided disc reluctance motor: the winding would consist of 'Gramme Ring' turns around the rotor core which are shorted together by inner and outer end rings. This winding configuration presents two parallel paths for the rotor currents: one is in the plane that corresponds to a 'surface' winding; and the other is in the plane of the Gramme Ring winding (see Section 1.2 above). At high slip frequencies the rotor currents will be mainly confined to the surface winding paths, as the Gramme Ring paths, which enclose the iron rotor core, have a relatively

* it is interesting to note that this constraint on rotor slot depth in a cylindrical machine is exchanged for the constraint on slot width at the inner diameter of a disc motor.

high impedance due to a large inductive component. At low slip frequencies, i.e. close to synchronism, the rotor slip frequency is small, the inductive reactance of the Gramme ring paths approaches zero, and the rotor currents can circulate around the shorter Gramme Ring paths. According to Section 1.5.3 above, for $D_o/D_i = \sqrt{3}$, the ratio of resistance of the surface winding and Gramme ring winding paths are as follows for a range of pole numbers:

Pole Number	Resistance of Surface Winding / Resistance of Gramme Ring Winging
1	1.7
2	1.3
3	1.0
4	0.8
5	0.7

Substantial improvements to the synchronising ability of small 2 and 4 pole single sided disc reluctance motors can therefore be expected if Gramme Ring type windings are used on their rotors.

iii) Airgap length

The rotor shaft of a cylindrical machine is mounted in bearings so that it is supported approximately concentrically inside the stator bore. It is a relatively simple matter to arrange the assembly of the motor casing and bearing housings so that a small running clearance between the stator and rotor surfaces can be used. In fractional horse power machines this clearance is commonly around 0.020 in.

It is more difficult to achieve such small running clearances in disc motors, by virtue of their geometry. For the planes of the stator and rotor surfaces must be set precisely with respect to the rotor axis, end float must be minimised, and the effect of any misalignment of the bearings is amplified at the outer diameter of the rotor. For example, a misalignment of one degree in the running axis of the rotor with respect to its true axis results in a displacement of almost 0.050 in. at a rotor diameter of six inches. So, while small running clearances may be achieved in precision-made disc motors, in which the stator and rotor are mounted in the same housing, for applications in which the stator

and rotor are separate items and are mounted independently, much greater airgaps usually obtain. Sadler and Davy[19] recommended clearances of around 2 mm (0.080") for industrial drives of the latter type in which linear stators were used to drive disc rotors. In addition to this, two airgaps are required in double sided machines so that the effective magnetic airgap is approximately equal to twice the running clearance; and in many single sided motor applications the stator and rotor will be separated from each other by a screen, which also results in increased airgap.

It may be concluded therefore that disc reluctance motors will often have to operate with larger airgaps than usually encountered in equivalent cylindrical machines, and this will have an adverse effect on their mean value of magnetising reactance, and on the X_d/X_q ratio. For example, if the running clearance, g_1, in a salient pole machine is doubled and g_2, the airgap length in the interpolar region, remains the same so that the ratio g_1/g_2 changes from 0.1,say, to 0.2, then for a pole arc to pole pitch ratio of 0.5, it can be shown from equations 2.5 that the x_d/x_q ratio is reduced by 25% from around 3.2 to 2.4. The mean value of the magnetising reactance is also reduced which further accentuates the impact of the leakage reactance on the X_d/X_q ratio.

From this brief discussion on the effect of the disc motor geometry on the general behaviour of a reluctance motor it appears that the increased leakage reactance and increased airgap of most configurations can worsen their performance, but that it is physically possible to provide low resistance rotor cages for some of them in order to improve their synchronising capability. A combination of reduced rotor resistance and increased leakage reactance in disc motors may usefully serve to limit their starting currents to acceptable levels.

Chapter One and Section 2.2 above suggest that innumerable designs for disc reluctance motors might be conceived. They would comprise various combinations of single or double sided axial or transverse flux stators, with sheet or cage rotors that have stationary or rotating backing iron and which incorporate one or more of the several types of reluctance features. Consideration is given to the likely alternatives in the following sections in order to identify the preferred configurations which offer good operating characteristics and/or simple manufacturing methods.

2.5 Single sided disc geometry reluctance motors

It can be assumed that a sensible single sided disc reluctance motor uses a rotor with attached backing iron. For this configuration gives the simple face-to-face assembly of stator and rotor with which disc motors are often identified. (Detached rotor backing iron would give the motor the same general construction as a double sided motor without the benefits accruing from the use of two sets of stator windings: it is therefore not entertained as a viable alternative). At synchronous speed the rotor of a single sided motor therefore experiences a strong magnetic pull towards the stator, which must be accommodated by a thrust bearing on the rotor shaft. This appears to constitute its main disadvantage.

Many alternative methods of introducing magnetic asymmetry into the disc rotor could be employed: these might include salient poles, flux guides or barriers and discrete segments. It is generally the case that salient pole reluctance motors give the worst overall performance, and it has therefore been assumed that the single sided disc motor will use segmented or flux guided rotors.

Several forms of disc motor stator have been identified, the axial flux stator in Fig. 1.2 and the 'L' core transverse flux stator in Fig.1.16 being the most prominent. As the airgap flux patterns emerging from both these stators will, to a first order, appear the same to the rotor, they can be considered simply as alternative methods of construction for the same basic stator. The topological study of single sided disc reluctance motors can therefore concentrate on the rotor geometries which are most compatible with this airgap flux pattern.

The 'C' core transverse flux stator in Fig. 1.12 is not considered to be a worthwhile alternative to the above stators for the present applications because it appears to offer no functional advantages to compensate for its greater constructional complexity.

One principal form of rotor emerges as the most effective for use with a single stator, and this is a segmented rotor. Illustrated in a developed form in Fig. 2.6(a), it utilises axial (i.e. circumferential) rotor flux paths and the segments can be made from a circular strip-wound core. Its methods of construction are consequently very similar to those required for an axial flux stator, and typically, the laminated rotor segments could be cast in aluminium in a non-magnetic annular channel.

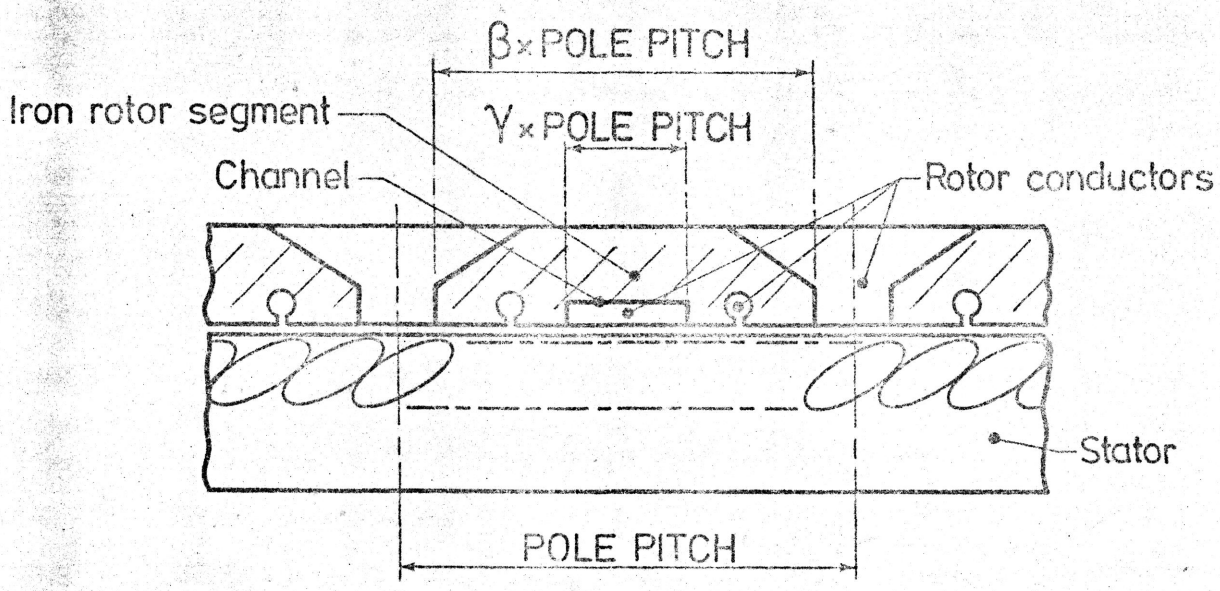

(a) SINGLE-SIDED, SEGMENTED-ROTOR, AXIAL FLUX, DISC RELUCTANCE MOTOR

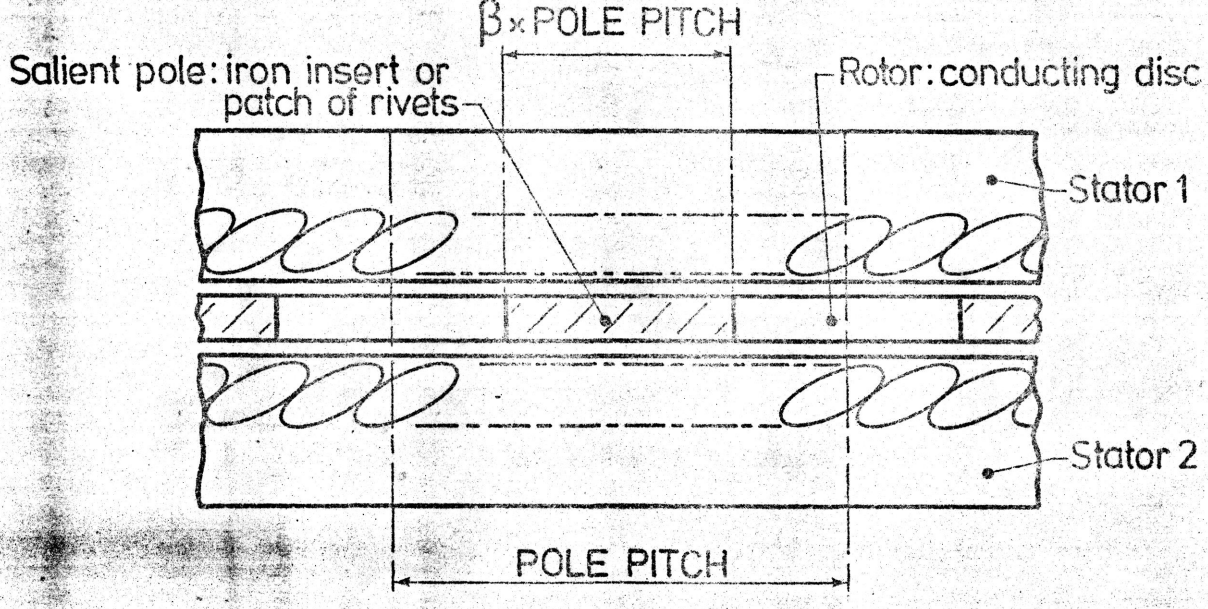

(b) DOUBLE-SIDED, SALIENT-POLE, AXIAL FLUX, DISC RELUCTANCE MOTOR

Fig. 2.6 ESSENTIAL FEATURES OF ALTERNATIVE DESIGNS FOR DISC GEOMETRY RELUCTANCE MOTORS

Gramme ring rotor current paths can be incorporated quite simply by this method. The performance of this type of motor is likely to be comparable to that of its cylindrical counterparts, with the exception of the effect of higher primary leakage reactance, and it can therefore be expected to function very effectively as a reluctance motor. A prototype motor of this type is described in Chapter 5 where theoretical and experimental performance data are presented.

Although the segmented rotor appears to be the simplest form for use with single sided motors (equivalent "essential barrier"[10] and "axially laminated"[2] rotors require more complex methods of construction, and in any case approximate very closely to segmented rotors in the disc geometry) it is nevertheless relatively difficult to make, and is not well-suited to low-cost production methods.

However one improved motor configuration also exists: it makes use of the stator and rotor shapes illustrated in Fig. 1.16. This is the motor which has the slightly cone shaped airgap and is able to utilise disc laminations for the rotor. For all intents and purposes, therefore, the rotor is the same as the rotor for a cylindrical machine, except for its non-uniform diameter. This being the case, it can be modified quite simply to include "essential barrier"[10] reluctance features, which are illustrated in Fig. 2.2(f). As in the case of the induction motor, the present reluctance version can consequently be made, except for the stator windings, from single punchings or pressings. In addition, the thrust force on the rotor shaft becomes the resolved component of the normal force between the stator and rotor surfaces. As the optimum angle of the cone with respect to the airgap plane of a pure disc motor would be around 30° to ensure uniform loading of the magnetic circuits of the stator and rotor, there will consequently be a reduction in this thrust force of almost 15%.

While more complex rotor shapes can be designed if solid iron is used instead of laminations, they would require relatively expensive production methods, and the cone shaped motor, with laminated rotor remains the most likely contender for a cheap, effective disc reluctance motor.

2.6 Double sided disc geometry reluctance motors

Three principle configurations for double sided stators were identified in Chapter 1. They consisted of:

- two axial flux stators (Fig. 1.3(c)).
- two 'L' core transverse flux stators (Fig. 1.16).
- the 'C' core double sided transverse flux disc stator with interconnected magnetic circuits (Fig. 1.18).

In so far as each of these configurations produces a rotating flux pattern which is directed normally across the airgap, they can therefore be considered simply as alternative methods of construction for one basic form of double sided disc motor. As with the single sided motor, differences between these stators that could be detected by the rotor would be, for present purposes, of a secondary nature.

A double sided disc motor can be considered as a stator plus a rotor with detached backing iron, the backing iron being stationary and supplied with a winding to form the second stator. Flux therefore passes directly through the rotor which itself contains no backing iron. An induction rotor consists of conducting material, in the 'sheet' rotor case; or conducting material plus 'teeth' in the 'cage' rotor (Section 1.3.2). Viewed in this way, it is apparent that a reluctance rotor that utilises the devices of flux guides, or flux barriers, or 'segments', cannot be conceived or constructed in a true double sided motor configuration. It seems therefore that the salient pole type of reluctance rotor is the only form of reluctance rotor that can be used with a double sided motor, and the general arrangement of it is illustrated in developed form in Fig. 2.6(b). The salient pole disc rotor can be considered to be derived either from a 'sheet' rotor, into which iron saliences have been inserted, or from the 'cage' rotor, from which some 'teeth' have been removed: the resulting form of rotor is the same. A rotor constructed by the latter method has been tested by Capaldi[20], but a simpler method of manufacture is achieved by adding patches of steel rivets[21] to a 'sheet' rotor.

This form of rotor is equivalent to a low inertia reluctance machine described by Lawrenson[22]. It is the lowest inertia form of disc rotor, but its inertia clearly exceeds by a considerable margin that of its

cylindrical counterpart. However, the disc shape is likely to be a more stable configuration for higher speed operation than the salient pole version of the 'drag-cup' rotor.

Section 2.4 above outlined the implications of leakage reactance and the two airgaps on the operation of double sided disc reluctance motors. It is therefore interesting to investigate the approximate characteristics that can be obtained from such motors. This will be done in terms of its X_d/X_q ratio. In the first instance, it is assumed that the pole arc to pole pitch ratio, β, is 0.5, that the running clearance between one side of the rotor and a stator surface, $0.5g_1$, is 0.020 inches (0.5 mm), and that the leakage factor k_1 of equation 2.7 above is 0.15. The maximum theoretical value of X_d/X_q that can be obtained if the distance between the stator surfaces, g_2, is very large compared with g_1 (i.e. the rotor is infinitely thick, and $g_1/g_2 = 0$) can be calculated from equations 2.7 above to be 2.9. This reduces for thinner rotors to the results tabulated below:

Rotor Thickness (inches)	g_1/g_2	X_d/X_q
1.0	0.04	2.7
0.5	0.08	2.4
0.25	0.16	1.8

They indicate that rotors down to half an inch thick are approximately representative of 'infinitely thick' rotors, but the reduction in X_d/X_q accelerates as thicknesses become one-quarter inch thick and less. Thick rotors are therefore required for an X_d/X_q ratio in excess of 2. If the rotor conductor thickness is maintained equal to the thickness of the iron rotor portions its resistance will be very low, and this will help to ensure that the motor has good synchronising properties. These results neglect the effect of fringe fields between the stator cores which will tend to increase the value of X_q more than the value of X_d and consequently reduce the X_d/X_q ratio slightly.

It appears therefore that double sided salient pole disc reluctance motors can never display X_d/X_q ratios greater than three (for $\beta = 0.5$), and that ratios in the range 1.5 to 2.0 are more likely to be feasible. The thick rotors which are required to achieve the upper section of the

range will, however, help to ensure good synchronising properties. These considerations do not make for a low cost machine.

A significant practical advantage of the double sided reluctance motor compared to the single sided version lies in the fact that the normal forces between the rotor and the stator balance out under ideal conditions, to leave zero net thrust force on the rotor shaft. Nevertheless a magnetic force exists between the two stators which must be mounted and secured to withstand it.

The design and analysis of a prototype double sided salient pole motor are described in Chapter 3, and experimental and theoretical results for it are reported in Chapter 4.

Chapter 2: References

1. Anderson, A.F., "A New Type of Reluctance Motor", IEE Students Quarterly Journal, September 1968, pp. 19-24.

2. Cruickshank, A.J.O., Anderson, A.F. and Menzies, R.W., "Theory and Performance of Reluctance Motors with Axially Laminated Anisotropic Rotors", Proc.IEE, 1971, 118, (7), pp. 887-894.

3. Bowers, B., "The Eccentric Electromagnetic Engine - a Chapter From the Very Early History of the Electric Motor", Electronics and Power, July 1972, pp. 269-272.

4. Kostko, J.K., "Polyphase Reaction Synchronous Motors", Journal AIEE, 1923, November, pp. 1162-1168.

5. Trickey, P.H., "Performance Calculations on Polyphase Reluctance Motors", Trans.AIEE, 1946, April, pp. 191-193.

6. Talaat, M.E., "Steady-state and Transient Synthesis of 3-Phase Reluctance Motors", Trans.AIEE, 1951, 70, pp. 1963-1970.

7. Lin, C.Y., "Characteristics of Reluctance Machines", Trans.AIEE, 1951, 70, pp. 1971-1977.

8. Risch, N.O., "Segmented Rotor Core Lamination for Use in a Synchronous Induction Motor.", US Patent 276 9108, 1956.

9. Lawrenson, P.J., "Development and Application of Reluctance Motors", Electronics and Power, June 1965, p.195-198.

10. Fong, W., "New Type of Reluctance Motor", Proc.IEE, 1970, 117, (3), pp.545-551.

11. Petrov, G.N., "Electric Machines, Part II - Induction and Synchronous Machines", National Electric Power Publisher, Moscow 1963 (in Russian).

12. Lawrenson, P.J., "Semipole Reluctance Motors", Electronics Letters, 1968, 4, (8), pp. 376-377.

13. Stephenson, J.M. and Lawrenson, P.J., "Average Asynchronous Torque of Synchronous Machines, with Particular Reference to Reluctance Machines", Proc.IEE, 1969, 116 (6), pp. 1049-1051.

14. Lawrenson, P.J. and Mathur, R.M., "Pull-in Criterion for Reluctance Motors", Proc.IEE, 1973, 120 (9), pp. 982-986.

15. Lawrenson, P.J. and Mathur, R.M., "Asynchronous Performance of Reluctance Machines Allowing for Irregular Distributions of Rotor Conductors", Proc.IEE, 1972, 119, (3), pp. 318-324.

16. Lawrenson, P.J. and Agu, L.A., "Theory and Performance of Polyphase Reluctance Machines", Proc.IEE, 1964, 111, (8), pp. 1435-1445.

17. Lawrenson, P.J. and Gupta, S.K., "Developments in the Performance and Theory of Segmental-Rotor Reluctance Machines", Proc.IEE, 1967, 114, (5), pp. 645-653.

18. Eastham, J.F., "Secondary for a Linear Induction Motor", U.K. Patent Application: 813/74.

19. Sadler, G.V. and Davey, A.W., "Applications of Linear Induction Motors in Industry", Proc.IEE, 1971, 118, (6), p. 765.

20. Capaldi, B., "The theory and Performance of a.c. Axial Flux Machines", Ph.D. Thesis 1973, University of Warwick.

21. Williams, F.C. and Laithwaite, E.R., "A Brushless Variable Speed Induction Motor", Proc.IEE, 1954, 102A, pp. 203-210.

22. Lawrenson, P.J. and Agu, L.A., "Low Inertia Reluctance Machines", Proc.IEE, 1964, 111, (12), pp. 2017-2025.

CHAPTER THREE

The Design and Analysis of a Double Sided Salient Pole Axial Flux Disc Reluctance Motor

3.1 Introduction

[illegible] topological characteristics of disc reluctance motors in Section 2.6 above suggested that a double-sided reluctance motor, in which the normal forces on the rotor were largely self-cancelling, could only operate with a salient-pole type of reluctance rotor. For this reason, the present chapter, and the following one, describe the analysis, design and testing of a prototype motor with this configuration. The design of the prototype is described before the analysis is undertaken in order that the features that must be taken into account are known more precisely.

The behaviour of a reluctance motor contains three distinct operating modes: start-up, under the influence of induction torques; synchronisation, where the subsynchronous pulsations of reluctance torque try to synchronise the rotor; and synchronous operation, relying on pure reluctance torque. Complete prediction of the performance of this type of motor under transient and steady state conditions therefore creates considerable difficulties.

Arockiasamy[1] developed a numerical technique for calculating the performance of electrical machines. It used a circuit approach, representing the machine by sets of electromagnetically coupled electric circuits, and solved the resulting voltage equations by step-by-step methods. This general method was adopted for the present analysis, but has been extended to take account of sheet rotors containing salient poles. These have a position-dependent effect on the magnetic circuit of the stator, and distort the current flow patterns in the rotor. Lawrenson et al[2] have described a similar method for segmented-rotor machines with discrete rotor conductors, but they adopted a two axis model for the motor. In the present case the stator phases have been treated separately in order to handle the space harmonics of the windings more readily.

Numerical methods enable complex problems to be solved more easily on a computer, and have therefore been used both for the calculation of the circuit parameters and for the solution of the machine equations. From the outset the method was designed for use with a digital computer. The result was computer programs which could handle a wide variety of motor designs and predict their performance under steady state, transient and fault conditions at both synchronous and asynchronous speeds.

3.2 Description of prototype motor

The general arrangement of the stators and rotor of an electrically double sided disc reluctance motor is illustrated in Fig. 1.3(a): a salient pole disc rotor is positioned between two stators which are interconnected so that the flux is directed normally across the airgap between them.

The stators for a prototype motor were designed in a conventional manner. A stator core, and a detailed semi-closed slot profile are shown in Fig. 3.1. The core was strip wound, like a swiss roll, using 0.013 inch thick grain oriented silicon steel. Its principal dimensions are:

Stator Core Dimensions

Inner diameter = 4.0 in
Outer diameter = 6.0 in
Total depth = 2.0 in

Each core contains 24 non-skewed, semi-closed radial slots which were machined individually. The uniform slot width of 0.33 inches gave a slot width:slot pitch ratio of approximately 0.5 at the mean stator diameter. Identical conventional double layer windings were inserted in both stators. The winding details are:

Winding Details

Number of poles = 4
Number of phases = 3
Coil details = 38 turns of 20 swg enamelled copper wire
Coil pitch = 5/6 of pole pitch

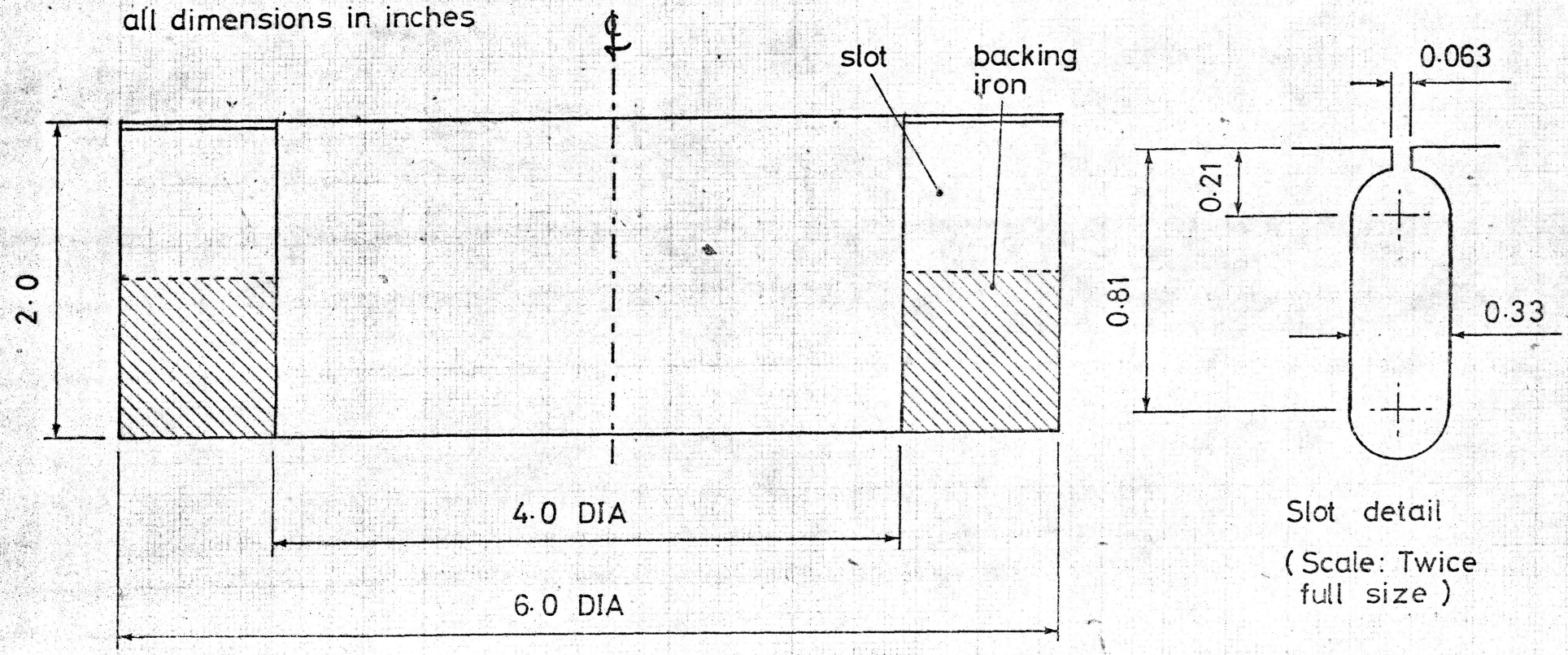

Diametral section of toroidal stator core
(Scale: Full size)

Slot detail
(Scale: Twice full size)

STATOR CORE

FIG. 3.1

The interconnection of the stator coils is illustrated in Fig. 3.2. The windings on the two stators were connected together in the manner shown in Fig. 3.3, i.e. with two phases on one stator interchanged with respect to the other so that the direction of rotation of the mmf wave is the same for both stators when they are set up face-to-face. The line terminals consequently appear on one stator, and the floating star point appears on the other. The double layer winding in each of the two stators effectively gives a four layer winding for the production of the airgap field, and the relative orientation of the two stators determines the shape of the airgap field. The stators were aligned so that slot number 1 of one stator was opposite slot number 24 of the other, and the resulting conductor pattern, which gives the best approximation to a sinusoidal winding distribution is illustrated in Fig. 3.4.

The salient pole disc rotor for the prototype machine is illustrated in Fig. 3.5. It consists essentially of a copper disc into which four pairs of arcuate iron portions have been inserted in a symmetrical pattern. These are to interact with the four pole stator field. Each pair of inserts extends over half a pole pitch (i.e. $\beta = 0.5$) which is generally recommended for the best all-round performance of a salient pole reluctance motor. A rotor thickness of approximately 0.2 inches was chosen. Greater thicknesses could be used to achieve higher X_d/X_q ratios but the chosen thickness enables the operating characteristics of this type of motor to be investigated satisfactorily and economically.

Two additional features of the rotor design require comment; they were both included to minimise the rotor resistance. They are:

- the thickened inner and outer rims of the conducting disc, (the average end ring factor according to the analysis of Russell and Norsworthy[3] is 3.2),
- and the radial copper rib between each pair of iron inserts.

The iron inserts were manufactured in the ideal arcuate shape for the prototype motor in order to facilitate the construction of a theoretical model which followed as closely as possible the physical shape of the rotor. The use of rivets for the rotor iron, as described in Section 1.3.2, would have been simpler to make but more difficult to analyse.

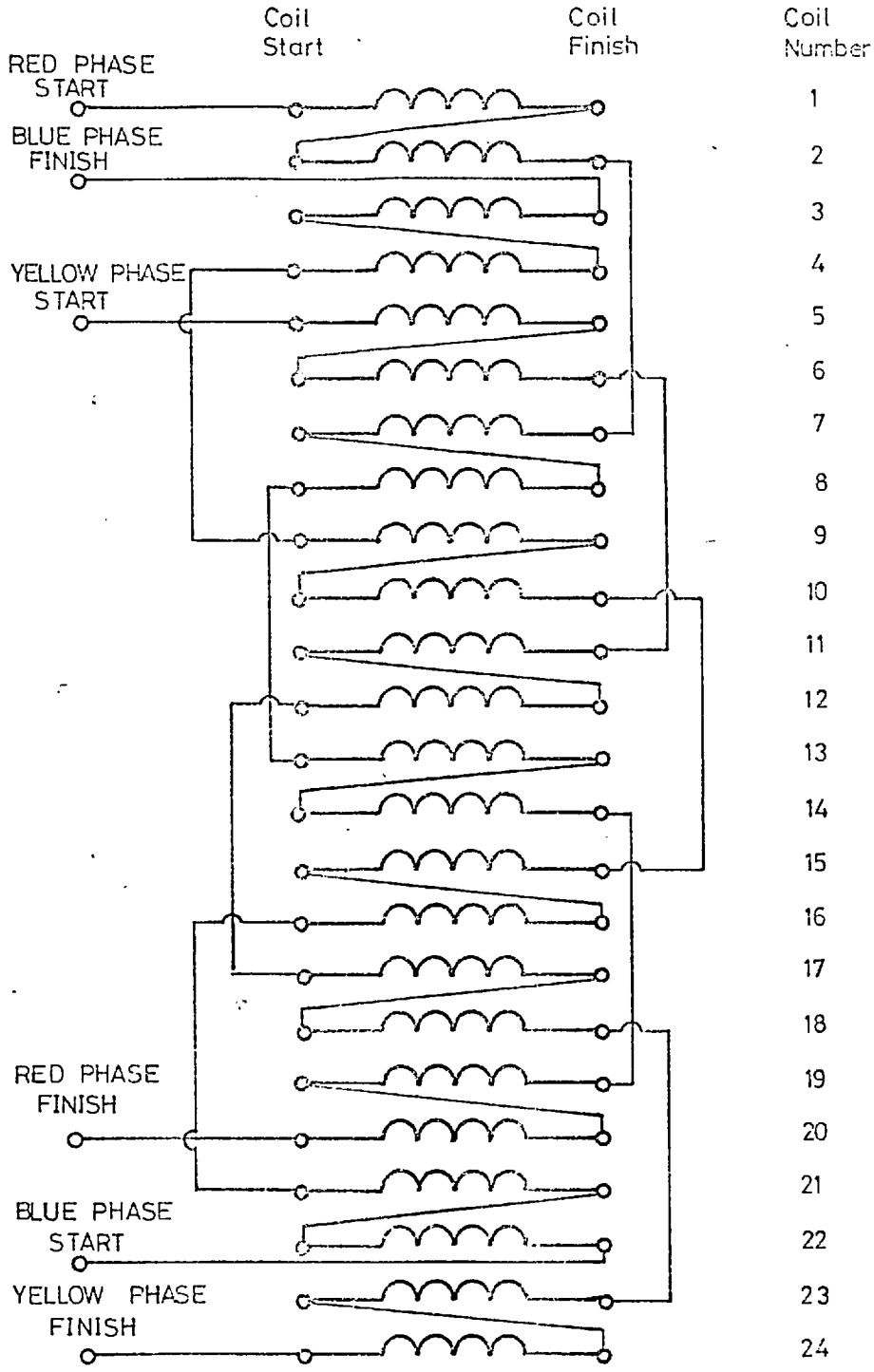

THE INTERCONNECTION OF STATOR COILS
(4- pole winding)

FIG. 3.2

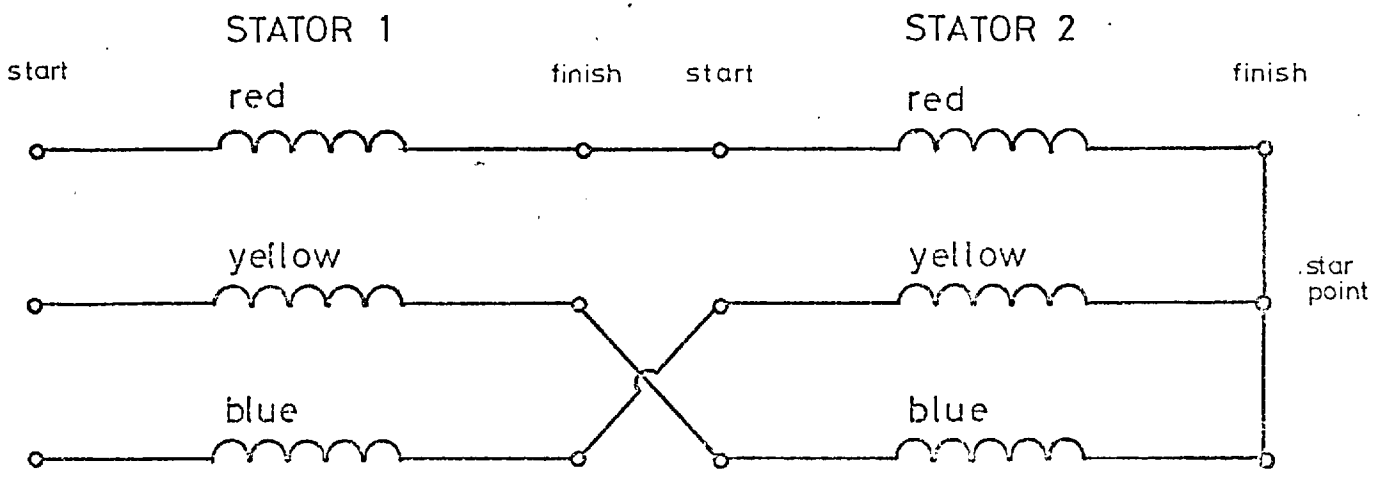

STATOR INTERCONNECTION

FIG. 3.3

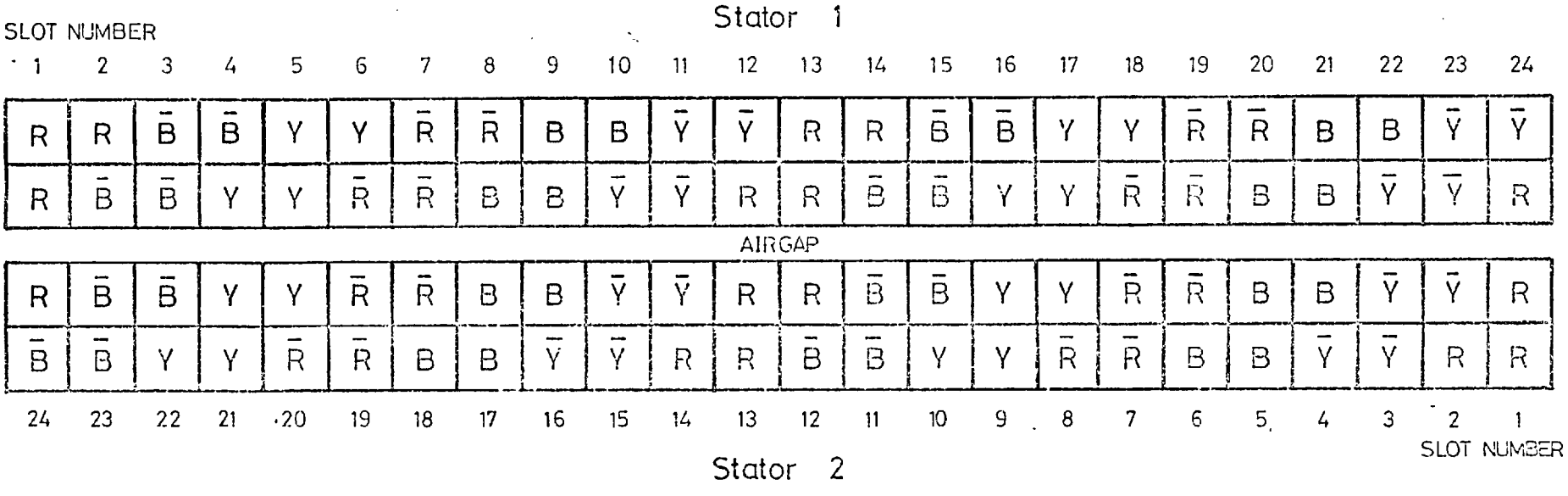

STATOR WINDING CONFIGURATION

4 - layer, 3 - phase, 4 - pole.

FIG. 3.4

all dimensions
in inches

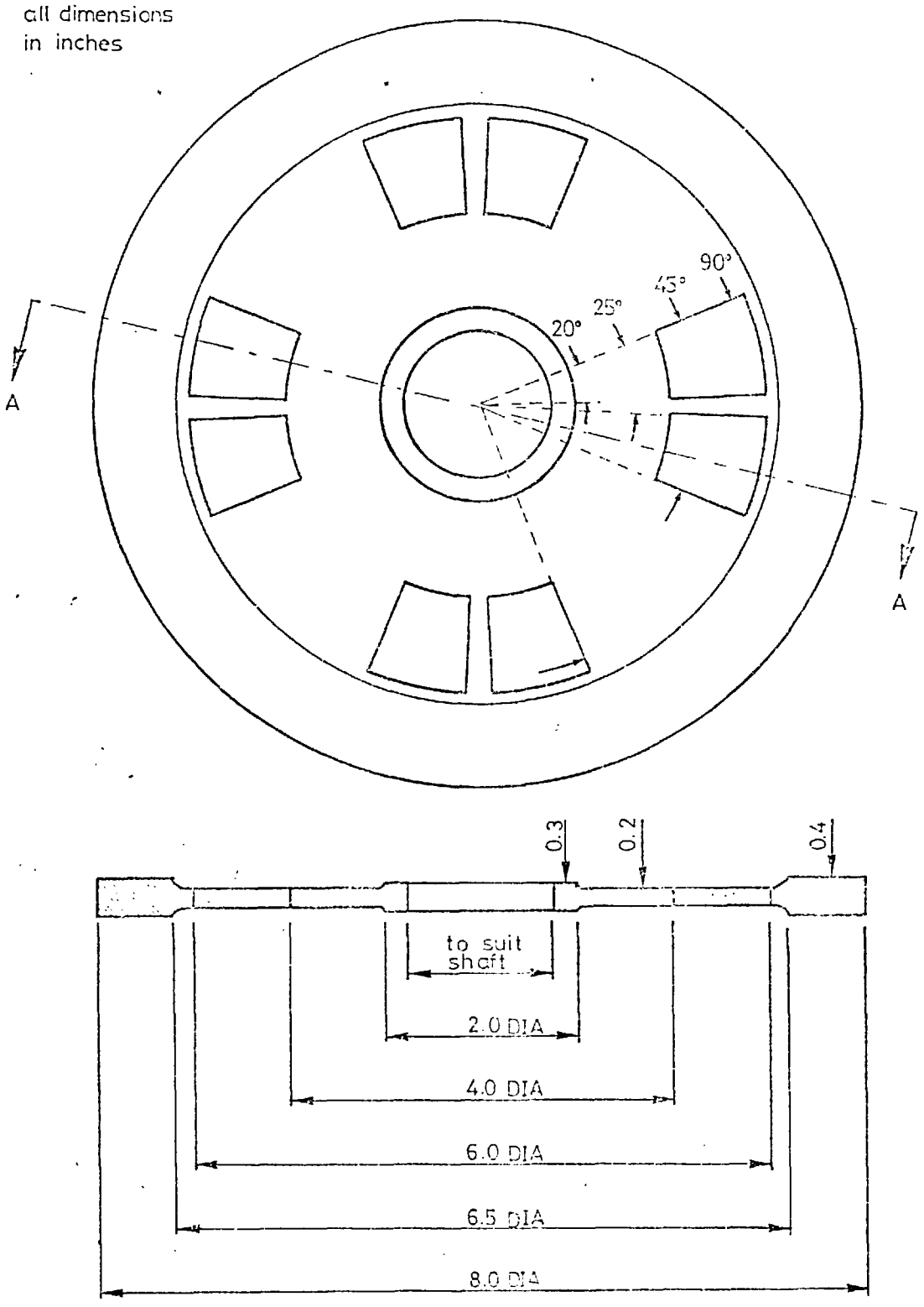

Section AA

MATERIALS:

Copper

Mild Steel

ROTOR DESIGN

FIG. 3.5

Photographs of the prototype motor are presented in Figs. 3.6, 3.7 and 3.8. Fig. 3.6 shows one stator mounted in its frame; Fig. 3.7 shows the copper rotor with iron inserts; and Fig. 3.8 shows the motor in an 'exploded' view.

3.3 Formulation of machine equations

3.3.1 Voltage equations

The voltage equations which describe the behaviour of an electric machine in terms of an equivalent set of coupled circuits can be written down quite easily, if at some length. They usually take the form:

$$v = iR + \frac{d}{dt}(\lambda) \qquad (3.1)$$

where v = instantaneous circuit voltage
i = instantaneous circuit current
R = circuit resistance
and λ = the total flux linkage for each circuit

Such equations are developed and explained in standard texts[4], and have been written out in full by Lipo and Krause[5]. The rate of change of the total flux linkages for the q^{th} circuit in a set of n can be re-written as:

$$\frac{d}{dt}(\lambda_q) = \sum_{r=1}^{n} \frac{d}{dt}(i_r M_{rq}) \qquad (3.2)$$

where M_{rq} is the mutual inductance between circuits r and q.

In which case, the set of n equations representing the n circuits can be summarised by:

$$v_q = i_q R_q + \sum_{r=1}^{n} \frac{d}{dt}(i_r M_{rq}) \qquad (3.3)$$

for all $q = 1, 2, \ldots n$.

In the present machine each of the stator phases is readily identifiable as a discrete circuit, but the rotor has no defined current paths. In order to overcome this problem, the rotor was represented by an equivalent electrical network. It is illustrated in Fig. 3.9 and

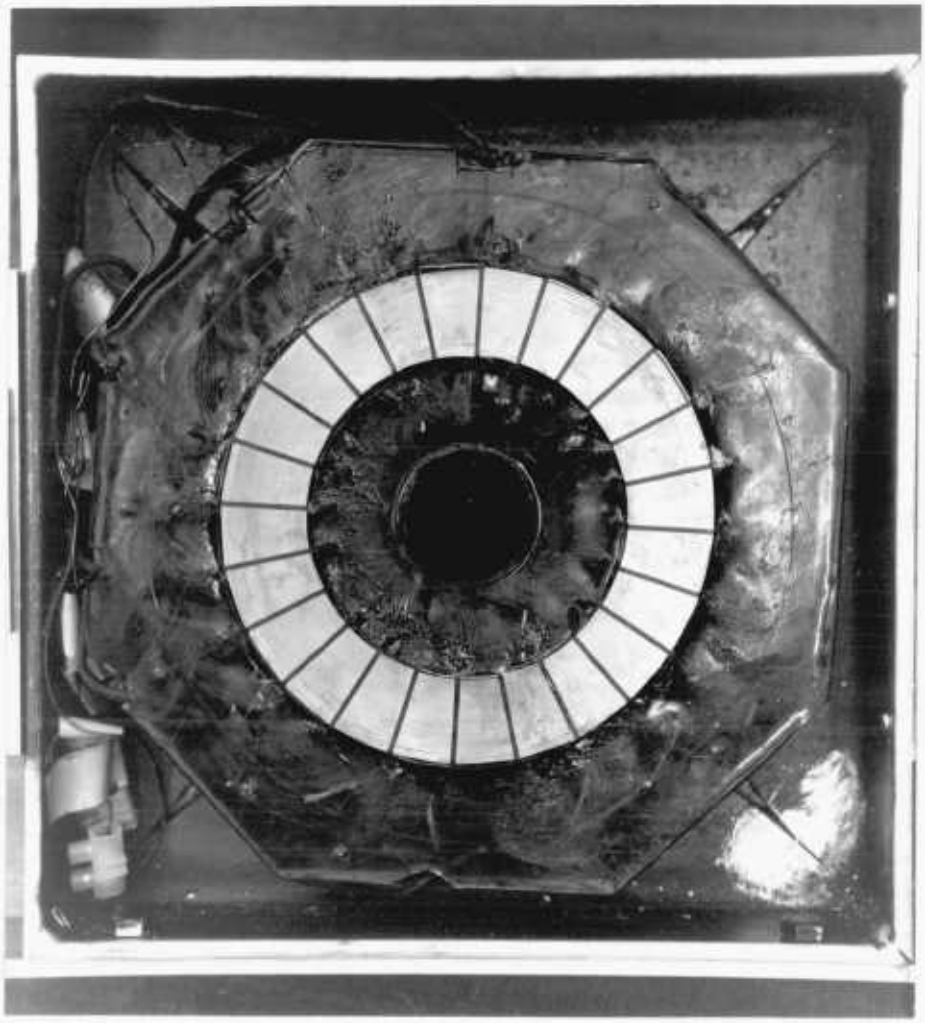

STATOR OF PROTOTYPE AXIAL FLUX DISC MOTOR

FIG. 3.6

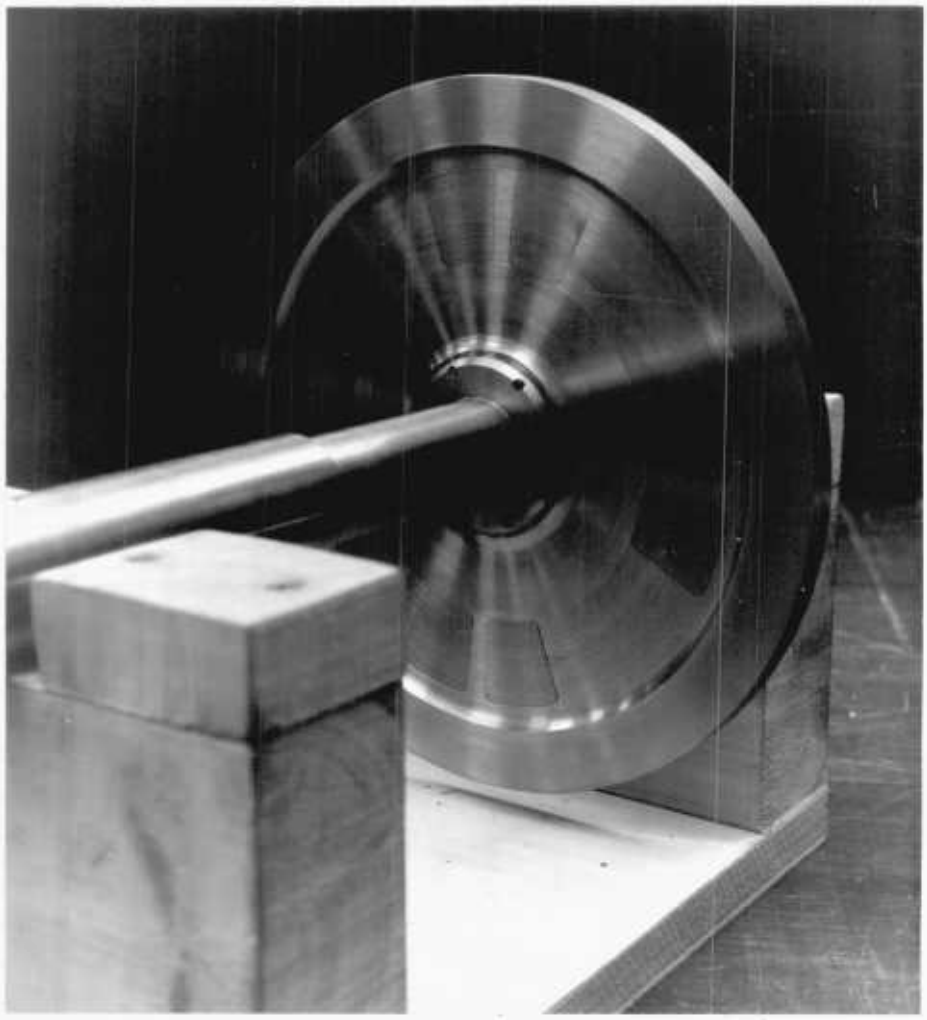

SALIENT-POLE ROTOR FOR DOUBLE-SIDED DISC RELUCTANCE MOTOR

FIG. 3.7

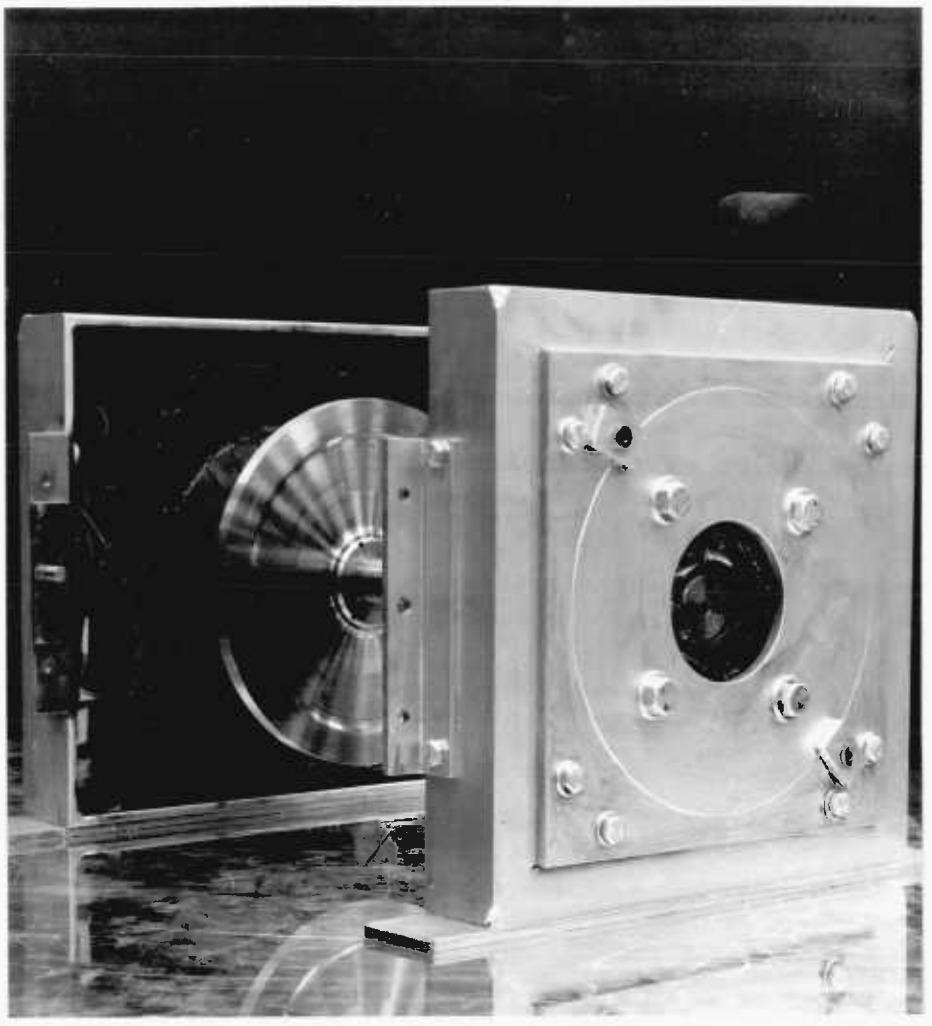

EXPLODED VIEW OF PROTOTYPE DOUBLE-SIDED SALIENT-POLE DISC RELUCTANCE MOTOR

FIG. 3.8

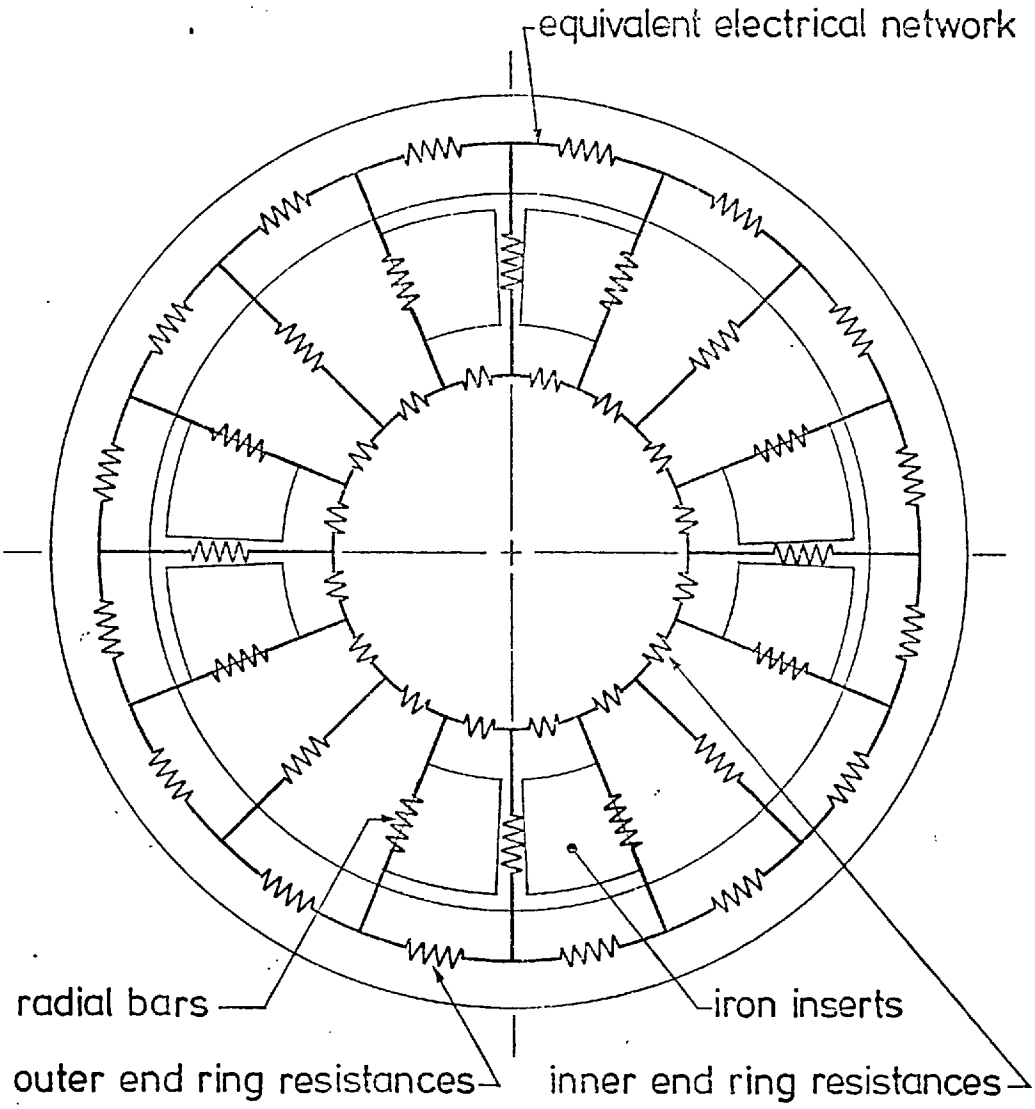

Fig.3.9 ILLUSTRATION OF THE NOTIONAL ELECTRIC NETWORK SUPERIMPOSED ON THE PHYSICAL ROTOR

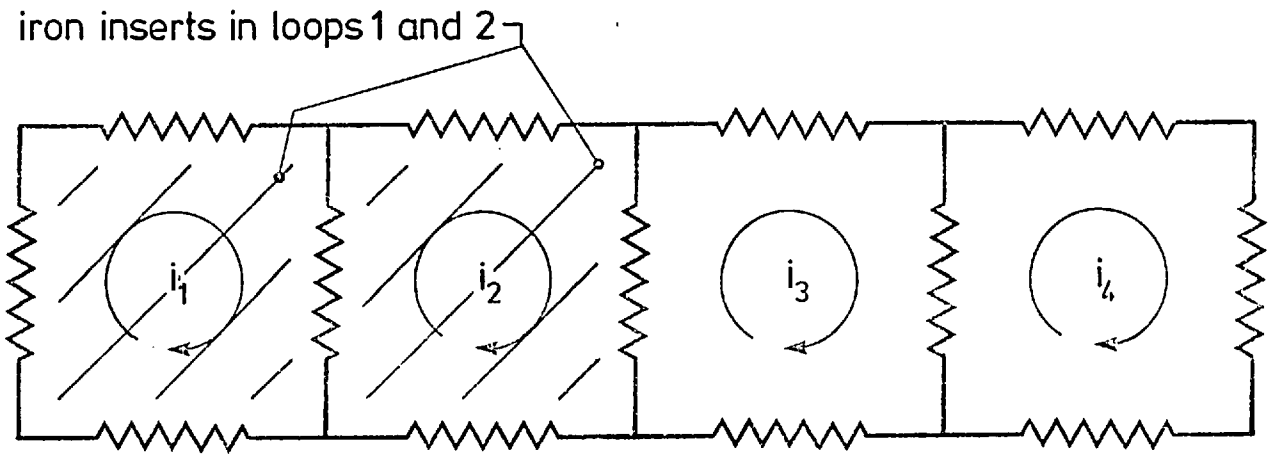

4-LOOP SYMMETRICAL PATTERN OF ROTOR MODEL

FIG. 3.10

consists of a 16 loop curvilinear ladder network arranged around the active annular section of the rotor. Each loop is coupled resistively with adjacent loops, and inductively with all others. This equivalent circuit model of the rotor is discussed further in Section 3.5 below.

The inductance terms that need to be inserted in equation 3.3 above therefore include the self and mutual inductances of the stator phases, the mutual inductances of the stator phases with the rotor loops, and the self and mutual inductances of the rotor loops. The self and mutual leakage inductances of the stator phases must also be included; the sheet rotor is assumed to produce negligible leakage flux.

By exploiting the symmetry of each pole of the rotor, voltage equations for just four of the rotor loops need be considered. These loops are illustrated in Fig. 3.10. Together with the three stator phases, these enable the machine to be represented by seven voltage equations.

The three voltage equations representing the stator phases can be written as follows:

$$\begin{aligned} v_R = {} & i_R R_R + \frac{d}{dt}(i_R M_{RR} + i_Y M_{RY} + i_B M_{RB}) \\ & + \frac{d}{dt}(i_R L_{RR} + i_Y L_{RY} + i_B L_{RB}) \\ & + \sum_{r=1}^{16} \frac{d}{dt}(i_r M_{rR}) \end{aligned} \qquad (3.4(a))$$

$$\begin{aligned} v_Y = {} & i_Y R_Y + \frac{d}{dt}(i_R M_{YR} + i_Y M_{YY} + i_B M_{YB}) \\ & + \frac{d}{dt}(i_R L_{YR} + i_Y L_{YY} + i_B L_{YB}) \\ & + \sum_{r=1}^{16} \frac{d}{dt}(i_r M_{rY}) \end{aligned} \qquad (3.4(b))$$

$$\begin{aligned} v_B = {} & i_B R_B + \frac{d}{dt}(i_R M_{BR} + i_Y M_{BY} + i_B M_{BB}) \\ & + \frac{d}{dt}(i_R L_{BR} + i_Y L_{BY} + i_B L_{BB}) \\ & + \sum_{r=1}^{16} \frac{d}{dt}(i_r M_{rB}) \end{aligned} \qquad (3.4(c))$$

where v, i, R, M and L are phase quantities,

suffices R, Y and B refer to the red, yellow and blue phases repectively,

and r = 1, 2, ... 16 refers to the 16 notional rotor loops.

The voltage equation for the q^{th} rotor loop takes the form:

$$v_q = i_q (2R_{b_q} + R_{oer_q} + R_{ier_q}) - i_{q-1}R_{b_q} - i_{q+1}R_{b_q}$$

$$+ \sum_{r=1}^{16} \frac{d}{dt} (i_r M_{qr})$$

$$+ \frac{d}{dt} (i_R M_{qR} + i_Y M_{qY} + i_B M_{qB}) \qquad (3.5)$$

where R_{b_q} is the bar resistance of the q^{th} loop

R_{oer_q} is the outer end ring resistance of the q^{th} loop

and R_{ier_q} is the inner end ring resistance of the q^{th} loop

These resistive elements of the rotor loops are indicated in Fig. 3.9.

The voltage equations, comprising three stator and four rotor equations of the type written out in equations 3.4 and 3.5 above, can be manipulated more conveniently in matrix format:

$$[v] = [R][i] + \frac{d}{dt}\{[M][I]\} \qquad (3.6)$$

- where [v] and [i] are column matrices. In the present case their order is seven, and elements 1, 2, 3, 4 refer to rotor loops, the fifth, sixth and seventh elements representing the red, yellow and blue phases respectively.
- where the resistance matrix [R] can be written by inspection as:

$$[R] = \begin{bmatrix} R_{T_1} & -R_{b_{12}} & 0 & R_{b_{16,1}} & 0 & 0 & 0 \\ -R_{b_{12}} & R_{T_2} & -R_{b_{2,3}} & 0 & 0 & 0 & 0 \\ 0 & -R_{b_{2,3}} & R_{T_3} & -R_{b_{3,4}} & 0 & 0 & 0 \\ R_{b_{4,5}} & 0 & -R_{b_{3,4}} & R_{T_4} & 0 & 0 & 0 \\ 0 & 0 & 0 & 0 & R_R & 0 & 0 \\ 0 & 0 & 0 & 0 & 0 & R_Y & 0 \\ 0 & 0 & 0 & 0 & 0 & 0 & R_B \end{bmatrix}$$

where $R_{T_r} = R_{b_{r-1,r}} + R_{b_{r,r+1}} + R_{oer_r} + R_{ier_r}$

the numerical subscripts to the bar resistances R_b refer to the rotor loops between which the bar is situated.

- where the inductance matrix, [M], can be written in full, as shown on the following page.

$$
M = \begin{bmatrix}
(M_{11} - M_{15} + M_{19} - M_{1,13})(M_{12} - M_{16} + M_{1,10} - M_{1,14})(M_{13} - M_{17} + M_{1,11} - M_{1,15})(M_{14} - M_{18} + M_{1,12} - M_{1,11}) & M_{1R} & M_{1Y} & M_{1B} \\
(M_{21} - M_{25} + M_{29} - M_{2,13})(M_{22} - M_{26} + M_{2,10} - M_{2,14})(M_{23} - M_{27} + M_{2,11} - M_{2,15})(M_{24} - M_{28} + M_{2,12} - M_{2,16}) & M_{2R} & M_{2Y} & M_{2B} \\
(M_{31} - M_{35} + M_{39} - M_{3,13})(M_{32} - M_{36} + M_{3,10} - M_{3,14})(M_{33} - M_{37} + M_{3,11} - M_{3,15})(M_{24} - M_{38} + M_{3,12} - M_{3,16}) & M_{3R} & M_{3Y} & M_{3B} \\
(M_{41} - M_{45} + M_{49} - M_{4,13})(M_{42} - M_{46} + M_{4,10} - M_{4,14})(M_{43} - M_{47} + M_{4,11} - M_{4,15})(M_{44} - M_{48} + M_{4,12} - M_{4,16}) & M_{4R} & M_{4Y} & M_{4B} \\
{}^{4}M_{1R} & {}^{4}M_{2R} & {}^{4}M_{3R} & {}^{4}M_{4R} & (M_{RR} + L_{RR})(M_{RY} + L_{RY})(M_{BR} + L_{BR}) \\
{}^{4}M_{1Y} & {}^{4}M_{2Y} & {}^{4}M_{3Y} & {}^{4}M_{4Y} & (M_{RY} + L_{RY})(M_{YY} + L_{YY})(M_{YB} + L_{YB}) \\
{}^{4}M_{1B} & {}^{4}M_{2B} & {}^{4}M_{3B} & {}^{4}M_{4B} & (M_{BR} + L_{BR})(M_{YB} + L_{YB})(M_{BB} + L_{BB})
\end{bmatrix}
$$

There are four distinct groups of terms in this inductance matrix:

- the left upper 4 x 4 block contains the self and mutual inductances of the rotor loops; these affect the magnitude and phase of the rotor currents, but do not depend upon the angular position of the rotor.

- the right upper 4 x 3 block and the left lower 3 X 4 block contain the mutual inductances between stator and rotor circuits; their cyclical variation with rotor position is responsible for the production of asynchronous (induction) torque.

- the right lower 3 x 3 block contains the total stator phase inductances (the main inductances plus their respective leakage inductances) which are modulated by the rotor saliency and are responsible for the synchronous (reluctance) torque component.

3.3.2 Torque equations

The equation for electrical torque, T_e, which can be derived by the application of the principle of virtual work to an expression for the energy stored in a set of mutually coupled coils is:

$$T_e = \frac{1}{2} \sum_{r=1}^{n} \sum_{q=1}^{n} i_r i_q \frac{d}{d\theta} (M_{rq}) \qquad (3.7)$$

where the suffices r and q relate to quantities for the r^{th} and q^{th} of a set of n coils.

Thus the electrical torque produced by a motor can be obtained from its circuit model providing the circuit currents, and the variation of the circuit inductances with rotor position are known. For the present application its advantage lies in the fact that both induction and reluctance torque components are calculated by the same method.

From the circuit model of the motor, described in Section 3.3.1 above, its total electrical torque is given by the expression:

$$T_e = \frac{1}{2} i_R^2 \frac{d}{d\theta}(M_{RR}) + \frac{1}{2} i_Y^2 \frac{d}{d\theta}(M_{YY}) + \frac{1}{2} i_B^2 \frac{d}{d\theta}(M_{BB})$$
$$+ i_R i_Y \frac{d}{d\theta}(M_{RY}) + i_Y i_B \frac{d}{d\theta}(M_{YB}) + i_B i_R \frac{d}{d\theta}(M_{BR})$$
$$+ 4 \sum_{n=1}^{4} i_n i_R \frac{d}{d\theta}(M_{nR}) + 4 \sum_{n=1}^{4} i_n i_Y \frac{d}{d\theta}(M_{nY}) + 4 \sum_{n=1}^{4} i_n i_B \frac{d}{d\theta}(M_{nB}) \quad (3.8)$$

where subscripts 1, 2, 3 and 4 refer to the four rotor loops which are considered explicitly.

3.3.3 Mechanical equations

The equation which relates the dynamic performance of the motor to the electrical torque produced by it takes the well known form:

$$T_e = T_b + J_k \ddot{\theta} \quad (3.9)$$

where T_e is the electrical torque produced by the motor
T_b is the total retarding torque produced by the load, and by the friction and windage forces
J_k is the total moment of inertia of the rotor plus the coupled load
and $\ddot{\theta}$ is the angular acceleration of the rotor

If the electrical torque produced by the motor can be calculated from equation 3.8 above, it is a relatively simple matter to predict its dynamic performance from equation 3.9. Solution of this equation, however, requires both the motor currents and the variation with position of the self and mutual inductances of the machine to be known. The first task therefore is to calculate the parameters of the equivalent circuit of the machine; this is done in Sections 3.4 and 3.5 below. The voltage equations (3.6 above) can then be solved for the motor currents, as explained in Section 3.7 below, and this ultimately enables the electrical and mechanical performance of the motor to be predicted.

3.4 Calculation of the stator circuit parameters

The manner in which the circuit parameters of the stator are calculated is described in this section. The required parameters are:

- the self and mutual inductances of the stator phases
- the self and mutual leakage inductances of the stator phase

and - the resistance of each phase winding

(The mutual inductances of the stator and rotor circuits are calculated in Section 3.5).

Measured values for the resistance of the stator windings, and for their leakage inductances were inserted into the theoretical model of the motor. Two reasons suggested that there was little to be gained from the use of theoretical values for these parameters:

- it is difficult to ascertain the true temperature of the windings during a test sequence (the windings were encapsulated), and hence it is difficult to allow for their increase in temperature in resistance calculations. More reliably, the resistance can be measured during the experimental work.

- leakage inductances are notoriously difficult to calculate precisely, even if the physical arrangement of the windings is assumed to be similar to the ideal configuration used for the calculations. In the present case the two stators were enclosed in steel frames (see Fig. 3.8) and the proximity of the iron has an effect on the leakage fields which is very difficult to predict. The self and mutual leakage inductances of the stator windings were therefore measured in the operating environment in order that reliable results could be used in the computations.

The main problem is to calculate the self and mutual inductances of the stator phases, and a difficulty arises because of the presence of the iron segments in the rotor. These create a non-uniform magnetic airgap and cause the stator inductances to be sensitive to rotor position.

The method used for these calculations has been designed to be "computer-friendly". It therefore relies heavily upon the principle of superposition, treating each phase winding coil-by-coil and summating the effects of the separate coils to find the overall properties of the winding. The principal steps in this procedure are as follows:

i) calculation of the flux density distribution produced by one short pitched stator coil in a uniform airgap

ii) calculation of the flux density distribution produced by a complete phase winding by summing the effects of the individual coils in the correct space-phase relationship

iii) modification of the flux density distribution in the uniform airgap to account for the effects of the iron rotor inserts. This is done for a range of rotor positions

iv) calculation of the self and mutual inductances of the stator phases by summing the appropriate flux linkages for each winding. This is also done for a range of rotor positions

The calculations for each of these steps is described in detail below.

i) Calculation of the flux density distribution produced by a short pitched coil in a uniform airgap

Fig. 3.11 illustrates a short pitched coil XY which spans β_p° (electrical). The current in each slot is assumed to be uniformly distributed across the width of the slot in an infinitely thin layer on the stator surface[6]. It therefore produces a trapezoidal instantaneous flux density distribution in an effective airgap of length 'g'. Flux densities b_1 and b_2 are indicated in Fig. 3.11; b_1 is greater than b_2 if β_p is less than the pole pitch.

By applying Ampere's Law, i.e. $\oint H.d\ell = I$ to the closed loop ABCD in Fig. 3.11, the following expression can be written down:

$$\frac{b_1(g + g_i)}{\mu_o} + \frac{b_2(g + g_i)}{\mu_o} = N_c\, i \qquad (3.10)$$

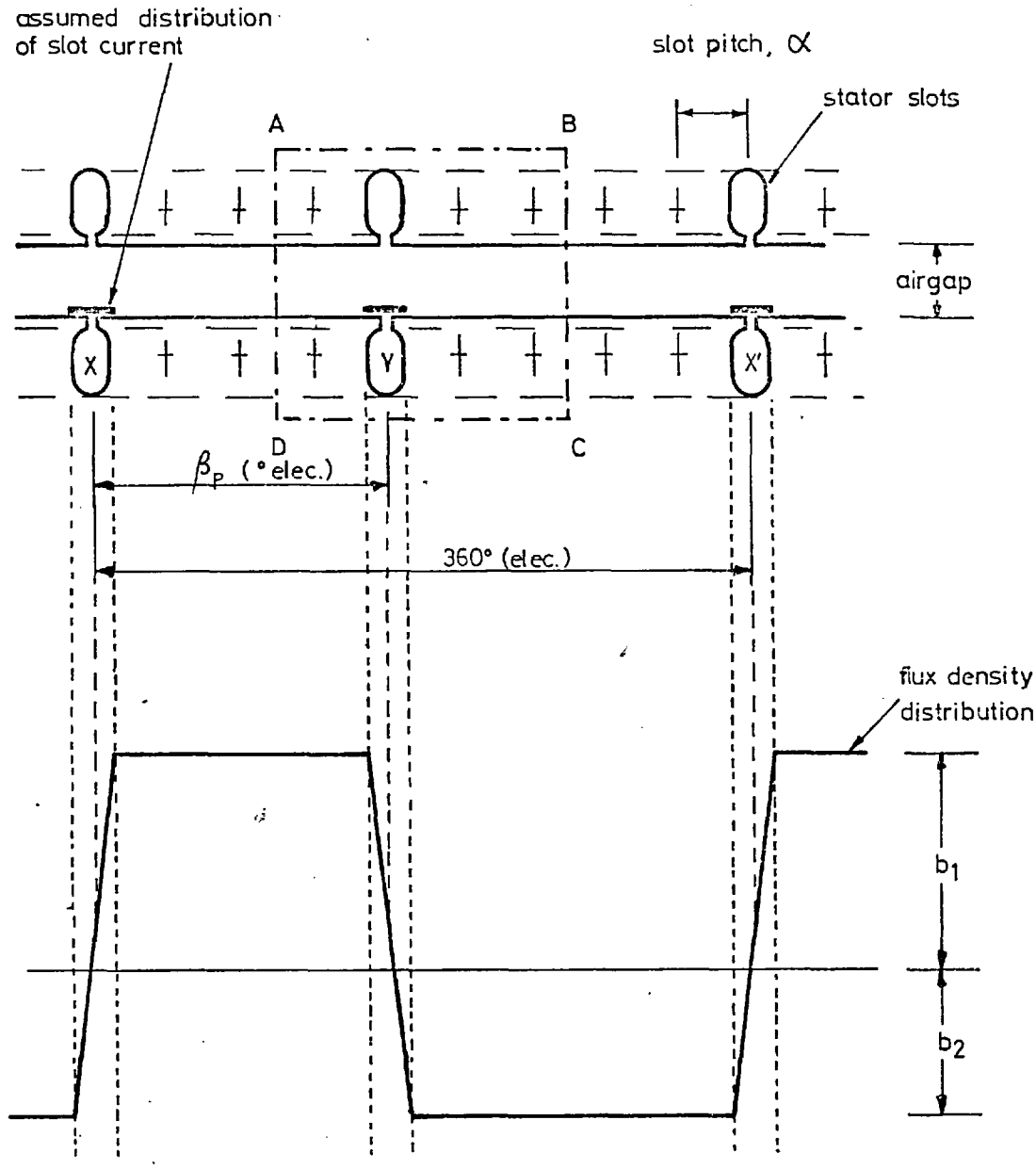

TRAPEZOIDAL FLUX DENSITY DISTRIBUTION FROM SHORT PITCHED STATOR COIL

FIG. 3.11

where N_c is the number of turns per coil

g is the airgap, including an allowance for the slot openings by the use of Carters Coefficient[7]

g_i is the equivalent airgap length of the flux path in the stator core

and i is the coil current

In fulfilment of the condition that the flux leaving one pole must enter an opposite pole, i.e. Div B = 0, the following equation also holds for the present case:

$$b_1 A_1 - b_2 A_2 = 0 \qquad (3.11)$$

where A_1 and A_2 are the active stator areas which correspond to a uniform flux density loading of b_1 and b_2 respectively.

i.e. $$A_1 = \pi D_m W \left(\frac{\beta_p}{360}\right) \qquad (3.12(a))$$

$$A_2 = \pi D_m W \left(\frac{360 - \beta_p}{360}\right) \qquad (3.12(b))$$

where D_m is the mean stator diameter

and W is the width of the stator core

Equations 3.10, 3.11 and 3.12 can be solved for b_1 and b_2, so that:

$$b_1 = \frac{N_c\, i\, \mu_o}{(g + g_i)} \left(\frac{360 - \beta_p}{360}\right) \qquad (3.13(a))$$

$$b_2 = \frac{N_c\, i\, \mu_o}{(g + g_i)} \left(\frac{\beta_p}{360}\right) \qquad (3.13(b))$$

which may be simplified to:

$$b_1 = B_c\,(360 - \beta_p) \qquad (3.14(a))$$

$$b_2 = B_c\,(\beta_p) \qquad (3.14(b))$$

where $$B_c = \frac{N_c\, i\, \mu_o}{360(g + g_i)}$$

For subsequent calculations the stator airgap is subdivided into 360 radial segments, each segment subtending an angle of 1° at the centre of the motor, and being denoted by subscript 'm', so that:

$$b_m = b_1 \quad \text{for} \quad m = 1, 2 \ldots \beta_p \qquad (3.15(a))$$

$$b_m = b_2 \quad \text{for} \quad m = \beta_p + 1 \ldots 360 \qquad (3.15(b))$$

ii) Calculation of the flux density distribution produced by a phase winding in a uniform airgap

The flux density distribution produced by a complete phase winding is obtained by summating the effects of each of the constituent coils at every radial segment, m. Thus for the winding of the test motor, which is shown on Fig. 3.4, the flux density which exists at each radial segment, m, due to each phase winding can be written down by inspection as:

$$\begin{aligned} B_{R_m} = {} & b_m + b_{(m-\alpha)} - b_{(m-6\alpha)} - b_{(m-7\alpha)} \\ & + b_{(m-12\alpha)} + b_{(m-13\alpha)} - b_{(m-18\alpha)} - b_{(m-19\alpha)} \\ & + b_m - b_{(m-5\alpha)} - b_{(m-6\alpha)} + b_{(m-11\alpha)} \\ & + b_{(m-12\alpha)} - b_{(m-17\alpha)} - b_{(m-18\alpha)} + b_{(m-23\alpha)} \end{aligned} \qquad (3.16(a)$$

$$\begin{aligned} B_{Y_m} = {} & b_{(m-4\alpha)} + b_{(m-5\alpha)} - b_{(m-10\alpha)} - b_{(m-11\alpha)} \\ & + b_{(m-16\alpha)} + b_{(m-17\alpha)} - b_{(m-22\alpha)} - b_{(m-23\alpha)} \\ & + b_{(m-3\alpha)} + b_{(m-4\alpha)} - b_{(m-9\alpha)} - b_{(m-10\alpha)} \\ & + b_{(m-15\alpha)} + b_{(m-16\alpha)} - b_{(m-21\alpha)} - b_{(m-22\alpha)} \end{aligned} \qquad (3.16(b))$$

$$\begin{aligned} B_{B_m} = {} & - b_{(m-2\alpha)} - b_{(m-3\alpha)} + b_{(m-8\alpha)} + b_{(m-9\alpha)} \\ & - b_{(m-14\alpha)} - b_{(m-15\alpha)} + b_{(m-20\alpha)} + b_{(m-21\alpha)} \\ & - b_{(m-\alpha)} - b_{(m-2\alpha)} + b_{(m-7\alpha)} + b_{(m-8\alpha)} \\ & - b_{(m-13\alpha)} - b_{(m-14\alpha)} + b_{(m-19\alpha)} + b_{(m-20\alpha)} \end{aligned} \qquad (3.16(c))$$

where B_{R_m} , B_{Y_m} , B_{B_m} are the flux densities at segment m due to the red, yellow and blue phase winding respectively, and α is the slot pitch.

The relationships in equation 3.16 depend upon the precise winding configuration that is under consideration, and include the effects of all winding space harmonics.

iii) Calculation of the flux density distribution in a non-uniform airgap

The iron rotor inserts in the motor under consideration create a non-uniform airgap, and the flux density is increased in the reduced airgap regions under them. As they are symmetrically positioned for one pole with respect to another, their effect can be taken into account by increasing the flux density of each of the radial segments that coincide with them by a using factor which corresponds inversely to the reduction in the airgap in this region. Thus the flux density of each radial segment, m, is increased by a 'gap factor', K_{gm}, which is given by:

$$K_{gm} = \frac{g + g_i}{g + g_i - t_r}$$

where t_r is the thickness of the iron insert.

It is particularly important that 'g_i' appears in this expression, for without it K_{gm} would be infinite when there was zero clearance between stator and rotor, i.e. when $g - t_r = 0$. As a result, in a practical machine, where $g - t_r$ is small compared with g, K_{gm} would tend to overestimate the local intensification of flux density under the iron inserts.

The modified flux density distribution produced by each phase winding when the iron rotor inserts are present can therefore be given in the form:

$$B'_{R_m} = B_{R_m} K_{gm} \qquad (3.18(a))$$

$$B'_{Y_m} = B_{Y_m} K_{gm} \qquad (3.18(b))$$

$$B'_{B_m} = B_{B_m} K_{gm} \qquad (3.18(c))$$

But K_{gm} must be defined with respect to a reference position on the stator, and will vary for each radial segment of the stator surface as the position of the rotor varies. Thus B_{R_m}, B_{Y_m} and B_{B_m} are independent of rotor position, but K_{gm} and hence B'_{R_m}, B'_{Y_m} and B'_{B_m} must be evaluated for a range of rotor positions. If K_{gm} is defined with respect to a reference position, m = 1, say - the flux density distributions produced by each phase winding when the rotor is displaced from the reference position by an angle 'δ_r' are given by:

$$B'_{R_m} = B_{R_m} k_{g(m-\delta_r)} \qquad (3.19(a))$$

$$B'_{Y_m} = B_{Y_m} k_{g(m-\delta_r)} \qquad (3.19(b))$$

$$B'_{B_m} = B_{B_m} k_{g(m-\delta_r)} \qquad (3.19(c))$$

for m = 1, 2, ... 360.

The $\delta_r = 0$ position used for computations was when the trailing edge of a pair of iron inserts was opposite slot 1 of stator 1 (see Fig. 3.4).

These flux density distributions enable the flux linkages, and hence inductances of the stator windings to be calculated.

iv) Calculation of the self and mutual inductances of the stator phase windings

The self inductance of a coil which comprises discrete conductors can be defined in simple terms as the flux linkage with itself per amp of current through itself. Similarly, the mutual inductance of the coil with another is equal to the linkage of flux produced by the first coil with the second coil, per amp of current flowing through the first coil. These definitions apply strictly when the coils consist of infinitely thin line conductors so that all the turns of a coil are linked by all the flux coupling it; it can be assumed to apply on average in the present case where the coils are embedded in the stator slots. The self and mutual inductances of the stator phase windings can therefore be calculated by summating the flux linked with each coil in a phase winding.

By this method the self inductance of the red phase winding, M_{RR}, can be obtained from the following summation series:

$$M_{RR} = \frac{N_c A_s}{i_R} \Big\{ \sum_{m=1}^{\beta_p} B'_{Rm} + \sum_{m=\alpha}^{\alpha+\beta_p} B'_{Rm} - \sum_{m=6\alpha}^{6\alpha+\beta_p} B'_{Rm} - \sum_{m=7\alpha}^{7\alpha+\beta_p} B'_{Rm}$$

$$+ \sum_{m=12\alpha}^{12\alpha+\beta_p} B'_{Rm} + \sum_{m=13\alpha}^{13\alpha+\beta_p} B'_{Rm} - \sum_{m=18\alpha}^{18\alpha+\beta_p} B'_{Rm} - \sum_{m=19\alpha}^{19\alpha+\beta_p} B'_{Rm}$$

$$+ \sum_{m=\alpha}^{\alpha+\beta_p} B'_{Rm} - \sum_{m=5\alpha}^{5\alpha+\beta_p} B'_{Rm} - \sum_{m=6\alpha}^{6\alpha+\beta_p} B'_{Rm} + \sum_{m=11\alpha}^{11\alpha+\beta_p} B'_{Rm}$$

$$+ \sum_{m=12\alpha}^{12\alpha+\beta_p} B'_{Rm} - \sum_{m=17\alpha}^{17\alpha+\beta_p} B'_{Rm} - \sum_{m=18\alpha}^{18\alpha+\beta_p} B'_{Rm} + \sum_{m=23\alpha}^{23\alpha+\beta_p} B'_{Rm} \Big\} \qquad (3.20)$$

where A_s is the surface area of one radial segment.

Similarly, the mutual inductance between the red and yellow phases, M_{RY}, can be obtained from:

$$M_{RY} = \frac{N_c A_s}{i_Y} \Big\{ \sum_{m=4\alpha}^{4\alpha+\beta_p} B'_{Rm} + \sum_{m=5\alpha}^{5\alpha+\beta_p} B'_{Rm} - \sum_{m=10\alpha}^{10\alpha+\beta_p} B'_{Rm} - \sum_{m=11\alpha}^{11\alpha+\beta_p} B'_{Rm}$$

$$+ \sum_{m=16\alpha}^{16\alpha+\beta_p} B'_{Rm} + \sum_{m=17\alpha}^{17\alpha+\beta_p} B'_{Rm} - \sum_{m=22\alpha}^{22\alpha+\beta_p} B'_{Rm} - \sum_{m=23\alpha}^{23\alpha+\beta_p} B'_{Rm}$$

$$+ \sum_{m=3\alpha}^{3\alpha+\beta_p} B'_{Rm} + \sum_{m=4\alpha}^{4\alpha+\beta_p} B'_{Rm} - \sum_{m=9\alpha}^{9\alpha+\beta_p} B'_{Rm} - \sum_{m=10\alpha}^{10\alpha+\beta_p} B'_{Rm}$$

$$+ \sum_{m=15\alpha}^{15\alpha+\beta_p} B'_{Rm} + \sum_{m=16\alpha}^{16\alpha+\beta_p} B'_{Rm} - \sum_{m=21\alpha}^{21\alpha+\beta_p} B'_{Rm} - \sum_{m=22\alpha}^{22\alpha+\beta_p} B'_{Rm} \Big\} \qquad (3.21)$$

Similar expressions can be written down for the other stator inductances. The limits of summation depend upon the winding configuration of the motor.

3.5 Calculation of the equivalent rotor circuit parameters

3.5.1 General method

The circuital representation of the rotor, the rotor model, requires a notional electrical network or mesh to be superimposed on the physical rotor geometry, as shown in Fig. 3.9. This network is then treated as follows:

- a regular pattern of currents is defined for a selected set of conducting circuits in the network. These must be capable of a unique solution.

- the resistance values of the resistive elements in the equivalent network are calculated from a knowledge of the physical dimensions and the electrical properties of the portion of the rotor they represent, and of the current distribution within them.

- the self and mutual inductances of the selected circuits are calculated from a knowledge of their respective magnetic circuits and current distributions.

With the resistances, and self and mutual inductances of the rotor circuits fully determined, these circuit parameters can be inserted in the set of voltage equations (equations 3.6 above) which describe the performance of the motor.

3.5.2 Factors which affect the choice of rotor model

Decisions need to be made regarding four principle features of the rotor model:

i) the physical shape of the conducting circuits which make up the equivalent electrical network representation of the rotor
ii) the number of such circuits
iii) the current pattern in the network
iv) the physical representation of the conductors which comprise the network

And there appear to be two prime considerations which affect the choice of these features. Firstly, it is important to maintain a close relationship between the electrical network and the physical rotor that it represents. This facilitates the interpretation and understanding of computed results and permits intermediate checks on the validity of the model to be undertaken more readily. It is achieved by choosing a network configuration which conforms to the natural geometry of the rotor, and by using a current pattern which reflects as closely as possible

the anticipated directions of current flow in the rotor. Secondly, it is desirable to choose the simplest electrical network that is consistent with effective rotor representation. Not only is it usually inadvisable to introduce undue complexity into any problem, but in the present method of solution each extra rotor circuit adds another equation to the set of simultaneous voltage equations that must be solved.

3.5.3 Description of the rotor model

With due regard for the considerations discussed above, the circuit model which was adopted to represent the rotor of the present double-sided salient pole disc reluctance motor is illustrated in Fig. 3.9. It can be seen to consist of sixteen conducting loops, each of which subtends 22.5° at the centre of the rotor, and which together make up a curvilinear ladder network around the active annulus of the rotor. Each loop consists of two radial bars and an inner and outer end ring portion. All loops carry a circulating current and they are arranged symmetrically around the iron portions set into the rotor. Adjacent loops are coupled resistively via the common radial bars, and all loops are coupled inductively via the common magnetic circuit provided by the stators. The loops are also coupled inductively with the stator phase windings. The resistances and the self and mutual inductances of the rotor loops are independent of rotor position if the effects of the slot openings are assumed to be negligible. In contrast, the mutual inductances of the rotor loops and the stator phases vary cyclically with rotor position. This feature is common to all induction motors.

Because four loops designated 1, 2, 3 and 4 form a symmetrical pattern which is repeated four times, once for each pole of the motor, the following relationships exist between the rotor currents:

$$\begin{aligned} i_1 &= -i_5 = i_9 = -i_{13} \\ i_2 &= -i_6 = i_{10} = -i_{14} \\ i_3 &= -i_7 = i_{11} = -i_{15} \\ i_4 &= -i_8 = i_{12} = -i_{16} \end{aligned} \qquad (3.22)$$

and just four equations can be used to describe the rotor behaviour completely.

Explanation of the present theoretical method has so far stated, without justification, that four rotor equations, representing four conducting loops per pole are used in the analysis. No evidence has been presented to indicate that this representation is adequate, and intuition might in fact suggest otherwise. For the radial conductors in the notional rotor loops are approximately one inch wide, and to represent these by line conductors gives a coarse model for the complex rotor under consideration.

There is no theoretical upper or lower limit to the number of loops by which the rotor can be represented. But there is every incentive to minimise the number of loops in order to reduce the computer time required for a solution of the machine equations. While the solution of these equations is described in detail in Section 3.7 below, it is sufficient at this stage to note that it requires the repeated inversion (usually many hundreds of times) of an n x n matrix, where n is the number of equations, and equals seven in the proposed analysis. As the computer time required to invert a matrix is proportional to more than the square of its order it is especially desirable that the minimum number of equations be used.

Preliminary investigations indicated that the simple rotor model, in which one radial rotor bar was represented by a line conductor, was indeed unsatisfactory, but an improved version was devised which raised the accuracy of the model to an acceptable level, without increasing the number of equations that need to be used. Results from the simple model, from the improved model, and from test work on the prototype motor are presented and discussed in Appendix I.

The technique used in the improved model was to subdivide the extensive bar conductors comprising each rotor loop into a concentric set of parallel-connected 'filament coils'. So that while parameters from only four rotor coils were finally required in seven machine equations, these parameters were calculated from the filament coils in a way that allowed for a non-uniform current distribution across the rotor conductors. The filament coils were assumed to be connected in parallel; the voltage equation for each filament coil was written down in terms of its resistance and self and mutual inductances; and this set of equations with an arbitrary excitation was solved for each of the filament currents.

These filament currents represent the current distribution across the rotor loops. It can now be taken as a better approximation than point conductors that this shape of current distribution will apply when all the coils are excited. From them the a.c. resistance of the loops is calculable, and their self and mutual inductances can be evaluated with due allowance for their distributed currents by a method described by Carter[8].

It can be seen that by this method the rotor parameters are calculated from the filament coils just once (or a few times if the effect of slip frequencies are to be taken into account) but that the step-by-step solution of the machine equations uses parameters relating to only four rotor loops.

It should be noted that this method is not unlike that used for the calculation of stator parameters in Section 3.4 above. In that case the effect of each stator coil connected in series contributed to a single equation for each phase. In this case the effect of each filament coil connected in parallel contributes to a single rotor loop equation.

The maximum width of a radial rotor bar is $\frac{1}{16}$ of the rotor circumference which subtends 22.5° at the centre of the rotor. The right hand radial bar of rotor loop number three (see Fig. 3.12 (a) and (b)) is this width as it is unrestricted by an iron rotor insert. The left hand bar of rotor loop number two, however, is 5° wide, due to the presence of the iron inserts. The size and position of each of the radial bars which make up rotor loops number one to four are tabulated below in terms of the 360 segments into which the rotor is subdivided (segment number one is at the trailing edge of a pair of iron inserts):

Loop Number	Extent of Radial Bars					
	L.H. Bar			R.H. Bar		
	From (segment Nos)	To	Width (°)	From (segment Nos)	To	Width (°)
1	350	360	11	21	25	5
2	21	25	5	46	56	11
3	46	55	10	57	78	22
4	57	78	22	80	90	11

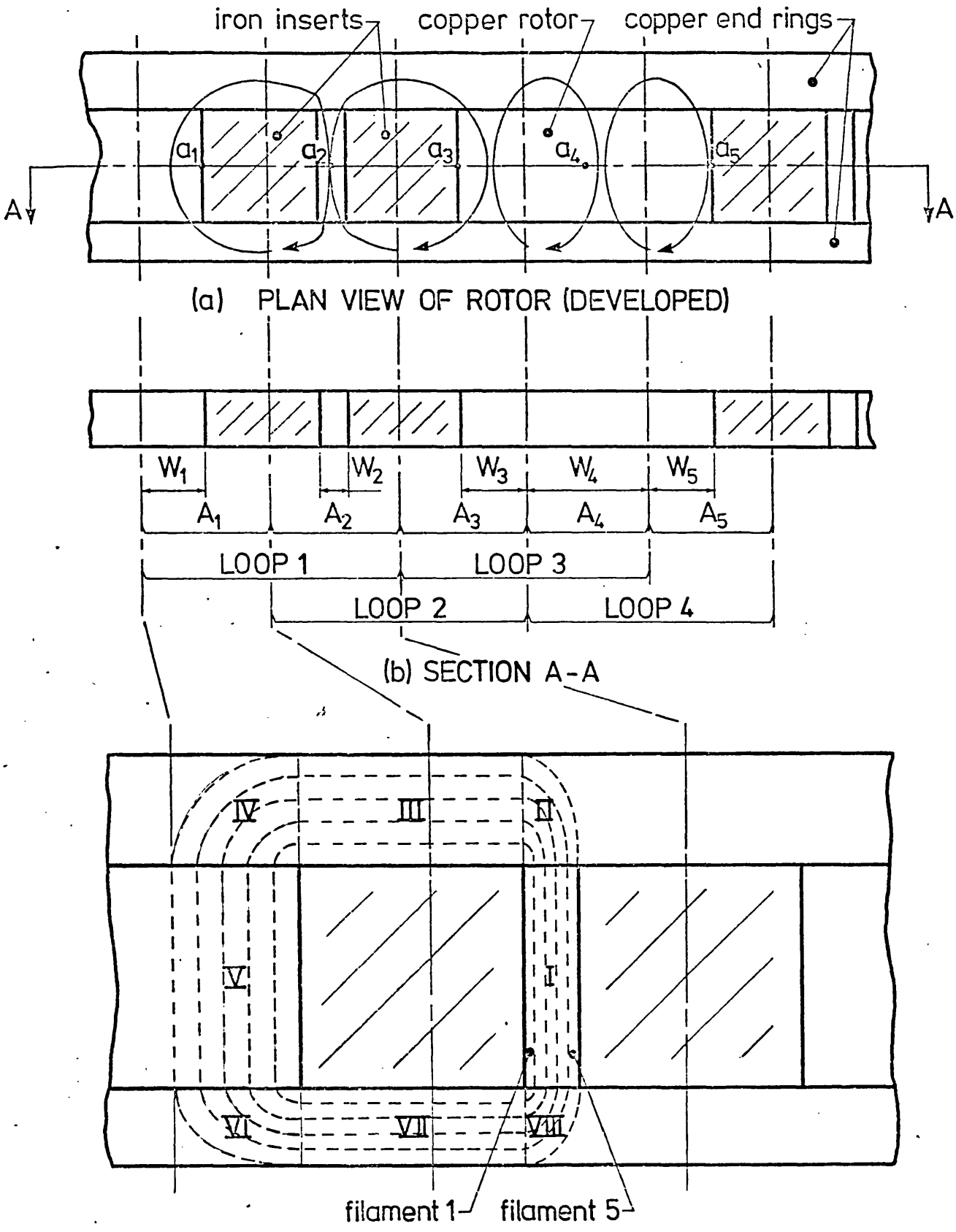

DETAILS OF ROTOR MODEL

FIG. 3.12

In the general case the right and left hand bars of a rotor loop have unequal widths. They are subdivided into a set of filament coils therefore in the manner shown in Fig. 3.12(c). The width of a filament coil in the right hand bar is made equal to one segment, i.e. one degree, and its width in the left hand bar and the end rings is scaled according to their respective widths.

From the tabulated details of the radial bars immediately above it is evident that one pole pitch of the rotor is effectively divided into a total of 49 filament coils. This gives a better representation for the rotor than point coils, but is not as good as 49 separate rotor loops: this is because a particular current distribution has been forced in the rotor bars. (A uniform distribution of current in the rotor conductors was also tried but was found to be less apt). However, the improvements in predicted results which were achieved while retaining a small number of machine equations by this method justified its application to the present case.

3.5.4 Assumptions for rotor model

Several assumptions were made in order that it was feasible to construct a theoretical rotor model:

- infinitely permeable and infinitely resistive rotor iron inserts
- radial current flow in the active annular section of the rotor. (The low resistance end rings help to ensure that this assumption applies)
- one dimensional current variations, i.e. there is no variation of rotor currents within the thickness of the rotor. This assumption is supported by the fact that the rotor half thickness, (2.5 mm) is approximately one quarter of the skin depth of copper at 50 Hz
- zero rotor leakage: the rotor loops were assumed to generate no leakage flux.

3.5.5 Calculation of filament coil parameters

The filament coil method of calculating the current distribution in conductors with a finite cross section has been used quite widely. For example, Popovitch[9] devised analytical methods for simple conductor geometries; and Sylvester[10] calculated the geometric mean distances of the filaments numerically in order to compute the inductances of each of the filaments. But the present complex geometry does not permit direct use to be made of previous experience. However, a novel method is devised below for calculating numerically the flux density distribution produced by a filament coil when it is situated in a non uniform airgap, and from this the filament coil inductances can be computed.

The four rotor loops that cover one pole pitch are illustrated in developed form in Fig. 3.12. The centre points of the bars A_1, A_2 ... A_n are denoted by a_1, a_2, ... a_n respectively. Bars A_1 and A_2 together with end ring interconnections make up loop 1; in general bars A_r and A_{r+1} form the radial sections of loop r. In the case of loop 1, an iron insert is enclosed by a conducting loop. The bar conductors have restricted widths w_1 and w_2 and are separated by non conducting but infinitely permeable iron portions. A different geometry exists for loop 3 where the radial bars meet at their inner edges. w_4 is the unrestricted bar width of 22.5° but w_3 is restricted to 10° by an iron portion.

The filament coils are illustrated in Fig. 3.12(c) for loop 1 only: they are determined in the following manner:

- w_r is defined for each loop by the physical geometry of the rotor
- the conducting section of the right hand bar is divided into filaments, each of which is one radial segment (1°) wide. The whole rotor loop is divided into this number of filament coils, their width in the left hand bar and in the end ring regions being scaled accordingly.
- the shape of the filament coils at the corners is assumed to be elliptical, the circumference of an ellipse being given approximately by $\pi[1.5(a+b)-\sqrt{ab}]$[11], where 'a' and 'b' are its major and minor semi-axes

- the filament coils so formed comprise a set of concentric, parellell-connected coils which are assumed to be connected to a common voltage source.

Filament coil no. 1 is innermost. The calculation of the filament coil parameters was undertaken as follows:

i) Filament resistance

Each concentric filament coil is subdivided into eight sections, numbered I, II ... VIII, as shown in Fig. 3.12(c). The resistance of each section can be calculated separately and added together to give the total filament coil resistance for the q^{th} filament, say, in the form:

$$R_q = \rho_c \left\{ \frac{\ell_{qI}}{s_I} + \frac{\ell_{qII}}{s_{II}} + \ldots + \frac{\ell_{qVIII}}{s_{VIII}} \right\} \qquad (3.23)$$

where ρ_c is the volume resistivity of the rotor conductor, and ℓ and s, the length and cross-sectional area respectively of each section, can be calculated simply from the rotor geometry.

ii) Filament inductance

Each filament coil can be considered to consist of an infinitely thin conductor, in which case the "flux linkage per amp" definition for inductance holds (see Section 3.4 above). The problem of calculating filament inductances therefore lies in calculating the flux density distribution produced by a filament coil in the non uniform airgap of the motor. In general terms this is the problem of calculating the flux density distribution produced by a short-pitched coil in a non-uniform airgap. The computer-oriented method which was developed to accomplish this makes use of the 360 radial segments into which the airgap of the machine is subdivided. It is assumed that for each segment 'm', the effective magnetic airgap is given by 'g_m', and the normal flux density prevailing over the segment is 'b_m'.

Ampere's Circuital Law can then be applied to 359 separate paths which pass through segments 1 and m, where m = 2, 3, ... 360. Typical paths of integration are shown in Fig. 3.13. For a filament coil which consists of N_f turns (in the present case N_f = 1) and carries a current i,

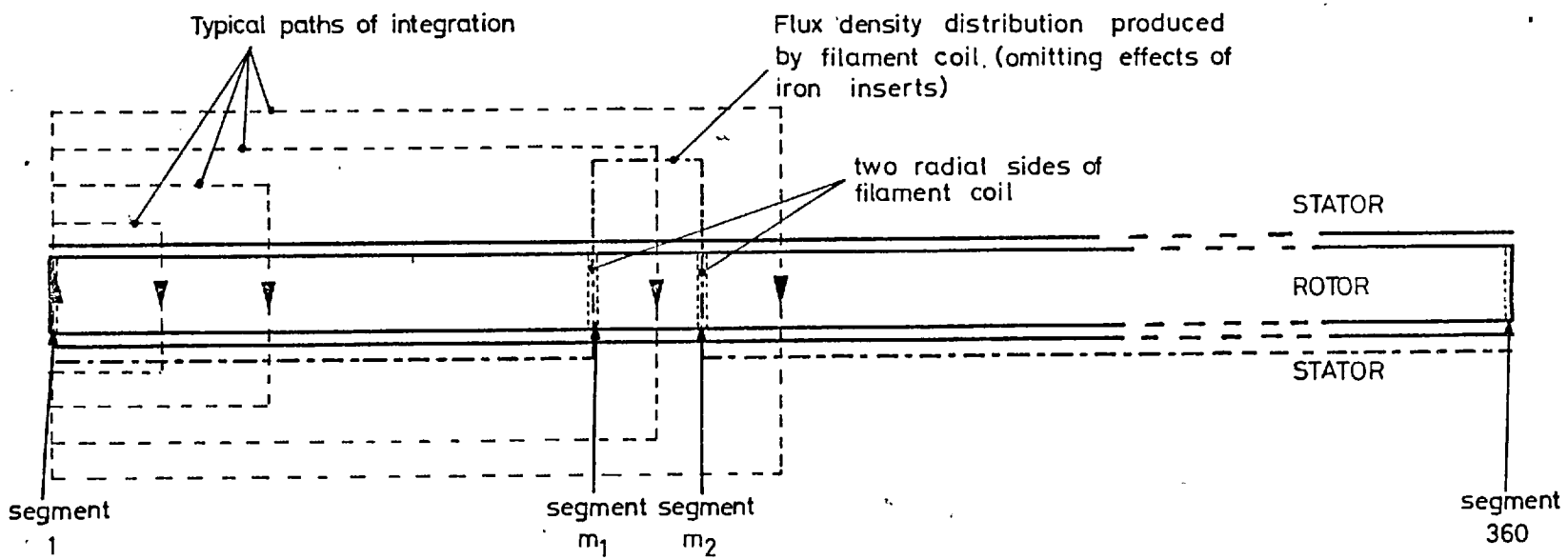

INTEGRATION PATHS FOR CALCULATION OF FLUX DENSITY DISTRIBUTION PRODUCED BY A SHORT PITCHED COIL IN A NON UNIFORM AIRGAP

FIG. 3.13

and is situated in segments m_1 and m_2, Ampere's Law for the 359 separate paths take the form:

$$\frac{b_1 g_1}{\mu_o} - \frac{b_m g_m}{\mu_o} = 0 \quad \text{for } m = 2, 3, \ldots m_1 \qquad (3.24(a))$$

$$\frac{b_1 g_1}{\mu_o} - \frac{b_m g_m}{\mu_o} = N_f i \quad \text{for } m = m_1+1, m_1+2 \ldots m_2 \qquad (3.24(b))$$

and $$\frac{b_1 g_1}{\mu_o} - \frac{b_m g_m}{\mu_o} = 0 \quad \text{for } m = m_2+1, m_2+2 + \ldots 360 \qquad (3.23(c))$$

Equations 3.24 may be re-arranged in the form:

$$b_m = \frac{b_1 g_1}{g_m} \quad \text{for } m = 2, 3 \ldots m_1 \text{ and } m = m_2+1, m_2+2 \ldots 360 \qquad (3.25(a))$$

and $$b_m = \frac{\mu_o}{g_m}\left(\frac{b_1 g_1}{\mu_o} - N_{fi}\right) \quad \text{for } m = m_1+1, m_1+2 + \ldots m_2 \qquad (3.25(b))$$

Equations 3.25 represent 359 expressions of Amperes Law which can be added together for all values of m, so that:

$$\sum_{m=2}^{m_1} b_m = b_1 g_1 \sum_{m=2}^{m_1} \frac{1}{g_m} \qquad (3.26(a))$$

$$\sum_{m=m_1+1}^{m_2} b_m = \mu_o \sum_{m=m_1+1}^{m_2} \frac{1}{g_m}\left(\frac{b_1 g_1}{\mu_o} - N_f i\right) \qquad (3.26(b))$$

$$\sum_{m=m_2+1}^{360} b_m = b_1 g_1 \sum_{m=m_2+1}^{360} \frac{1}{g_m} \qquad (3.26(c))$$

And equations 3.26(a), 3.26(b), 3.26(c) can also be added, to give:

$$\sum_{m=1}^{360} b_m = b_1\left[1 + g_1 \sum_{m=2}^{m_1} \frac{1}{g_m} + \sum_{m=m_2+1}^{360} \frac{1}{g_m}\right] + \mu_o \sum_{m=m_1+1}^{m_2} \frac{1}{g_m}\left(\frac{b_1 g_1}{\mu_o} - N_f i\right) \qquad (3.27)$$

From the fundamental relationship:

$$\text{div } B = 0 \qquad (3.28)$$

it can be seen that the algebraic sum of all the flux crossing the airgap of a machine must equal zero.

$$\text{i.e.} \quad \sum_{m=1}^{360} b_m = 0 \qquad (3.29)$$

In which case the right hand side of equation 3.27 equals zero, and can be solved for b_1 in the form:

$$b_1 = \frac{\mu_o N_f i \sum_{m=m_1+1}^{m_2} \frac{1}{g_m}}{1 + g_1 \sum_{2}^{360} \frac{1}{g_m}} = K_b \qquad (3.30)$$

Equation 3.30 illustrates that for a constant value of N_f and i, the flux density in segment 1 can be written in terms of the geometry of the airgap. Denoting the value of b_1 in equation 3.30 above by K_b, the values of b_m can be obtained directly by substituting for b_1 in equations 3.25 above:

$$\text{i.e.} \quad b_m = K_b \frac{g_1}{g_m} \quad \text{for } m = 2, 3 \ldots m_1 \text{ and } m = m_2+1, m_2+2 \ldots 360 \qquad (3.31(a))$$

$$\text{and} \quad b_m = \frac{\mu_o}{g_m} \left(\frac{K_b g_r}{o} N_f i\right) \quad \text{for } m = m_1+1 \ldots m_2 \qquad (3.31(b))$$

The self and mutual inductances of the filament coils which comprise each rotor loop can now be calculated. The self inductance of the q^{th} filament coil M_{qq} in a given rotor loop which extends physically between segments m_1 and m_2 of the rotor is given by:

$$M_{qq} = dA \sum_{m=m_1}^{m_2} b_{mq} \qquad (3.32)$$

where dA is the area of one segment and b_{mq} is the flux density at segment m which is produced when filament q is excited by one amp, and is given by equation 3.31 above.

Similarly, the mutual inductance M_{qr} between the q^{th} filament above, and the r^{th} filament coil which extends between rotor segments m_1' and m_2'

is given by:

$$M_{qr} = dA \sum_{m=m_1'}^{m_2'} b_{mq} \qquad (3.33)$$

iii) Voltage equations for the filament coils

The purpose of subdividing each rotor loop into a set of filament coils was stated above to be to calculate the current in each filament coil, and then to use the filament coil currents to represent the distribution of current across the flat bar conductors of the rotor loops. The filament coil currents can be calculated by writing down the voltage equation for each of the parallel connected filaments in terms of its resistance and inductances calculated above. Thus, for the p filaments comprising a rotor loop the voltage equations can be written in the form:

$$\begin{aligned}
v_1 &= i_1R_1 + j\omega(i_1M_{11} + i_2M_{12} + \ldots + i_qM_{1q} + \ldots + i_pM_{1p}) \\
v_2 &= i_2R_2 + j\omega(i_1M_{21} + i_2M_{22} + \ldots + i_qM_{2q} + \ldots + i_pM_{2p}) \\
&\vdots \\
v_q &= i_qR_q + j\omega(i_1M_{q1} + i_2M_{q2} + \ldots + i_qM_{qq} + \ldots + i_pM_{qp}) \\
&\vdots \\
v_p &= i_pR_p + j\omega(i_1M_{p1} + i_2M_{p2} + \ldots + i_qM_{pq} + \ldots + i_pM_{pp})
\end{aligned} \qquad (3.34)$$

where $v_1 = v_2 = \ldots v_q = \ldots v_p$ because all the filaments are assumed to be connected in parallel and excited from the same voltage source. Sinusoidal excitation was assumed for these calculations. Equations 3.34 can be written in matrix format:

$$[v] = [R][i] + j\omega[M][i] \qquad (3.35)$$

and can be solved for the filament currents by rearranging in form:

$$[i] = [v]\{[R] + j\omega[M]\}^{-1} \qquad (3.36)$$

and inverting the impedance matrix.

The resistance matrix [R] contains terms on the major diagonal only, and the inductance matrix [M] is symmetrical about the major axis, for $M_{12} = M_{21}$. Equation 3.36 can be solved by assuming an arbitrary voltage level for the voltage matrix and using conventional matrix inversion techniques. The filament coil currents so calculated give the distribution of current across the rotor bars in terms of the total loop currents.

3.5.6 Calculation of rotor parameters

The rotor parameters which are required for substitution into the voltage equations which describe the performance of the machine relate to the conducting loops into which the rotor has been subdivided. These parameters are:

- the bar and end ring resistances of the rotor loops
- the self and mutual inductances of the rotor loops
- the mutual inductances of the rotor loops with the stator phase windings

Their calculation uses the filament coil currents described above to give the distribution of the currents in the bars. As this current distribution depends upon the frequency of the currents in the rotor loops, the calculations were made for p.u. slip speeds of 1.0, 0.8, 0.6, 0.4, 0.2 and 0.0 and the parameter values for intermediate speeds were obtained by linear interpolation between the computed values.

The methods of calculation used for the above sets of parameters were as follows:

i) Bar and end ring resistances

The impedance of a rotor loop, loop q, say, at the slip frequency under consideration can be obtained from the equations relating to its constituent filament coils, equations 3.35 and 3.36 above in the form

$$Z_q = \frac{v_q}{i_q} = R_q + j\omega M_q \qquad (3.37)$$

where Z_q is the impedance of rotor loop q
v_q is the arbitrary voltage applied in equation 3.36 above
i_q is the sum of all the filament currents flowing in the loop under the influence of voltage v_q

and R_q and ωM_q are the real and imaginary parts of the loop impedance

'R_q' is therefore the a.c. resistance of the complete rotor loop.

For the purposes of the machine voltage equations (3.6 above), the end-ring and radial bar components of this total a.c. loop resistance, R_q, are required. These were obtained approximately by dividing the total a.c. resistance in proportion to the d.c. resistances of the component parts. Thus if R' and R denote d.c. and a.c. resistances respectively, and suffices:

q denotes the total loop q
b_{r_q} denote the right hand bar of loop q
b_{ℓ_q} " " left " " " " "
oer_q " " outer end ring of loop q
ier_q " " inner " " " " "

the following relationships can be written:

$$R_{b_{rq}} = \frac{R'_{b_{rq}}}{R'_q} R_q \qquad (3.38(a))$$

$$R_{b_{\ell q}} = \frac{R'_{b_{eq}}}{R'_q} R_q \qquad (3.38(b))$$

$$R_{oer_q} = \frac{R'_{oer_q}}{R'_q} R_q \qquad (3.38(c))$$

and $$R_{ier_q} = \frac{R'_{ier_q}}{R'_q} R_q \qquad (3.38(d))$$

ii) Self and mutual inductances of the rotor loops

The simple definition of inductance in terms of "flux linkage per amp" can be written as:

$$M = \frac{\lambda}{I} \qquad (3.39)$$

with the usual notation. It applies to discrete circuits in which the current distribution in the conductors is known. Inductance calculated by this method is a function of geometry, and is constant providing that:

- the relationship between flux and current is linear, i.e. when the magnetic materials in the relevant magnetic circuit are operating under linear conditions
- the current distribution is defined

The first of these two limitations has been taken into account by the assumption that all the iron paths are unsaturated. The second is particularly relevant to the present case, however, in which the rotor loop currents are non-linearly distributed across the flat rotor bars and end rings. The definition of inductance can be extended to cover this situation, and takes the form[8]:

$$M = \frac{1}{i^2} \Sigma \lambda \delta i \qquad (3.40)$$

where λ is the flux linking with each elemental portion 'δi' of the total current i.

This relationship can be used in conjunction with the rotor loop and filament coil parameters calculated and described above. Thus for the q^{th} rotor loop (excited by a voltage v_q which is the same for all loops) which has been subdivided into'p' filaments the total loop current, i_q, is given by:

$$i_q = \sum_{r=1}^{p} i_{r_q} \qquad (3.41)$$

where i_{r_q} is the current flowing in the r^{th} filament in the q^{th} loop.

Furthermore, the flux density distribution created by the q^{th} loop in each segment 'm' is given by:

$$b_{m_q} = \sum_{r=1}^{p} b_{m_{rq}} \quad \text{for } m = 1, 2, \ldots 360 \qquad (3.42)$$

where $b_{m_{rq}}$ is the flux density produced by the r^{th} filament of loop q in segment m.

Substituting these parameters into the definition of inductance given in equation 3.40 above, the mutual inductance between the q^{th} and s^{th} loops can be written as:

$$M_{qs} = \left(\frac{1}{i_q}\right)^2 \left\{ \sum_{r=1}^{p} i_{rq} \left(dA \sum_{m=m_{1r}}^{m_{2r}} b_{ms} \right) \right\} \left(\frac{i_q}{i_s}\right) \qquad (3.43)$$

where the r^{th} filament coil in the q^{th} loop (there are a total of 'p' filament coils in the loop) spans the rotor segments m_{1r} and m_{2r}, and is linked by the total flux that is produced between these segments by the s^{th} loop.

The different impedances of the different rotor loops - some comprise copper conductors, others enclose iron inserts - result in different total currents being driven around the loops when excited by the same voltage. The current scaling factor in equation 3.43, $(\frac{i_q}{i_s})$ enables the filament coil currents to be used to give the current distribution across the loop conductors, but scales them so that the same total current flows in each loop. The assumption implicit in this method of calculating the mutual inductance between rotor loops is that the distribution of current across the loop conductors is the same whether it is driven by an external source, or by an internal emf induced by an incident time-varying flux field.

The general expression for mutual loop inductances, equation 3.43 above, covers the special case of self loop inductances when q = s. However, the self inductances of each loop is also calculated by equation 3.37 above where it appears in the imaginary part, ωM_q, of the loop impedance Z_q.

As stated above, four rotor loops are necessary to describe the behaviour of the rotor, because of its symmetrical pole pitch pattern. It should be noted however that it is necessary during the calculation of the mutual inductance of four rotor loops to consider more than four loops. This arises because adjacent loops share a common conducting bar in which loop currents are distributed, and over which the generated flux density is also distributed. The mutual inductance of one loop with an adjacent loop is therefore not the same as with a non-adjacent loop of the same type. Referring to a rotor loop which encloses an iron segment as an 'iron loop', and one that contains copper only as a 'copper loop', it can be seen that for the rotor under consideration, with the rotor model described above, there are eight types of inductances:

- self inductance of an iron loop
- mutual inductance of an iron loop with an adjacent iron loop
- mutual inductance of an iron loop with a non-adjacent iron loop

- mutual inductance of an iron loop with an adjacent copper loop
- mutual inductance of an iron loop with a non-adjacent copper loop
- self inductance of a copper loop
- mutual inductance of a copper loop with an adjacent copper loop
- mutual inductance of a copper loop with a non-adjacent copper loop

With reference to Fig. 3.9, it can be seen that in order to calculate:

- the mutual inductance of an iron loop with a non-adjacent iron loop
- and, the mutual inductance of a copper loop with a non-adjacent copper loop

a total of seven loops must be considered.

3.5.7 Calculation of the mutual inductances of the stator phase windings and rotor loops

The technique for calculating the so-called 'stator-rotor' inductances is derived from the methods described above for calculating the stator inductances, Section 3.4 above, and the rotor inductances, Section 3.5.6 above. The linkage of the flux density distribution created by each rotor loop (equation 3.42) with the phase winding of each stator phase was computed by the summation methods set out in equations 3.20 and 3.21 above.

These inductances depend upon rotor position and vary cyclically as the rotor moves; the computations were consequently repeated for a range of rotor positions.

3.5.8 Conclusions

This concludes the descriptions of the methods used to calculate the equivalent circuit parameters of a disc reluctance motor with a conducting sheet rotor that contains iron portions to create salient poles. The method is designed for programming on a digital computer. The airgap was represented by a 360 element array which defined the length of the effective magnetic airgap in each of the 1° segments. As described

above, inductance calculations could then be made using summation procedures between easily defined limits. A flow chart of the program which calculates all the stator and rotor parameters is illustrated in Fig. 3.14.

The circuit model which has been adopted represents the behaviour of the motor by an equivalent electrical network, and the circuit parameters of this network relate to the primary interactions within the main air-gap of the motor. Secondary effects, notably fringe fields at the edge of the airgap also affect the behaviour of the machine, and the manner in which they were taken into account in the present model is described below.

3.6 Treatment of fringe fields

Fringe flux fields commonly occur in electrical machines at discontinuities or irregularities in their iron circuits which are carrying flux. They arise because of the imperfections of iron and air as magnetic conductors and insulators respectively. A strict treatment of fringe fields usually requires analytical or numerical methods to be employed. Circuital methods for machines analysis require that secondary field effects, such as fringe fields, be taken into account by appropriate factors, and these are usually based on field considerations. The common example of this is Carters Co-efficient[7] which allows for the way in which slot openings in the airgap of a machine tend to increase the effective magnetic length of that gap.

In the present case, the main fringe fields occur at the inner and outer diameters of the machine where the flux crosses the airgap. The effect of the fringe field is particularly important in the motor under consideration because the pole width is small compared to the length of the airgap. The pole width/airgap ratio is in fact between 3 and 4: for conventional machines it is more typically between 100 and 200.

The effect of a fringe flux field is to leave the uniform flux density within the airgap substantially unchanged, but for extra flux to traverse the airgap at the edges. Hence the total flux crossing the airgap is greater than predicted by a method which assumes a uniform flux field within the confines of the airgap. For this reason, although fringe fields leave the theoretical and experimental values of airgap flux

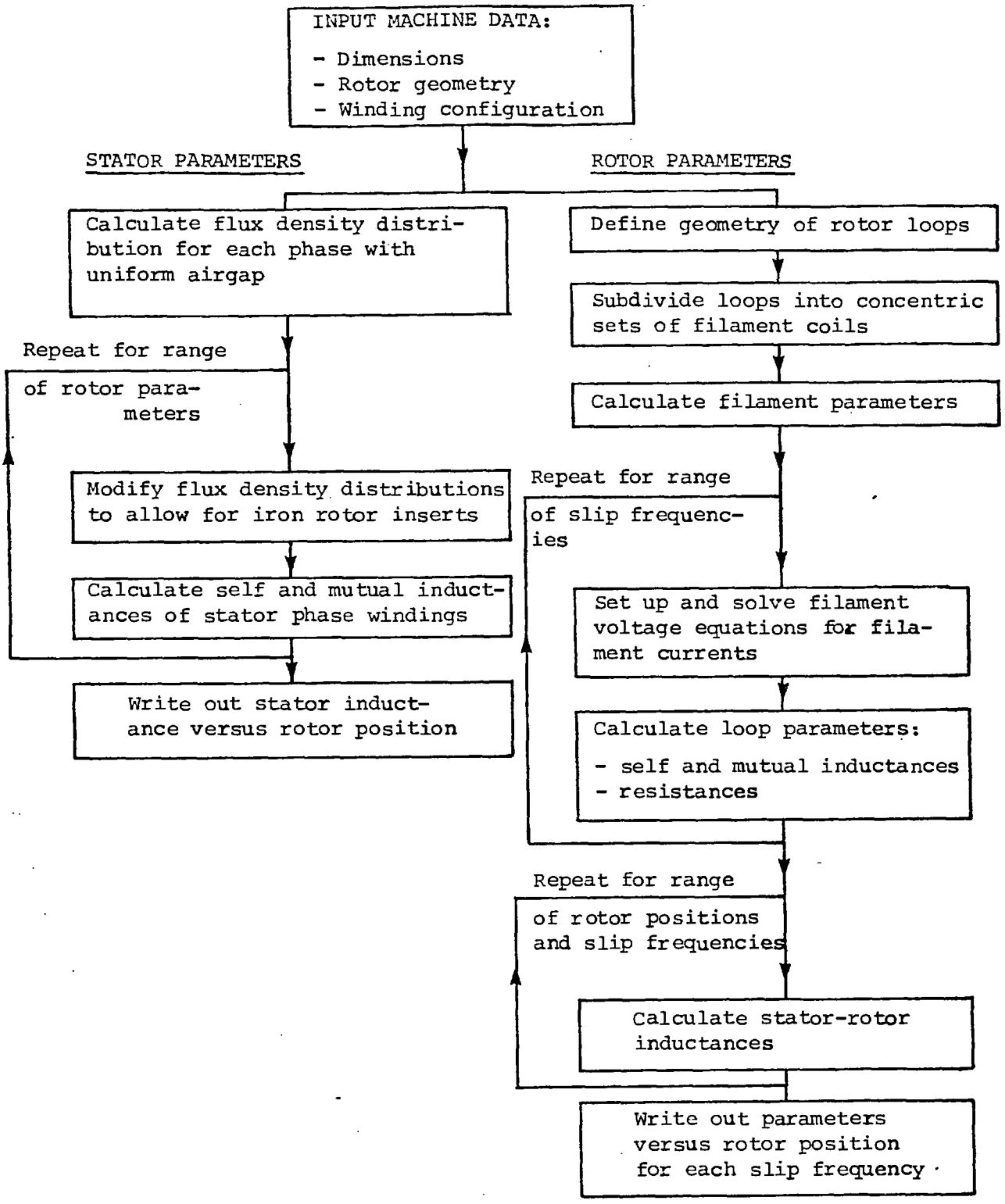

Fig. 3.14 Flow chart of computer program to calculate equivalent circuit parameters of a double sided salient pole axial flux disc reluctance motor

density unaffected, the theoretical value of the total flux crossing the airgap - and hence the related inductances - must be amended to allow for the fringe flux. A corollary of this is that search coils which are placed in the airgap for the purpose of measuring flux linkages, and hence inductances, must be remote from the edges of the stator by sufficient distance that the fringe flux is enclosed.

Two ways can be used to compensate for the fringe flux, both of which assume that the flux density is uniform within the airgap of the machine and zero outside it. Either the theoretical stator width can be increased by an amount, such that the total flux crossing the enlarged stator width is equal to the actual airgap flux plus the fringe flux: the predicted flux density is equal to the actual flux density in this case. Or the stator width can remain unchanged, but the length of the airgap be reduced so that an increased flux density is used to account for the extra flux: the predicted flux density is therefore intentionally greater than the actual flux density. Bolton[12] used the former method, finding that for a certain range of linear motor geometries the stator width should be increased by the length of the airgap to give satisfactory results. This method might be preferred because the predicted and actual flux densities should be the same. For the present analysis, however, the method of reducing the effective airgap was used. This was because the iron inserts in the rotor produced variable fringe fields around the stator, and if the 'stator width' method were used, the width of the stator would have to vary around the machine. By using the 'reduced airgap' method a fringe factor could be calculated for each of the 360 airgap segments, and could be included in the array which defined the airgap data in the computer program.

The effect of the fringe fields on all the inductances that appear in the voltage equations (equations 3.6 above) must be taken into account. The manner in which this was accomplished for the stator, stator-rotor, and rotor inductances is now described.

i) The effect of fringe fields on the stator inductances

A cross section through the two stators showing the two cores, their end windings and the airgap between them in a position remote from the iron rotor inserts is illustrated in Fig. 3.15(a). The shape of the

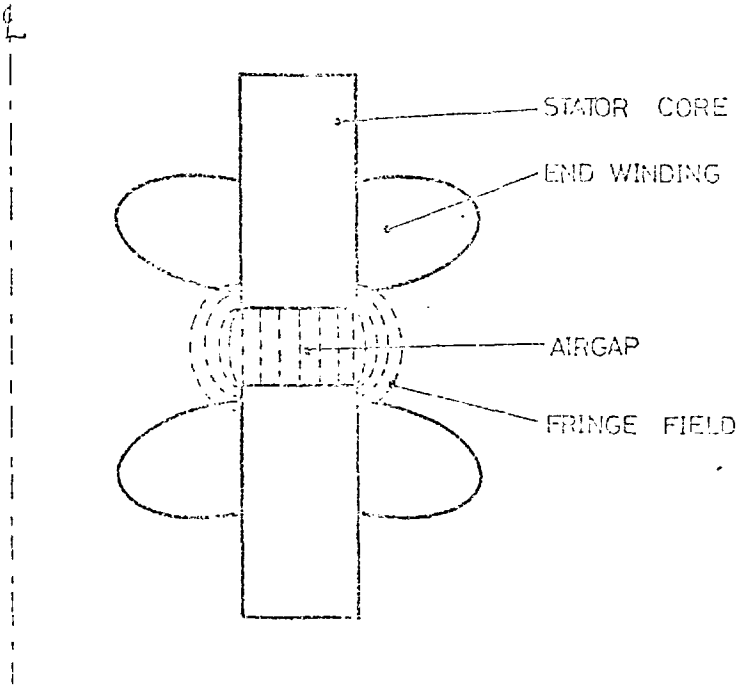

A. FRINGE FLUX BETWEEN STATOR CORES

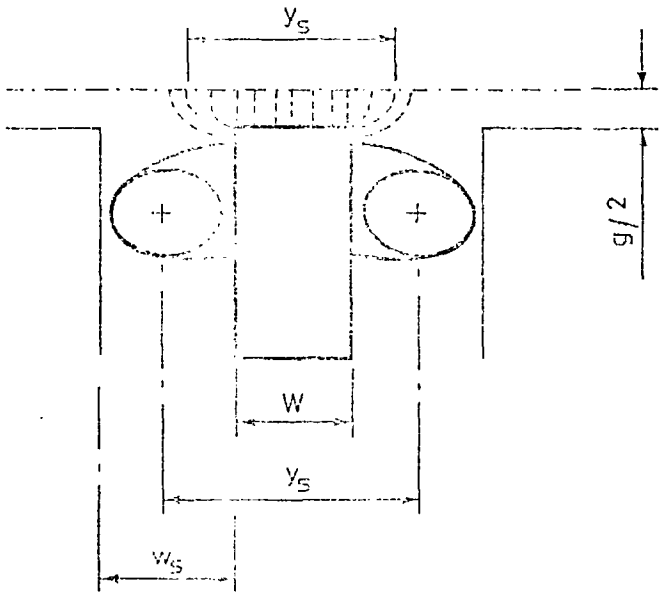

B. CALCULATION OF EFFECTIVE STATOR WIDTH

TREATMENT OF FRINGE FIELDS

FIG. 3.15

fringe fields is also indicated and it can be seen that the majority of the fringe flux links the main windings and therefore contributes to their self and mutual inductances. It was found that the effect of the fringe flux could be taken into account by recognising that, as shown in Fig. 3.15(b) the two stator cores are like the teeth of a doubly salient device, with the end windings in the 'slots' either side of them. And therefore a modified Carter Co-efficient can be applied. With reference to Fig. 3.15(b), it can be shown that according to Carter[7]:

$$y'_s = y_s - k_o w_s \qquad (3.44)$$

where y'_s is the effective width of the stator surface
y_s is the slot pitch
k_o is Carter's Coefficient
and w_s is the slot width

By symmetry, the distance of the centre of the end winding bundle from the stator core was assumed to be equal to half the slot width.

Also, it can be seen from Fig. 3.15(b) that:

$$y_s = W + w_s \qquad (3.45)$$

so that the effective increase in stator width due to fringing, y'_s/W is given by:

$$\frac{y'_s}{W} = 1 + \frac{w_s}{W}(1 - k_o) \qquad (3.46)$$

This factor was used to reduce the airgap length in positions from which the iron inserts were absent so that the total predicted airgap flux included the fringe flux.

It was difficult to measure precisely the effective position of the centre of the 'slot' containing the end windings, but the two possible extreme positions gave fringe factors of 1.42 and 1.51: an average rounded value of 1.5 was used for computations to support experimental work described in Chapter 4 below. Approximate numerical field solutions also indicated that this was a reasonable value.

In the area of the iron rotor inserts the above method cannot be applied, because of the geometry of the situation: the mid-point of the airgap between the two stator cores is no longer equivalent to an iron surface of infinite width. An approximate numerical field solution indicated that the main flux crossing the gap in these regions was increased by around 10% by fringe flux. A fringe factor of 1.1 was therefore used.

In the calculation of the stator inductances therefore the natural magnetic airgap at each position of the machine was reduced by the following fringe factors, k_{fm}:

k_{fm} = 1.5 when segment m contains no rotor iron
k_{fm} = 1.1 when segment m contains rotor iron

ii) The effect of fringe fields on rotor inductances

For the calculation of the rotor inductances the stator cores act as magnetic paths for the flux that would be generated if each hypothetical rotor loop were excited in turn. The fringe flux under these conditions appears to depend upon the position of the rotor end ring conductors with respect to the inner and outer edges of the core. If the end rings were assumed to be infinitely thin conductors, aligned with the inner and outer diameters of the cores and situated half way between the two cores, there would be no fringe flux. In reality the end rings have finite width, the current is distributed across them, and there is a certain amount of fringe flux. The rotor end rings and the position of the notional filament coils were illustrated in Fig. 3.12(c). Any flux generated elsewhere around the stator will tend to fringe across the airgap in the region of the rotor loop under consideration and will link to a varying degree with the currents flowing in the filament coils of the rotor loop shown. The calculation of a fringe factor for these conditions depends upon:

- a knowledge of the fringe fields at the edges of the stators
- a knowledge of the current distribution in the filament coils
- the arc subtended by each filament coil in the end ring region

The fringe field in the region of the stator core was calculated theoretically by an approximate numerical method; and the theoretical filament coil currents were used to give the end ring current distribution. The results obtained by this method were as follows:

Rotor Loop No.	Fringe Factor
1	1.05
2	1.05
3	1.10
4	1.10

The rotor inductances calculated on the assumption of zero fringe flux were increased by the above factors to allow for the fringe fields. As might be expected from the symmetry of the rotor, fringe factors for loops 1 and 2 are the same, as are those for loops 3 and 4. For the mutual inductances between loops, the average of the fringe factors for the individual loops was used.

iii) The effect of fringe fields on stator-rotor inductances

Fringe factors for the mutual inductances between the stator phases and the rotor loops are identical to those for the self inductances of the rotor loops. This is because the shape of the fringe field at the edges of the stator core is the same whether the flux is caused by excitation of a stator phase or by a rotor loop at another position in the airgap.

3.7 Solution of the machine equations

The set of voltage equations which describe the reluctance motor under consideration as an equivalent electrical network was expressed in matrix form by equation 3.6 above as

$$[v] = [R][i] + \frac{d}{dt}\{[M][i]\}$$

The [R] and [M] matrices contain the equivalent circuit parameters, the calculation of which has been described in Sections 3.4 and 3.5 above. In order to predict the performance of the machine, therefore, it is now necessary to solve this equation for the motor currents [i] when a specified set of voltages [v] are applied to it. A knowledge of the motor

currents enables the electrical torque produced by the motor to be estimated (Section 3.3.2, equation 3.7) and hence the dynamic behaviour of the motor (Section 3.3.3, Equation 3.9).

The difficulties surrounding the general solution of equation 3.6 can be seen by expanding the time-differential term, i.e.

$$[v] = [R][i] + \left\{[M]\frac{d}{dt}[i] + [i]\frac{d}{dt}[M]\right\}$$

$$\therefore [v] = [R][i] + \left\{[M]\frac{d}{dt}[i] + [i]\frac{d}{d\theta}[M]\frac{d\theta}{dt}\right\} \qquad (3.47)$$

for it can be seen that the final term in equation 3.47, $\frac{d}{dt}[M]\frac{d\theta}{dt}$, is in general the product of two variables, thus making the equation non-linear.

Arockiasamy[1] developed numerical "step-by-step" methods for solution of equations of the type given in 3.47 above, and applied them with success to induction motors and single phase variable airgap reluctance motors. There is in essence no difference between the equations governing those machines and the present equations, and the same general methods of solution have therefore been used here.

Numerical step-by-step procedures need make no assumptions of sinusoidal variation with time of voltage and current and therefore are ideally suited for prediction of transient behaviour. By considering the change in motor parameters over small time intervals, equation 3.6 can be re-written in the form:

$$\frac{[v]' + [v]''}{2} = [R]\cdot\frac{[i]' + [i]''}{2} + \frac{[M]''[i]'' - [M]'[i]'}{\Delta t} \qquad (3.48)$$

where superscripts ' and " indicate quantities prevailing at the beginning and end of the time interval respectively.

It can be seen that the average values of [v] and [i] over the time interval are taken, and that the term $\frac{d}{dt}\{[M][i]\}$ is expressed in a finite difference form. After specifying a set of initial conditions, the principle of this method of solution is to apply equation 3.48 to successive time intervals, for the duration of the period under consideration: the values prevailing at the end of one time interval become the starting values for the next interval. The basic requirement of the method is to calculate [i]" for each time step, the other parameters being known, or determinable. Thus, equation 3.48 can be re-arranged in the form:

$$[i]'' = \frac{\left\{ \frac{[v]'+[v]''}{2} - \frac{[R][i]'}{2} + \frac{[M]'[i]'}{\Delta t} \right\}}{\left\{ \frac{[R]}{2} + \frac{[M]''}{\Delta t} \right\}} \qquad (3.49)$$

The denominator of this equation is a matrix in its own right, the inverse of which is required for a solution. But it also contains [M]" which is the cause of the non-linearity of equation 3.49. The physical meaning of the non-linearity is as follows: in order to calculate the currents at the end of a time interval, the machine inductances at the end of that time interval are required. These inductances depend upon the rotor position at that time which clearly depends upon the angle of rotation during the time interval. This in turn depends upon the average torque produced by the motor, which however depends upon the motor currents at the end of the time interval - and these are the parameters that were to be calculated.

Two methods were adopted by Arockiasamy[1] to overcome the intrinsically non-linear nature of the machine equations. These were a "constant speed" solution, and a full transient solution.

i) The "constant speed" solution

This method provides a solution to the machine equations for any fixed motor speed. Equation 3.47 is therefore linearised by this expedient, $d\Theta/dt$ being made constant. In terms of equation 3.49, it means that the rotor position is known at every instant in time, which enables [M]" to be determined. The solution at constant speed can therefore be used to predict the steady state performance of the motor at that speed.

ii) Transient solution

The transient solution to the machine equations uses an iterative procedure within each time interval to overcome the non-linear nature of the equations. As the dynamic characteristics of the rotor depend upon its coupled load, the voltage equations (3.6) must be solved in conjunction with the torque equation (3.7) and the mechanical equation (3.9). The procedure is as follows:

1) the speed of the rotor at the end of a time interval Δt, is given by:

$$u'' = u' + \frac{T_e - T_b}{J_k} \Delta t \qquad (3.50)$$

if Δt is sufficiently small for the rate of angular acceleration to be deemed constant,

where u'' is the speed at the end of Δt
u' is the speed at the beginning of Δt
T_e is the average electrical torque exerted during Δt
T_b is the average total load torque during Δt
and J_k is the moment of inertia of the rotating parts

An estimate for the value of T_e is obtained by extrapolating from the results of previous time steps.

2) the rotor angle at the end of the time interval is given by:

$$\theta'' = \theta' + \frac{u' + u''}{2} \Delta t \qquad (3.51)$$

where θ' is the rotor angle at the beginning of Δt
and θ'' is the rotor angle at the end of Δt

3) the matrix [M]" can therefore be written down, and equation 3.49 solved for [i]"

4) inserting [i]" into the torque equation enables the average electrical torque produced during the time interval to be calculated and compared with the value estimated at (1) above. If this value is the same as the estimated value (within prescribed limits) the next step of the procedure can be started; if it is not, it is inserted as the new estimated value of torque for a second iteration. This procedure is repeated until the test for convergence is satisfied at each step.

The time-step length, Δt, used for the above computations, was set as a fixed fraction of the period of the sinusoidal applied voltage. It was found that step lengths of up to one-twentieth of this period could be used without an unacceptable loss of precision, and without signs of numerical instability. More sophisticated methods of determining and varying step length are available, such as the Runge-Kutta-Merson 4th Order variable step length method, but their added complications did not appear to be justified for the present work.

It can be seen that the "transient solution" to the machine equations, described above, can be used to simulate the behaviour of a motor under any conditions that are programmed into it. Fault and transient conditions can be investigated in this way. In Chapter 4 it is used to simulate the behaviour of the motor from the instant at which the supply is switched on until it reaches synchronous speed.

Flow charts for the computer programs which were written to undertake the above "constant speed" and "transient" solutions are given in Figs. 3.16 and 3.17.

Chapter 4, which follows, provides theoretical results from computerised solutions of the methods described above, and compares them with experimental data obtained from a prototype motor.

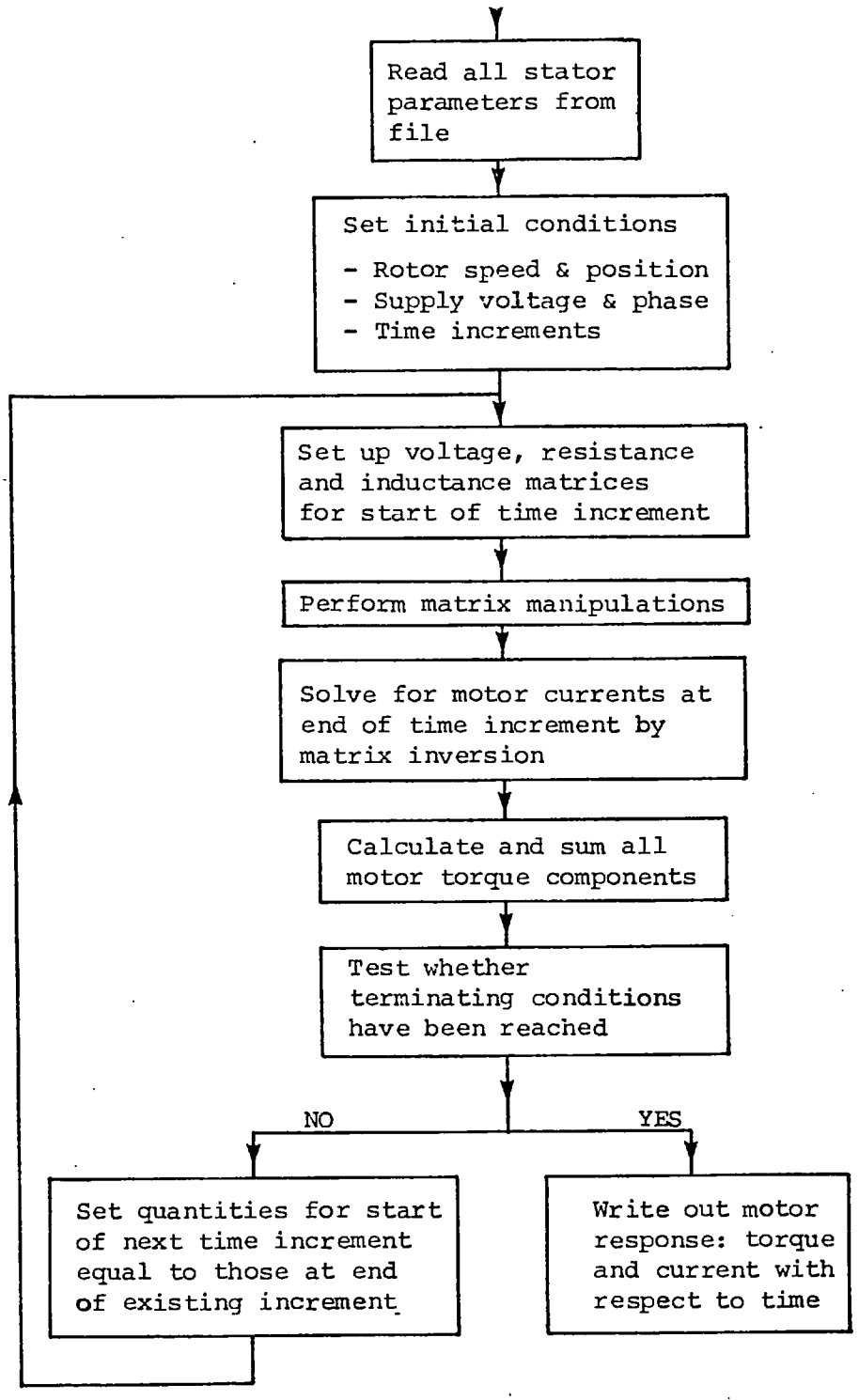

Fig. 3.16 Flow chart of computer program for "constant speed" solution of motor voltage equations

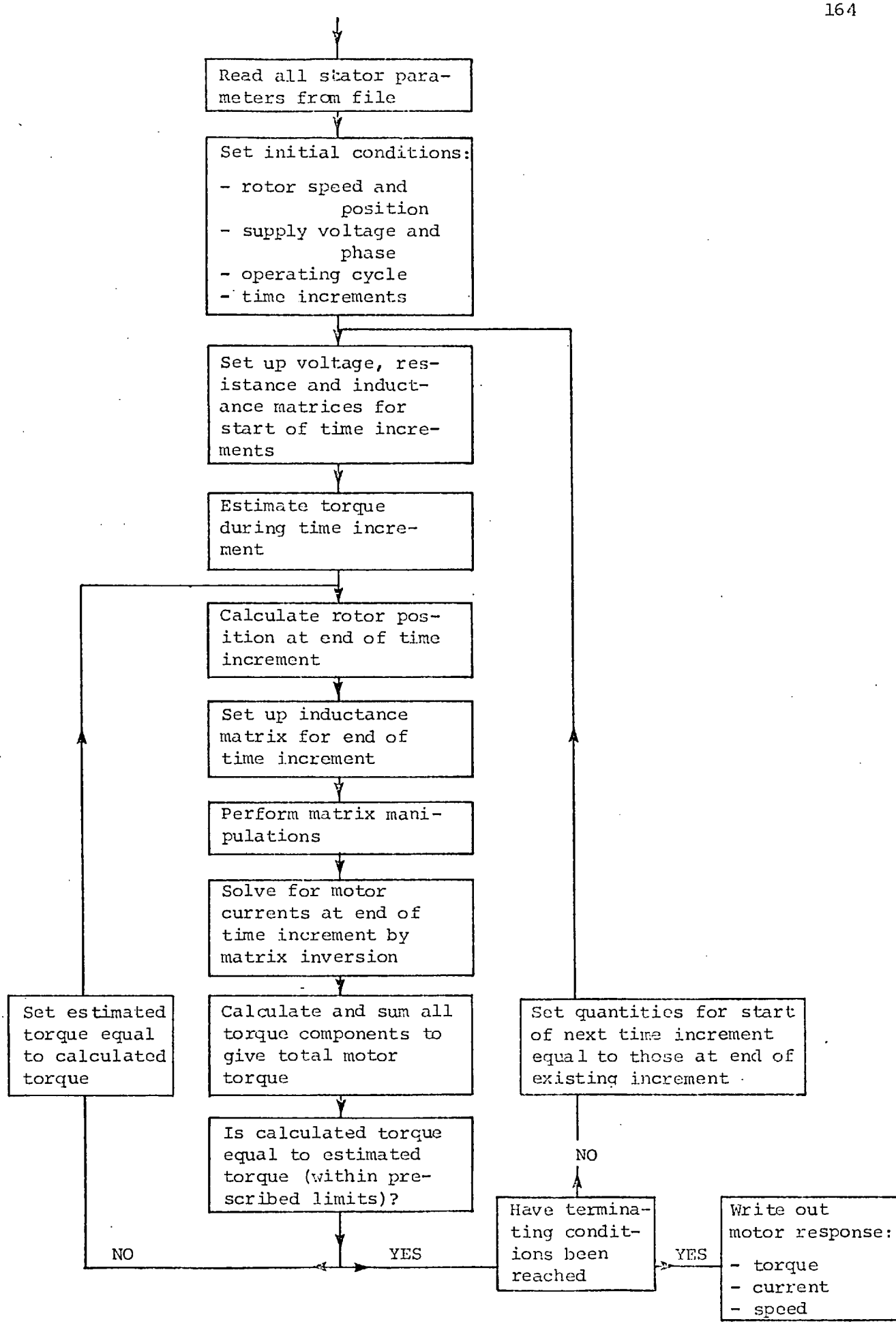

Fig. 3.17 Flow chart of computer program for full 'transient' solution of motor voltage equations

Chapter 3: References

1. Arockiasamy, R., "Development and Analysis of Thyristor Controlled Induction Motors", Ph.D. Thesis 1969, Imperial College, University of London.

2. Lawrenson, P.J., Mathur, R.M. and Stephenson, J.M., "Transient Performance of Reluctance Machines", Proc.IEE, 1971, 118, (6), pp. 777-783.

3. Russell, R.L. and Norsworthy, K.H., "Eddy Currents and Wall Losses in Screened-Rotor Induction Motors", Proc.IEE, 1958, 105A, pp. 163-175.

4. Fitzergerald, A.E., Kingsley, C. and Kusko, A., "Electric Machinery", 1971 (Third Edition), McGraw-Hill Inc.

5. Lipo, T.A. and Krause, P.C., "Stability Analysis of a Reluctance-Synchronous Machine", Trans.IEEE, 1967, PAS-86, (7), pp. 825-834.

6. Saunders, R.M., "Electromechanical Energy Conversion in Double Cylindrical Structures", Trans.AIEE, 1963, 82, pp. 631-638.

7. Carter, F.W., "Note on Airgap and Interpolar Induction", JIEE, 1900, 29, pp. 925-933.

8. Carter, G.W., "The Electromagnetic-Field in its Engineering Aspects", 1954, Longmans, Green & Co.

9. Popovic, B.D. and Popovic, Z.D., "Method of Determining Power-Frequency Current Distribution in Cylindrical Conductors", Proc.IEE, 1972, 119, (5), pp. 569-574.

10. Sylvester, P., "Model Theory of Skin Effect in Straight Flat Conductors", 1966, IEEE Internat. Convention Rec.

11. Tuma, J.J., "Engineering Mathematics Handbook", 1970, McGraw-Hill.

12. Bolton, H.R., "The Design of Special Purpose Induction Machines", Ph.D. Thesis 1971, Imperial College, University of London.

CHAPTER FOUR

Theoretical and Experimental Performance of the Double-Sided Salient Pole Axial Flux Disc Reluctance Motor

4.1 Introduction

The double-sided salient pole disc reluctance motor with axial stator flux paths was identified in Section 2.6 above as one of the preferred types of axial flux disc reluctance motor. A method of analysis for this type of motor was derived in Chapter 3; and the purpose of the present section is to verify experimentally the validity of that method. Also, the intention is to use these theoretical and experimental results to suggest the quality of performance that might be achieved from improved designs of motors of this type.

The method of analysis that has been described above can handle steady state and transient, synchronous and asynchronous performance of the reluctance motor. An attempt has therefore been made to prove that the computer model can perform satisfactorily under these various conditions by comparing the performance predicted for them with the results achieved in practice. In addition, the calculated values for the stator and rotor parameters were also checked by measurements. These parameter values were in fact the first to be checked as the ultimate success of the computer model depended upon its ability to calculate the equivalent circuit parameters of the motor.

Unless otherwise stated, all tests were carried out with the rotor illustrated in Fig. 3.5 which was 0.190 inches thick situated in the middle of a 0.285 inch airgap between the two stators.

4.2 Calculation and measurement of the equivalent circuit parameters of the motor

The following reluctance motor parameters appear in the voltage equations which are used to describe its behaviour:

i) Resistance of stator phase windings
ii) Self and mutual inductances of the stator phase windings
iii) Self and mutual components of the stator leakage inductances
iv) Self and mutual inductances of the notional rotor loops
v) Resistive components of the equivalent electrical network of the rotor
vi) Mutual inductances of the rotor loops and the stator phase windings

The extent to which the computer model is capable of predicting these parameters reliably is demonstrated in this section. Each of the above sets of parameters is considered in turn.

4.2.1 Resistance of stator phase windings

The four pole phase winding on each stator of the test motor consists of 8 coils connected in series, each coil being made up of 38 turns of 20 swg enamelled copper wire. The windings of the two stators are connected in series. The value of the resistance of a complete motor phase can be calculated theoretically[1] by:

$$R_1 = L_{mc} N_{ph} R_s (1 + \alpha t) \qquad (4.1)$$

where L_{mc} is the length of the mean conductor
N_{ph} is the number of turns per phase
R_s is the resistance per unit length of the conductor
α is the temperature co-efficient of resistance
and t is the temperature rise of the windings

The value of resistance predicted by this method for a 40°C temperature rise is 4.8 Ω. The measured value of 5.2 Ω was used in the computer model, however, because it is difficult to estimate and allow for the effective operating temperature of encapsulated windings.

4.2.2 Self and mutual inductances of stator phases

The important feature of the self and mutual inductances of the stator phases of a reluctance motor is that they are modulated by the position of the iron rotor inserts. The effect of these inserts was

introduced for the static measurement of stator inductances by means of a dummy rotor. This consisted of the iron rotor inserts supported in a non-magnetic and insulating disc. It enabled the magnetic circuits of the rotor to be used in isolation from the electric circuits. 'Open circuit' tests could therefore be carried out at standstill. The stator inductances were measured by the use of airgap shadow windings which extended outside the stator core diameters by a distance of one-quarter of an inch in order to enclose the fringe flux (see Section 3.6 above). An approximate numerical field solution of the fringe fields indicated that this was the appropriate position for the shadow coils.

Accurate calculation of the self and mutual inductances of the stator phases relies upon the ability to predict precisely the flux density distribution in the airgap of the machine when the iron inserts are present. Some preliminary measurements were therefore made using a proprietary Hall probe flux meter to check this aspect of the computer model:

Fig. 4.1 illustrates measured and computed flux densities in a uniform airgap of 0.25 inches when the red phase is excited. The maximum flux density level is predicted accurately but the detailed slot effects are not taken into account by the model.

Fig. 4.2, Fig. 4.3 and Fig. 4.4 illustrate the flux density distribution in an airgap of 0.25 inches for red, yellow and blue phase excitation respectively when the position of the iron inserts correspond to the $\delta_r = 0$ rotor position (see Section 3.4 above). The effect of the iron rotor inserts on the flux density distribution can be seen to be taken fully into account by the computer model.

Preliminary measurements and calculations were also made for the self and mutual inductances of the stator windings when the two stators were set with a uniform airgap of 0.3 inches between them. The inductances were measured; calculated with the computer model; and calculated theoretically on the assumption that the windings were sinusoidally distributed. The results were as follows:

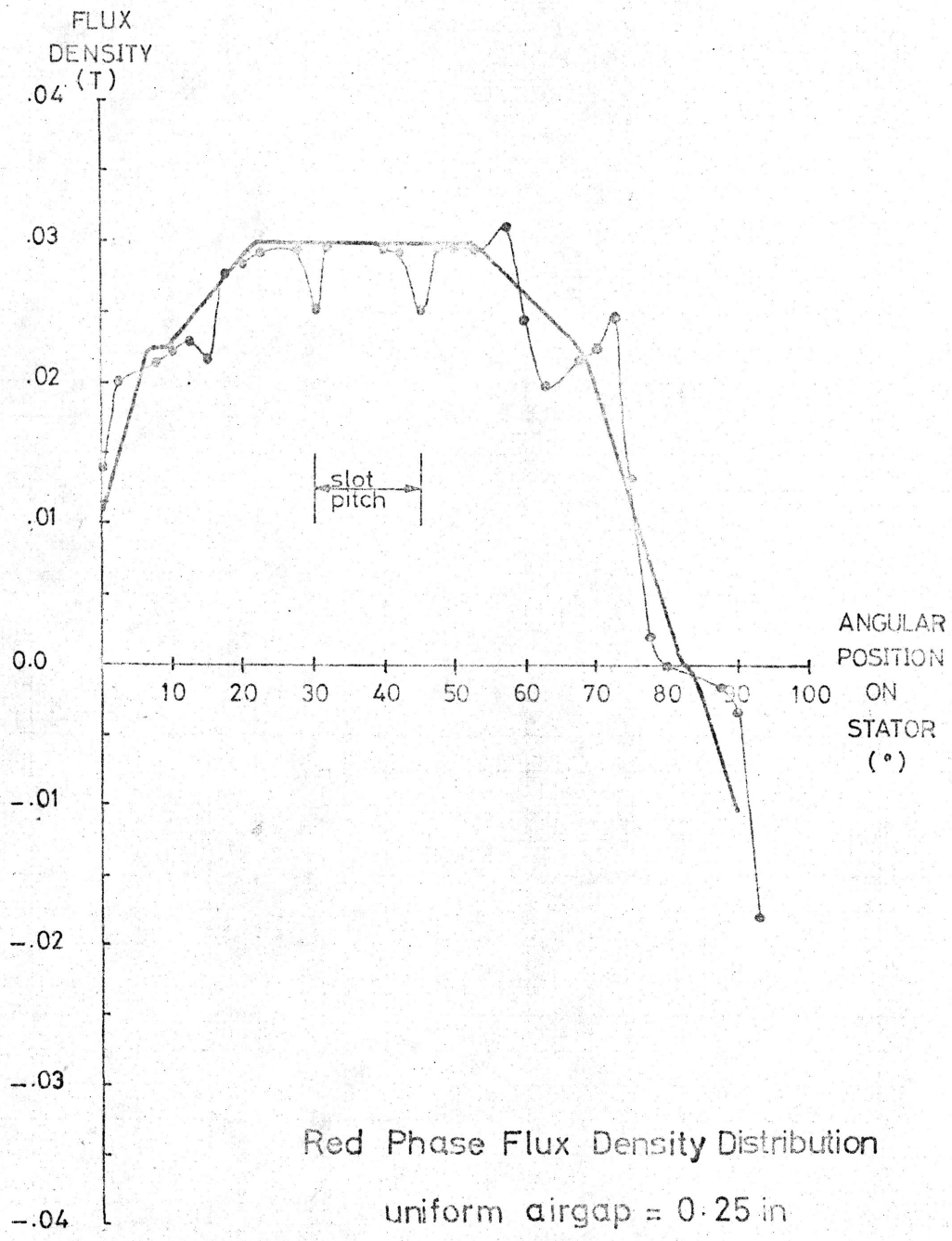

Red Phase Flux Density Distribution

uniform airgap = 0·25 in

experimental results —o—
computer results ——

FIG. 4.1

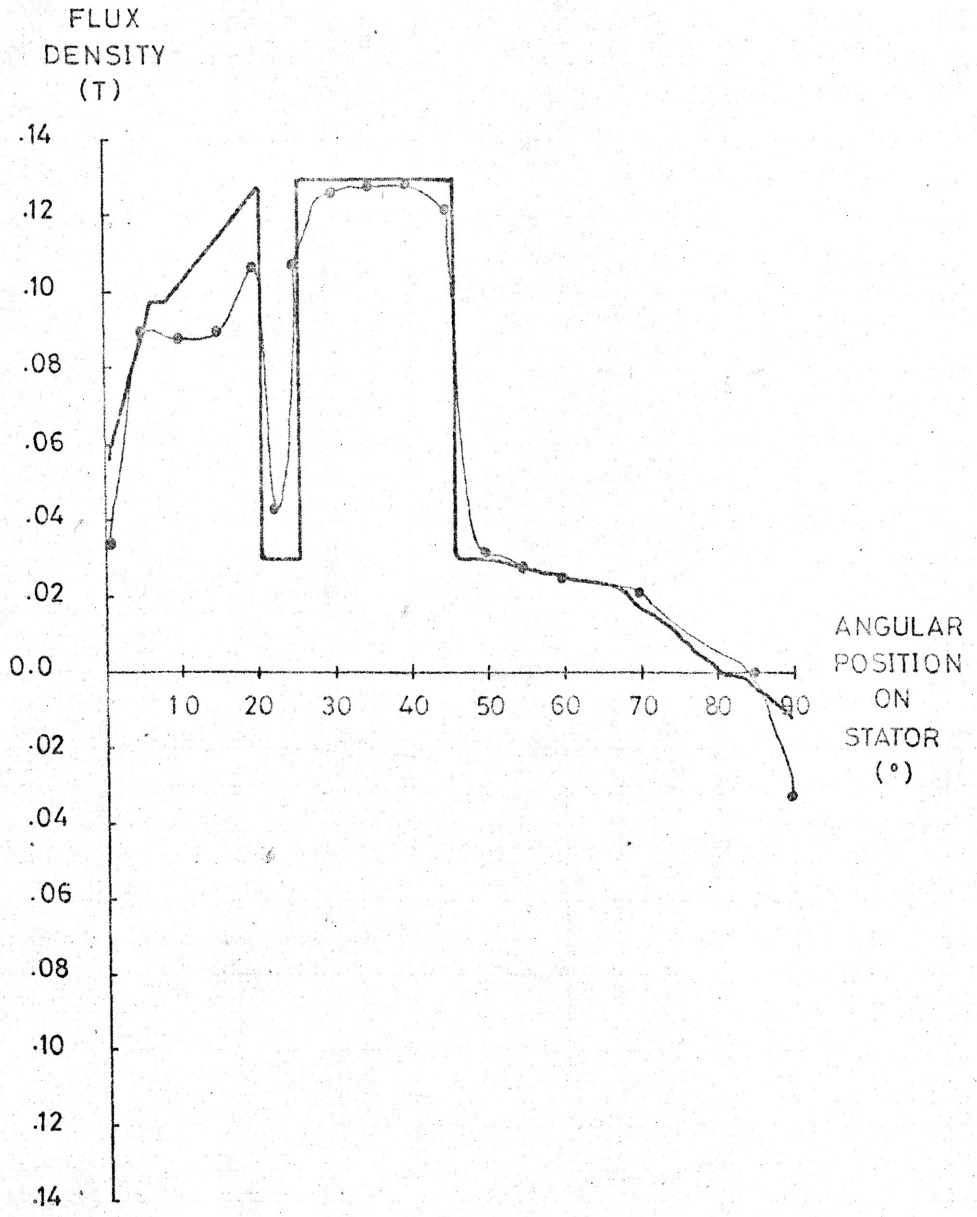

RED PHASE FLUX DENSITY DISTRIBUTION

non uniform airgap
$g = 0{\cdot}25$ in, $\delta_r = 0$

experimental results —●—
computer results ——

FIG. 4.2

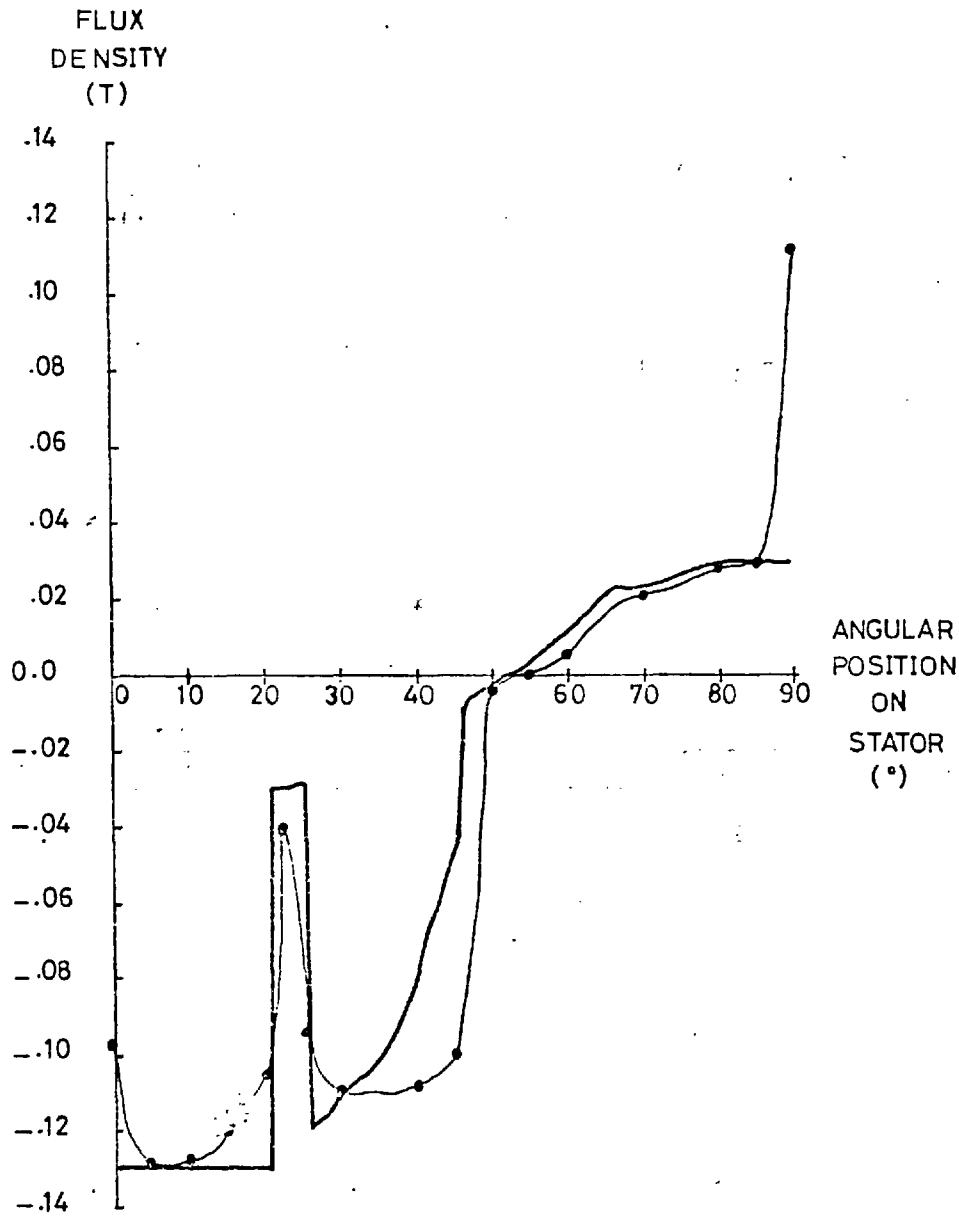

YELLOW PHASE FLUX DENSITY DISTRIBUTION

non uniform airgap

$g = 0{\cdot}25$ in, $\delta_r = 0$

experimental results —•—

computer results ——

FIG. 4.3

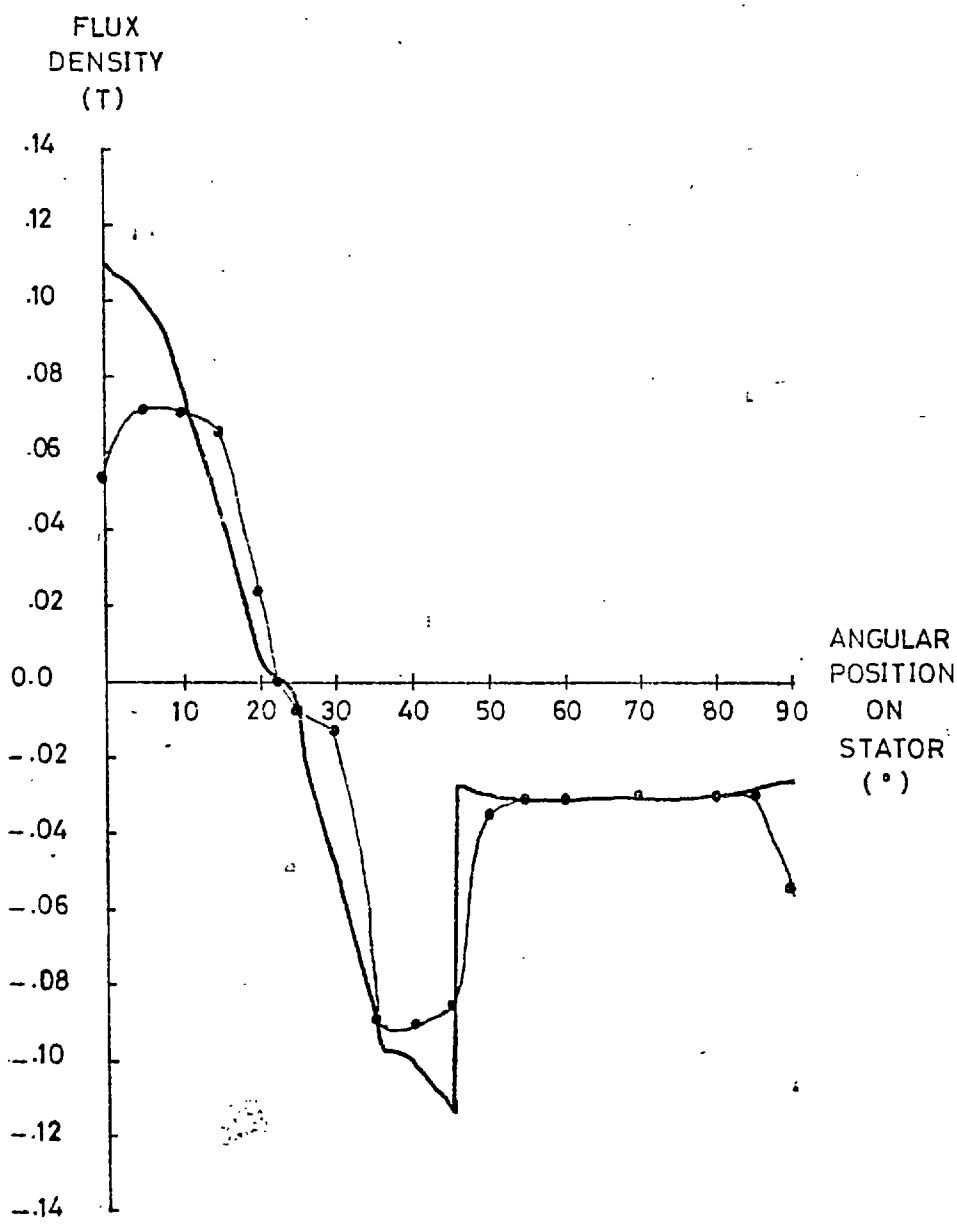

BLUE PHASE FLUX DENSITY DISTRIBUTION

non uniform airgap

$g = 0.25$ in, $\delta_r = 0$

experimental results —•—

computer results ——

FIG. 4.4

	Measured Inductance (H)	Theoretical Inductances	
		Computer Model (H)	Sinusoidal Winding Distribution (H)
Blue Phase Self Inductance	0.28	0.26	0.32
Blue/Red Phase Mutual Inductance	-0.13	-0.12	-0.16
Blue/Yellow Phase Mutual Inductance	-0.13	-0.12	-0.16

There is close agreement between the measured values and the results of the computer model which take the actual winding distribution into account; but the results based on the assumption of perfectly sinusoidally distributed windings are somewhat higher.

The variation of the self and mutual inductances of the stator phases with rotor position is illustrated in Figs. 4.5 and 4.6: predicted and measured results are shown. It can be seen that the computed results correlate well with the experimental data.

4.2.3 Self and mutual components of the stator leakage inductances

As stated in Section 3.4 above it is difficult to calculate precisely the leakage reactances of a stator winding. Measured values, which allow for the operating environment, were therefore used in the computations. They were:

self component of stator leakage inductance = 0.0165 H

mutual component of stator leakage inductance = -0.0046 H

These components were the same for all phases, and were substantially independent of motor airgap and rotor position.

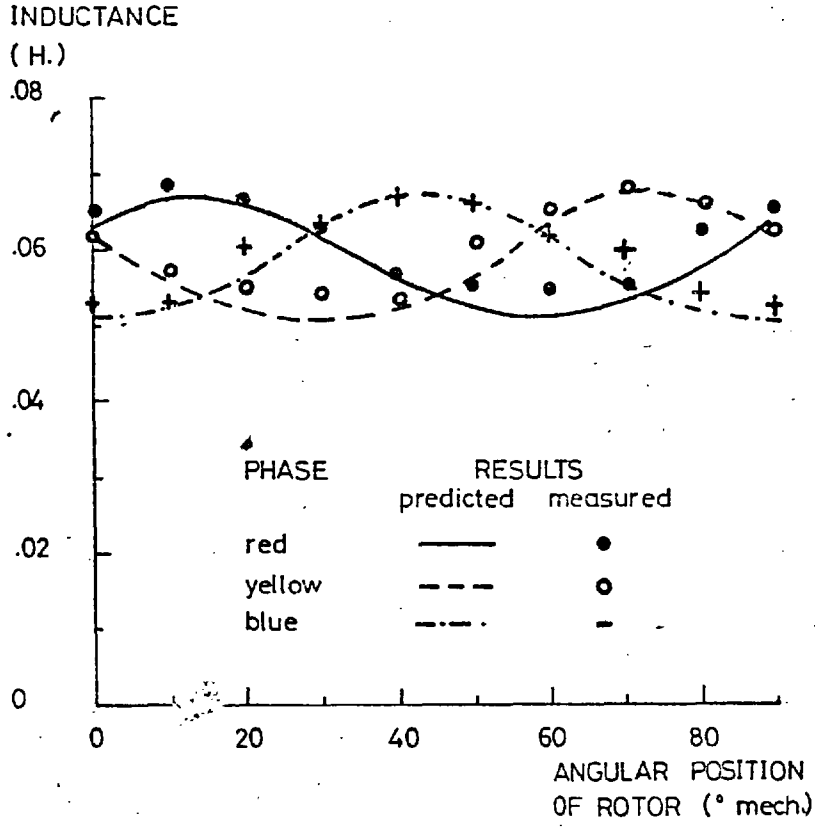

VARIATION OF SELF INDUCTANCES OF STATOR PHASES WITH ROTOR POSITION

FIG. 4.5

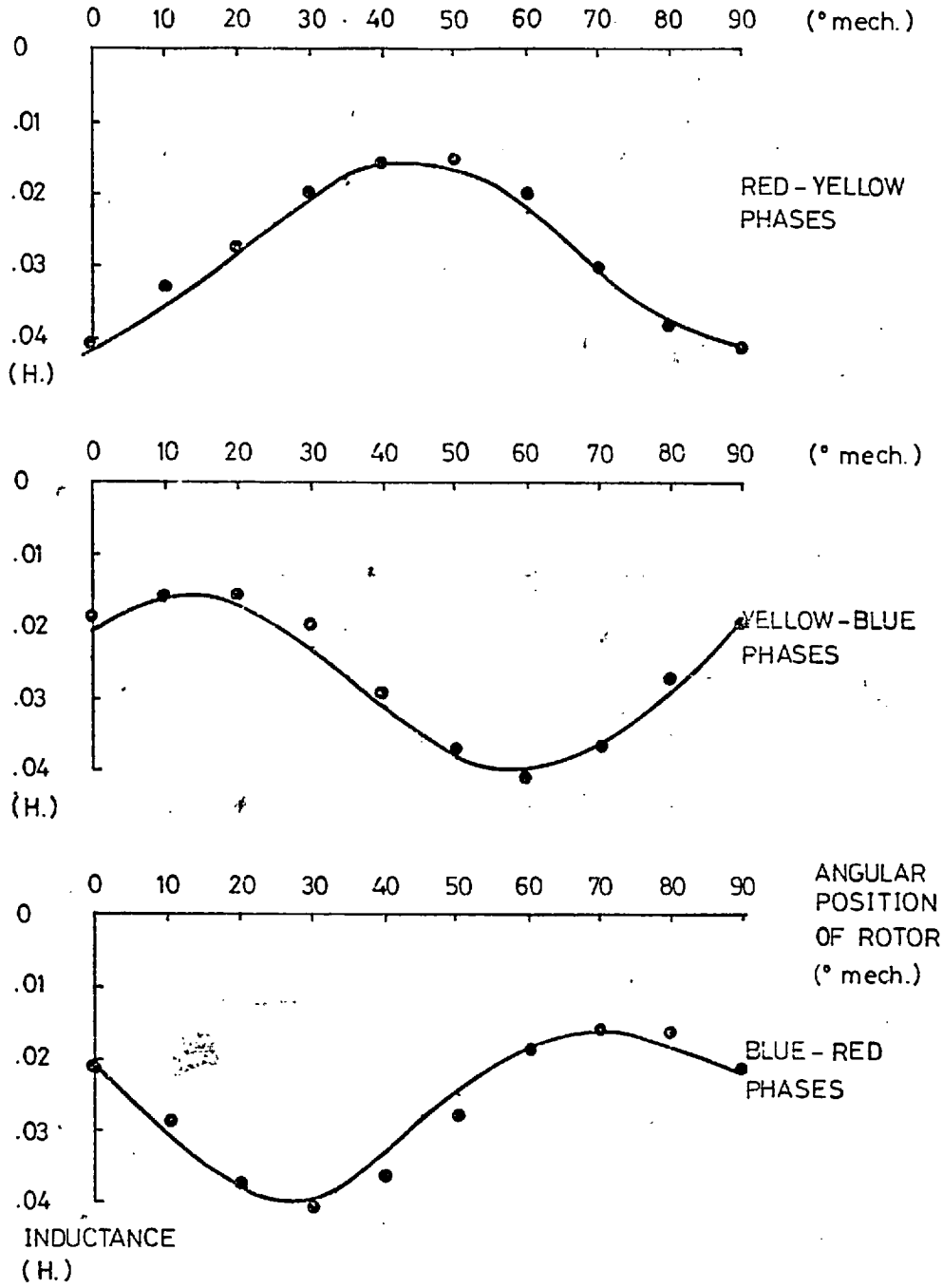

VARIATION WITH ROTOR POSITION OF MUTUAL INDUCTANCES BETWEEN STATOR PHASES

FIG. 4.6

4.2.4 Self and mutual inductances of rotor loops

Measurement of the rotor parameters presents considerable difficulties. This is because there is no access to the notional elements which make up the equivalent electrical network of the rotor. It is possible to measure the parameters of a physical reproduction of the equivalent network, but this gives no indication of whether that network is a valid representation of the rotor.

The first aspect of the rotor model that was checked was the filament coil method of predicting the current distribution in the rotor bars. This was achieved by placing an aluminium sheet in the airgap between two laminated iron cores as shown in Fig. 4.7. The aluminium sheet was slit along four-fifths of its length to force transverse current flow under the iron blocks. In Fig. 4.7(c) the flux density distribution measured across the aluminium plate when it was excited is compared with the predictions for it from a filament coil analysis. An acceptable level of agreement can be seen to exist. The discrepancy might well arise from the theoretical assumption of zero flux leakage from the ends of the iron blocks. On the basis of these results it can be assumed that the filament coil method is capable of giving a good estimate of the current distribution across a wide conductor; and the theoretical distribution of currents across the bars of the notional rotor loops was therefore utilised to enable the circuit parameters of the loops to be measured experimentally. The principle of the method is to replace the bar conductors of the rotor loops by a discrete coil so that the total flux linkage of the coil carrying the total loop current is equal to the total flux linkage of the rotor loop with distributed currents. Expressed mathematically, the total flux linkage of a set of 'n' parallel connected concentric coils which is subjected to a uniform magnetic field normal to the plane of the coils is given by:

$$\lambda_c = bW\,(y_1\delta_{i1} + y_2\delta_{i2} + \ldots y_r\delta_{ir} + \ldots y_n\delta_{in})$$
$$= bW \sum_{r=1}^{n} y_r\delta_{ir}$$

where b is the flux density of the incident field
W is the width of the coil
y_r is the breadth of the r^{th} coil
δ_{ir} is the current in the r^{th} filament coil

FLUX DENSITY DISTRIBUTION PRODUCED BY STRIP CONDUCTORS IN A UNIFORM AIRGAP

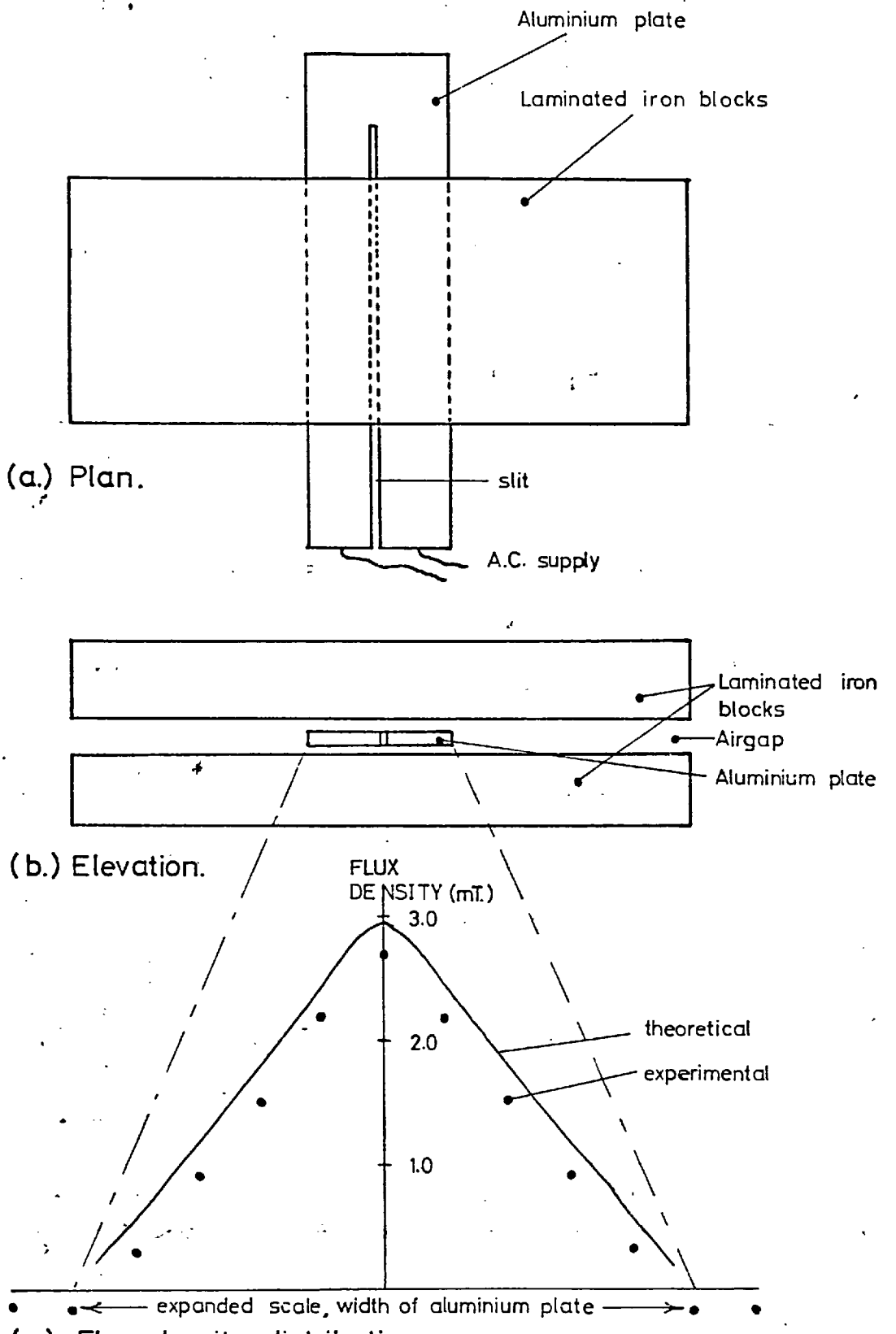

FIG. 4.7

If y_m is the breadth of an equivalent coil, its total flux linkage, λ_m, is given by:

$$\lambda_m = bW\, y_m \sum_{r=1}^{n} \delta_{ir} \qquad (4.3)$$

And for $\lambda_m = \lambda_c$

$$y_m = \frac{\sum_{r=1}^{n} y_r \delta_{ir}}{\sum_{r=1}^{n} \delta_{ir}} \qquad (4.4)$$

Hence a single coil which spans y_m can be substituted for the set of concentric coils described above, for the purposes of inductance calculations.

Computation of the dimensions of single coils that were equivalent to rotor loops 1 and 3, using their theoretical current distributions, gave the following results:

Rotor Loop Number	Coil Span (in degrees)	Position on Rotor (in degrees)	
		From	To
1('iron' loop)	27	355	22
3('copper' loop)	15	51	66

Rotor inductances measured by means of these equivalent coils are compared below with their theoretical values.

Rotor Inductance	Measured (H)	Computed (H)
Self Inductance of Loop 1	2.16×10^{-7}	2.61×10^{-7}
Mutual Inductance, Loops 1 & 3	-5.04×10^{-9}	-6.13×10^{-9}
Mutual Inductance, Loops 1 & 9	-1.91×10^{-8}	-2.84×10^{-8}
Mutual Inductance, Loops 1 & 11	-5.51×10^{-9}	-6.18×10^{-9}

The level of agreement between the two sets of results gives some indication that the computed parameters for the rotor model are representative of the rotor characteristics.

4.2.5 End ring and bar resistances of rotor loops

No way could be devised to measure the resistances of the bar and end ring components of the rotor model. These were the only elements of the model which could not be measured directly or indirectly, however, and the shape of the asynchronous torque curve of the motor will give some indication of the precision with which they were computed.

4.2.6 Mutual inductances between rotor loops and stator phases

These inductances were measured by exciting each of the stator phases in turn and measuring the flux linkage with the equivalent single coil versions of the rotor loops (see Section 4.2.4 above) for a range of rotor positions. The theoretical and experimental results are illustrated in Fig. 4.8 for two loops: rotor loop 1 which contains an iron portion; and rotor loop 3 which is plain copper. Close correlation can be seen to exist between predicted and measured results in both cases.

The rotor inductances and resistances, and the stator rotor inductances were calculated by the filament coil method for a range of slip frequencies, i.e. 1.0, 0.8, 0.6, 0.4 and 0.0 per unit slip. The percentage changes in the various parameters between unity and zero slip are summarised below:

Parameter	Percentage Change in Value between Unity and Zero Slip
Rotor Inductances:	
Self inductance of rotor loop 1 (encloses iron segment)	0.4%
Self inductance of rotor loop 3 (plain copper)	1.7%
Mutual inductance of rotor loops 1 and 2	0.4%
Mutual inductance of rotor loops 1 and 3	0.7%
Mutual inductance of rotor loops 3 and 7	3.0%

Rotor Resistances:

Rotor Bar between loops 1 and 2	0.5%
Rotor Bar between loops 3 and 4	8.7%
Outer end ring resistance of loop 1	0.4%
Outer end ring resistance of loop 3	8.2%

Stator-Rotor Inductances:

Maximum mutual inductance between rotor loop 1 and the red phase	0%
Maximum mutual inductance between rotor loop 3 and the red phase	1.9%

It is noticeable from these results that the larger parameters which dominate the performance of the motor - those associated with the 'iron' loops - are least sensitive to rotor frequency. This is because the circulating currents are constrained to narrow rotor bars in which there can be little variation in current distribution with the frequency of excitation; and the infinitely permeable iron rotor segments ensure that the flux distribution is substantially independent of rotor frequency. This leads to the conclusion that it is probably an unnecessary refinement to make these parameters slip dependent. Such a precaution is possibly more necessary in a sheet rotor induction motor, for as can be seen above, the resistance of the 'copper' loops varies by almost 10% between unity and zero slip frequency.

This concludes the comparison of the theoretical and experimental values of the static motor parameters. The following sections investigate its dynamic performance.

4.3 Steady state performance

4.3.1 Introduction

This section is concerned with the steady state performance of the double sided salient pole disc reluctance motor under synchronous and

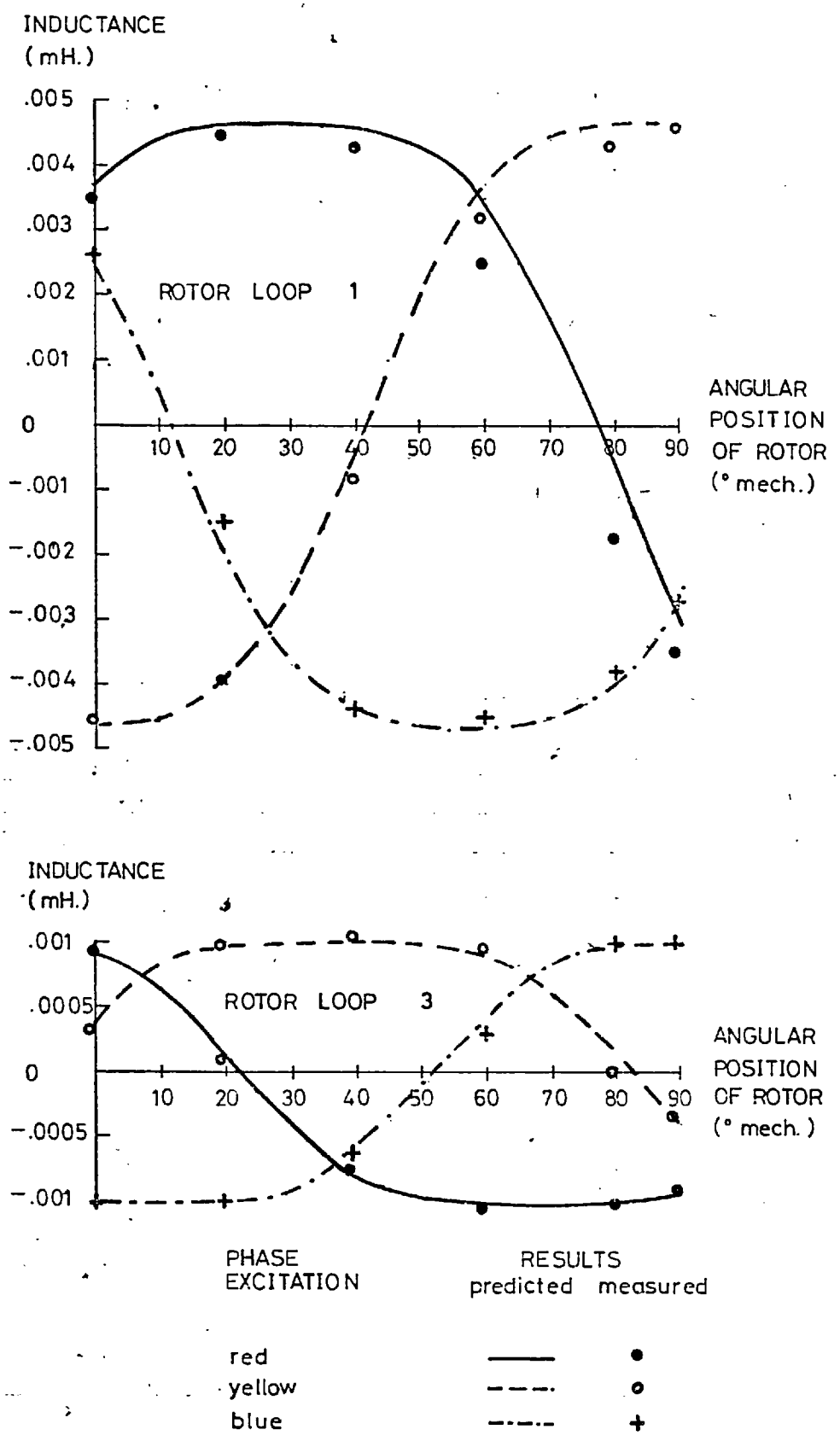

VARIATION WITH ROTOR POSITION OF MUTUAL INDUCTANCES BETWEEN STATOR PHASES AND EQUIVALENT ROTOR COILS

FIG.4.8

asynchronous conditions: measured and predicted performances are compared.

The motor was arranged with the 0.19 inch thick rotor situated centrally in an airgap of 0.285 inches between the two stators; this left a mechanical clearance of .047 inches between the rotor and each of the stator surfaces. The benefits to be gained from using smaller airgaps are assessed theoretically in the conclusions at the end of this section, but to achieve them in practice would require many precautions to be taken in manufacturing the motor assembly. These would appear to include ground stator surfaces, bored-in-line bearing housings and a rigid, precise rotor assembly.

The motor tests were carried out with the series-connected stators supplied from a line voltage of 300 V rms. As illustrated in Fig. 4.9, the stator windings were then loaded at around 3,500 A/in^2, and the rapidly increasing level of iron losses indicated that the stator core was operating at an acceptably high flux density. Under these conditions it exhibited an X_d/X_q ratio of 1.4, when unloaded it could achieve synchronism from start-up within two revolutions of the rotor, it was able to synchronise twice its own inertia against rated synchronous torque, and it operated stably at synchronous speed.

4.3.2 Asynchronous performance

The steady state torque vs speed and current vs speed characteristics of the motor at speeds from standstill to a p.u. slip of 0.2 are shown in Fig. 4.10. At speeds above 0.2 slip the reluctance torque pulsations become noticeable, and this speed range has therefore been excluded from the present results.

The main conclusion that can be deduced from these results is that the correlation between the theoretical and experimental characteristics is quite good. There is particularly close agreement between the torque characteristics, but the predicted phase current is some 15%-20% less than measured. These results can be taken as a general vindication of the method used for modelling the conducting circuits of the rotor. The shape of the torque speed curve is indicative of a "high resistance" rotor. In the present case it is caused by a low value of X_m/R_2, the

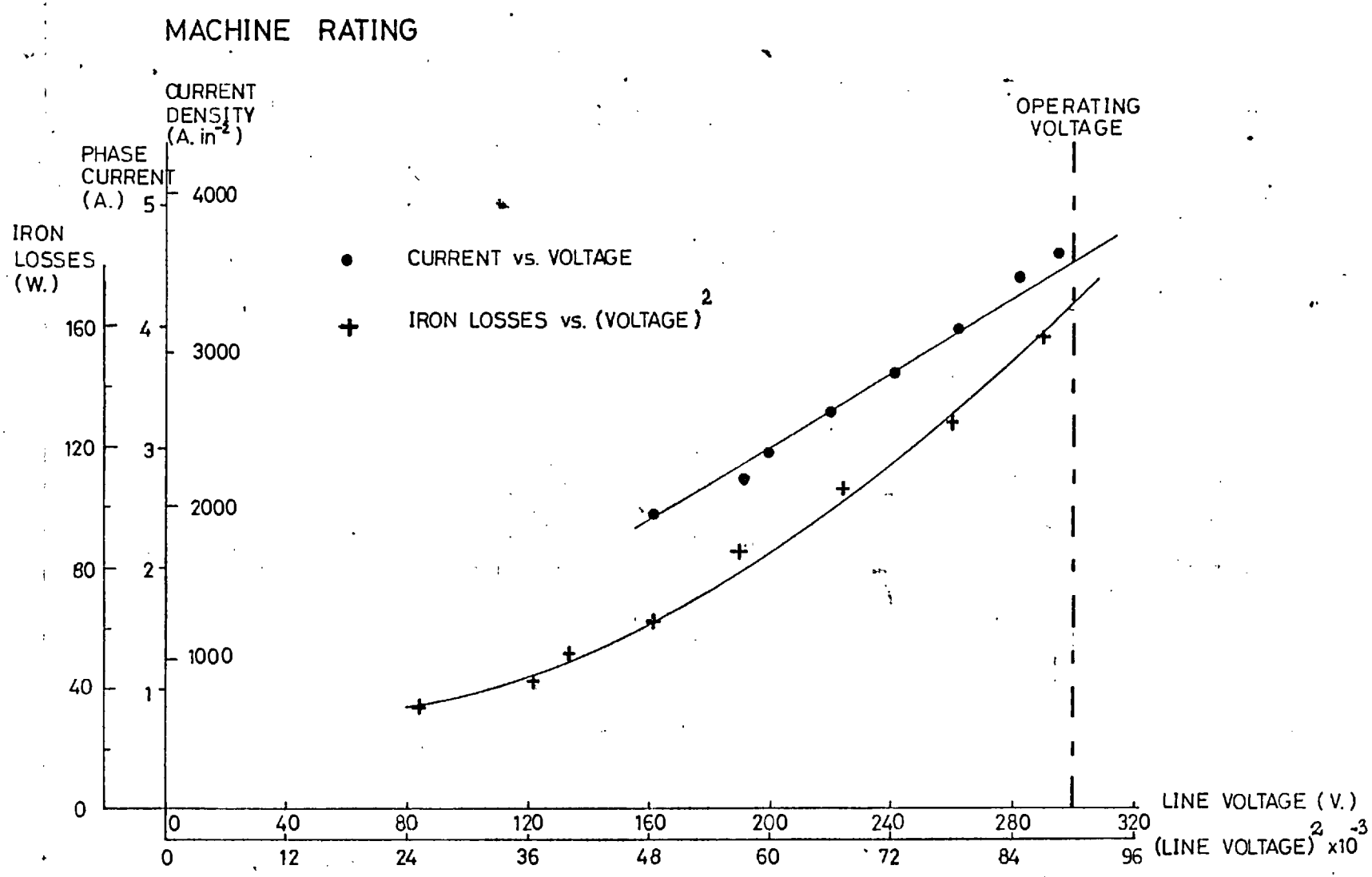
MACHINE RATING
CURRENT DENSITY (A. in^{-2})
PHASE CURRENT (A.)
IRON LOSSES (W.)
OPERATING VOLTAGE
CURRENT vs. VOLTAGE
IRON LOSSES vs. (VOLTAGE)^2
LINE VOLTAGE (V.)
(LINE VOLTAGE)^2 x10^{-3}
0
40
80
120
160
200
240
280
320
12
24
36
48
60
72
84
96
1000
2000
3000
4000
1
2
3
4
5

FIG. 4.9

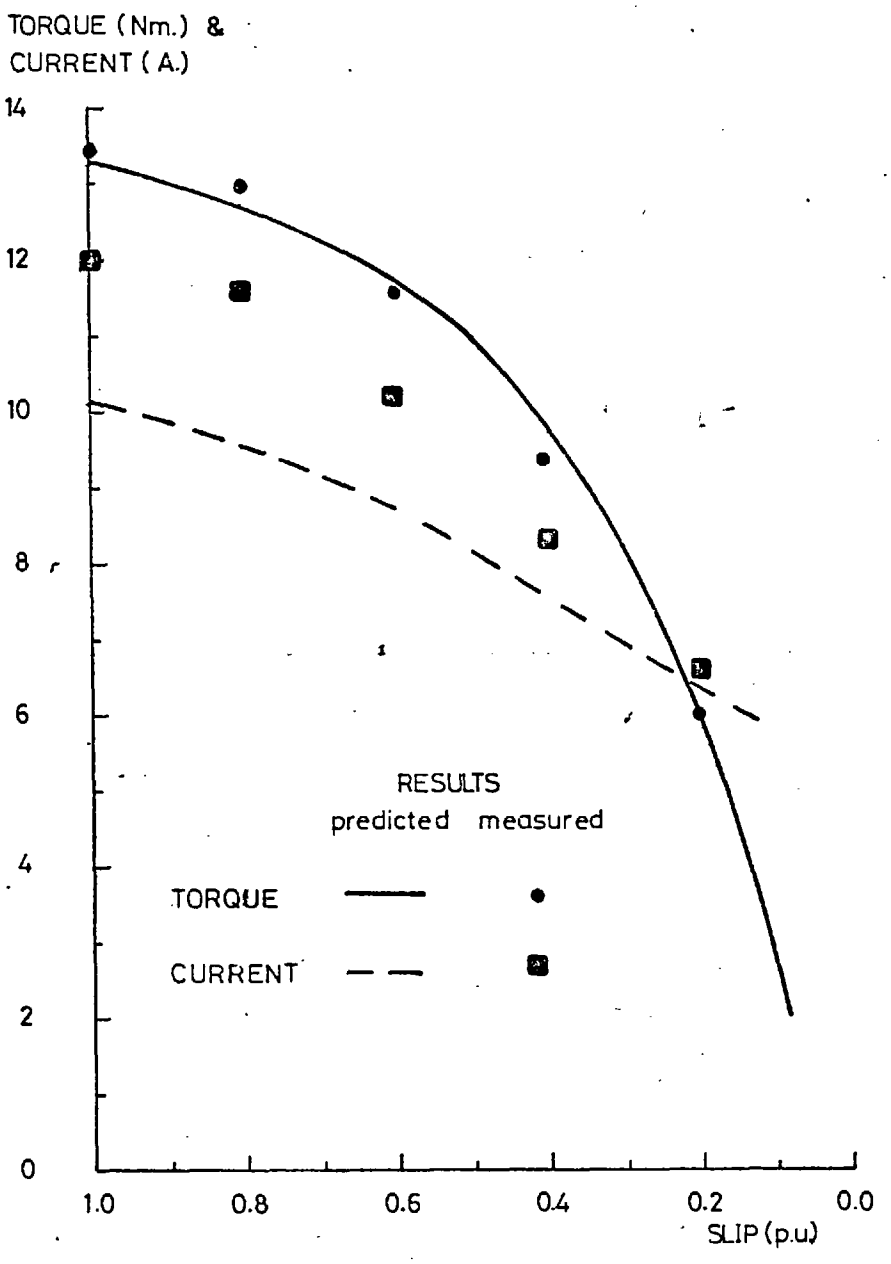

ASYNCHRONOUS STEADY-STATE CHARACTERISTICS

FIG. 4.10

small magnetising reactance being a result of the large airgap between the stators. The value of the X_m/R_2 ratio for an induction motor which is "equivalent" to the present reluctance motor, i.e. one obtained if the iron inserts are 'spread' uniformly around airgap, and the rotor copper is redistributed uniformly, can be shown to be approximately 4. The computer model predicted a torque vs speed curve which was almost identical to that shown in Fig. 4.10 when fed with input data for the "equivalent" induction motor.

An estimated power balance for the asynchronous operation of the present reluctance motor is shown in Fig. 4.11. The main purpose of this diagram is to show that a large proportion of the input power is dissipated as stator copper losses - approximately half the total input power is accounted for in this way. It is a direct result of the high magnetising current required to drive flux across the large airgap of the machine, and makes it impossible to achieve a good efficiency from a motor of this type.

4.3.3 Synchronous performance

At synchronous speed the induction torque of the motor is substantially zero, and the drive is produced by the reluctance effect of the salient rotor poles interacting with the stator field. In terms of the torque components identified in equation 3.8, the variation with angular position of the mutual inductances between the stator phases and the rotor loops is zero; the only inductances which vary with rotor position are the self and mutual inductances of the stator windings which are modulated by the iron rotor portions.

The synchronous characteristics of the motor, with respect to load angle are illustrated in Fig. 4.12. The load angle concerned is the angle between the applied voltage and the quadrature axis (or induced voltage, in excited synchronous machines). The choice of load angle, and the reason for non-zero torque at zero load angle are discussed in detail in Section 5.3.2 below. The torque can be seen in Fig. 4.12 to increase in a predominantly sinusoidal manner with increasing load angle, the current, power factor and efficiency increasing in step with it. The steady state synchronous behaviour of the motor can be predicted by the computer model which has been described above. It is more economic in

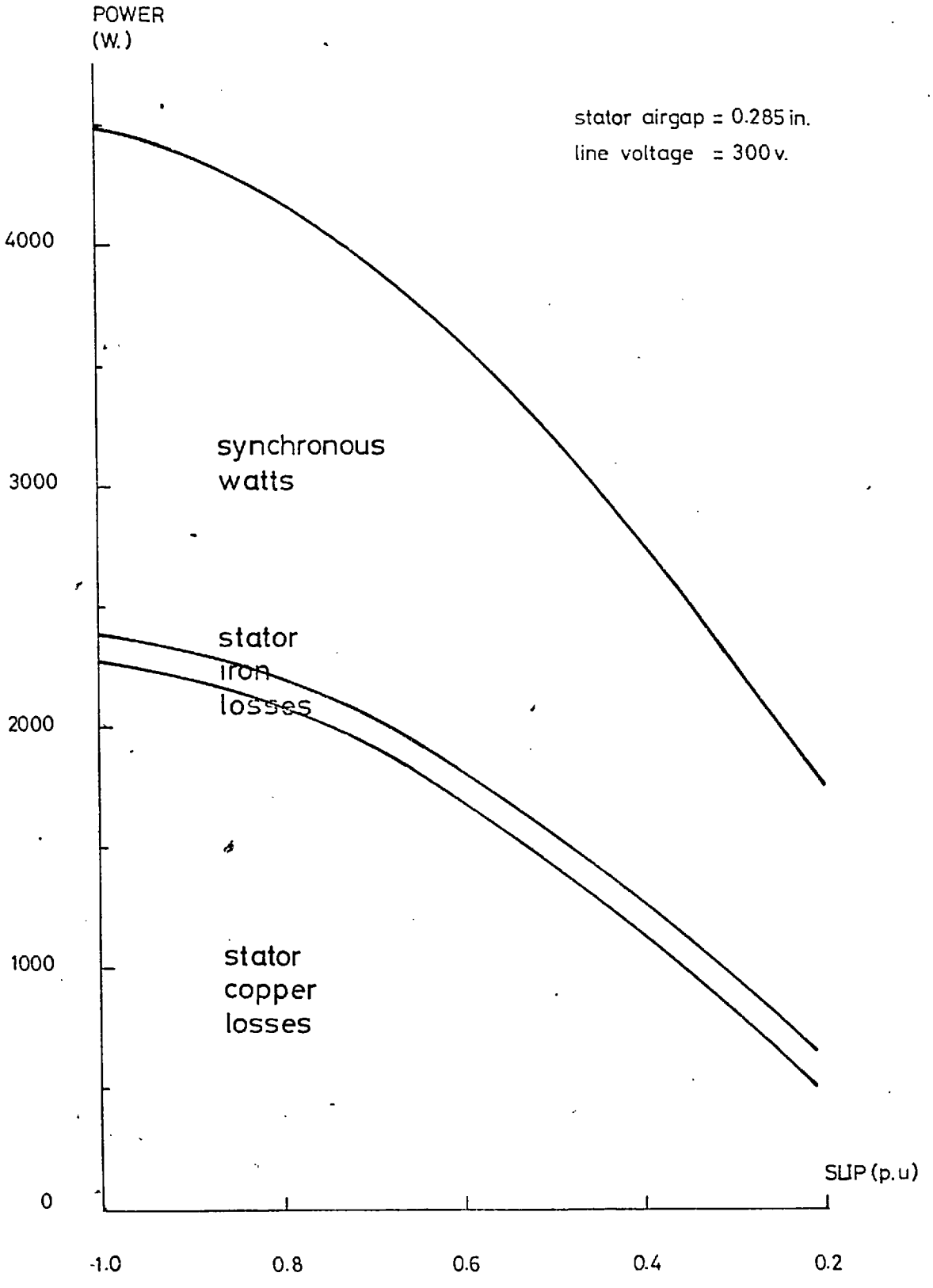

INPUT POWER BALANCE

FIG. 4.11

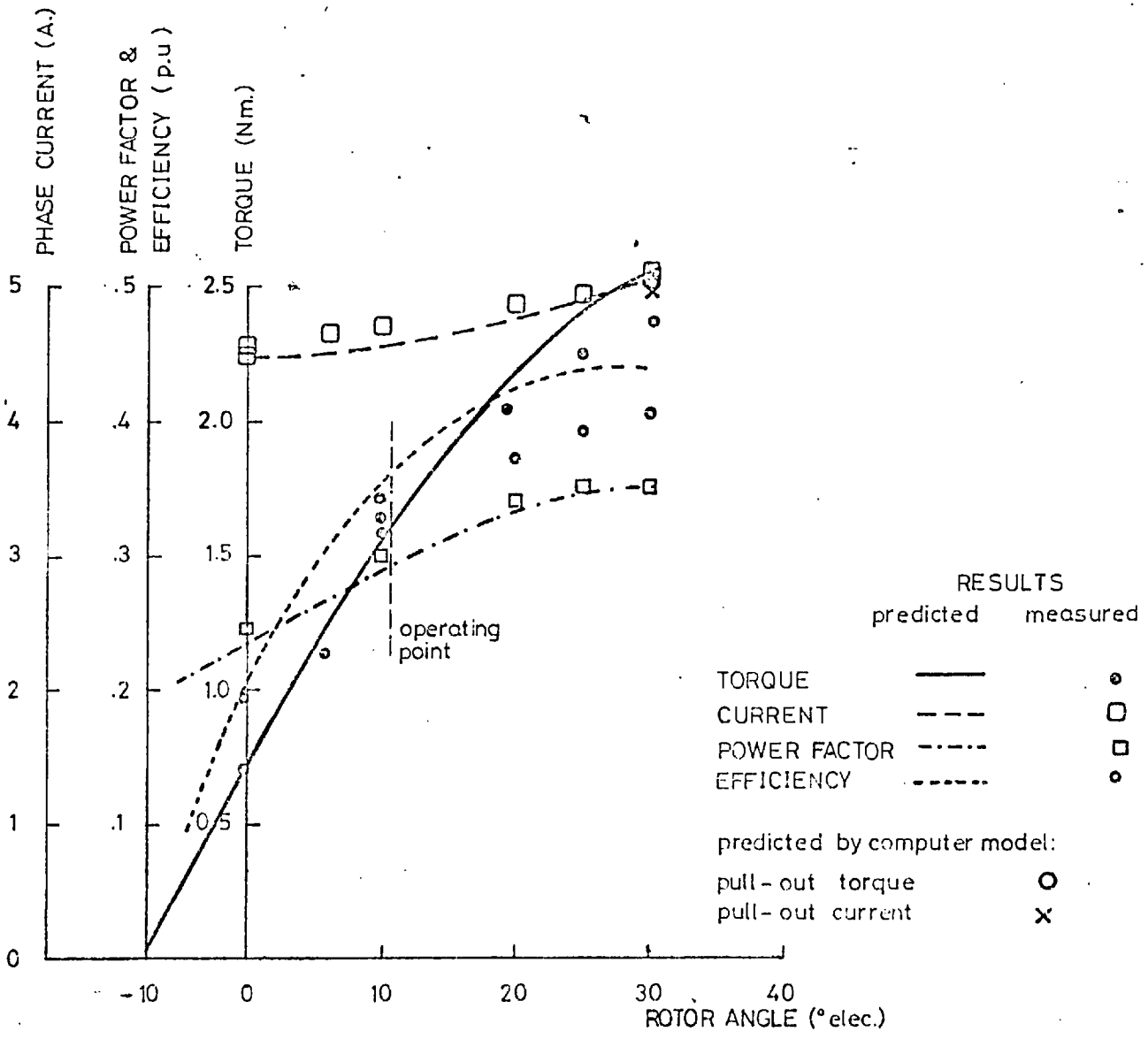

FIG. 4.12

SYNCHRONOUS CHARACTERISTICS

terms of computer time, however, to use the standard two axis representation of the motor to obtain its theoretical behaviour at synchronous speed. The method of doing this is described in Section 5.3.3 and the theoretical results in Fig. 4.12 were obtained by this method. The motor current and torque at pull-out, as calculated by the computer model, are also shown in Fig. 4.12, and agree very well with the other predictions. These predictions are generally in close agreement with the measured results, although they appear to overestimate by almost 10% the pull-out torque which can be produced by the motor. This is mainly caused by a theoretical underestimation of the quadrature axis reactance of the motor. It is interesting to note that the direct and quadrature axis reactances which were derived from the single phase quantities calculated by the computer model agree well with the measured values, while those calculated by the theoretical method suggested by Lawrenson[2] seriously overestimate the direct axis reactance. The results are as follows:

Method of Calculation	X_d (Ω)	X_q (Ω)	X_d/X_q
By analytical method	47.2	27.5	1.72
From computer model	38.6	28.4	1.36
Measured results	38.4	29.5	1.30

This is because the variable fringe fluxes around the stator periphery cannot be taken into account by the analytical method.

The normal steady-state synchronous operating point for a reluctance motor is often taken to be at two-thirds of its pull-out capacity. At this point, which is indicated on Fig. 4.12, the motor is producing a torque of 1.6 Nm (250 watts) at a power factor and efficiency of 0.3 and 34% respectively. The direct-on-line starting current of the motor can be seen, from Fig. 4.10, to be some two-and-a-half times the current at its synchronous operating point.

It is interesting to investigate the improvements in performance that might be gained if the motor were to be constructed to very close tolerances, and the running clearances between the stators and rotor reduced to 0.020 inches, say. According to the theoretical method used above the motor parameters and its performance at two thirds of its pull-out capacity would be:

	Test Motor	Improved Motor
Running Clearance (in)	.045	.020
X_d (Ω)	38.6	65.1
X_q (Ω)	28.4	37.2
X_d/X_q	1.36	1.75
At $\frac{2}{3}$ pull-out capacity		
Torque (Nm)	1.6	2.1
Phase current (A)	4.7	2.9
Power factor (p.u.)	0.29	0.38
Efficiency (%)	34	56

It appears that a reduced running clearance would enhance the performance of the test motor but nevertheless, even with these improvements the motor would still have the characteristically poor performance of a salient pole reluctance motor.

4.4 Transient performance

4.4.1 Introduction and experimental method

In the present context the transient performance of the reluctance motor includes its behaviour from the instant at which the supply is switched on at an arbitrary instant in time until it achieves stable synchronous operating conditions. It therefore includes asynchronous acceleration under the influence of electrical transients, the synchronisation process and the attainment of a stable synchronous state. In the general case the synchronisation process takes place before the electrical transients have died away.

The starting sequence of a reluctance motor therefore creates suitably arduous conditions under which to assess the effectiveness of a theoretical method which purports to handle the transient performance of a motor, and was consequently used as a test sequence in this case. The experimental behaviour of the motor was monitored from the instant of switch on to synchronous speed; and the theoretical performance, for

the same starting conditions, was computed. The experimental and theoretical results are presented and discussed in Section 4.4.2 below.

The motor voltages and currents during the starting sequence were monitored by conventional techniques on a U-V recorder; and the motor torque characteristic was obtained by a photographic method. A six inch diameter disc which had three hundred equal divisions engraved around its periphery was attached to the motor shaft. This disc was photographed at a rate of 1000 frames per second during the starting sequence of the motor. Angular displacement versus time data were obtained from the film which was processed numerically to provide, in conjunction with the moment of inertia of the rotating parts, the torque versus speed characteristic of the motor.

4.4.2 Comparison of experimental and theoretical results

For the transient starting sequence described in the previous section the motor was set up in the manner described in Section 4.3.1 above, and when switched on was connected direct-on-line to a 300 V rms 3-phase supply. No external load was coupled to the motor shaft. The predicted and measured variations in current and torque with respect to time from the instant of switch on are plotted on Fig. 4.13. The predicted current, in Fig. 4.13(b) can be seen to be cophasal with the measured current; but as found in the steady state performance in Fig. 4.10 the peak amplitudes of the predicted currents are some 15% less than measured. It appears from Fig. 4.13(b) that current transients due to switch on have largely died away after six cycles; and distortion of the theoretical current waveform thereafter is due to second harmonic modulation by the salient poles. The apparent freedom of the measured current waveform from this distortion was thought to be due to the effect of the leakage reactance of the variable autotransformer which was connected between the 415 V, 3 phase supply and the motor. For as shown in Fig. 4.14 the voltage waveform appearing at the motor terminals was non-sinusoidal, unlike the theoretical applied voltage waveform, and this may be attributed to harmonic voltage drops across the leakage reactance of the variable autotransformer. This effect, however, did not appear to be sufficiently serious to warrant re-winding the motor for direct operation from a 415 V supply.

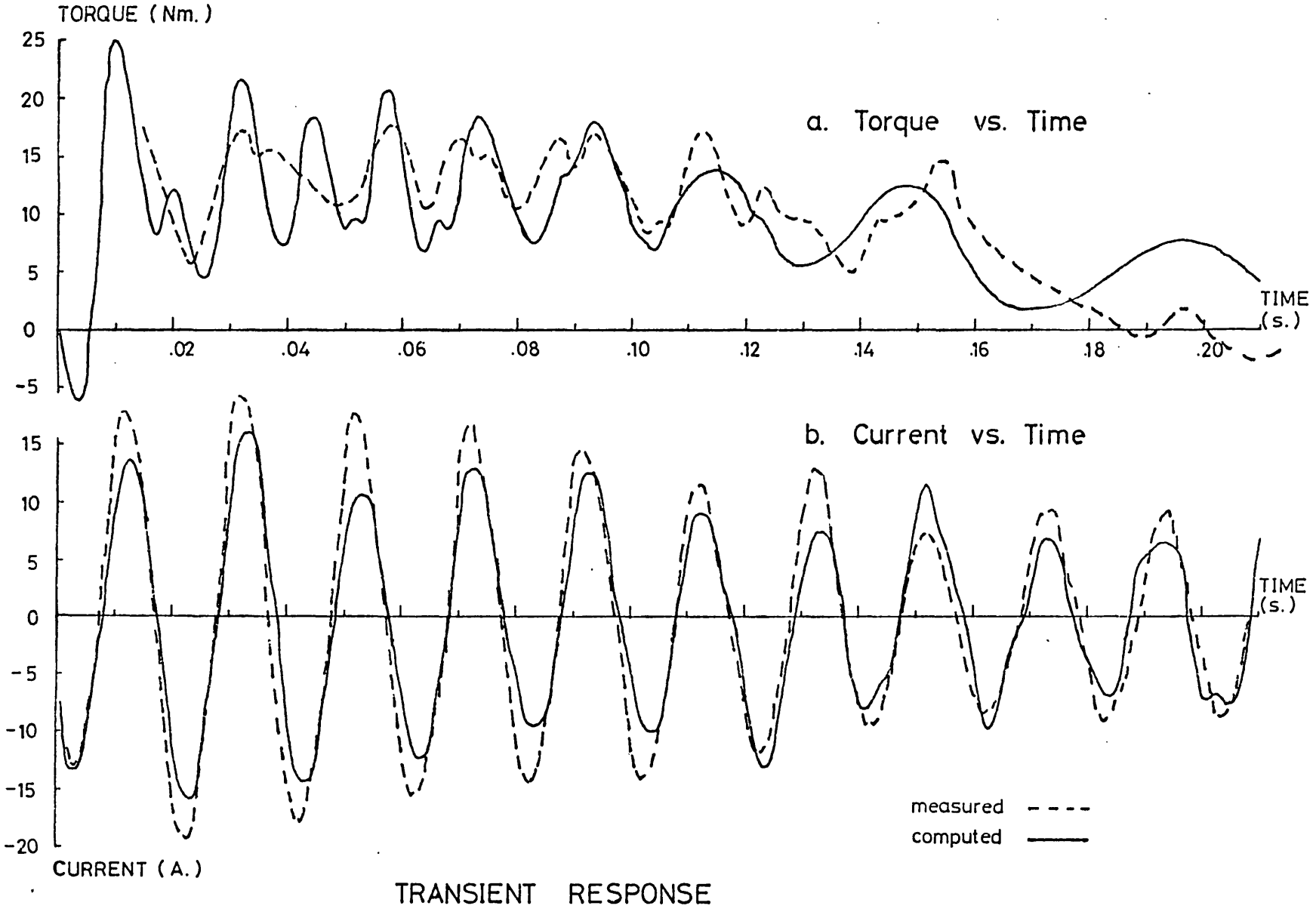

FIG. 4.13 TRANSIENT RESPONSE

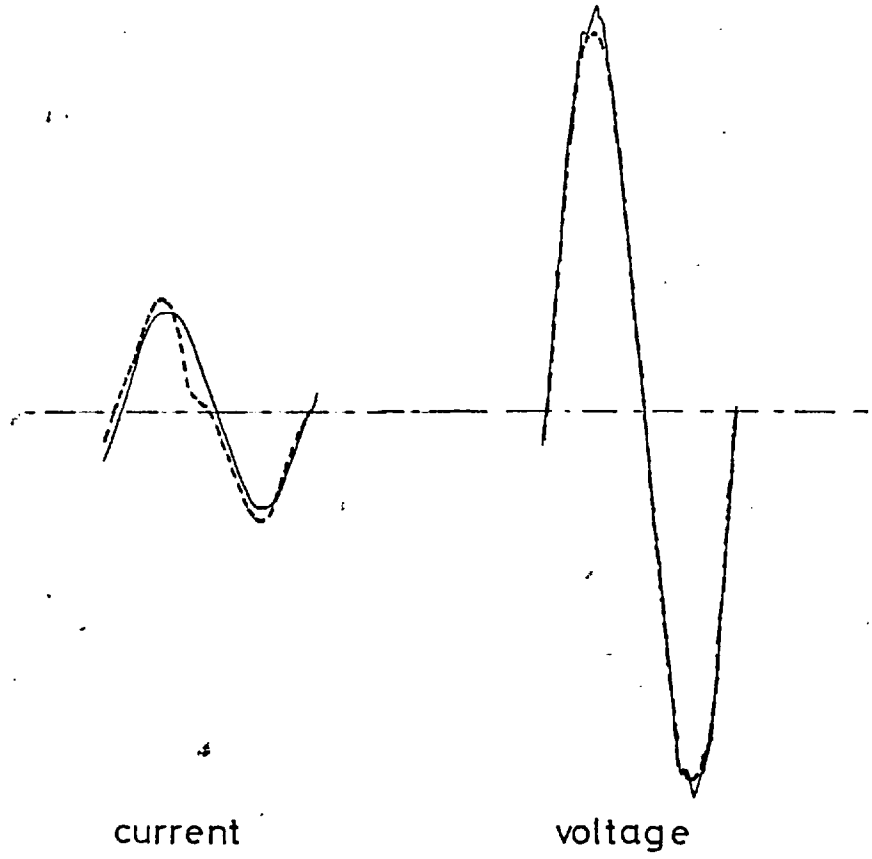

PHASE CURRENT AND VOLTAGE WAVEFORMS AT SYNCHRONOUS SPEED

THEORETICAL ----

EXPERIMENTAL ——

FIG. 4.14

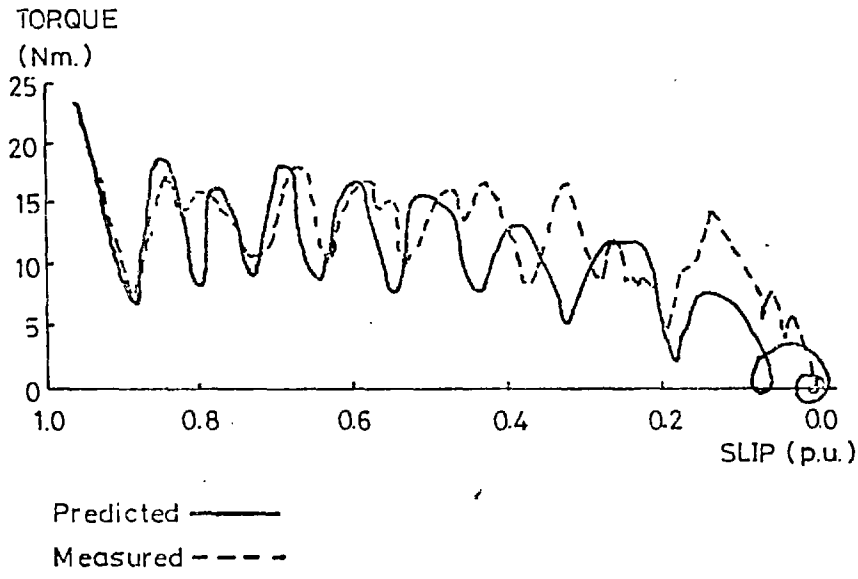

TRANSIENT PERFORMANCE

FIG. 4.15

The predicted and measured torque versus time characteristics are compared in Fig. 4.13(a) and display some measure of agreement. The two torque characteristics become progressively out of phase however. This is inevitable, as any error between the predicted and measured torque during the run up period will give an accumulating error between the angular displacements of the theoretical and actual rotors. For example, 0.2 secs after switch-on, the theoretical and experimental angular displacements of the rotor were 1004° and 1054° respectively.

The frequency of reluctance torque pulsations, f_r, at a slip speed, s, can be shown to be equal to:

$$f_r = (\frac{f}{p} - s)\ 2p \qquad (4.5)$$

for a 2p pole motor connected to an fHz supply.

At the right hand end of Fig. 4.13(a) the frequency of torque pulsation,when the measured motor speed is 20 Hz, also corresponds to a motor speed of 20 Hz from equation 4.5 above; the torque pulsation in that area of Fig. 4.13(a) is therefore due to reluctance torque at a slightly subsynchronous speed. It is impractical to illustrate more of the torque vs time characteristics as the torque pulsations become very slow and would require a long time axis to display them. The synchronisation process is displayed more effectively on a torque vs speed curve (which is derived from the torque vs time results) as shown in Fig. 4.15. In this graph also, the theoretical and measured reluctance torque pulsations become out of phase at subsynchronous speeds, for the reasons given above, but the computer model otherwise gives a sensible prediction of the transient behaviour of the motor.

The synchronisation process of a reluctance motor is an essentially transient phenomenon. It is a vital part of reluctance motor operation as the rating of the motor is largely determined by the coupled load that it can drive into synchronism. Given a set of operating conditions, such as load inertia, friction and windage torques, line voltage and starting conditions, the computer model can simulate the behaviour of the motor during the synchronisation cycle. This can be useful for a study of the behaviour of a given motor design under prescribed conditions, but does not easily help to evaluate the maximum synchronising capability of a motor. It could only be achieved by repetitive running of the

computer programme for a range of starting conditions, friction losses and coupled loads, until its maximum capability was discovered. Apart from the expense, in terms of computing time, that is involved in an exercise of this nature, it is in any case an unsatisfying approach to the problem. A less arduous solution was offered by Lawrenson and Mathur [3]. They established a synchronisation criterion which defines the maximum inertia that a reluctance motor can synchronise for specified motor parameters and load conditions. This criterion is explained in Section 5.3.3 below, but results from it are compared with experimental performance in Fig. 4.16. It can be seen that excellent agreement exists between the synchronising capability of the motor for a range of load inertias and supply voltages with a constant friction torque of 0.51 Nm. This shows again that the prediction of the motor parameters by the computer model is acceptable and indicates that the synchronisation criterion is reliable. The full-load torque of this motor was established as 1.6 Nm in Fig. 4.12. At this load torque, its predicted synchronisable inertia is indicated in Fig. 4.16: it can synchronise a total inertia of 0.023 Kgf.m^2, which includes the inertia of its own rotor of 0.013 Kgf.m^2.

4.5 Conclusions

Conclusions can be drawn on two aspects of the work presented in this Chapter: on the quality of performance that can be obtained from a double sided salient pole disc motor; and on the effectiveness of the theoretical method of analysis.

The conclusions about the quality of motor performance have a negative slant. Following the conclusions in Section 2.4, and the foregoing results, it appears that the double sided disc reluctance motor will be inferior to an equivalent cylindrical machine. This is for three reasons:

i) The disc motor contains a second airgap which makes the machine generally worse and reduces the x_d/x_q ratio.

ii) The disc motor usually has a high end winding leakage reactance which serves to reduce the X_d/X_q ratio. This is especially the case for low pole number machines.

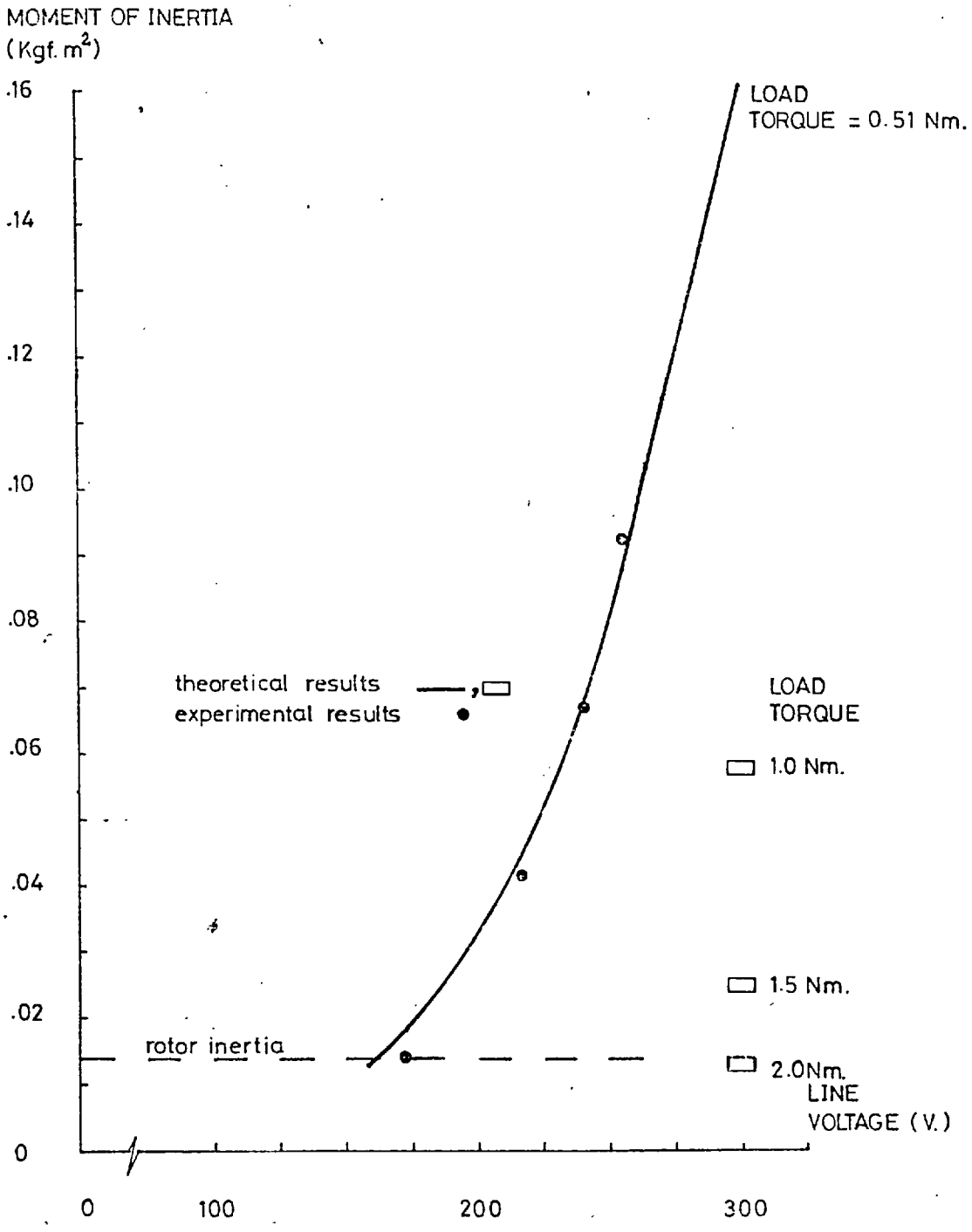

SYNCHRONISING CAPABILITY OF DOUBLE SIDED SALIENT POLE RELUCTANCE MOTOR

FIG. 4.16

iii) The high inertia of the disc rotor, higher than the equivalent cylindrical rotor, reduces the inertia of the coupled load that can be synchronised.

The performance of the prototype motor which possessed these defects to a relatively high degree has been shown to be unimpressive. At its synchronous operating point its power factor and efficiency were 0.3 and 35% respectively, and it could synchronise just as much again as its own rotor inertia. By improved designs it has been shown that the operating power factor and efficiency might be raised to say 0.4 and 60%, but its performance is inherently limited to the low standard which is characteristic of salient pole machines. The disc geometry appears to aggravate the design problems with this type of motor. As shown in Section 2.6, however, the salient pole rotor is the only type of reluctance rotor that will operate with the double sided stator configuration.

The use of double sided disc reluctance motors is therefore likely to be limited to applications where both brushless synchronous operation and a disc rotor geometry are essential. Typically these might occur when the rotor shaft must be allowed a degree of eccentric movement; or when a reduced rotor shaft length is at a premium.

The computer model which was described in Chapter 3 has been shown in this Chapter to be capable of predicting the performance of a sheet rotor salient pole reluctance motor under arduous operating conditions. It is noticeable, however, that this type of method cannot easily be used to establish design criteria for these motors. It seems therefore that the appropriate function of this theoretical method is for the simulation of the behaviour of a given motor design under prescribed operating sequences. These may include transient and fault conditions. It does not therefore supplement the analytical methods for the prediction of motor behaviour, but rather complements them by extending the range of conditions under which the motor performance can be predicted. The analytical methods, which are in many cases very approximate, are therefore essential to aid the initial understanding of motor behaviour, and to establish criteria for their design.

In the present case the computer model has been shown to be capable of simulating the behaviour of a complex motor - the rotor has no defined

current paths and contains asymmetrically positioned iron inserts - under arduous transient conditions. For this, computation of the motor parameters is the important process. The 'filament coil' model of the rotor circuits appears to have been particularly successful in deriving adequate rotor parameter values without increasing beyond four per pole pitch the number of notional rotor coils - and hence equations - that need to be considered.

Chapter 4: References

1. Say, M.G., "The Performance and Design of Alternating Current Machines", 1958, 3rd Edition, Pitman.

2. Lawrenson, P.J. and Agu, L.A., "Theory and Performance of Polyphase Reluctance Machines", Proc.IEE, 1964, 111, (8), pp. 1435-1445.

3. Lawrenson, P.J. and Mathur , R.M., "Pull-in Criterion for Reluctance Motors", Proc.IEE, 1973, 120, (9), pp. 982-986.

CHAPTER FIVE

Theory and Performance of a Single-Sided Segmented-Rotor Axial Flux Disc Reluctance Motor

5.1 Introduction

A segmented rotor reluctance motor was identified in Section 2.5 as one of the more attractive forms of single sided disc reluctance motor. Together with the 'essential barrier' machine of Fong[1] and the axially laminated reluctance motor of Cruickshank[2] the segmented rotor reluctance motor design provides a standard of performance which is superior to that of the salient pole machine. But between these three types of machine there is perhaps little to distinguish them in terms of their performance. The segmented rotor configuration has been chosen for the disc motor geometry, however, because the manufacturing processes required for its construction would be very similar to those for the disc induction motor. The strip wound core required for an induction rotor, would be divided into segments for the reluctance rotor.

The cylindrical form of the segmented rotor machine has been given considerable attention by Lawrenson et al[3,4,5,6,7,8,9,10,11,12,13] since the early 1960's. A method of analysis, and design criteria for it are consequently well established. Some special features of the disc reluctance motor alter its quality of performance, however, so that, although it seems that Lawrenson's analytical methods[6] can be adopted, the per unit values of several important parameters bear a different relationship to each other. Important in this respect is the leakage reactance of disc shaped stators. But the general area of application of disc shaped motors also has an influence on another motor parameter - its airgap - and this has an impact on the machine inductances. The geometry of a single sided motor makes it very suitable for special duty as a "glandless drive". The rotor can be attached to a pump impeller and be situated in, for example, a toxic fluid and be driven by the stator which is situated outside the pump chamber. The stator therefore drives the rotor through a static screen, obviating the need for a liquid seal around a rotating shaft. The screened-rotor motor described by Russell and

Norsworthy[14] is an example of the way in which this type of drive has been achieved using conventional cylindrical motors: a simpler arrangement appears to be feasible using the disc motor geometry. Furthermore, a brushless synchronous disc motor such as the segmented-rotor machine under consideration has two possible advantages over an asynchronous motor for this application:

- the speed of the rotor is fixed by the supply frequency and is therefore known under most conditions. This may be especially important if the speed cannot be monitored by other means. Loss of synchronism can be detected by harmonics which appear in the supply lines at twice the rotor slip frequency.

- the level of thermal dissipation in the rotor of a synchronous reluctance motor will usually be lower than in an induction motor. Such considerations may be important in vacuum systems.

For these areas of application, however, the disc motor is inevitably required to operate with a larger magnetic airgap than is usually encountered in conventional cylindrical machines.

The main purpose of this chapter therefore is to investigate the quality of performance that can be achieved from a large airgap segmented rotor reluctance motor.

The design of a prototype motor is described in the following section, and in subsequent sections various aspects of the motor performance and behaviour are investigated theoretically and experimentally. These include the direct and quadrature axis reactances; the synchronous and asynchronous performance; the synchronising ability; and the normal force which exists between the stator and rotor. These investigations serve to confirm that the method of analysis is applicable to disc motors, and enable the potential of this type of motor to be assessed. All tests were carried out with two airgap settings: around 0.045 in (1.1 mm) and 0.095 in (2.4 mm). (The precise airgap length is defined for each set of tests). These airgaps cover the range within which single sided motors might be required to operate.

5.2 Motor design

A single sided segmented rotor disc reluctance motor comprises a stator and a rotor. One of the two stators that were used for the double sided motor tests in Chapter 4 was also used for the present motor, and a description of it was given in Section 3.1.

The rotor consists of three main components: the iron segments, the conducting circuits and the support structure. Design details of one of the iron rotor segments are shown in Fig. 5.1. Values of β (pole arc:pole pitch ratio) and γ (channel width:pole pitch ratio) recommended by Lawrenson[6] for good all round performance were adopted for the present design, i.e. $\beta = 0.85$ and $\gamma = 0.27$.

One additional slot was provided either side of the central channel for the purpose of accommodating conducting rotor bars. In conventional segmented rotor designs most of the benefit is derived from the channel when its depth is some ten times the main airgap length; no observable improvements are made when the above ratio exceeds 25. For the present large airgap motor such ratios are not feasible, and consequently the depth was set at 0.3 inches. This was sufficient to accommodate the rotor conductors, and gave ratios of channel depth to airgap length in the range 3-7 for the tests that were carried out on the motor. The four segments were of laminated construction, being made from a single circular strip wound core (0.013" lamination strip) which was machined into four of the segments illustrated in Fig. 5.1.

The rotor cage is illustrated in Fig. 5.2. It was machined from a solid copper disc, the non-uniform radial bars being arranged to fit in the channels, slots and interpolar gaps of the rotor segments. The average surface resistivity of this rotor was designed to be approximately one-half the value of the salient pole rotor of the double sided motor described in Section 3.1. A low resistance rotor was chosen to give improved synchronisation properties.

The four rotor segments were fitted into the rotor cage so that their non-slot and non-channel portions were flush with the airgap side of the copper grid, and this assembly was supported in a thick aluminium alloy disc which was recessed to accept the rear portions of the iron segments that protruded from the rear surface of the copper grid. The

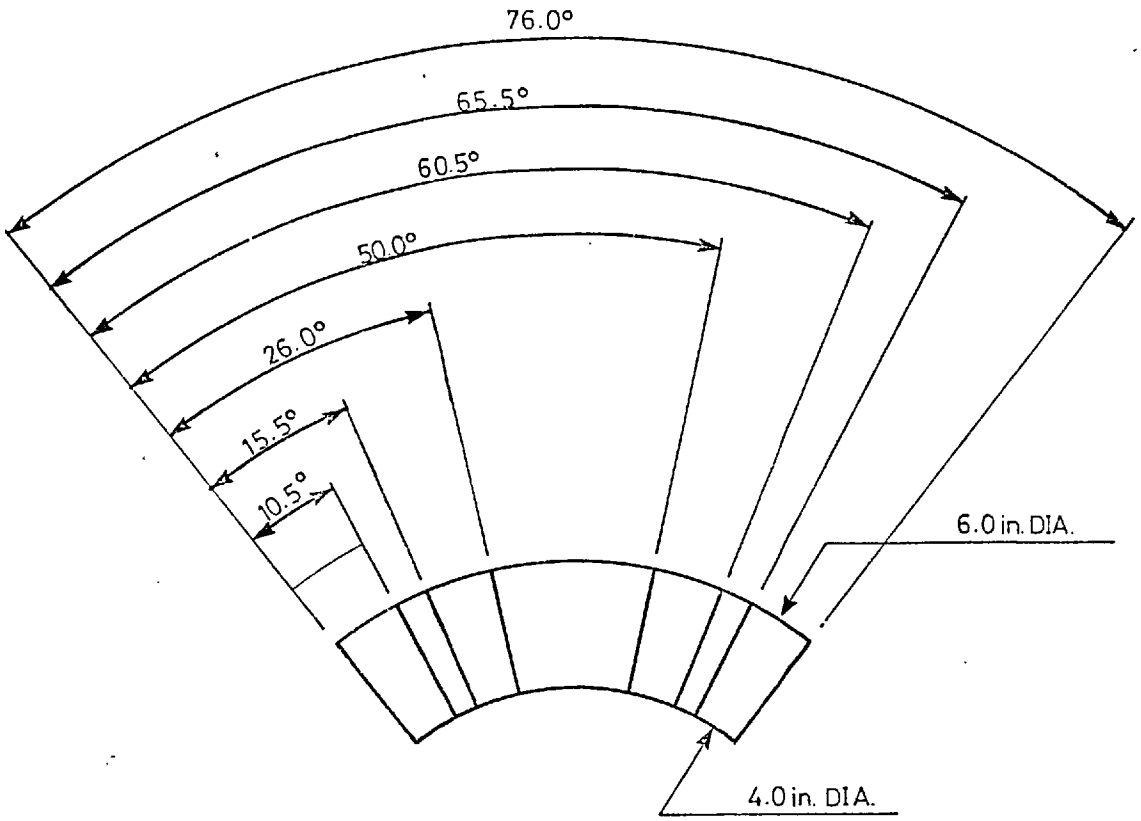

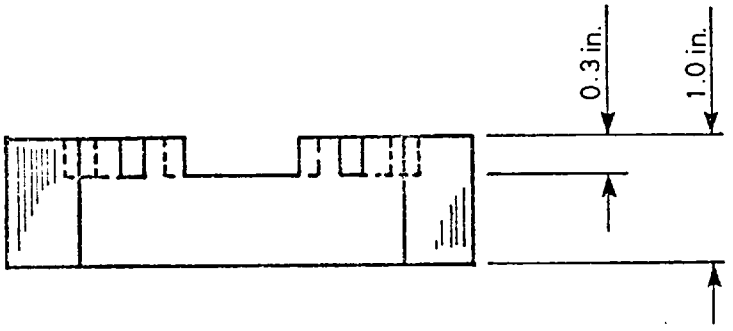

LAMINATED IRON ROTOR SEGMENT

FIG. 5.1

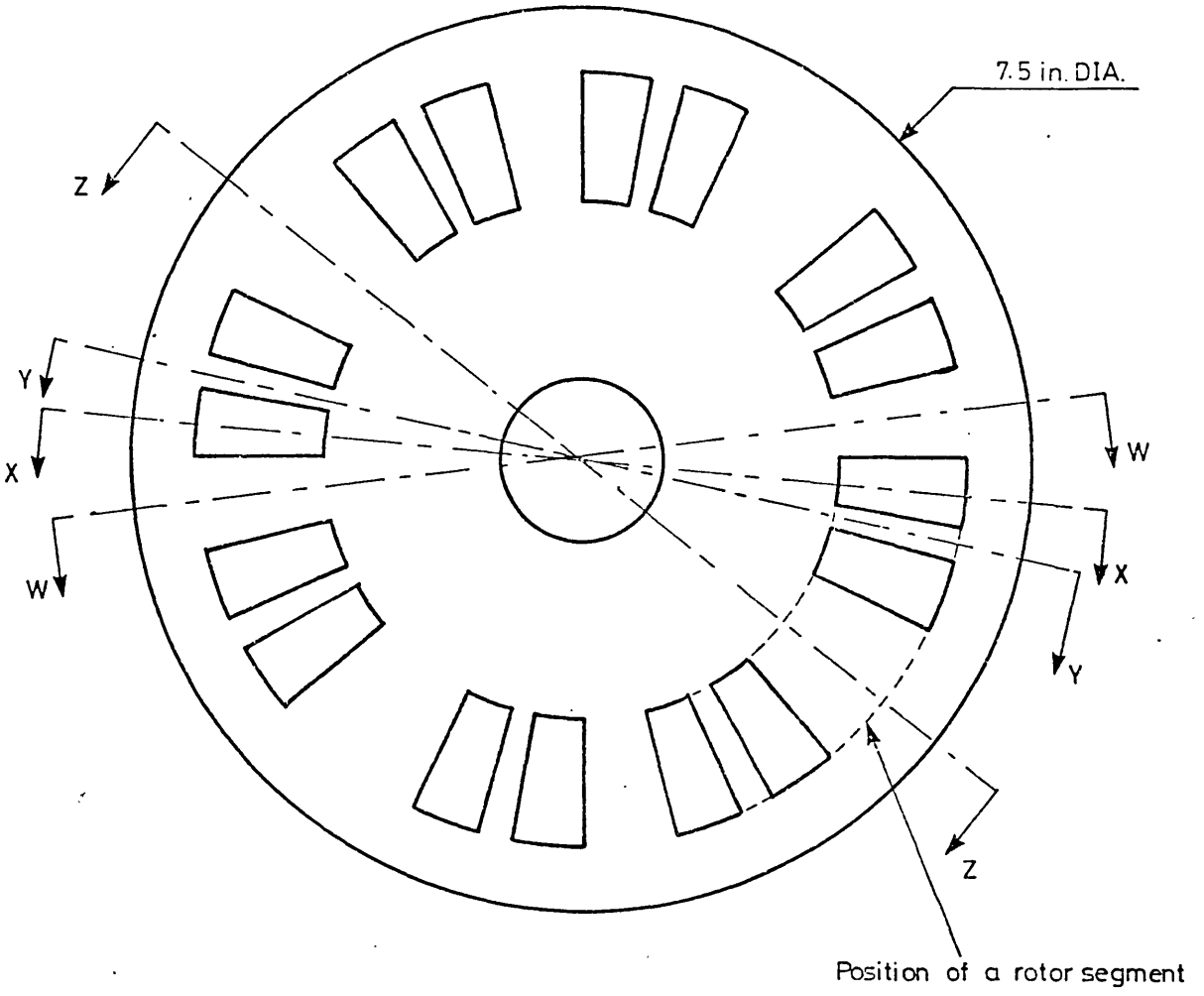

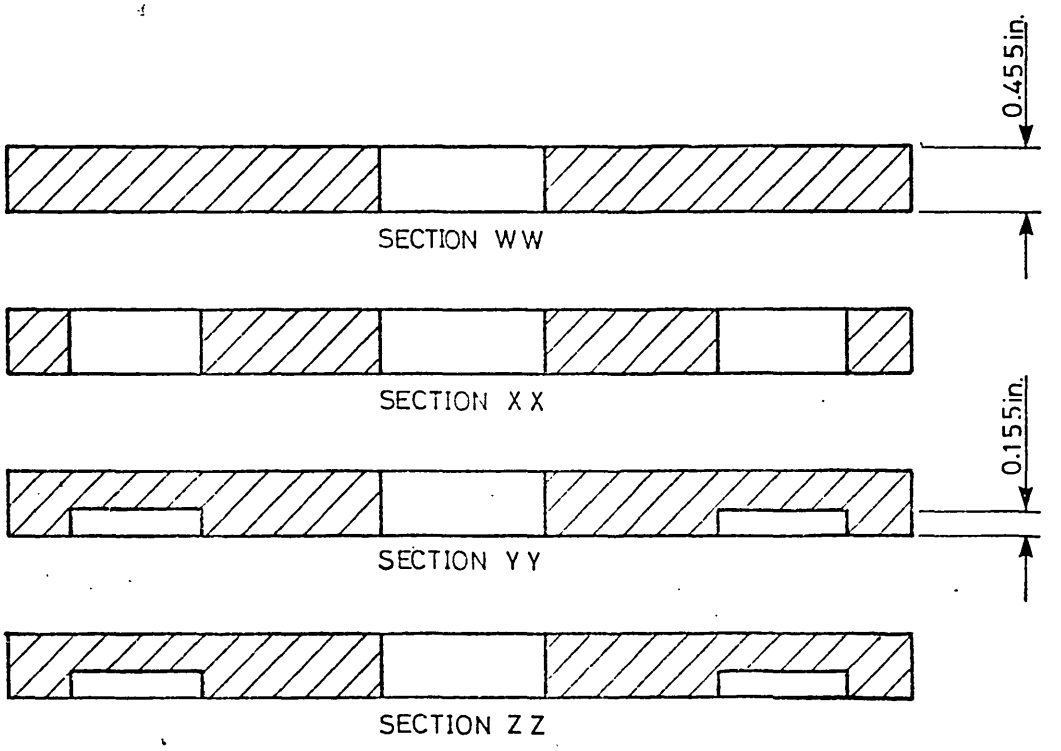

COPPER ROTOR CAGE

FIG. 5.2

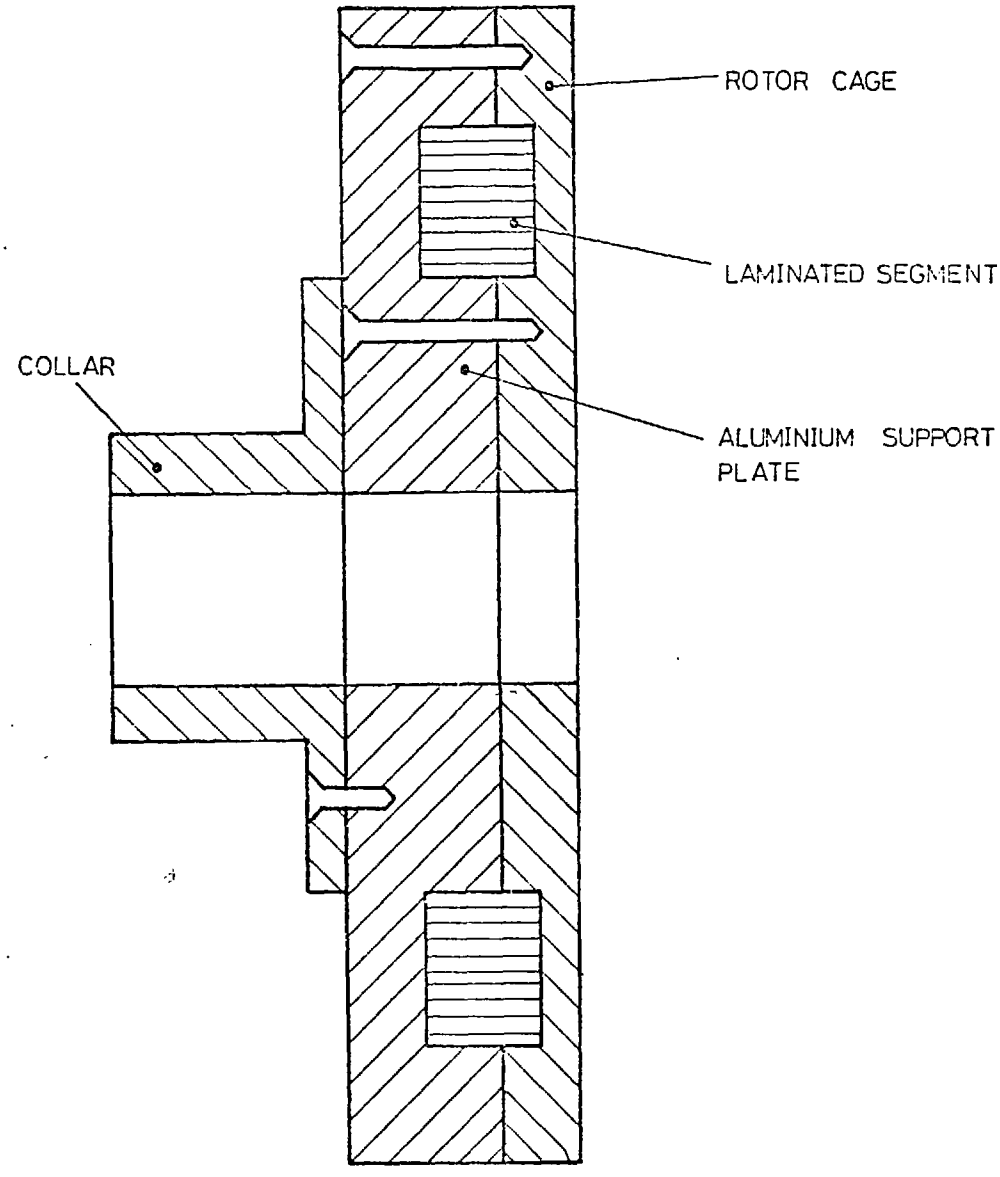

DIAMETRAL SECTION

SEGMENTED ROTOR ASSEMBLY

FIG. 5.3

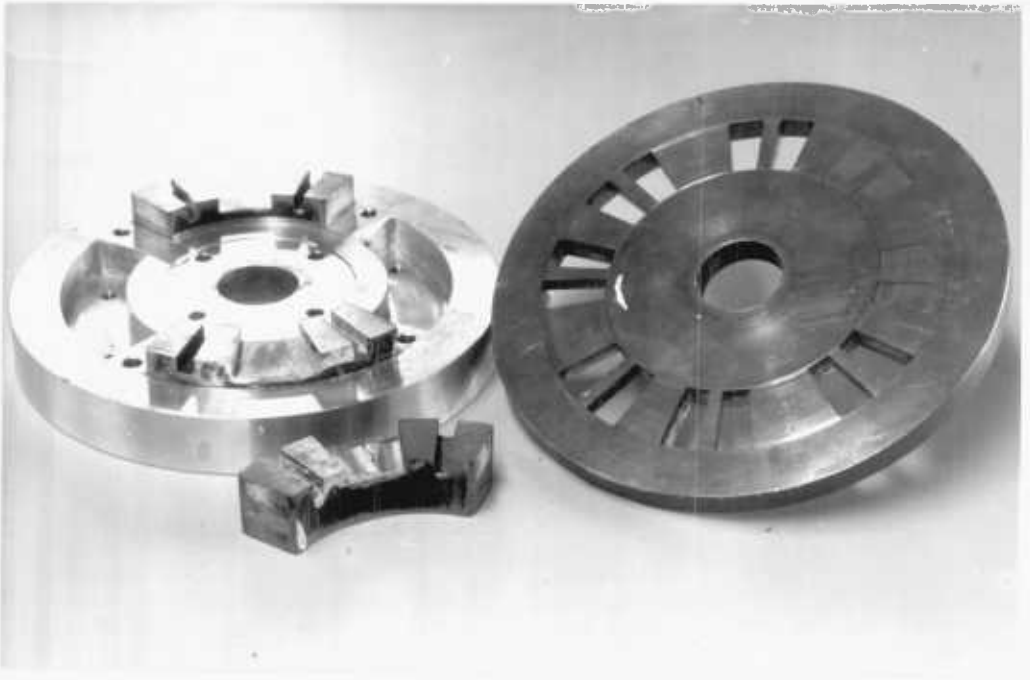

COMPONENTS OF SEGMENTED ROTOR FOR SINGLE SIDED DISC RELUCTANCE MOTOR

FIG. 5.4

assembly is shown in section in Fig. 5.3. A non-magnetic support plate was used to preserve magnetic isolation between the rotor segments.

Photographs of the components of the rotor are shown in Fig. 5.4.

5.3 Direct and quadrature axis reactances

The segmented rotor motor is just one form of synchronous reluctance motor. Its performance can accordingly be defined in terms of the direct and quadrature axis reactances X_d and X_q. (Primary resistance R_1 must also be taken into account in small machines in which its per unit value is usually significant). However, the calculation of X_d and X_q presents particular problems in the segmented rotor machine because of the 'flux reversal' which occurs under most operating conditions. This phenomenon implies that the rotor assumes a magnetic potential with respect to the stator, which makes the normal analytical concept of airgap mmf inapplicable.

The main problem in the analysis of the present machine therefore lies in the calculation of its direct and quadrature axis reactances. A method for undertaking this, which is due to Lawrenson and Gupta[6] is described briefly.

To overcome the problem presented by the magnetic potential of the rotor segments, the analysis of the machine is undertaken in terms of stator and rotor potential functions. Thus, the calculation of the airgap flux density distribution can be made via the relationship:

$$B_\alpha = \Lambda_\alpha (P_{s_\alpha} - P_{r_\alpha}) \qquad (5.1)$$

where, at any angular position α in the airgap:

B_α is the flux density
Λ_α is the airgap permeance
P_{s_α} is the magnetic potential of the stator
and P_{r_α} is the magnetic potential of the rotor

The airgap permeance Λ_α, is effectively the function $\frac{1}{g_\alpha}$ where g_α is the airgap length at α. It can be expressed in the form of a Fourier series which takes account of the shape of the rotor segment - notably the inter-

polar gap and the central channel. Typically, it takes the form:

$$\Lambda_\alpha = \frac{\mu_o R}{g}\left[\beta - \gamma(1-c) + \frac{2}{\pi}\sum_{n=1}^{\infty}\frac{1}{n}\left\{\sin n\beta\pi - (1-c)\sin n\gamma\pi\right\}\right]$$

$$\times\left\{\cos 2np\left(\alpha - \frac{\omega t}{p} - \frac{\pi}{2p} - \delta_i\right)\right\} \qquad (5.2)$$

where R is the radius of the machine

g is the airgap length

g_1 is the channel depth

$c = g/(g + g_1)$

and n is an integer which defines the order of rotor permeance harmonics

The stator magnetic potential P_s is the well known result for the airgap mmf distribution:

$$P_s = \frac{6NI}{\pi}\left[K_1\cos(p\alpha - \omega t) \pm \sum_{k=1}^{\infty}(-1)^K\frac{K_{6k\pm1}}{6k\pm1}\right.$$

$$\left.\times\cos\left\{(6k\pm1)p\alpha \pm \omega t\right\}\right] \qquad (5.3)$$

where I = the maximum current

N = the turns per pole and phase

K_1 = product of pitch and distribution factors

k = an integer defining harmonics of stator potential

The peak value of the rotor potential, $\hat{P}_r$, is derived by establishing the condition that the algebraic sum of the flux entering the segment is zero. It takes the form:-

$$\hat{P}_r = \frac{2A\left\{(1-c)\sin\frac{\gamma\pi}{2} - \sin\frac{\beta\pi}{2}\right\}}{\pi\left\{\beta - \gamma(1-c) + 2g\ h'p/\pi R\ell\right\}}\cdot\sin p\delta_i \qquad (5.4)$$

where A = the peak value of stator potential

h' = effective rotor segment depth

ℓ = half the interpolar distance

The rotor potential has a sign which varies cyclically from one pole to the next, and can therefore be considered as a wave of rotor potential which is given by:

$$P_r = \hat{P}_r \frac{4}{\pi} \sum_{n=1,3,5\ldots} \frac{1}{m} \sin\left(\frac{m\beta\pi}{2}\right) \cos mp(\alpha - \theta) \qquad (5.5)$$

The complete expression obtained for the flux density distribution B_α, by substituting expressions 5.2, 5.3, 5.4 and 5.5 in equation 5.1 is given below:

$$B_\alpha = ID[K_1 \cos(p\alpha - \omega t) + \sum_{k=1}^{\infty} G_{(+)} \cos\{(6k+1)p\alpha - \omega t\} - \sum_{k=1}^{\infty} G_{(-)} \cos\{(6k-1)p\alpha + \omega t\}]$$

$$+ IE[K_1 \sum_{n=1}^{\infty} \frac{1}{n}\{\sin n\beta\pi - (1-c)\sin n\gamma\pi\} \times \cos\{(2n \pm 1)p\alpha - (2n \pm 1)\omega t - 2np\delta - n\pi\}$$

$$+ \sum_{k=1}^{\infty}\sum_{n=1}^{\infty} G_{(+)} \frac{1}{n}\{\sin n\beta\pi - (1-c)\sin n\gamma\pi\} \times \cos\{(2n \pm 6k \pm 1)p\alpha - (2n \pm 1)\omega t - 2np\delta - n\pi\}$$

$$- \sum_{k=1}^{\infty}\sum_{n=1}^{\infty} G_{(-)} \frac{1}{n}\{\sin n\beta\pi - (1-c)\sin n\gamma\pi\} \times \cos\{(2n \pm 6k \mp 1)p\alpha - (2n \mp 1)\omega t - 2np\delta - n\pi\}]$$

$$- IF[K_1\pi\{\beta - \gamma(1-c) \sum_{m=1}^{\infty} \frac{1}{m} \sin(m\beta\pi/2) \times \cos(pm\alpha - m\omega t - mp\delta - n\pi/2)$$

$$+ K_1 \sum_{m=1}^{\infty}\sum_{n=1}^{\infty} \frac{1}{mn}\{\sin n\beta\pi - (1-c)\sin n\gamma\pi \sin(m\beta\pi/2) \times \cos\{(2n \pm m)(p\alpha - \omega t - p\delta - \pi/2)\}] \qquad (5.6)$$

where $D = \frac{6N\mu_o R}{g\pi}\{\beta - \gamma(1-c)\}$

$E = \frac{6N\mu_o R}{g\pi^2}$

$F = \frac{24NH\mu_o R}{g\pi^3}$

$$G_{\pm} = (-1)^k K_{(6k\pm1)}/(6k\pm1)$$

and $$H = \frac{\hat{P}_r \pi}{6NK_1 I}$$

The generated voltage can be calculated from the airgap flux density. Taking into account the fundamental and all higher harmonics it can be written as:

$$\sum_{q=1}^{\infty} e_q = -2pN \sum_{j=1}^{\infty} \frac{d}{dt} \left(\int_{-\pi/2jp}^{\pi/2jp} K_j B_j d\alpha \right) \qquad (5.7)$$

From the full equation for generated voltage which is obtained by substituting for the flux density from equation 5.6 into equation 5.7, the terms contributing to the fundamental component can be picked out and an equation written for the instantaneous terminal voltage. The inductive component in this equation takes the form:

$$X_{eff} = x_c \{D' + F''' - (E'' + F''') \cos 2p\delta_i\} \qquad (5.8)$$

where $$x_c = \frac{24\mu_o (K_1 N)^2 \omega R}{\pi g}$$

i.e. the magnetising reactance of a round rotor, uniform airgap machine.

$$D' = \beta - \gamma(1 - c)$$

$$E'' = \frac{1}{\pi} \{\sin \beta\pi - (1 - c) \sin \gamma\pi\}$$

and $$F''' = \frac{2HK_1}{\pi} \left[\pi\{\beta - \gamma(1 - c)\} \sin \frac{\beta\pi}{2} + \sum_{m=1}^{\infty} \sum_{n=1}^{\infty} \frac{1}{mn} \{\sin n\beta\pi - (1 - c) \sin n\gamma\pi\} \sin \frac{m\beta\pi}{2}\right]$$

with $2n - m = \pm 1$

and $$H = \frac{\hat{P}_r \pi}{6NKI}$$

And the values of x_d and x_q are obtained from equation 5.8 when $\delta_i = 0$ and $\frac{\pi}{2p}$ respectively.

The separate leakage reactance of the windings must be added to the armature reaction values of x_d and x_q to give:

$$X_d = x_l + x_d \qquad (5.9(a))$$

$$X_q = x_l + x_q \qquad (5.9(b))$$

Refinement of the above method of calculating the direct and quadrature axis reactances of a segmented-rotor motor is usually required in order to take account of the fringe fields which occur at the discontinuities of the iron surfaces of the rotor segments. In particular the inter-segmental spacing, the effective depth of the segments, and the width of the channel are modified by the fringe fields. Lawrenson and Gupta[10] used numerical methods to obtain solutions to the field patterns in these regions for a wide range of dimensions, and in much the same way as Carter's Coefficient is usually presented, provided a series of graphs from which appropriate fringe factors can be obtained. In the present case allowance was also made for fringe flux passing between the stator and rotor cores at their inner and outer peripheries in the manner described in Section 3.6.

Thus the details of the prototype motor could be inserted in equation 5.8 and its direct and quadrature axes calculated for a range of magnetic airgaps. These predictions were compared with measured values for the motor.

The two axis reactances were obtained from standstill measurements. This was achieved by using a 'dummy rotor' which consisted of the iron rotor segments embedded in a non-magnetic and non-electrically conducting disc. Each stator phase was excited separately and its self inductance and mutual inductances with the other phases were measured. The direct and quadrature axis positions of the rotor for each phase were identified as the rotor positions at which the phase exhibited maximum and minimum reactance. The single phase quantities so measured were transformed into the reactances X_d and X_q by the conventional method.

Predicted results and measured inductances are compared in Fig. 5.5. These are values of X_d and X_q, i.e. they include the winding leakage inductances, and the measurements were made using the actual stator windings. The leakage reactance was also separated from the magnetising component

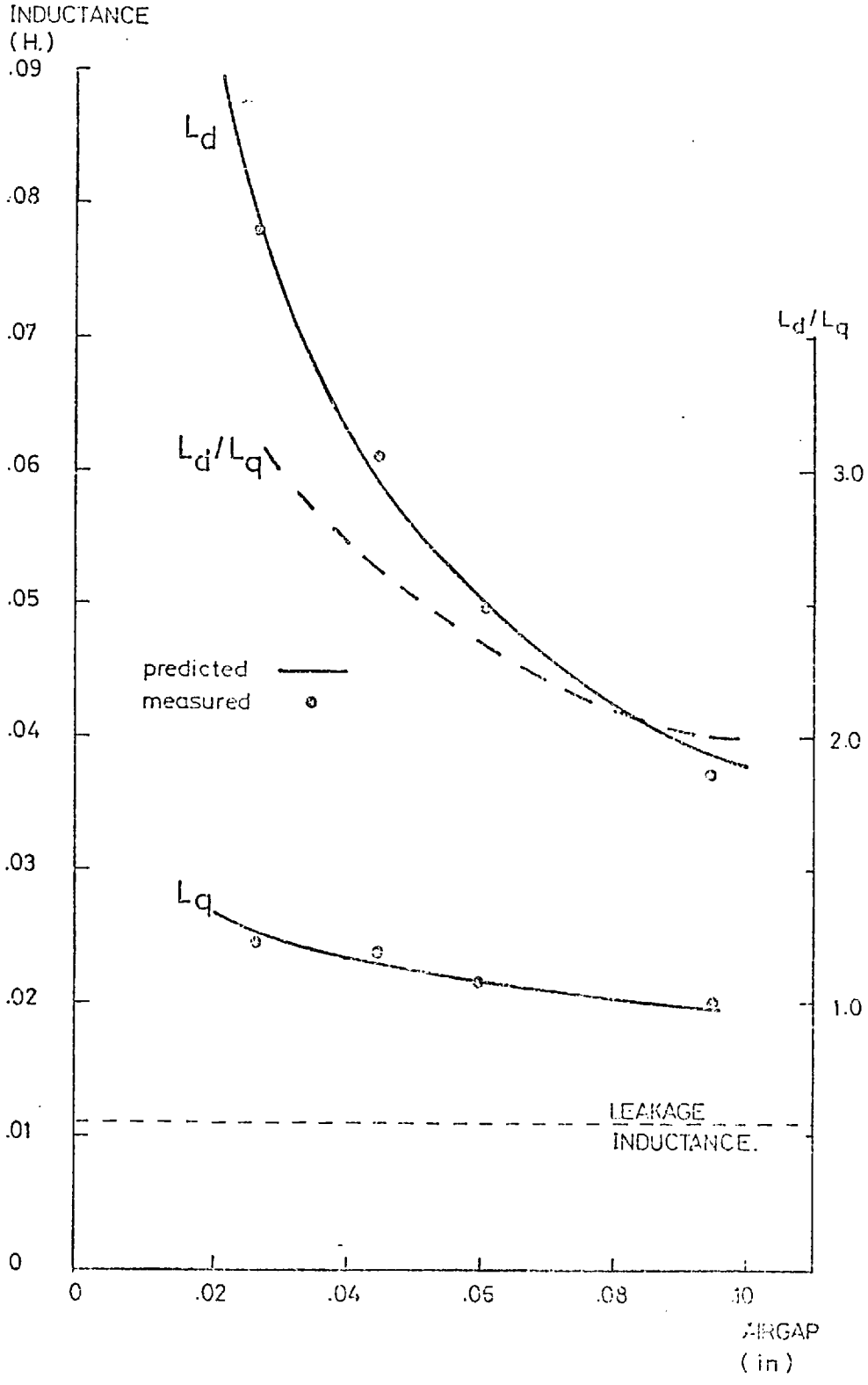

VARIATION OF DIRECT AND QUADRATURE AXIS INDUCTANCES WITH AIRGAP

FIG. 5.5

by using airgap shadow windings and is indicated on Fig. 5.5. It was found to be substantially independent of rotor position and is therefore the same for the direct and quadrature axis inductance components.

The theoretical and experimental results are clearly in close agreement. The predictions were made with the assumption that the disc motor was equivalent to a cylindrical motor with bore diameter equal to $\frac{1}{2}(D_o + D_i)$ and core width equal to $\frac{1}{2}(D_o - D_i)$, where D_o and D_i are the external and internal diameters of the disc motor core. This assumption appears to be amply justified.

The dominating role of the leakage reactance, especially in the quadrature axis reactance can be seen in Fig. 5.5. Its deleterious effect on the X_d/X_q ratio is also shown. This ratio lies between about 2.0 and 3.0 for the airgap range under consideration: for conventional segmented rotor machines values of 5 or 6 are more typical. For the airgap sizes under consideration the X_d/X_q ratio is as follows:

Airgap (inches)	X_d/X_q
.043	2.5
.095	1.9

There is a noticeably small decrease in the X_d/X_q ratio for a large increase in airgap.

5.4 Synchronous characteristics

The phasor diagram for a synchronous reluctance motor is illustrated in Fig. 5.6. From it the synchronous characteristics of the motor can be derived in terms of X_d, X_q and R_1, and for this reason the successful method of calculation of X_d and X_q described in the previous section is particularly important.

Three angles are indicated on Fig. 5.6: the power factor angle between voltage and current, ϕ; the torque angle between the direct axis and the stator mmf wave, δ_i; and the load angle, δ, which is commonly used for synchronous machines, between the applied and induced emfs. The torque

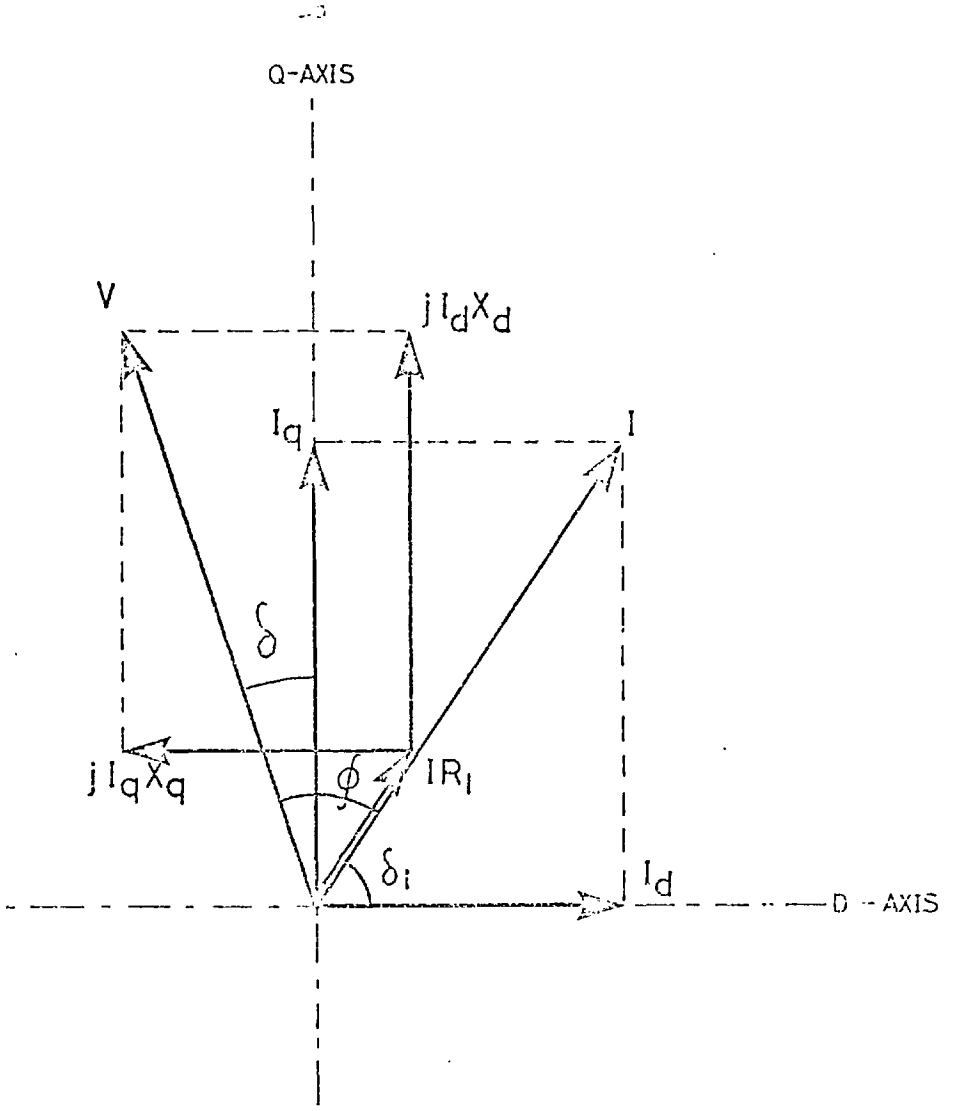

PHASOR DIAGRAM FOR A SYNCHRONOUS RELUCTANCE MOTOR.

FIG. 5.6

angle δ_i is most directly associated with the physical action in reluctance motors, and is used by Lawrenson in his analyses[3,6]. From Fig. 5.6 it can be seen that the three angles are related:

$$\delta = \delta_i + \phi - \frac{\pi}{2} \qquad (5.10)$$

The synchronous torque characteristics with respect to δ and δ_i are therefore different because the power factor of the motor changes with load. The torque characteristic with respect to the load angle, δ, has the predominantly sinusoidal shape normally associated with reluctance torque. The torque characteristics of the present motor are therefore calculated in terms of the load angle δ. (Stephenson discusses and compares the two angles, δ and δ_i, in an extended correspondence article[15]).

With reference to the phasor diagram in Fig. 5.6 the phase current can be calculated in terms of X_d, X_q, R_1, δ and the phase voltage V,

$$\text{for} \quad I = \sqrt{I_d^2 + I_q^2} \qquad (5.11)$$

$$\text{and} \quad V \sin\delta = I_q X_q - I_d R_1 \qquad (5.12(a))$$

$$V \cos\delta = I_d X_d + I_q R_1 \qquad (5.12(b))$$

Solving equations 5.12 for I_d and I_q, substituting into 5.11 and simplifying gives the result:

$$I = \frac{V}{\sqrt{2}(X_d X_q + R_1^2)} \left\{2R_1(X_d - X_q)\sin 2\delta - (X_d^2 - X_q^2)\cos 2\delta + 2R_1^2 + X_d^2 + X_q^2\right\}^{\frac{1}{2}} \qquad (5.13)$$

This enables the synchronous power output, P_{out}, to be derived, for:

$$P_{out} = P_{in} - 3I^2R_1 \qquad (5.14(a))$$

$$= 3IV\cos\phi - 3I^2R_1 \qquad (5.14(b))$$

Substituting from equation 5.13, and noting that $I\cos\phi = I_q\cos\delta - I_d\sin\delta$, the expression for P_{out} can be expressed as:

$$P_{out} = \frac{3V^2(X_d - X_q)}{2(X_d X_q + R_1^2)^2}\left\{R_1(X_d + X_q)\cos 2\delta + (X_d X_q - R_1^2)\sin 2\delta - R_1(X_d - X_q)\right\} \qquad (5.15)$$

The notable feature of this expression is that the synchronous power is non-zero when the load angle is zero, unless R_1 is zero, i.e.

$$P_{out}\Big|_{\delta=0} = \frac{3V^2 R_1 X_q (X_d - X_q)}{(X_d X_q + R_1^2)^2} \qquad (5.16)$$

And when R_1 is zero, equation 5.15 reduces to give the well-known expression for pull-out torque as:

$$P_{pull\text{-}out} = \frac{3V^2}{2}\left(\frac{1}{X_q} - \frac{1}{X_d}\right) \qquad (5.17)$$

A further parameter of the machine at synchronous speed, the power factor, can also be calculated with reference to the phasor diagram, Fig. 5.4, and can be shown to be:

$$\cos\phi = \frac{1}{\sqrt{2}} \frac{2R_1 + (X_d - X_q)\sin 2\delta}{[2R_1(X_d - X_q)\sin 2\delta - (X_d^2 - X_q^2)\cos 2\delta + 2R_1^2 + X_d^2 + X_q^2]^{\frac{1}{2}}} \qquad (5.18)$$

The results given in equations 5.13, 5.15 and 5.18 above enable the current, torque and power factor of the reluctance motor to be calculated for a range of values of δ at synchronous speed.

Calculations were therefore carried out and the theoretical results obtained are compared with experimental results in Figs. 5.7, 5.8, 5.9 and Fig. 5.10. All tests were carried out at a phase voltage of 50V rms in order to maintain a similar airgap flux density level for both airgap settings. At this voltage the motor currents were approaching their thermal limits, but the iron cores of the stator and rotor were operating at flux densities of about 0.3T - 0.5T.

Taking each of the Figures in turn, it can be seen that:

Fig. 5.7: Torque

The torque vs load angle characteristics for the two airgaps are very similar in shape and magnitude. Viewed simply, in terms of equation 5.17, it can be seen that for a fixed voltage the pull out torque is largely dependent upon X_q - especially if X_d is considerably greater than X_q. In the present motor therefore, where X_q changes very slowly with airgap, the pull out torque does not change greatly as the airgap is changed.

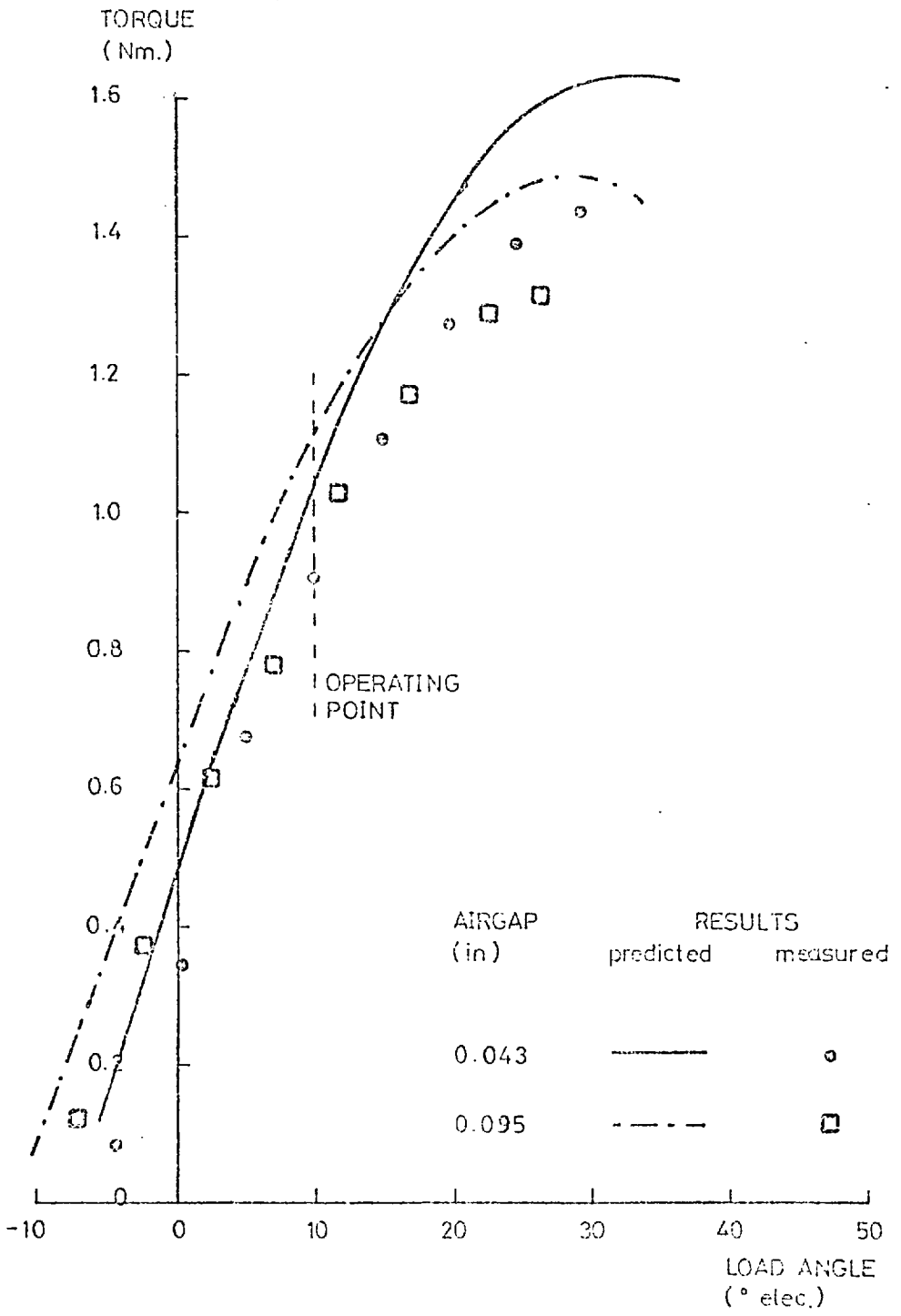

SYNCHRONOUS TORQUE CHARACTERISTICS

FIG. 5.7

As predicted in equation 5.16 the torque characteristic does not pass through the origin; torque is zero when δ is between -5° and -10°. This shift in the torque characteristic causes the pull-out torque to occur at a load angle of around 30°. A typical operating point, which is indicated on Fig. 5.7 at two-thirds of the pull-out torque, therefore seems to occur at a load angle of around 10°.

At pull-out the motor is producing 200-250 watts, which would give a usable steady state power output of around 150 watts.

Fig. 5.8: Power Factor

The two power factor characteristics of the motor with 0.043 inch and 0.095 inch airgaps are seen to intersect at a small positive load angle of just over 3°. The stator I^2R losses associated with the larger magnetising current for the bigger airgap setting appear to dominate the real power intake at low output levels, and give the larger airgap motor the better power factor. As power output increases with load angle however, the smaller airgap motor setting achieves the better power factor, but in the operating region, δ = 10°, power factors of the two machines are very similar, and not much less than their maximum values:

Airgap	Power Factor in Operating Region (δ = 10°)	Maximum Power Factor
0.043 in	0.5	0.6
0.095 in	0.45	0.55

Fig. 5.9: Efficiency

The effect of the motor airgap on motor performance is indicated clearly in Fig. 5.9, which compares the synchronous efficiencies for the two airgaps. A maximum efficiency exceeding 65% can be achieved with the smaller airgap of 0.043 in compared with 55% for the 0.095 in gap. It is interesting to notice that with the present motor design the efficiency characteristics are remarkably flat, and that an efficiency within 5% of the maximum value is obtained for values of load angle, δ, from about 5° to pull out, i.e. when less than half the pull out torque

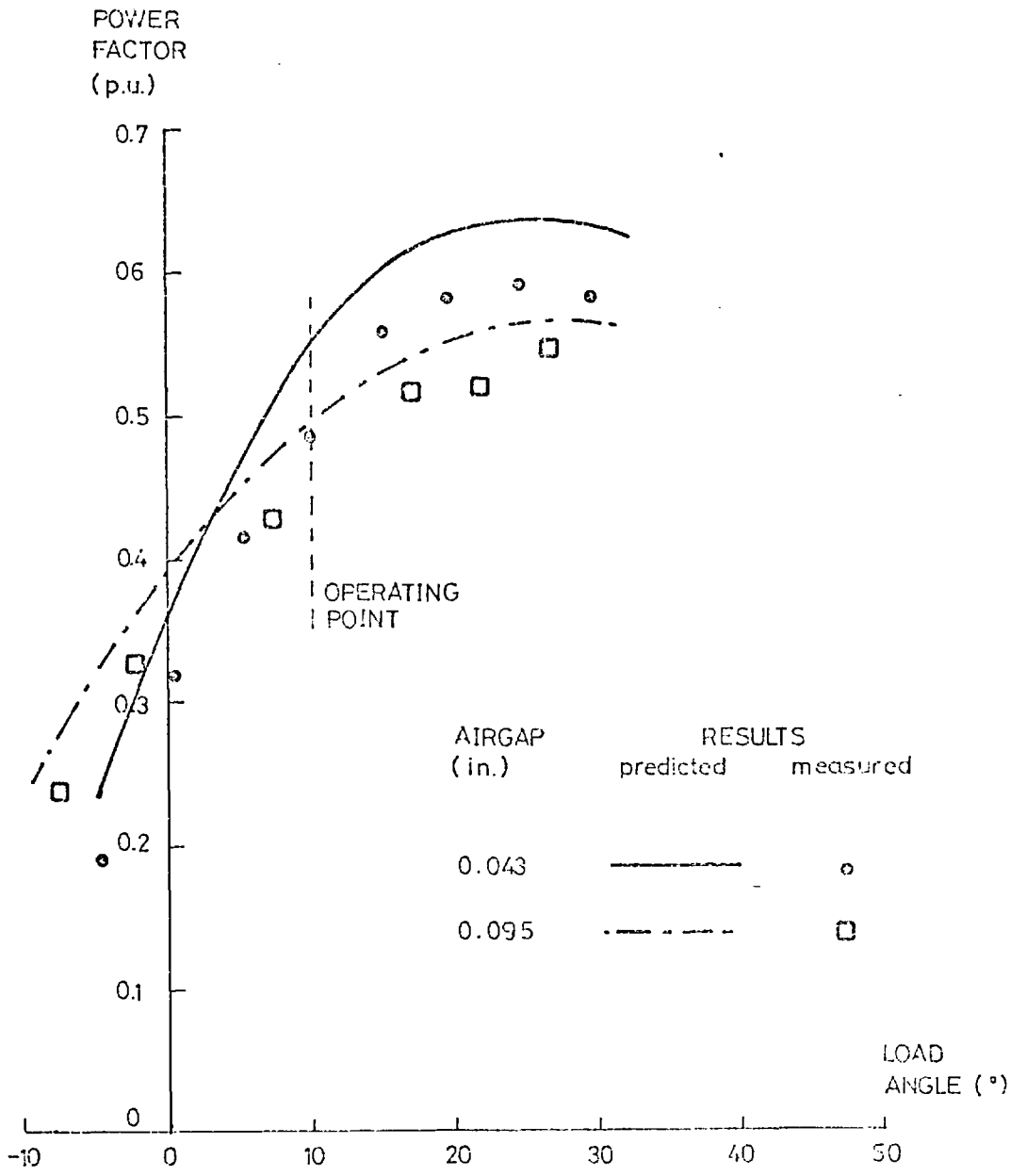

POWER FACTOR AT SYNCHRONOUS SPEED

FIG. 5.8

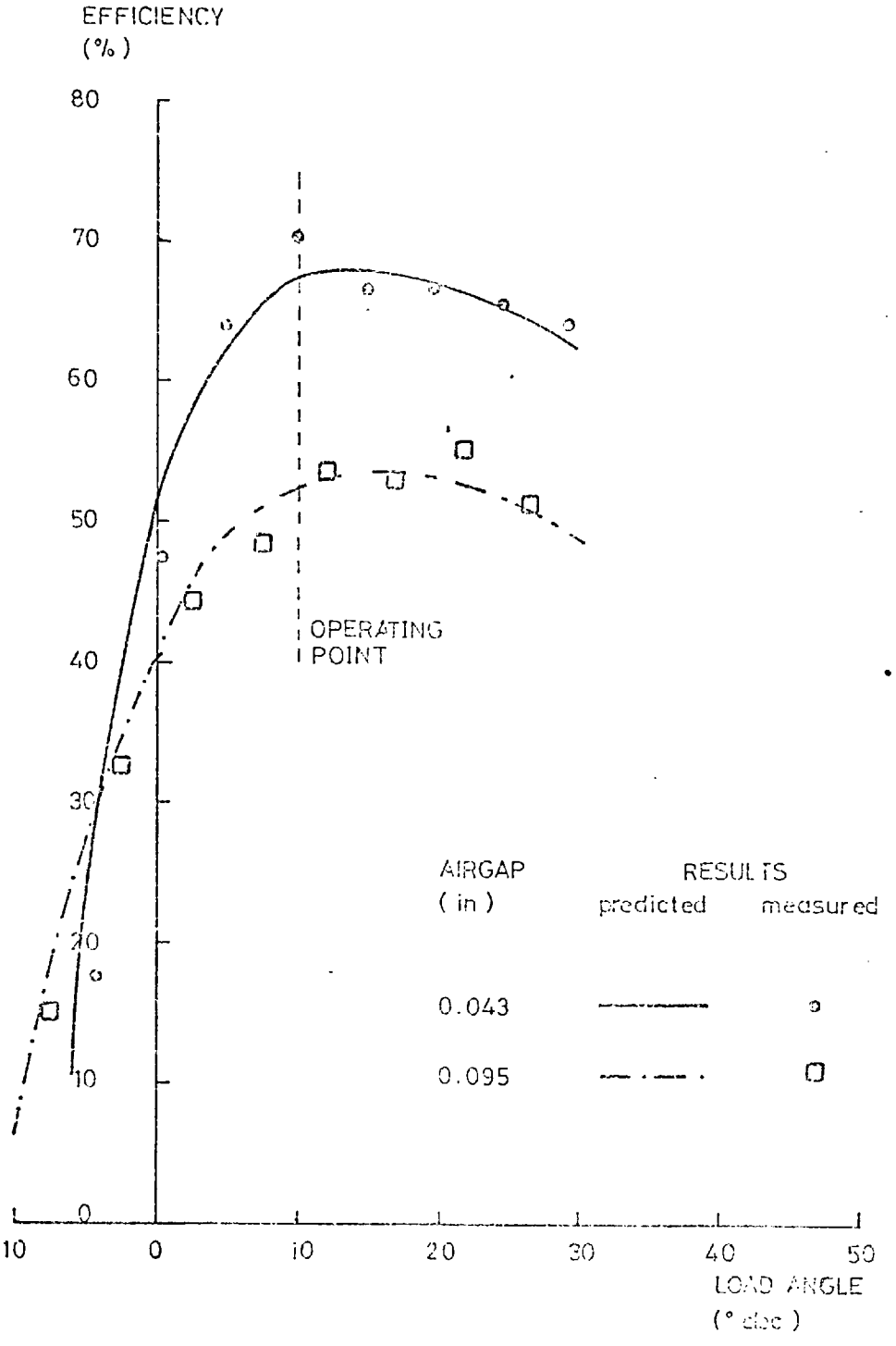

EFFICIENCY AT SYNCHRONOUS SPEED

FIG. 5.9

is being produced.

The flatness of efficiency curve is apparently due to the opposing effects of increased power output with load angle which tends to increase the efficiency; and increased stator I^2R losses due to the higher phase current that is drawn as load angle increases, which tends to reduce the efficiency.

From Fig. 5.9 it can be seen that typical efficiencies that might be expected from large airgap reluctance motors operating at two-thirds of their pull out power are:

Airgap (inches)	Efficiency at Operating Point (%)
0.043	65-70
0.095	50-55

Fig. 5.10: Phase Current

The phase current increases slowly as power output and load angle increase. The ratios of the currents when the motor is running light and close to pull out are as follows:

Airgap (inch)	Current at Pull Out / Current Running Light
0.043	1.71
0.095	1.29

the smaller change for the large airgap setting being due to its smaller change of reactance from the direct to the quadrature axis positions.

The increase in current that is required for the larger airgap is less than proportional to the increase in airgap because of the buffering effect of the stator resistance and leakage reactance. Hence for an increase in airgap by a factor of 2.2 from 0.043 in to 0.095 in the current increases by some 50%.

A well designed motor usually operates near its optimum magnetic and electric loadings, i.e. the flux density in the core will be close to the

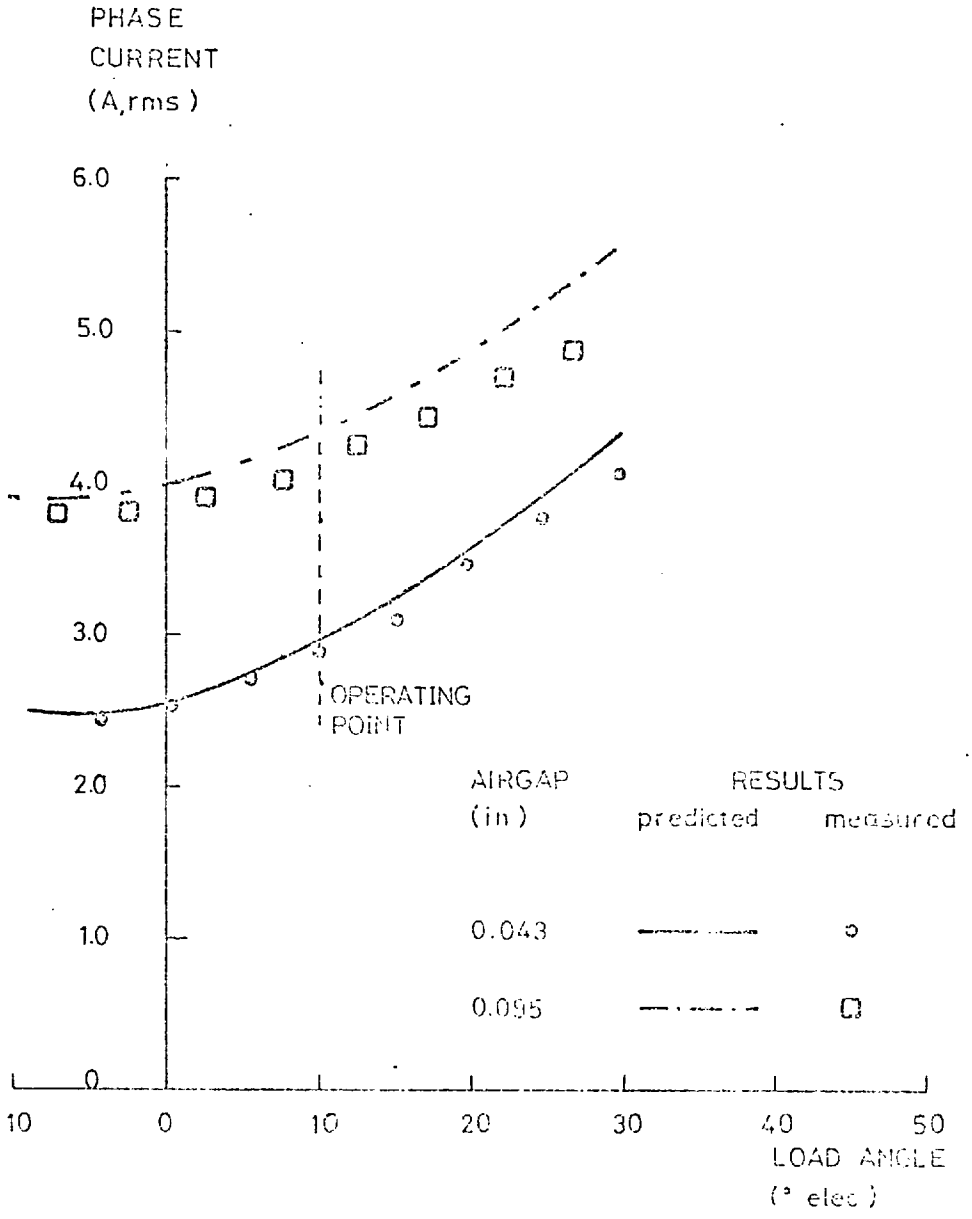

PHASE CURRENT AT SYNCHRONOUS SPEED

FIG. 5.10

saturation level, and the current density in the windings will be near its thermal limit. In conventional small airgap machines it is possible to use a 1:1 tooth width to slot width ratio with which the tooth iron can operate near its saturation level and the output of the machine can be maximised (see Section 1.5.2) - without the copper and iron losses in the stator causing an unacceptable temperature rise. In the present case, the large airgaps with which the motor has been tested prevent this condition being achieved. For the greater copper losses associated with the higher magnetising current reduce the flux density level that can be set up in the airgap. In general, therefore, the stator designed for use with a large airgap will have narrower teeth than usual, and a correspondingly reduced backing iron section. The prototype motor was designed with a 1:1 tooth to slot width ratio so that tests with small airgaps might also be undertaken. For large airgap tests therefore the iron circuit was underloaded and the output of the motor was limited by stator I^2R losses. It is interesting, however, on the basis of experimental results obtained for it, to estimate the maximum synchronous output that might be obtained from the prototype motor if for each airgap setting it were to operate at its maximum permissible current loading. This loading depends largely upon the operating environment and cooling conditions, and for the present purposes a current density of 3,000 A/in^2 (4.65 A/mm^2) has been chosen. This sets the steady state operating current of the motor at 3.8 Amps, and implies a total stator copper loss of around 100 watts.

From the results in Fig. 5.10 which give the motor current for a phase voltage of 50V rms, the approximate voltages for the motor at the different airgap settings if they are to operate on 3.8A rms at two-thirds pull out power are:

Airgap (in)	Phase Voltage (V,rms)
0.043	65
0.095	45

The steady state synchronous outputs that can be achieved from the motor under these conditions, assuming that their power factors and efficiencies do not change from the values obtaining at 50V phase are

illustrated in Fig. 5.11. Both torque and power are indicated on the ordinate axis of the graph.

The advantages of the smaller airgap are very pronounced; and the steady state operating conditions at two-thirds pull out power are as follows:

Airgap (inches)	Power Output at Operating Point (watts)	Power Factor (p.u.)	Efficiency (%)
.043	270	.53	67
.095	120	.43	50

More than twice the output is obtainable with the smaller airgap compared to the larger; but the performance of both should perhaps be compared with that of the same motor operating with a small airgap of 0.020 inches, say. According to predictions for this condition, using the above methods, a segmented rotor disc motor with a 0.020 inch airgap could operate from a phase voltage of 90V rms and at two-thirds of its pull out power would provide 600 watts. This would be achieved at a power factor and efficiency of 0.75 and 80% respectively.

The steady state synchronous operation of a segmented rotor disc motor with a large airgap is therefore significantly inferior to its usual mode of operation but can nevertheless achieve operating characteristics which are far from unacceptable.

5.5 Synchronising capability

The steady state synchronous performance of a large airgap segmented rotor disc motor has been discussed in the previous section. It is also necessary, however, to investigate the synchronising capability of this motor, i.e. the load and inertia that can be synchronised by it. For in most applications the motor must be capable of achieving synchronous speed when supplied from its rated voltage and coupled to its rated load. It is well known[16] that the ultimate rating of a reluctance motor is often determined by its synchronising ability.

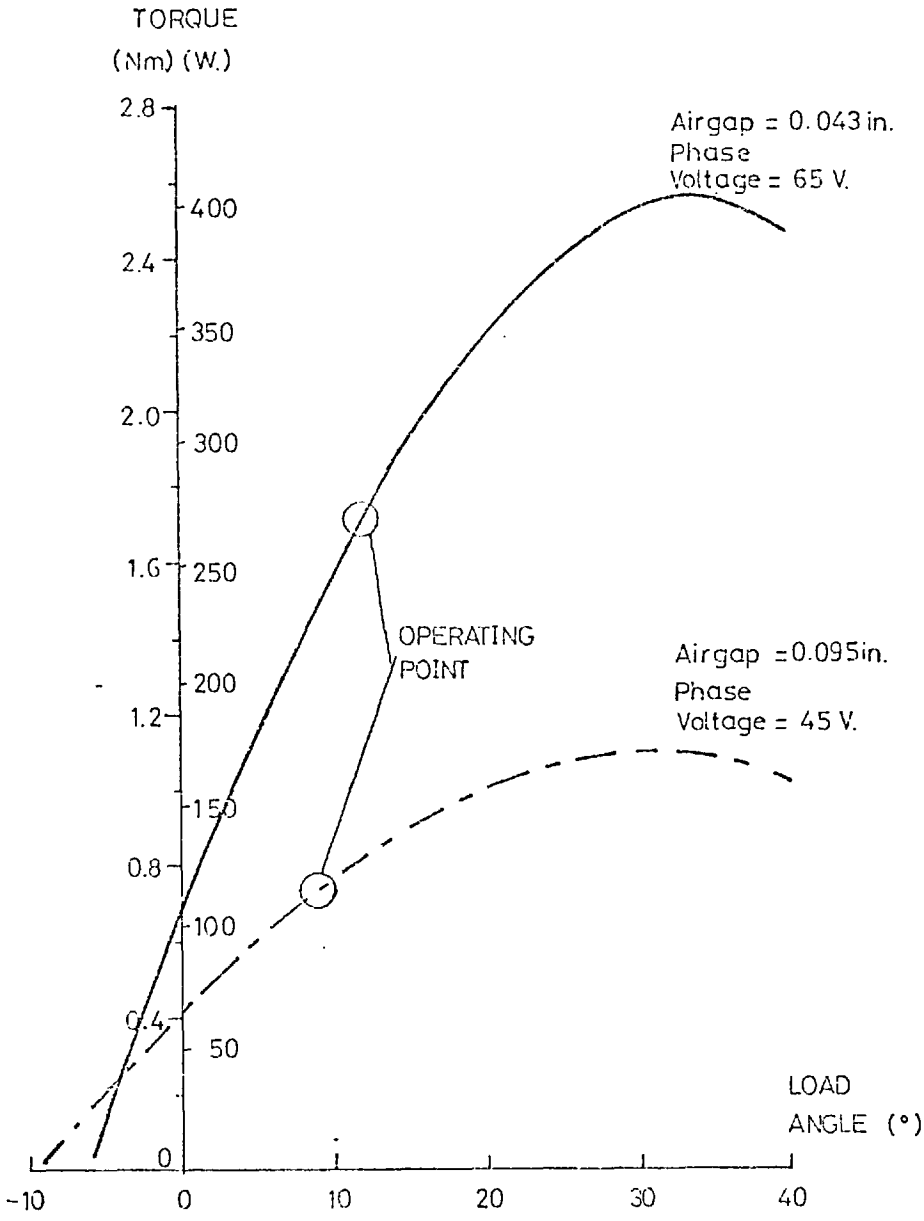

VARIATION OF SYNCHRONOUS OUTPUT WITH AIRGAP

FIG. 5.11

This section therefore investigates the synchronising capability of the prototype motor experimentally, and compares it with predictions from a theoretical method.

Lawrenson and Mathur[13] published a "pull-in criterion" for reluctance motors in 1973. It enables the maximum inertia that the motor can synchronise to be calculated for specified load torque conditions. A knowledge of the motor's two axis reactances and primary resistance, and the slope of the asynchronous torque characteristic near synchronous speed are required. This method is deemed to be an improvement on earlier methods, notably by Talaat[17], Douglas[18] and Burian[19], because it takes into account the fact that the asynchronous torque of a salient pole machine is negative at zero slip[15]. For this reason it has been used to estimate the pull-in performance of the present prototype disc reluctance motor, and is described briefly below.

Lawrenson and Mathur[13] identified a 'limiting synchronisation cycle', in which the greatest inertia can be synchronised against a given load: it is illustrated in Fig. 5.12. It is the case in which the reluctance torque is still just equal to the load torque by the time the rotor has achieved zero slip, but with the rotor at a load angle δ_f' in the unstable region of the reluctance torque characteristic. This cycle gives the largest possible accelerating torque in the attempt to achieve synchronisation, and leads to synchronous running directly, or after pole slipping once. Other typical successful and unsuccessful synchronisation attempts are also indicated on Fig. 5.12.

To arrive at a quantitative evaluation of the synchronising performance, it is necessary to define the asynchronous torque characteristic near to synchronous speed, the reluctance torque characteristic at synchronous speed, and the initial and final conditions for the synchronisation cycle. The latter cause the most difficulties. The asynchronous torque, T_a, can be expressed as:

$$T_a = As^2 + Bs - C \qquad (5.19)$$

and an expression for reluctance torque, T_r, can be written in the form:

$$T_r = D \cos 2\delta + E \sin 2\delta - C \qquad (5.20)$$

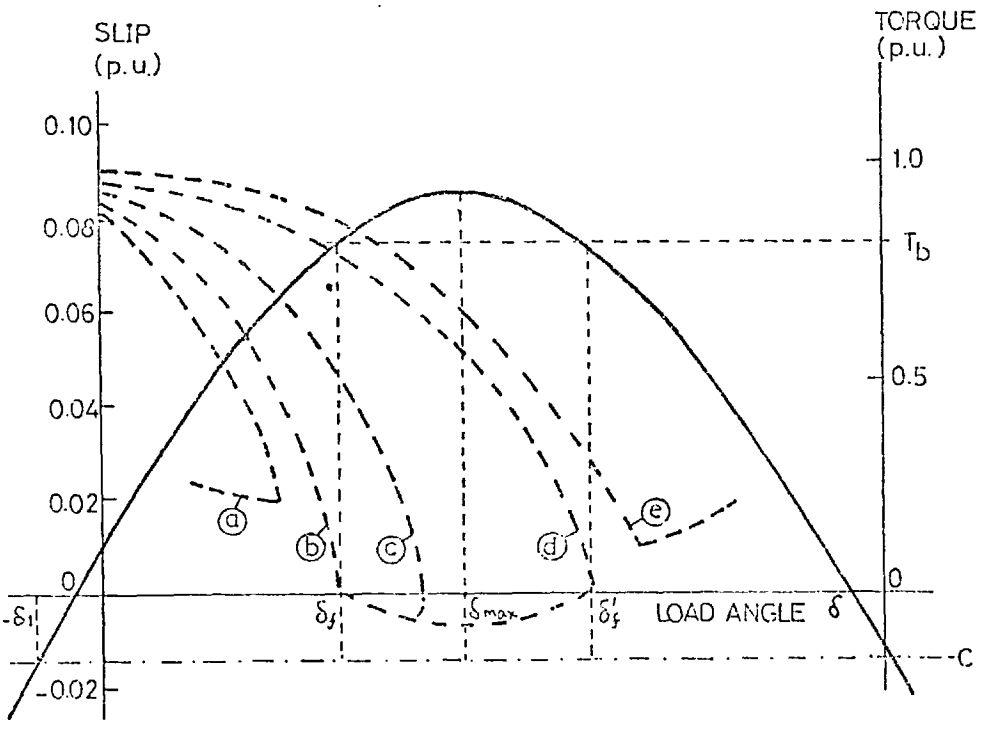

ⓐ fails to synchronise
ⓑ direct (critical) synchronisation
ⓒ synchronisation
ⓓ limiting synchronisation cycle
ⓔ fails to synchronise

SLIP vs. LOAD ANGLE TRAJECTORIES FOR SYNCHRONISING CYCLES.
(after Lawrenson and Mathur, 1973)

FIG. 5.12

where A and B are constants which are most reliably obtained from experimental data, and C, D and E are given in the full expression for reluctance torque in equation 5.15 above.

The coefficient C which appears in the expressions for synchronous and asynchronous torque is worthy of comment. Equation 5.19 shows that the asynchronous torque intercept at zero slip has a negative value, and is not zero as would be expected with cylindrical rotor machines. The physical meaning of this term is that power is required to rotate a salient pole rotor at very low slip speeds. This power supplies the copper losses in the primary windings which are due to the modulation of the stator currents by the rotor saliency. The same term C appears in the expression for synchronous torque, equation 5.20. It indicates that the losses in the stator winding resistance cause the maximum torque in the motoring (positive) mode to be less than that in the generating (negative) mode.

The equation of motion for the motor and its load during synchronisation can be written as:

$$T_a + T'_r - T_b = J_k \frac{d^2\delta}{dt^2} \qquad (5.21)$$

where T_b is the load torque

$T'_r = T_r + C$

J_k = moment of inertia of rotor plus coupled load

A change of variables puts equation 5.21 into a more convenient form, for

$$s = \frac{d\delta}{dt} \quad \text{and} \quad \frac{d^2\delta}{dt^2} = \frac{ds}{dt} = s\frac{ds}{d\delta} \qquad (5.22)$$

Thus the equation of motion can be expressed in terms of s and δ, which are the important variables during synchronisation:

$$T_a + T'_r - T_b = J_k s \frac{ds}{d\delta} \qquad (5.23)$$

The solution of equation 5.23 between appropriate limits establishes the synchronisation criterion that is required. Definition of the limits is described below.

Expressing equation 5.20 in the form:

$$T_r = K \cos 2(\delta_{max} - \delta) - C \qquad (5.24)$$

where $K = \sqrt{D^2 + E^2}$ and $\delta_{max} = \frac{1}{2} \tan^{-1} \frac{E}{D}$ the angles which appear on Fig. 5.12 can be shown to be:

$$\delta_1 = \frac{\pi}{4} - \delta_{max} \qquad (5.25(a))$$

$$\delta_f = \delta_{max} - \frac{1}{2} \tan^{-1} \left\{ \frac{[K^2 - (T_b + C)^2]^{\frac{1}{2}}}{T_b + C} \right\} \qquad (5.25(b))$$

and $$\delta'_f = \frac{\pi}{2} - \delta_f - 2\delta \qquad (5.25(c))$$

As explained above, the conditions at the end of the synchronisation attempt are:

$$\delta = 0 \text{ and } \delta = \delta'_f \qquad (5.26)$$

But in order to obtain an analytical solution to equation 5.23, a cosinusoidal relationship between s and δ was assumed, in the form:

$$s = s_o \cos(\delta + \delta_f + 2\delta_1) \qquad (5.27)$$

where s_o is the slip at the beginning of the synchronisation cycle. From which the load angle at the beginning of the cycle is given by:

$$\delta_o = -(\delta_f + 2\delta_1) \qquad (5.28(a))$$

and by using equation 5.19 with the condition that $T_a + T'_r - T_b = 0$ at the beginning of the cycle, the value of s_o can be shown to be:

$$s_o = \frac{1}{2A} [-B + \{B^2 + 4A(T_b + C - T'_{r_o})\}^{\frac{1}{2}}] \qquad (5.28(b))$$

where T'_{r_o} is the value of T'_r corresponding to slip s_o.

Hence, equations 5.26 and 5.28 define the limits for the solution of equation 5.23, which gives a value for the maximum inertia $J_{k_{max}}$, that can be synchronised under given load conditions as:

$$J_{k_{max}} = \frac{2}{s_o^2} \left\{ -D \sin 2\delta_o + E \cos 2\delta_o + Bs_o - (T_b + C - \frac{As_o^2}{2}) \frac{\pi}{2} \right\} \qquad (5.29)$$

Predictions using this criterion are compared with experimental evidence below.

The asynchronous performance of the motor was tested near synchronous speed to assist in calculating the synchronising capability of the motor (for calculating the constants A and B in equation 5.19). The torque vs. slip curves are shown in Fig. 5.13. Their shape indicates that the rotor resistance is sufficiently low for the motor to reach a small slip under the influence of induction torque. In accordance with equation 5.19 the induction torque characteristics approach zero torque at a small positive slip speed. It can also be seen that the experimental curves are approximately asymptotic to the predicted negative values of torque at zero slip.

Theoretical and experimental results for the synchronising performance of the prototype motor are presented in Figs. 5.14 and 5.15 for the airgaps of 0.043 inch and 0.095 inch respectively. The motors were tested for a range of load torques and coupled inertias. There is some agreement between the experimental and theoretical results under most conditions, although significant errors are seen to emerge for the higher inertia tests on the motor with the 0.043 in airgap. The most probable reason for this is the onset of saturation in the stator teeth[20].

The significance of the synchronising performance of the motor is brought out by comparing it with the steady-state synchronous performance of which it is capable. For if a motor is to start up under full load and at rated voltage it is essential that it is capable of synchronising under these conditions. Or conversely, the rated output of the motor can be no more than the load which it can synchronise.

The steady state synchronous output of the motor which was established in the preceding section (two-thirds of the pull out power at rated voltage) is compared below with the synchronising capability of the motor against a friction load (i.e. no added inertia):

Airgap (in)	Rated Voltage (V,rms)	Rated Synchronous Output (watts)	Synchronising Capability (watts)
0.043	65	270	120
0.095	45	120	35

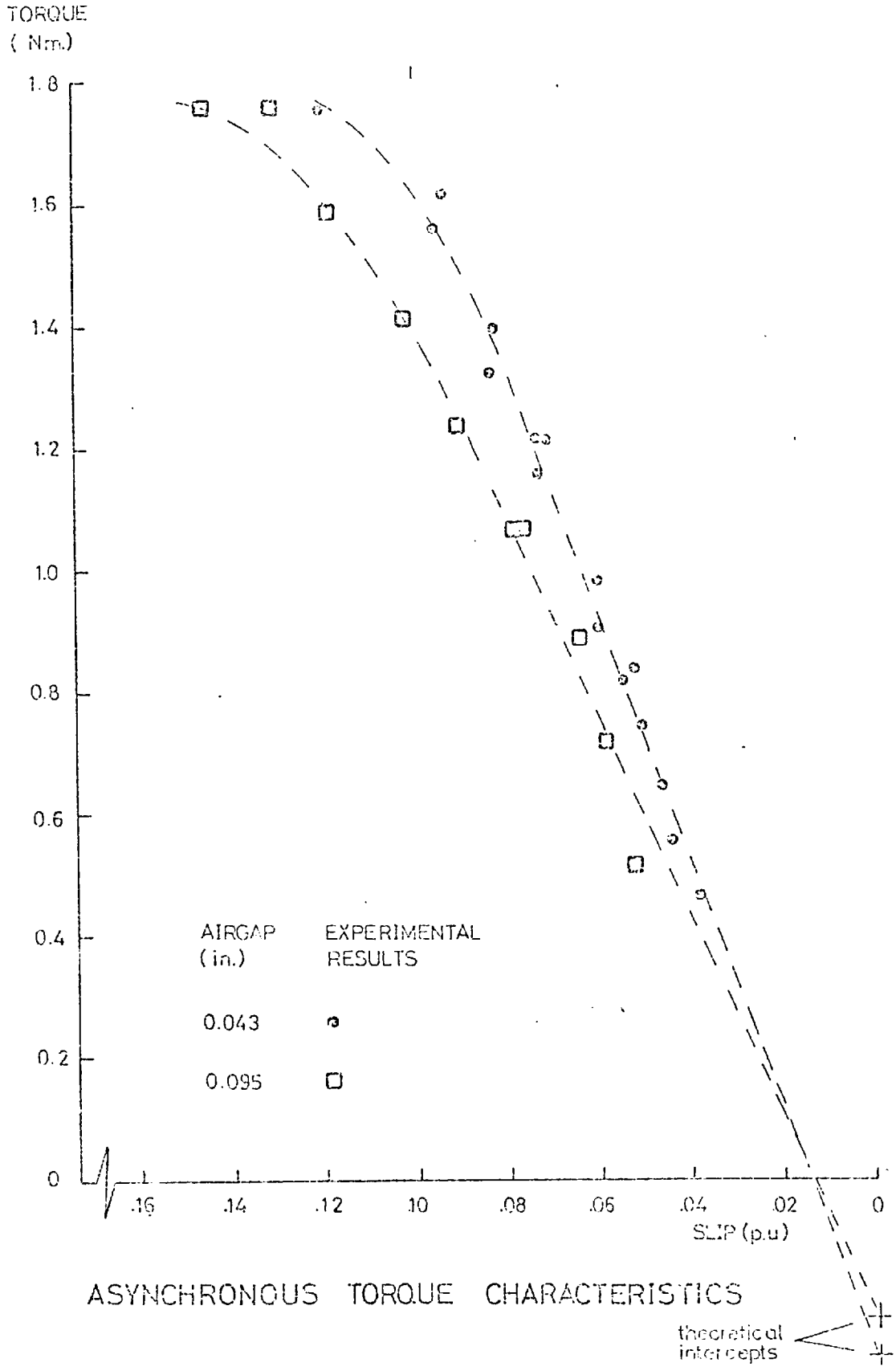

ASYNCHRONOUS TORQUE CHARACTERISTICS

FIG. 5.13

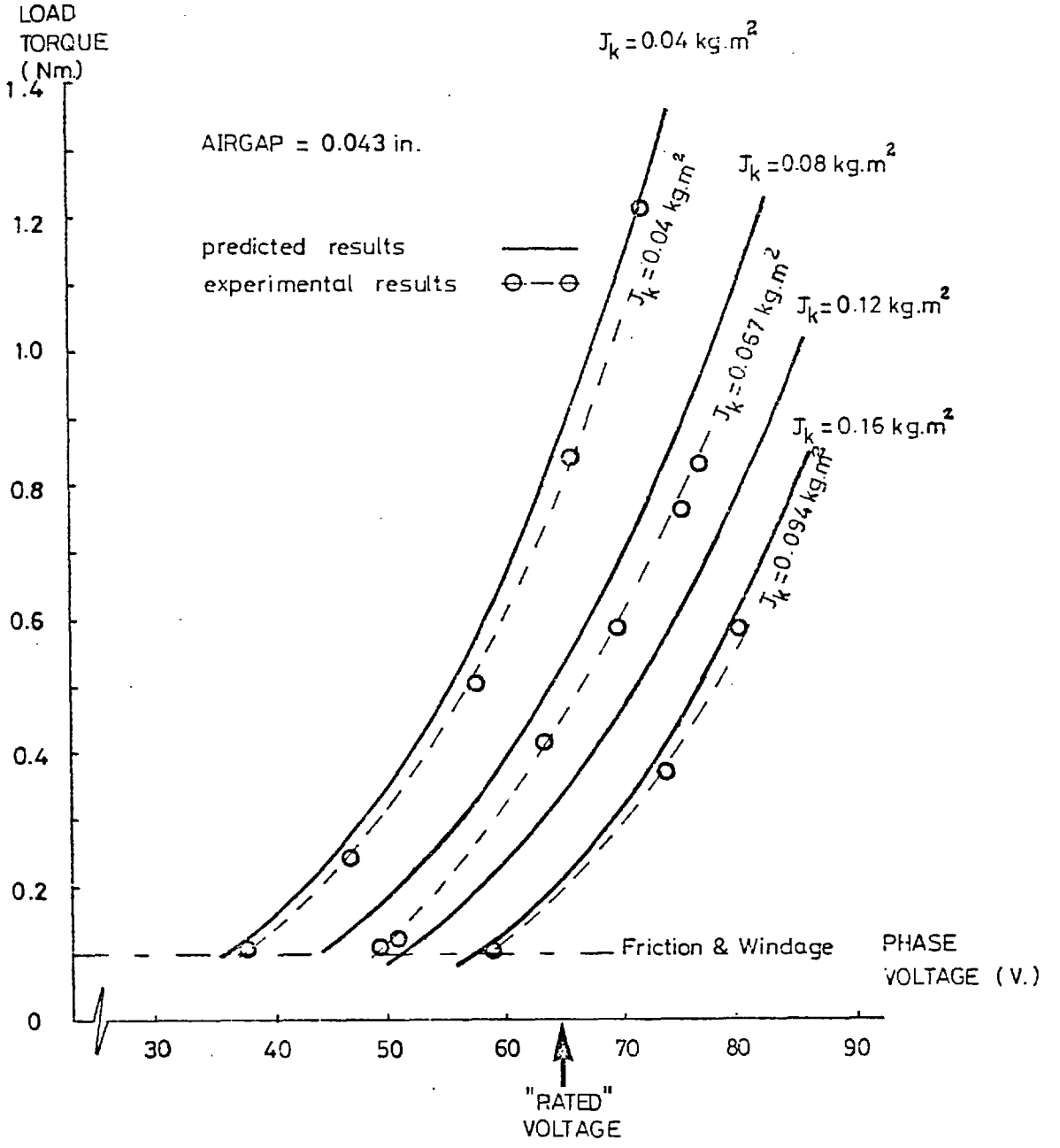

SYNCHRONISING PERFORMANCE OF A SEGMENTED ROTOR DISC RELUCTANCE MOTOR

FIG. 5.14

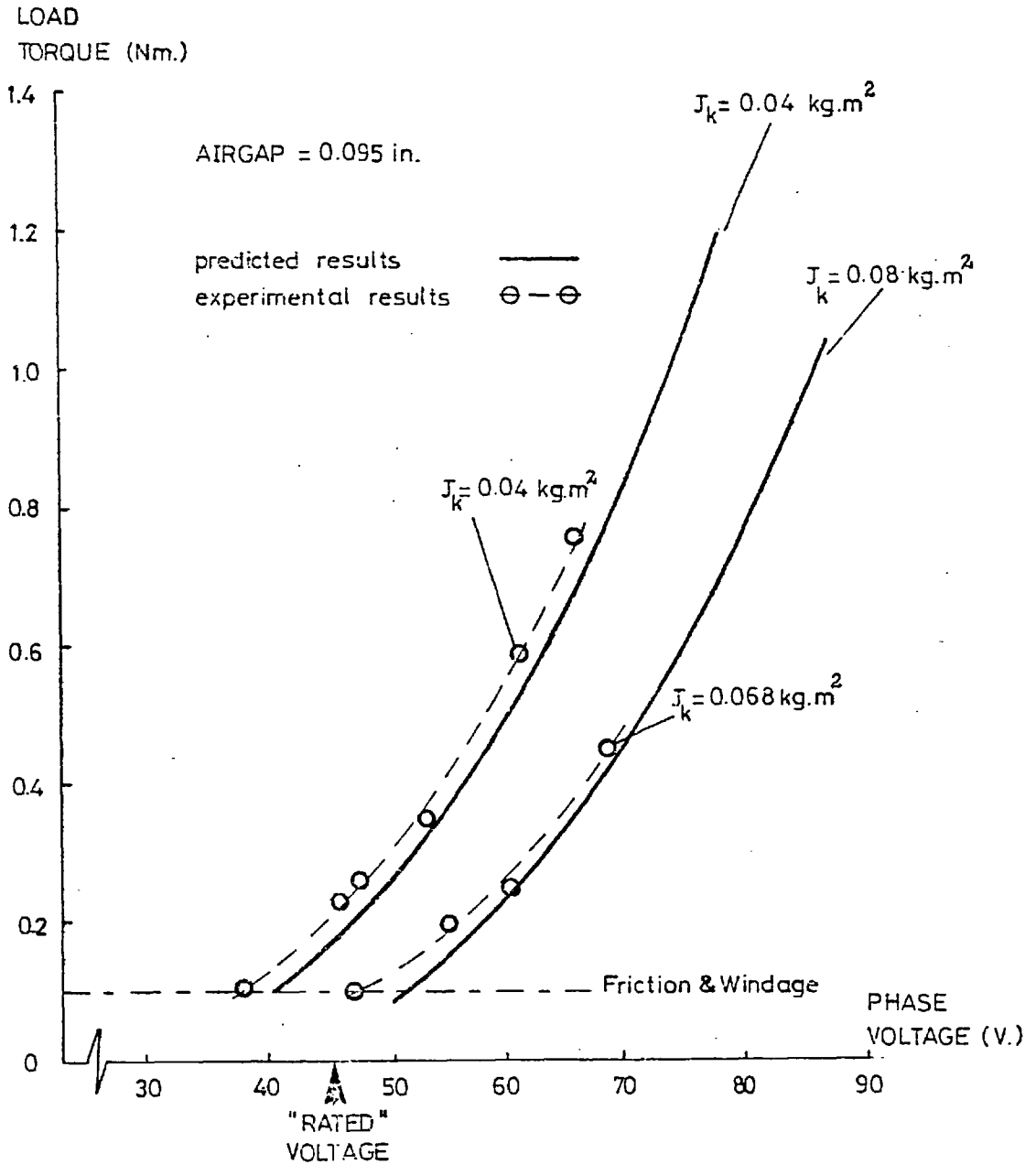

SYNCHRONISING PERFORMANCE OF A SEGMENTED ROTOR DISC RELUCTANCE MOTOR.

FIG. 5.15

It can be seen that in neither case does the synchronising capability of the motor permit its full synchronous output to be utilised if start-up is undertaken in the manner specified above. Indeed, with the airgap of 0.095 inches, the motor is able to do little more than synchronise itself against the bearing friction torque. It is in this respect therefore that the penalties associated with the large airgaps of the motor under consideration are most noticeable.

However, taking the motor with an airgap of 0.043 inches, operating at a synchronous power of 120 watts, after synchronising itself it is still capable of an efficiency greater at 50%, but its power factor is slightly less than 0.4. Its current at this operating point is less than the rated value, 3.4 Amps instead of 3.8 Amps. A case therefore exists for its nominal rated voltage to be increased so that the steady state current at synchronous speed, after synchronising the maximum load of which it is capable is 3.8 Amps. This will increase the specific output of the motor, but do little to improve its power factor and efficiency as it will still be operating at a small load angle.

The inevitable conclusion arising from the theoretical and experimental evidence presented above is that the output capability of a large-airgap segmented-rotor disc reluctance motor is very poor compared with a conventional machine. This is for three main reasons: high leakage reactance, high I^2R losses and a high self inertia of the rotor. Some reductions in these quantities can clearly be achieved by better design, but the inherent disadvantages of a disc geometry for this type of motor appear to be serious.

The disc motor is however a special type of motor which would be used in specialised applications for which its geometry gives it particular suitability. Having established that its performance when operated in a conventional way is poor, therefore, the problem that presents itself is how to overcome these drawbacks so that it can be used effectively when required.

Voltage boosting during synchronisation provides the most convenient way of enhancing the synchronising capability of a reluctance motor. Providing that the magnetic circuit of the motor is designed to permit this without excessive saturation - and this is quite possible as the

normal airgap flux density of the motor will be relatively low - two ways of voltage boosting suggest themselves:

i) If the motor is driven from a solid-state supply it is clearly possible to provide it with a voltage boost facility. If the supply were a variable frequency drive, then running the motor up to speed synchronously might also overcome the problem.

ii) An alternative method uses a star-delta switch, of the type used for starting induction motors. By this method the motor would typically be star connected during run-up from standstill to a sub-synchronous speed from which it will not synchronise. Switching the stator windings to a delta connection at this stage boosts the line voltage by a factor of $\sqrt{3}$ and the synchronising torque by a factor of 3. Once synchronism has been achieved the windings can be restored to their star connected configuration for normal running. Preliminary tests on the prototype motor have shown that this procedure gives a very positive synchronising torque, and that once synchronised, the re-switching from delta to star connection can be accomplished, under full load, without loss of synchronism.

These methods of overcoming the poor synchronising of a large airgap disc reluctance motor effectively increase its cost, but at least they make its use technically feasible. Its adoption for potential applications therefore rests on purely economic considerations, and will clearly depend on the cost of alternative solutions.

5.6 Normal force

A magnetic force exists between the stator and rotor of a single sided disc motor. This force is not self cancelling, as in cylindrical machines, and manifests itself as a net force to be accommodated by thrust bearings on the rotor shaft. It is therefore an important feature that must be taken into account in the design of disc motors.

The problem is to calculate the force between the stator, and a rotor which consists of a conducting grid and magnetically anisotropic iron circuits. This section discusses methods of predicting these forces and presents a comparison between theoretical and experimental results.

Two principal methods are available for calculating the electromagnetic forces. The first is generally applicable and relies upon the principle of Maxwell's stresses. (It is discussed in some detail by Carpenter[21]). The second is less generally applicable and uses the principle of conservation of energy, usually via the method of 'virtual work'. Harris[22] has identified some of the conditions under which it may be used. Appendix 2 shows that under most practical conditions, it can be applied to machines that have rotor saliency, but it is given no further consideration in the present section.

According to the first Maxwell stress system, the time average force between two electromagnetically coupled units may be written as:

$$F_n = \frac{Wp}{\mu_o T} \int_o^{\tau_p} \int_o^T \left\{ [b_n(x,t)]^2 - [b_t(x,t)]^2 \right\} dt\, dx \qquad (5.30)$$

where p is the number of pairs of poles
T is the period of time
τ_p is the pole pitch of the fundamental
W is the uniform width of the units
$b_n(x,t)$ and $b_t(x,t)$ are the normal and tangential components of flux density respectively which vary with position, x, and time, t.

In most analyses of electrical machines, and in the present case, the flux is assumed to traverse the airgap normally so that the tangential component of flux density, $b_t(x,t)$, is zero. Thus, when the normal component of flux density varies sinusoidally in space and time, equation

5.30 reduces to:

$$F_n = 2p\,\tau_p\,W\,\frac{B_N^2}{2\mu_o} \qquad (5.31)$$

where B_N is the rms value of the flux density.

These relationships were applied in two ways for the prototype segmented rotor motor:

i) True airgap flux density

The airgap flux density distribution derived by Lawrenson and Gupta presented in equation 5.6 above gives, within the limits of the stated approximations[6] the true flux density distribution in the airgap of the segmented rotor motor. It takes account of the stator winding harmonics and the rotor permeance harmonics, and of the flux which bypasses the interpolar gap by re-entering the stator core.

The normal force between the stator and rotor was therefore calculated directly by programming equation 5.6, feeding in parameters and operating conditions for the prototype motor, and computing the time average force over a cycle for a range of load angles.

ii) Two axis model

The airgap flux density distribution in the segmented rotor reluctance motor was represented by direct and quadrature axis components in the manner of the conventional two axis model of a machine. This method assumes fundamental components of stator mmf only, and recognises the direction of the airgap flux paths only in so far as they affect the calculated values of the two axis reactances X_d and X_q. By consideration of the phasor diagram for the two axis model of the motor in Fig. 5.6, an expression for the normal force was derived as follows.

Working in rms quantities, the airgap voltages V_{dm} and V_{qm} induced by the rotating direct and quadrature axis airgap flux density components are given by:

$$V_{dm} = I_d\,x_d \qquad (5.32(a))$$

$$V_{qm} = I_q\,x_q \qquad (5.32(b))$$

but, using e = Blv (usual notation),

$$V_{dm} = B_d W 2\tau_p f 4pk_w N = K_v B_d \qquad (5.33(a))$$

$$V_{qm} = B_q W 2\tau_p f 4pk_w N = K_v B_q \qquad (5.33(b))$$

where $K_v = 2\tau_p f 4pk_w W N$

From equations 5.32 and 5.33,

$$B_d = \frac{V_{dm}}{K_v} = \frac{I_d x_d}{K_v} \qquad (5.34(a))$$

$$B_q = \frac{V_{qm}}{K_v} = \frac{I_q x_q}{K_v} \qquad (5.34(b))$$

The resultant normal flux density, B_N, is related to B_d and B_q by

$$B_N^2 = B_d^2 + B_q^2 \qquad (5.35)$$

so that substituting from equations 5.34 into 5.35 gives:

$$B_N^2 = \frac{1}{K_v^2} \{I_d^2 x_d^2 + I_q^2 x_q^2\} \qquad (5.36)$$

Expressions for I_d and I_q derived from Fig. 5.6 are:

$$I_d = V \frac{(X_q \cos\delta - R_1 \sin\delta)}{(R_1^2 + X_d X_q)} \qquad (5.37(a))$$

$$I_q = V \frac{(X_d \sin\delta + R_1 \cos\delta)}{(R_1^2 + X_d X_q)} \qquad (5.37(b))$$

Substituting the values of I_d and I_q from equations 5.37 into equations 5.36, and remembering that the normal force is $B_N^2/2\mu_o$ per unit area, the normal force exerted between stator and rotor is given by:

$$F_n = \frac{p \tau_p W}{\mu_o K_v^2} \frac{V^2}{(R_1^2 + X_d X_q)^2} \{x_d^2 (X_q \cos\delta - R \sin\delta)^2 + x_q^2 (X_d \sin\delta + R \cos\delta)^2\} \qquad (5.38)$$

The factor $\frac{p \tau_p W}{\mu_o K_v^2}$ which appears in equation 5.38 can be re-arranged into a more convenient form. Substituting for K_v the factor becomes:

$$\frac{1}{64 \mu_o W \tau_p f^2 p (K_w N)^2}$$

Comparing this with an expression for the magnetising reactance of a conventional machine, with uniform magnetic airgap, g:

$$x_c = \frac{\mu_o \omega}{\pi^2 g} 24p\ \tau_p\ W\ (K_w\ N)^2 \qquad (5.39)$$

it can be seen that the above factor is equal to $\frac{3}{2}\ \frac{1}{\omega K_c}$ where $x_c = \frac{K_c}{g}$. Hence, the expression for normal force can be written in the form:

$$F_n = \frac{3}{2\omega}\ \frac{1}{K_c}\ \frac{V^2}{(R_1^2 + X_d X_q)^2} \{x_d^2 (X_q \cos\delta - R_1 \sin\delta)^2 + x_q^2 (X_d \sin\delta + R \cos\delta)^2\} \qquad (5.40)$$

It is interesting to note that when primary resistance and leakage reactance are zero, the normal force is independent of load angle, and is given by:

$$F_n\Big|_{\substack{R_1=0 \\ x_1=0}} = \frac{3V^2}{2\omega K_c} \qquad (5.41)$$

Equation 5.40 is an expression for the normal force in a reluctance motor, derived from conventional two axis theory. It was used to predict the forces present in the prototype motor.

Theoretical and experimental results of the normal force investigation are presented on Fig. 5.16. Results from both the theoretical methods described above are shown in this figure. The general conclusion is that both methods give commendable agreement with experiment, especially in the motoring region, but they deserve individual comments. The simple two axis model gives its best agreement with practice with the larger airgap of 0.090 inches. Predictions can be seen to depart further from experiment with the smaller airgap of 0.040 inches especially as the rotor approaches the quadrature axis position in both the motoring and generating regions. It is under these conditions that the harmonic distortion of the airgap flux pattern becomes most severe, and evidently cannot be handled effectively by the two axis model. It would appear that this model could not be applied with confidence for airgaps less than 0.040 inches.

Use of the true airgap flux density distribution, however, appears to predict normal force equally competently at both airgap settings. The shapes of the theoretical and experimental force characteristics are very

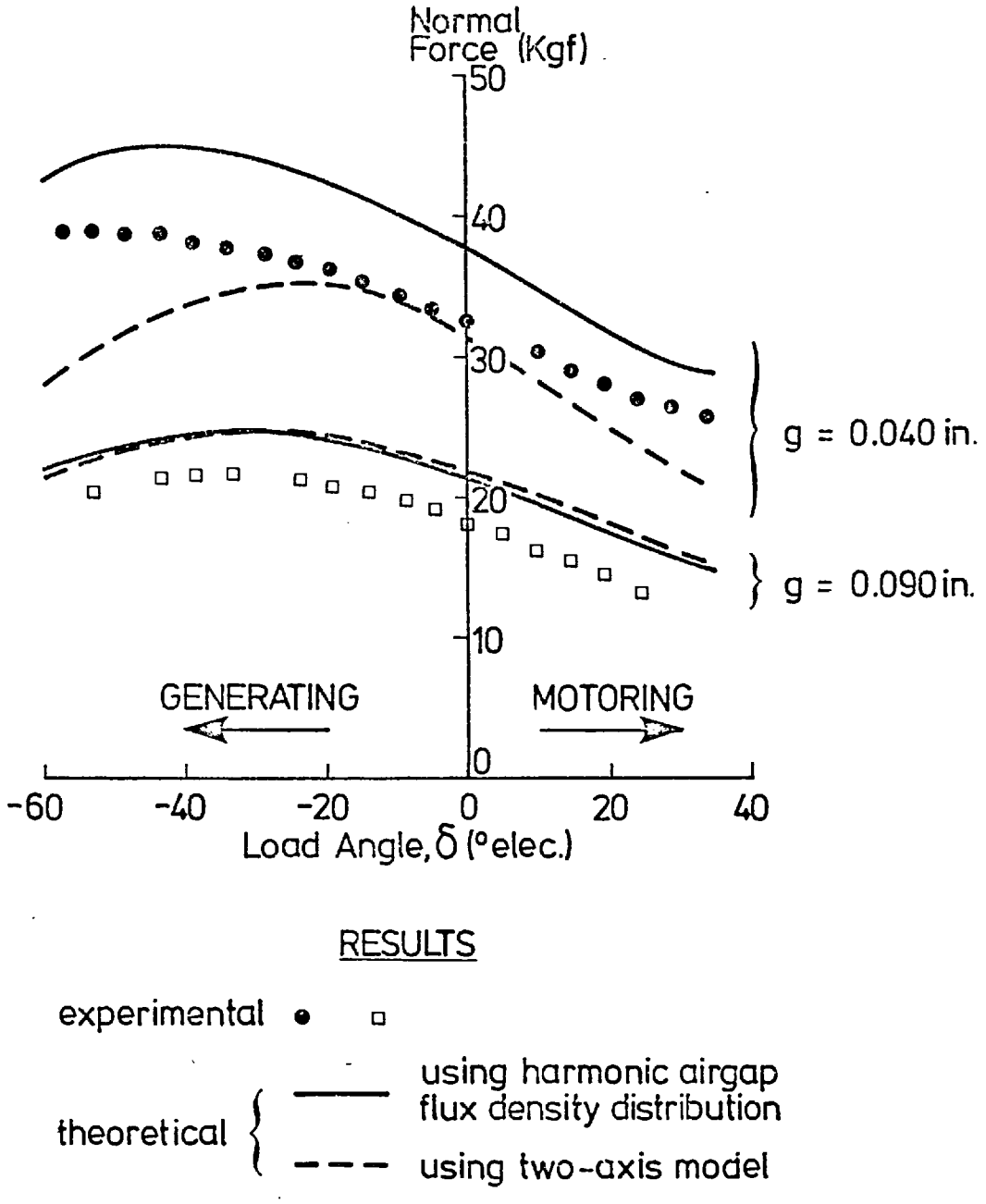

Fig.5.16 VARIATION OF NORMAL FORCE WITH LOAD ANGLE

similar in both cases, and the theory overestimates the force consistently by around 15%. There are no reasons to suggest that this method could not be used for even smaller airgaps.

The two theoretical methods deserve comparison in two respects.

i) Transient Forces

The results presented in Fig 5.16 are time-average forces. There are indications however that the normal force has a pulsating component. This is predicted by calculations using the true airgap flux density, which show a strong pulsation at twice the fundamental frequency. The most probable cause of this is a backward rotating field of fundamental frequency interacting with the main field. The backward rotating field appears to be produced by interaction of the second permeance harmonic with the fifth mmf harmonic. Clearly the two axis model does not predict this aspect of the normal force characteristic. It can therefore be used for calculating time-average forces, but not peak forces. Experiments have not been performed to investigate this aspect of normal force and it is therefore not discussed further in this thesis. It deserves investigation, however, as the life of a thrust bearing will depend upon the magnitude and frequency of these pulsations.

ii) Computational complexity

It can be seen from equation 5.40 that normal force predictions from the two axis model are very simple to make. They can be tackled by hand, or with a short computer program. The method is useful, therefore, bearing in mind how closely it predicts the forces for larger airgaps. Calculations from the true airgap flux density could not be contemplated by hand, however, as it was found that some 5 winding harmonics (including the fundamental) and 40 permeance harmonics needed to be inserted into equation 5.6 to give reliable results. Computations at not less than 20 intervals in a voltage cycle were required to obtain the time average force. The results shown on Fig. 5.16 were obtained by making calculations at six load angles and for each airgap setting the computation absorbed over 300 minutes of c.p.u. time on an ICL System 4-70 computer. This method is therefore expensive to use and apparently need only be resorted to for very small airgap segmented rotor machines.

Two features of the normal forces present in a disc reluctance motor can be extracted from Fig. 5.16. These are the magnitude of the force with respect to the output of the motor, and the variation of the force with load angle at synchronous speed. For the prototype motor operating from a phase voltage of 50V the size of the normal and tractive forces are summarised below:

Airgap Setting (in)	Normal Force at $\delta = 10°$ (Kgf)	Tractive Force at $\delta = 10°$ (Kgf)	Normal Force / Tractive Force
0.040	30.5	1.6	19
0.090	18.5	1.6	11.5

From these results it appears that the normal force is between 10 and 20 times greater than the tractive force. The normal force is therefore large, but there seems to be no reason why it could not be accommodated by conventional thrust bearings in many applications. It is interesting to compare simple expressions for normal and tractive force. Equation 5.41 above gives the normal force produced by a motor that possesses no primary resistance and leakage reactance and is driven from a constant voltage supply, i.e.

$$F_n\Big|_{\substack{R_1=0\\X_1=0}} = \frac{3V^2}{2\omega k_a} \qquad (5.41)$$

The tractive force produced at pull out by the same motor, in which the direct axis reactance is assumed to be very large compared to the quadrature axis reactance is given by simplifying equation 5.17 as:

$$T_{po}\Big|_{\substack{R_1=0\\X_1=0}} = \frac{3V^2 g_q}{2\omega k_c} \qquad (5.42)$$

where g_q is the effective airgap of the quadrature axis, and according to previous representation, is given by

$$g_q = \frac{g}{k_q} \qquad (5.43)$$

Hence the torque is g_q times the normal force where g_q, in metres, is a very small number.

The variation of normal force with load angle can be observed in Fig. 5.16. The force reduces in the motoring region as load angle increases. The reduction is caused by a fall in the airgap voltage as an increasing current increases the voltage drop across the primary resistance and leakage reactance. For the prototype motor a reduction in normal force of between 25% and 30% can be seen to occur as the motor load increases from zero to pull-out. As shown in equation 5.41 above the force would be constant if the primary resistance and leakage reactance were absent. And this condition might be approached in large machines in which these parameters have low per unit values.

Chapter 5: References

1. Fong, W., "New Type of Reluctance Motor", Proc.IEE, 1970, 117, (3), pp. 545-551.

2. Cruickshank, A.J.O., Anderson, A.F. and Menzies, R.W., "Theory and Performance of Reluctance Motors with Axially Laminated Anisotropic Rotors", Proc.IEE, 1971, 118, (7), pp. 887-894.

3. Lawrenson, P.J. and Agu, L.A., "Theory and Performance of Polyphase Reluctance Machines", Proc.IEE, 1964, 111, (8), pp. 1435-1445.

4. Lawrenson, P.J. and Agu, L.A., "Low Inertia Reluctance Machines", Proc.IEE, 1964, 111, (12), pp. 2017-2025.

5. Lawrenson, P.J., "Two Speed Operation of Salient-pole Reluctance Machines", Proc.IEE, 1965, 112, (12), pp. 2311-2316.

6. Lawrenson, P.J. and Gupta, S.K., "Developments in the Performance and Theory of Segmental-Rotor Reluctance Motors", Proc.IEE, 1967, 114, (5), pp. 645-653.

7. Lawrenson, P.J., Gupta, S.K. and Murthy Vamaraju, S.R., "Multispeed Performance of Segmental Rotor Reluctance Machines", Proc.IEE, 1968, 115, (5), pp. 695-702.

8. Lawrenson, P.J., Mathur, R.M. and Murthy Vamaraju, S.R., "Importance of Winding and Permeance Harmonics in the Prediction of Reluctance Motor Performance", 1969, 116, (5), pp. 781-787.

9. Lawrenson, P.J. and Bowes, S.R., "Stability of Reluctance Machines", Proc.IEE, 1971, 118, (2), pp. 356-369.

10. Lawrenson, P.J. and Gupta, S.K., "Fringe and Permeance Factors for Segmented-Rotor Reluctance Machines", Proc.IEE, 1971, 118, (5), pp. 669-674.

11. Lawrenson, P.J., Mathur, R.M. and Stephenson, J.M., "Transient Performance of Reluctance Machines", Proc.IEE, 1971, 118, (6), pp. 777-783.

12. Lawrenson, P.J. and Mathur, R.M., "Asynchronous Performance of Reluctance Machines Allowing for Irregular Distributions of Rotor Conductors", Proc.IEE, 1972, 119, (3), pp. 318-324.

13. Lawrenson, P.J. and Mathur, R.M., "Pull-in Criterion for Reluctance Motors", Proc.IEE, 1973, 120, (9), pp. 982-987.

14. Russell, R.L. and Norsworthy, K.H., "Eddy Currents and Wall Losses in Screened-Rotor Induction Motors", Proc.IEE, 1958, 105A, pp. 163-175.

15. Stephenson, J.M. and Lawrenson, P.J., "Average Asynchronous Torque of Synchronous Machines with Particular Reference to Reluctance Machines", Proc.IEE, 1969, 116, (6), pp. 1049-1051.

16. Discussion on "Reluctance Motors", Proc.IEE, 1968, 115, (9), pp. 1283-1285.

17. Talaat, M.E., "Steady-state and Transient Synthesis of 3-phase, Reluctance Motors", Trans.AIEE, 1951, 70, pp. 1963-1970.

18. Douglas, J.F.H., "Pull-in Criterion for Reluctance Motors", Trans. AIEE, 1960, 79, pp. 139-142.

19. Burian, K., "Pulling-into-step of Reluctance Synchronous Motors", Trans.IEEE, 1965, PAS-84, pp. 349-352.

20. Williamson, A.C., "Calculation of Saturation Effects in Segmented-Rotor Reluctance Machines", Proc.IEE, 1974, 121, (10), pp. 1127-1133.

21. Carpenter, C.J., "Surface Integral Methods of Calculating Forces on Magnetised Iron Parts", IEE monograph No. 342, August 1959.

22. Harris, M.R., "Circuit Analysis of Electromagnetic Force in Terms of Effective Inductance", Proc.IEE, 1966, 113, (11), pp. 1873-1875.

CHAPTER 6

General Conclusions

On the basis of the studies described in the five preceding chapters of this thesis the following observations on disc motors can be made.

1. Disc-geometry machines constitute a class of electric machines, in addition to the conventional class of cylindrical machines, which utilise continuous rotary motion for the interconversion of electrical and mechanical energy. In general there are equivalent disc machines for the many varieties of cylindrical machines, but the "double-sided" disc machine also exists.

2. The "double-sided" disc motor can be considered as a special machine which is suitable only for special applications. The single sided motor on the other hand, by virtue of the simple and separate arrangement of stator and rotor can reasonably be considered as a serious contender for some of the drive applications now met by cylindrical machines.

3. Traditionally disc machines have been excluded from many uses for two principal reasons:

- the high cost of manufacture
- the normal force between stator and rotor

The transverse flux disc motor designs which utilise pre-punched laminations for the stator core construction appear to open the path for the development of low cost disc motor designs. In many cases the normal forces can be accommodated by standard thrust bearing arrangements. Other methods of reducing and eliminating the normal forces are under consideration.

4. Conventional methods of analysis for cylindrical machines apply equally well, in many cases, for disc machines. Design criteria cannot be carried over with equal success, however, and new ones for disc motors are required. Stator design - specifically slot depth and stator

width - requires optimisation so that the motor operates under acceptable thermal conditions.

5. Further development of disc motors, along the aforementioned lines appears to be worthwhile, in order to establish whether commercially viable units are feasible.

Appendix 1

Justification of Improved Rotor Model

A description of the theoretical rotor model in Section 3.5.3 of the main text stated that the use of a "simple" model gave unsatisfactory torque predictions, while an "improved" model, which required the same number of rotor loops, produced more representative results. This appendix presents theoretical and experimental evidence to support this statement. As described in Section 3.5.3, the "simple" model represented the radial bar conductors by infinitely thin conductors, while the "improved" model subdivided the rotor loops into concentric, parallel-connected filament coils.

The rotor parameter values by the two models are compared below:

i) Loop resistance

Loop No.	Loop Resistance (μΩ)		
	Simple Model	Improved Model (slip=0)	(slip=1.0)
1	25.7	37.4	38.1
2	25.7	37.8	38.4
3	15.0	18.6	19.9
4	15.0	18.0	19.4

It can be seen that the resistance of the loops which contain iron segments, loops 1 and 2, is predicted to be almost 50% higher by the improved model, than by the simple model. The difference is less marked for loops 3 and 4, but is still in the order of 25%. The "improved" model, unlike the "simple" model, can also take account of the rotor slip frequency on current distribution in the rotor loop conductors, and its effect on rotor resistance. The resistances of loops 3 and 4 decrease by almost 8% from standstill to synchronous speed.

ii) Self and mutual inductances of rotor loops

Loop Parameter	Inductance (H)	
	Simple Model	Improved Model
M_{11}	2.5×10^{-7}	2.6×10^{-7}
M_{22}	2.6×10^{-7}	2.6×10^{-7}
M_{33}	10.6×10^{-8}	4.1×10^{-8}
M_{44}	11.4×10^{-8}	4.0×10^{-8}
M_{12}	-2.6×10^{-8}	-2.6×10^{-8}
M_{13}	-9.8×10^{-9}	-6.2×10^{-9}
M_{14}	-1.1×10^{-8}	-6.2×10^{-9}
M_{23}	-1.0×10^{-8}	-5.5×10^{-10}
M_{24}	-1.1×10^{-8}	-6.3×10^{-9}
M_{34}	-4.1×10^{-9}	8.0×10^{-9}

The inductances of the 'iron' rotor loops, i.e. M_{11}, M_{22} and M_{12} are approximately the same with both models. This can be explained by the fact that the current is largely constricted within a relatively narrow conductor (the radial rib between two segments) and the flux is concentrated through the iron insert. On the other hand, there is considerable reduction in the values of inductances of 'copper' loops, loops 3 and 4, predicted using the 'improved' model compared with the simple model, because of the incomplete linkage of the flux generated by one loop with the currents distributed over the extent of a wide radial bar.

iii) Mutual inductances between rotor loops and stator phases

The peak values of the mutual inductances between the rotor loops and the stator phases are tabulated below:

Parameter	Inductance (H)	
	Simple Model	Improved Model
M_{1R}, M_{1Y}, M_{1B}	4.3×10^{-5}	4.6×10^{-5}
M_{2R}, M_{2Y}, M_{2B}	4.3×10^{-5}	4.7×10^{-5}
M_{3R}, M_{3Y}, M_{3B}	1.7×10^{-5}	1.0×10^{-5}
M_{4R}, M_{4Y}, M_{4B}	1.8×10^{-5}	1.0×10^{-5}

Noticeable here are the reduced mutual inductances of loops 3 and 4 with the stator phases when predicted using the improved model. This again is thought to arise from the greater distribution of the current in the 'copper' loops.

The most conclusive evidence of the superior quality of the improved model is gained from Fig. A1.1 in which asynchronous torque vs speed curves for the motor tests reported in Section 4.3.2 are illustrated. It can be seen that while the predictions from the improved model are almost coincident with the test results, the simple model results are indicative of underestimated rotor resistances. The results for theoretical and measured phase currents in Fig. A1.1 do not show the improved model in as favourable a light. It can be seen that the theoretical currents predicted by the simple model are closer to the measured results than those of the improved model. The fact that the simple model currents are greater than the improved model currents is consistent with an underestimation of the rotor resistance by the simple model.

However, it is apparent from the results presented in Fig. A1.1 that the improved model gives a reasonable representation of the rotor impedance while a simple model, with four rotor loops per pole, is unsatisfactory for most purposes.

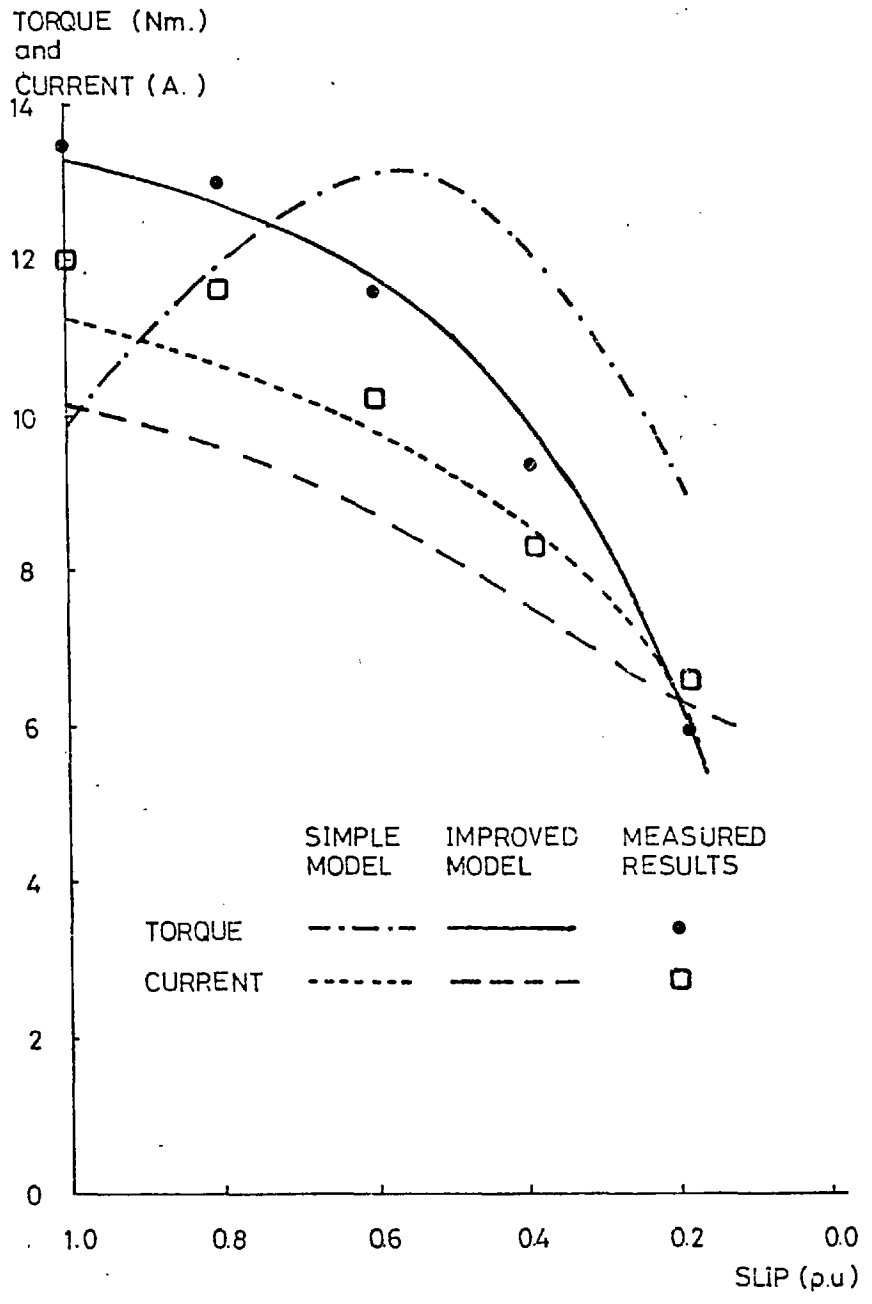

COMPARISON OF RESULTS PRODUCED BY ALTERNATIVE ROTOR MODELS

FIG. A1.1

Appendix 2

Energy Methods for the Calculation of Normal Forces in Disc Reluctance Motors

The normal force between stator and rotor of a segmented rotor disc reluctance motor was investigated in Section 5.6. Experimental results were compared with theoretical predictions that were made on the basis of the first Maxwell stress system. Correlation was found to be good.

The Maxwell stress method is the fundamental method for calculating magnetic forces, and it offers a useful physical picture of the mechanisms of force production. A second general method of calculating forces also exists which is often called the 'energy method'. It complements the Maxwell method, and is sometimes more convenient to apply, but does not give as useful a physical explanation of the mechanisms involved.

The energy method is based on the principle of virtual work. If a force, F, is acting on part of a magnetic system, and if this part is allowed a small displacement δx, say, then work, δW, will be done:

$$\delta W = F\,\delta x \qquad \text{(A2.1)}$$

The displacement δx may increase the stored energy of the system by an amount δW_m, and voltages induced in coils in the system would also require some electrical energy δW_e to be supplied. The balance of energy exchanges caused by the displacement δx can therefore be written as:

$$\delta W_e = \delta W_m + \delta W \qquad \text{(A2.2)}$$

where $\delta W = F\,\delta x$. i.e. the electrical energy input to the system supplies the increase in stored energy and mechanical work done. Carter[1] has shown that if the current to the system is held constant the electrical energy is divided equally between the stored energy and mechanical work done so that

$$\delta W_m = F\,\delta x$$

$$\text{and} \quad F = \frac{\delta W_m}{\delta x} \qquad \text{(A2.3)}$$

i.e. the mechanical force is equal to the rate of change with respect to displacement of the stored energy.

The field-stored energy in a constant current system is given by:

$$W_m = \int_0^{\lambda} id\lambda \qquad (A2.4)$$

where λ is the flux linkage of the system. A linear relationship exists between flux linkage and current in air cored systems, and exists approximately in iron cored systems operating under unsaturated conditions, the constant of proportionality being inductance, L, so that:

$$\lambda = Li \qquad (A2.5)$$

Substituting equation A2.5 into A2.4 gives:

$$W_m = \int_0^{\lambda} \frac{\lambda}{L} d\lambda$$

$$\text{and } W_m = \frac{1}{2} \frac{\lambda^2}{L} = \frac{1}{2} Li^2 \qquad (A2.6)$$

Equation A2.6 is the well known expression for the stored energy in an inductive system, and it can be combined under the prescribed constant current conditions with equation A2.3 above to give:

$$F = \frac{1}{2} i^2 \frac{dL}{dx} \qquad (A2.7)$$

The mechanical force existing in a simple magnetic system can therefore often be calculated from a knowledge of the dependence of the inductance of the system on its airgap. This forms the basis of the energy method for calculating forces in magnetic systems.

In complex systems, however, such as provided by electrical machines, the energy method must be used with caution. It is not generally applicable. Harris[2] has identified the conditions under which it may be applied and has pointed out its limitations. In fact the energy method appears to be inapplicable to the present prototype segmented rotor disc reluctance motor because it contains secondary conductors with non-zero resistance (c.f. "Class 2", Harris[2]), but in reality it means that the method can be used for steady state conditions only, in which the airgap is constant. Under transient conditions, in which the airgap is changing, energy dissipation in the rotor conductors would make the method inapplicable. Harris[2] made no mention of the use of energy methods in salient pole machines; but Boldea and Nasar[3,4] presented theoretical results for the normal forces in a linear segmented rotor machine. This is identical to

the problem presented by the present disc motor, as they neglected entry and exit edge effects. But direct use of their method produced results which did not agree with the theoretical or experimental results presented in Section 5.6 above. A closer investigation of the application of the energy method to salient pole machines is therefore presented below. It is found that it can be used, and from the two axis model of the machine an expression for the normal force is derived by the energy method. This expression is identical to that derived in equation 5.40 by the Maxwell stress method.

By inspection of Fig. 5.6, the total reactive VA of the motor can be expressed as:

$$\begin{aligned} VAr &= 3\{I_d(x_d + x_1) + I_q R\}I_q + 3\{I_q(x_q + x_1) - I_d R\}I_q \\ &= 3\{I_d^2(x_d + x_1) + I_q^2(x_q + x_1)\} \end{aligned}$$

The airgap field-stored energy, W_m, is therefore given by:

$$W_m = \frac{3}{2\omega}(I_d^2 x_d + I_q^2 x_q) \qquad \text{(A2.9)}$$

This can be seen to be in the form:

$$W_m = W_{md} + W_{mq} \qquad \text{(A2.10(a))}$$

where $$W_{md} = \frac{3}{2\omega} I_d^2 x_d \qquad \text{(A2.10(b))}$$

and $$W_{mq} = \frac{3}{2\omega} I_q^2 x_q \qquad \text{(A2.10(c))}$$

The fundamental assumption of the two axis model of a salient pole machine is that it can be represented by two machines with uniform airgaps g_d and g_q, say, for the direct and quadrature axis machines respectively. The behaviour of the actual machine is then obtained by superposition of the behaviour of the two uniform airgap machines. Hence equations A2.10(b) and A2.10(c) can be re-written in the form:

$$W_{md} = \frac{3}{2\omega} I_d^2 \left(\frac{k_c}{g_d}\right) \qquad \text{(A2.11(a))}$$

$$W_{mq} = \frac{3}{2\omega} I_q^2 \left(\frac{k_c}{g_q}\right) \qquad \text{(A2.11(b))}$$

where k_c was defined at equation 5.39.

According to equation A2.7 the normal forces exerted by the direct and quadrature axis machines are given by:

$$F_{nd} = \frac{3}{2\omega} I_d^2 \frac{d}{dg_d} \left(\frac{k_c}{g_d}\right)\Big|_{I_d=\text{const}} \qquad \text{(A2.12(a))}$$

$$F_{nq} = \frac{3}{2\omega} I_q^2 \frac{d}{dg_q} \left(\frac{k_c}{g_q}\right)\Big|_{I_q=\text{const}} \qquad \text{(A2.12(b))}$$

The total normal force between the stator and rotor is given by:

$$F_n = F_{nd} + F_{nq} \qquad \text{(A2.12(c))}$$

$$\text{Hence } F_n = \frac{3k_c}{2\omega} \left\{I_d^2 \frac{d}{dg_d} \left(\frac{1}{g_d}\right) + I_q^2 \frac{d}{dg_q} \left(\frac{1}{g_q}\right)\right\} \qquad \text{(A2.13)}$$

$$\text{And } F_n = -\frac{3k_c}{2\omega} \left\{\frac{I_d^2}{g_d^2} + \frac{I_q^2}{g_q^2}\right\}$$

$$= -\frac{3}{2\omega} \frac{1}{k_c} \left\{I_d^2 x_d^2 + I_q^2 x_q^2\right\} \qquad \text{(A2.14)}$$

Substituting for I_d and I_q, using equation 5.37, equation A2.14 expands to:

$$|F_n| = \frac{3}{2\omega} \cdot \frac{1}{k_c} \frac{V^2}{(R_1^2 + X_d X_q)^2} \left\{x_d^2 (X_q \cos\delta - R_1 \sin\delta)^2 + x_q^2 (X_d \sin\delta + R_1 \cos\delta)^2\right\} \qquad \text{(A2.15)}$$

which can be recognised to be identical to equation 5.40, the expression for normal force derived by the Maxwell Stress method.

Energy method of Boldea and Nasar

Boldea and Nasar[3][4] adopted a different approach to that described above for the calculation of normal forces in a reluctance motor. They also used the energy method, but proceeded from equation A2.9 above with the step:

$$\bar{F}_n = \frac{3}{2\omega} I^2 \frac{\partial}{\partial g} \left\{\frac{x_d \alpha_d^2 + x_q \alpha_q^2}{\alpha_d^2 + \alpha_q^2}\right\}\Big|_{I=\text{const}} \qquad \text{(A2.16)}$$

where $$\alpha_d = \frac{X_q \cos\delta - R_1 \sin\delta}{R_1^2 + X_d X_q} \qquad \text{(A2.17(a))}$$

$$\alpha_q = \frac{X_d \sin\delta + R_1 \cos\delta}{R_1^2 + X_d X_q} \qquad \text{(A2.17(b))}$$

This results in an expression which is not readily simplified. However, it disagrees with the equation derived by the Maxwell's stress method, and this casts doubt on its validity.

Further points which question the validity of the method are set out below.

i) Fig. A2.1 compares normal force calculations using Boldea and Nasar's method with those presented in section 5.6 above. They can be seen to disagree with the experimental results, and with two independent sets of theoretical results.

ii) Fig. A2.2 illustrates three sets of theoretical results for the linear reluctance motor considered by Boldea and Nasar. Two observations can be made:

a) normal forces, calculated independently using Boldea and Nasar's method, do not agree with the results published by Boldea and Nasar.

b) normal forces calculated by the Maxwell Stress method, which proved successful for the prototype disc motor in section 5.6 above differ from both the other two.

iii) It can be shown that the expression derived by Boldea and Nasar predicts that normal force is independent of leakage reactance, and is therefore independent of the airgap voltage. The principal steps which indicate this are as follows:

Differentiating equation A2.16 numerically, and allowing superscripts + and - to denote parameter values at airgaps of $g + \frac{\Delta g}{2}$ and $g - \frac{\Delta g}{2}$ respectively,

$$\bar{F}_n = -\frac{3}{2\omega}\frac{I^2}{\Delta g}\left\{\left[\frac{(X_d^+ - x_1)(\alpha_d^+)^2 + (X_q - x_1)(\alpha_q^+)^2}{(\alpha_d^+)^2 + (\alpha_q^+)^2}\right] - \left[\frac{(X_d^- - x_1)(\alpha_d^-)^2 + (X_q^- - x_1)(\alpha_q^-)^2}{(\alpha_d^-)^2 + (\alpha_q^-)^2}\right]\right\}$$

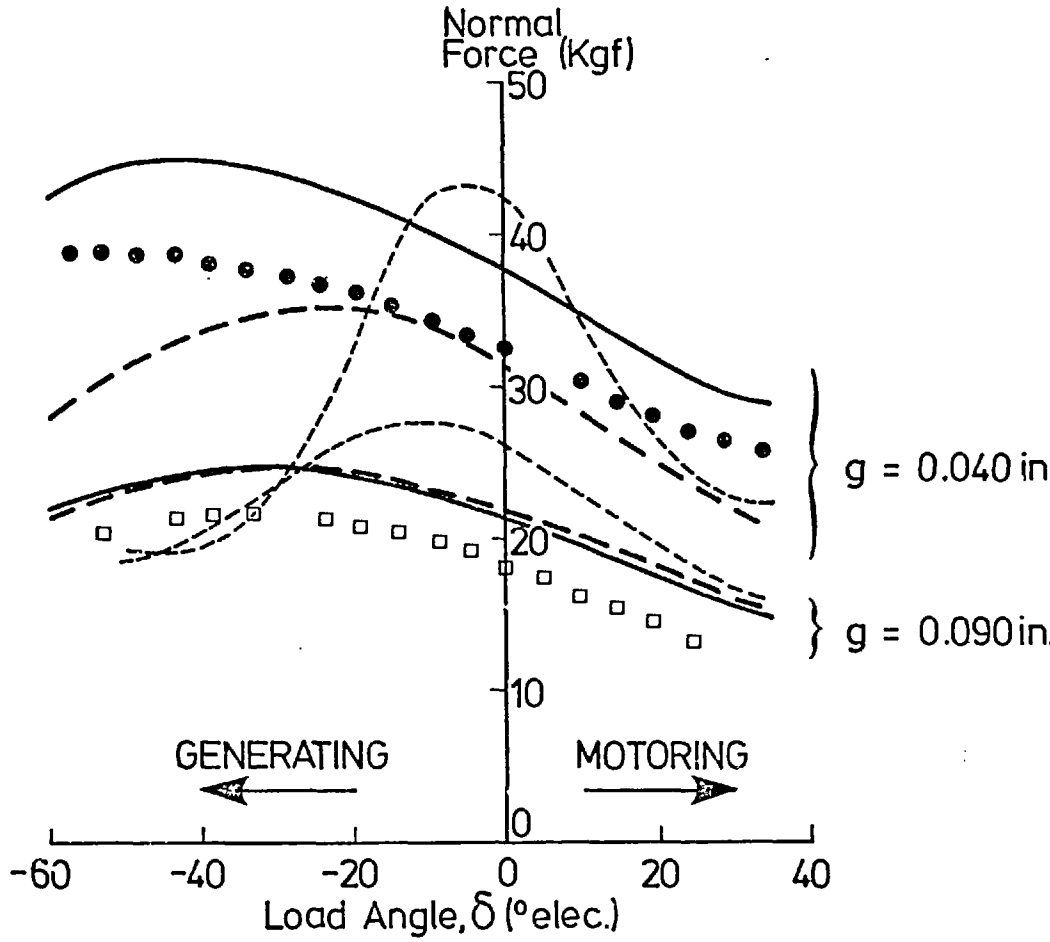

RESULTS

experimental ● □

theoretical
——— using harmonic airgap flux density distribution
– – – using two-axis model
------ using Boldea and Nasar's method

Fig.A2.1 VARIATION OF NORMAL FORCE WITH LOAD ANGLE

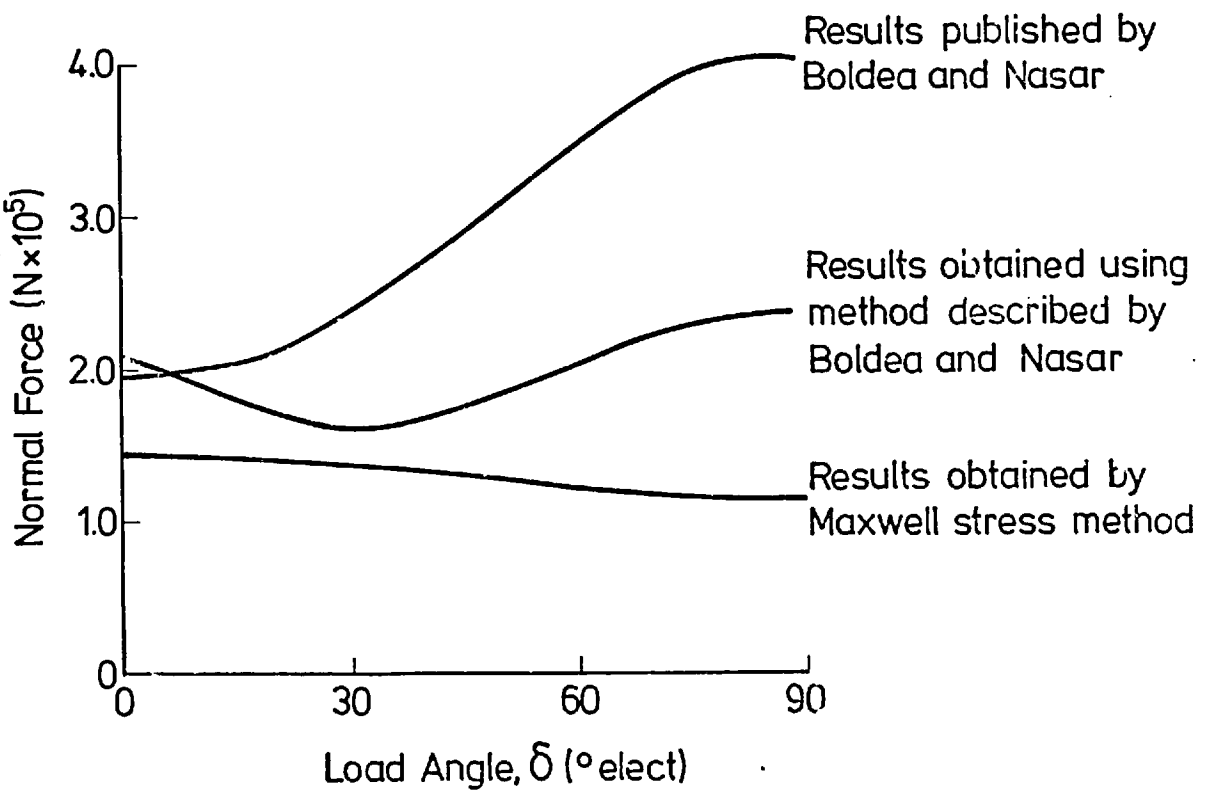

Fig. A2.2 NORMAL FORCE RESULTS FOR LINEAR RELUCTANCE MOTOR OF BOLDEA AND NASAR (Ref. 3 and 4)

$$= -\frac{3}{2\omega}\frac{I^2}{\Delta g}\left[\frac{X_d^+(\alpha_d^+)^2 + X_q^+(\alpha_q^+)^2}{(\alpha_d^+)^2 + (\alpha_q^+)^2}\right] - \left[\frac{X_d^-(\alpha_d^-)^2 + X_q^-(\alpha_q^-)^2}{(\alpha_d^-)^2 + (\alpha_q^-)^2}\right]$$

$$- x_1\left[\frac{(\alpha_d^+)^2 + (\alpha_q^+)^2}{(\alpha_d^+)^2 + (\alpha_q^+)^2}\right] + x_1\left[\frac{(\alpha_d^-)^2 + (\alpha_q^-)^2}{(\alpha_d^-)^2 + (\alpha_q^-)^2}\right]\Big\} \qquad \text{(A2.18)}$$

The terms in x_1 cancel out, and the normal force is dependent only on X_d and X_q: the partition of X_q into x_q and x_1, and X_d into x_d and x_1, is apparently irrelevant.

iv) Use of the Boldea and Nasar expression for normal force would seem to predict different normal forces for equivalent salient pole and segmented rotor machines, for example. This is because the variation of x_d and x_q with g depends upon the rotor geometry. These differences are not taken into account in the two axis model, upon which the method is based. The predicted normal force for any type of reluctance motor should therefore be identical for specified values of X_d, X_q and x_1. This means, in the present context, that the normal force must be independent of the variation of x_d and x_q with g.

Evidently, to start by differentiating x_d and x_q with respect to g, and to end with equation A2 9 above, the analysis should proceed as follows:

$$F_n = -\frac{3}{2\omega}\left\{I_d^2\frac{dx_d}{dg}\left.\frac{dg}{dg_d}\right|_{I_d=\text{const}} + I_q^2\frac{dx_q}{dg}\left.\frac{dg}{dg_q}\right|_{I_q=\text{const}}\right\} \qquad \text{(A2.19)}$$

But $$\frac{dx_d}{dg} = \frac{k_c}{g^2}(gk_d' - k_d) \qquad \text{(A2.20(a))}$$

and $$\frac{dg_d}{dg} = -\frac{1}{k_d^2}(gk_d' - k_d) \qquad \text{(A2.20(b))}$$

so that $$\frac{dx_d}{dg}\frac{dg}{dg_d} = -\frac{k_c}{g_d^2} = -\frac{x_d^2}{k_c} \qquad \text{(A2.21)}$$

where $k_d' = \frac{d}{dg}(k_d)$; similar expressions apply for the q-axis.

Substituting equation A2.21 into equation A2.19 now gives:

$$F_n = \frac{3}{2\omega}\frac{1}{k_c}[I_d^2X_{dm} + I_q^2X_{qm}] \qquad \text{(A2.22)}$$

and this is identical to equation A2.9.

The evidence of the four points outlined above suggests that the energy method described in this Appendix can be recommended in preference to that put forward by Boldea and Nasar[3].

Appendix 2: References

1. Carter, G.W., "The Electromagnetic Field in its Engineering Aspects", 1954, Longmans, Green and Co.

2. Harris, M.R., "Circuit Analysis of Electromagnetic Force in Terms of Effective Inductance", Proc.IEE, 1966, 113, (11), pp. 1873-1875.

3. Boldea, I and Nasar, S.A., "Thrust and Normal Forces in a Segmented-Secondary Linear Reluctance Motor, Proc.IEE, 1975, 122, (9), pp. 922-924.

4. Nasar, S.A. and Boldea, I., "Linear Motion Electric Machines". Wiley, 1976.